CALIFORNIA INSTITUTE OF TECHNOLOGY

EARTHQUAKE ENGINEERING RESEARCH LABORATORY
Center for Research on the Prevention of Natural Disasters

EARTHQUAKE-INDUCED SOIL PRESSURES ON STRUCTURES

by
John H. Wood

EERL 73-05

A Report on Research Conducted under Grants
from the National Science Foundation and
the Earthquake Research Affiliates Program
at the California Institute of Technology

Pasadena, California
August 1973

EARTHQUAKE-INDUCED SOIL PRESSURES ON STRUCTURES

Thesis by

John H. Wood

In Partial Fulfillment of the Requirements

for the Degree of

Doctor of Philosophy

EERL 73 - 05

California Institute of Technology

Pasadena, California

1973

(Submitted May 21, 1973)

ACKNOWLEDGMENTS

The author sincerely thanks his research advisor, Professor George W. Housner, for his guidance and suggestions during the course of research and preparation of this thesis. Additional thanks are owed to other faculty members and students at Caltech for the informative course work and discussions which formed the basis for this research. In particular the author wishes to extend his thanks to Professor Ronald F. Scott for many helpful discussions and to Dr. Gerald A. Frazier for his invaluable assistance with the development of the finite element programs used for part of this work.

The award of study leave with financial support from the New Zealand Ministry of Works made the author's graduate work possible and this assistance as well as the tuition and Fellowship support from the California Institute of Technology is gratefully acknowledged. The travel grant received from the United States Educational Foundation in New Zealand is also acknowledged.

Appreciation is extended to the National Science Foundation and the Earthquake Research Affiliates of California Institute of Technology for financial support of the research work.

ABSTRACT

The earthquake-induced pressures on soil-retaining structures are investigated. The study was motivated by the lack of suitable earthquake design data for relatively rigid structures on firm foundations in situations where the foundation, structure and retained soil remain essentially elastic.

Pressures and forces on the walls of a number of idealized wall-soil problems are analyzed. The solutions obtained are evaluated for a range of the important parameters to give results useful for design. In the idealized problems the soil is represented by an elastic layer of finite length bonded to a rigid foundation or rock layer. The wall or structure is represented by a rigid element resting on the rock layer and is permitted to undergo rotational deformation about the base. The mass or moment of inertia of the structure and its rotational stiffness are included as parameters in the idealization. Static and dynamic solutions are obtained using both analytical and finite element methods. Solutions are evaluated for the assumption of perfectly rigid behavior of the wall. The general solution for the deformable wall case was developed by superposition of the solution for the perfectly rigid case and solutions derived for displacement forcing of the wall structure.

The assumption of linear elastic behavior of the wall- soil system is likely to be approximately satisfied in situations where a building or other large civil engineering structure is founded on

firm soil or rock strata. In contrast to the linearly elastic assumption made in this study, the commonly used Mononobe-Okabe method employs the assumption of sufficiently large wall deformations to induce a fully plastic stress condition in the soil. It was concluded that both the elastic theory and the Mononobe-Okabe method have valid applications in the design of wall structures subjected to earthquake motions, but that because of significant differences in the solutions obtained from each method, care is required in selecting the most appropriate method for a particular situation.

TABLE OF CONTENTS

LIST OF FIGURES

1. INTRODUCTION

In this investigation a study is made of the earthquake-induced pressures on the vertical or nearly vertical walls of structures embedded in, or supporting a soil layer, and results are presented that have application in the design of these structures.

The behavior of wall structures during earthquakes can be broadly classified into three categories, which can be defined by the maximum stress condition that develops in the soil near the wall. For earthquake and gravity load-induced displacements of the structure that are small, measured relative to a point in the soil at a moderate distance from the structure, the soil near the wall will respond in an essentially linearly elastic manner. In the second category the induced wall displacements are sufficiently large to produce significant nonlinear soil response. With increasing relative displacement of the wall the third category, a fully plastic stress state in the soil, develops. It should be noted that these definitions are to some extent over-simplifications since in general the stress condition in the soil will be influenced by other factors in addition to the load-induced displacements of the structure. For example, very strong earthquake ground motions may induce a nonlinear or even a fully plastic condition in the soil for the case of a perfectly rigid wall supporting a weak soil. It should also be mentioned that gravity loads acting alone may produce a fully plastic stress state in the soil. This is frequently the case for cantilever retaining walls which in general are very flexible structures. The method used to estimate the earthquake-induced wall pressures should depend on the category

of the predominant behavior during the earthquake. In general the stress state that develops will be basically a function of the structure stiffness, structure dynamic properties, foundation stiffness, soil stiffness, soil strength and magnitude of the earthquake motions. A discussion is given in Section 1.2 of the likely deformational characteristics of a number of wall types and some indications are given as to their likely classification. Because of the large number of possible wall types and configurations it is not possible to make precise statements regarding wall classifications and frequently preliminary estimates of earthquake behavior may be necessary.

This study was motivated by the lack of well defined design procedures and design data for evaluating earthquake pressures on structures supporting a soil which remains in an essentially elastic state during an earthquake. A problem that was considered to be of practical interest was the analysis of earthquake-induced soil pressures on soil-supporting walls in large power stations founded on rock strata. The analysis methods given in this study have been developed with this particular problem in mind; however, it is likely that the results will be useful for other wall types in which predominantly elastic soil behavior is expected. At the present time the most generally accepted method of computing the earthquake-induced pressures on walls is based on an approximate plasticity theory and is known as the Mononobe-Okabe method. Although this method has a number of limitations, which are discussed in more detail later, it appears to be reasonably

satisfactory for most cases in which the basic underlying assumptions of the method are approximately satisfied. One of the most important assumptions made in the Mononobe-Okabe method is that the wall structure displaces a sufficient amount to develop a fully plastic stress state in the soil near the wall. For the case of basement or soil-retaining walls in buildings or other large civil engineering structures, that are founded on a firm soil or rock stratum, this assumption is unlikely to be satisfied and the method is considered by the writer to be unsuitable for many walls of this type. A detailed comparison between the Mononobe-Okabe method and the elastic theory is presented later but it is worthy of mention here that the Mononobe-Okabe method will give, for certain cases, wall pressures that are significantly less than computed by elastic theory. No relatively simple analysis methods can be suggested at the present time for cases in which the soil stresses reach values intermediate between the essentially elastic and fully plastic conditions. Numerical methods, such as the finite element method, can be employed or alternatively bounds for the pressure distribution can be found by using both elastic theory and an approximate plasticity theory.

Relatively small wall displacements can result in appreciable modification of the wall pressure distribution computed on the basis of perfect rigidity of the wall. Even displacements sufficiently small to satisfy the essentially elastic stress condition in the soil may result in significant changes from the perfectly rigid case. In some applications the perfectly rigid wall assumption may be satisfactory but in general an estimate of the effect of wall deformation should

be made. In studying earthquake-induced deformations of a wall structure it is informative to consider two limiting types of behavior. For a wall having a small mass in comparison to the mass of the soil retained in the vicinity of the wall, deformation of the wall will result essentially from the lateral soil pressure distribution produced by the soil inertia forces, and the deformation may be due to both strains in the wall structure and strains in the soil or rock foundation of the wall. In the other limiting type of behavior, the wall structure is considered to be massive with respect to the retained soil and in this case the dynamic properties of the structure (mass and stiffness) will become important parameters in determining the wall displacements. Behavior intermediate between the cases may occur and frequently can be satisfactorily analyzed by superimposing solutions based on the limiting cases.

An essentially exact formulation of the interaction of wall structures and the supported soil during earthquakes yields a highly interactable problem governed by nonlinear three-dimensional wave equations for an inhomogeneous medium. Even if the problem is simplified by assuming that the soil medium is homogeneous and responds in a linearly elastic manner, exact analytical solutions of the wave equations are only possible for a very limited number of simple boundary conditions that have little relevance to the analysis of wall problems. In many cases the soil properties will not be accurately known. This is because in most practical situations it is considered uneconomic to carry out soil investigations that are sufficiently detailed to give a good prediction of the soil behavior

during dynamic loading. Furthermore, quite a large number of soil-retaining structures are of insufficient importance to warrant more than a very basic soil study. Even if a very detailed investigation were undertaken, because of the inherent differences between the soil in laboratory simulated conditions and in the field at the time of the earthquake, it is unlikely that the dynamic soil properties could be precisely defined. Because the soil properties are not accurately known and also because of the uncertainty in predicting both the magnitude and frequency composition of the incoming earthquake waves a precise statement of the practical problem to be solved is not possible. Thus, even if a method were developed to give an essentially exact solution of the governing wave equations, the solution would be bounded by a significant range of uncertainty, or alternatively extensive computations would be required to define the sensitivity of the solution to the inexactly defined input parameters.

With the recent advances made in the application of numerical techniques, such as the finite element method, the solution of very complex dynamic continuum problems is feasible. Complexities such as irregular boundary configurations, material inhomogeneity and material nonlinearity can be handled by the finite element method. Although these complexities can be treated in an almost routine manner by standard programs, their inclusion generally results in an increase in computational effort for the user and an increase in computer running times. In particular, the inclusion of nonlinear material behavior may considerably increase

the machine time required to compute a solution, and in view of this increase in cost of the analysis and the inherent uncertainty in specifying the soil properties and the character of the earthquake ground motion, such refinements may seldom be justifiable.

In this study, solutions are obtained for certain idealized wall-soil problems that have been sufficiently simplified to enable analytical methods to be employed. The finite element method has been used to extend the range of applicability of the solutions. By considering readily solvable idealized problems it was found possible to identify the parameters that significantly influence the wall pressures and to vary these over a relatively wide range of values. Although in most practical cases the wall-soil system will be more complex than the relatively simple problems studied, it is believed that the results will be informative in the design of many firmly-founded wall structures. The results given are suitable for direct application in cases that approximately satisfy the basic assumptions made in this study. For complex structures or for structures of particular importance a finite element study may be warranted, but even for these cases the results of simplified studies are of use for preliminary design and can also assist the interpretation of the results of the more sophisticated analysis. Because of the uncertainties in the inputs mentioned above, the application of the results of the simplified problems to the design of more complex cases can probably be justified in many situations.

It is convenient to present the results of this investigation in three parts. Firstly solutions are presented for the case of a

perfectly rigid wall. In this case the earthquake-induced pressures are the result of inertia body forces within the soil layer. In the second part of the study solutions are given for the pressures resulting from the earthquake-induced displacements of the structure. Finally the solutions of the first and second cases are combined by using superposition in the frequency domain to give a general solution for the total earthquake-induced pressures on a deformable structure. Using this approach solutions are presented in a form that have general applicability for many practical cases. Quite a significant part of this investigation was devoted to the derivation of equivalent static solutions for the dynamic problems of interest. In general, static solutions are more readily obtainable than dynamic solutions and frequently the static solution can be used to give a good approximation to the maximum dynamic response to earthquake excitation. Also, the static solutions were found to have application in extending and simplifying the dynamic solutions.

The rigid-wall solutions presented are for the case of a rigidly-founded structure supporting a soil layer of finite length that is bonded to a rigid base. Both static and dynamic analytical solutions are derived for a homogeneous linearly elastic soil in smooth contact with the wall structure. In the static solutions, the wall pressures are given for the case of a uniform horizontal body force in the soil. The dynamic solutions are presented in terms of the natural frequencies and normal modes of the soil body. Expressions are derived that demonstrate the method of using the normal

mode solutions to compute the wall pressures resulting from an arbitrarily time-varying horizontal acceleration applied at the base of the soil. The steady-state solutions for the wall moment and forces are derived for the case of harmonic forcing at the base of the soil layer and it is shown how random vibration theory enables these results to be used to compute statistical estimates of the forces and moments induced by earthquake forcing. The effects of a bonded assumption for the soil-wall interface and a nonuniform soil on both the static and dynamic solutions were investigated using the finite element method.

The influence of the displacement of the structure on the rigid-wall pressures was studied by using an idealized soil-wall system similar to that described for the rigid-wall solutions. The system was modified for this case by allowing a specified displacement of the wall boundary. Analytical solutions were derived for both static and harmonic forcing of the wall boundary. Solutions were evaluated for the case of a rotational deformation of the wall about its base. Static solutions for other types of wall deformation were computed using the finite element method. Finite element solutions were also computed to investigate the influence of a bonded wall-soil interface and nonuniform soil properties on the pressure distributions.

Expressions for the total wall forces and moments on a deformable wall structure, forced by a horizontal earthquake motion at its base, were derived by superposition of the rigid-wall and forced-wall solutions in the frequency domain. The application of

the solutions presented is demonstrated by an analysis of the earthquake-induced pressures on a soil-supporting wall in a large power-generating plant constructed on a rock foundation.

1.1. BASIC ASSUMPTIONS

The basic assumptions made throughout this investigation are discussed in this section. In the derivation of particular solutions and results it was necessary to make other assumptions and these are discussed in the relevant sections of the text.

1.1.1. Earthquake Ground Motion

In an earthquake, strains are produced in the soil by the passage of a complex wave function that propagates from the causative fault through or along the surfaces of the soil and the bedwork strata. Stresses develop at the soil-structure boundaries as a result of wave reflection and transmission into and out of the structure. Strong ground-shaking in the vicinity of structures located essentially on top of soil or rock surfaces consist of a superposition of body (shear and compressional) and surface waves that have propagated a significant distance through an inhomogeneous nonlinear medium and that impinge on the structure from a wide range of directions. The detailed nature of the mechanism generating the waves at the source is not known and only a limited amount of information is available regarding the influence on the propagating waves of the generally complex geology between the

source and the site of the structure.

In this investigation it is assumed that the earthquake ground shaking can be represented by an arbitrarily time-varying horizontal acceleration applied at the base of the structure or at some convenient horizontal plane below the structure. It is further assumed that this motion is spatially constant over a horizontal length at least several times greater than the wall height. The time-dependence or the frequency components of this acceleration are taken to be similar to existing strong-motion earthquake records. The above assumptions are essentially equivalent to assuming that the incoming waves are vertically propagating plane shear waves. However, the assumptions made are approximately satisfied by shear waves at a moderate angle of incidence and surface waves,provided the wave lengths are at least 10 times longer than the wall height.

1.1.2. Soil-Wall Systems

The soil-wall systems studied are assumed to satisfy the usual conditions of the theory of elasticity. This assumption is likely to be satisfied or approximately satisfied by relatively rigid wall structures, and in particular when significant translation or rotation of the structure in the soil is prevented by either the structural configuration or the presence of a relatively rigid foundation.

The soil is assumed to be in an unsaturated condition and no account of water pressures has been made in this study. Saturated conditions and water pressures on walls have been investigated by

Matuo and Ohara[32,33]*.

The soil is assumed to be an isotropic material. Anisotropic behavior can be readily handled by the finite element method; however, in general the soil properties will not be sufficiently well determined to warrant this refinement.

The problems investigated are assumed to satisfy the conditions of plane strain. That is, the wall is assumed to be long in comparison to its height. Many building basement walls will only approximately satisfy this condition; however, the considerable increase in complexity and computational effort introduced by a three-dimensional approach severely restricts the possibility of more refined studies. The limitations of the plane strain assumption are discussed in further detail in Section 9.1.

1.2. WALL TYPES

A large variety of types of soil-supporting wall structures are employed in civil engineering works. Some of the more common types of wall structures are shown schematically in Fig. 1.1. A brief description of the basic behavior of these structures under the action of horizontal earthquake motions is given below.

TYPE I. Cantilever Retaining Wall

Many relatively low retaining walls are of cantilever type construction. Lateral stresses resulting from vertical gravity and horizontal earthquake body forces in the soil generally produce

*Numbers in parenthesis designate references listed on page 259

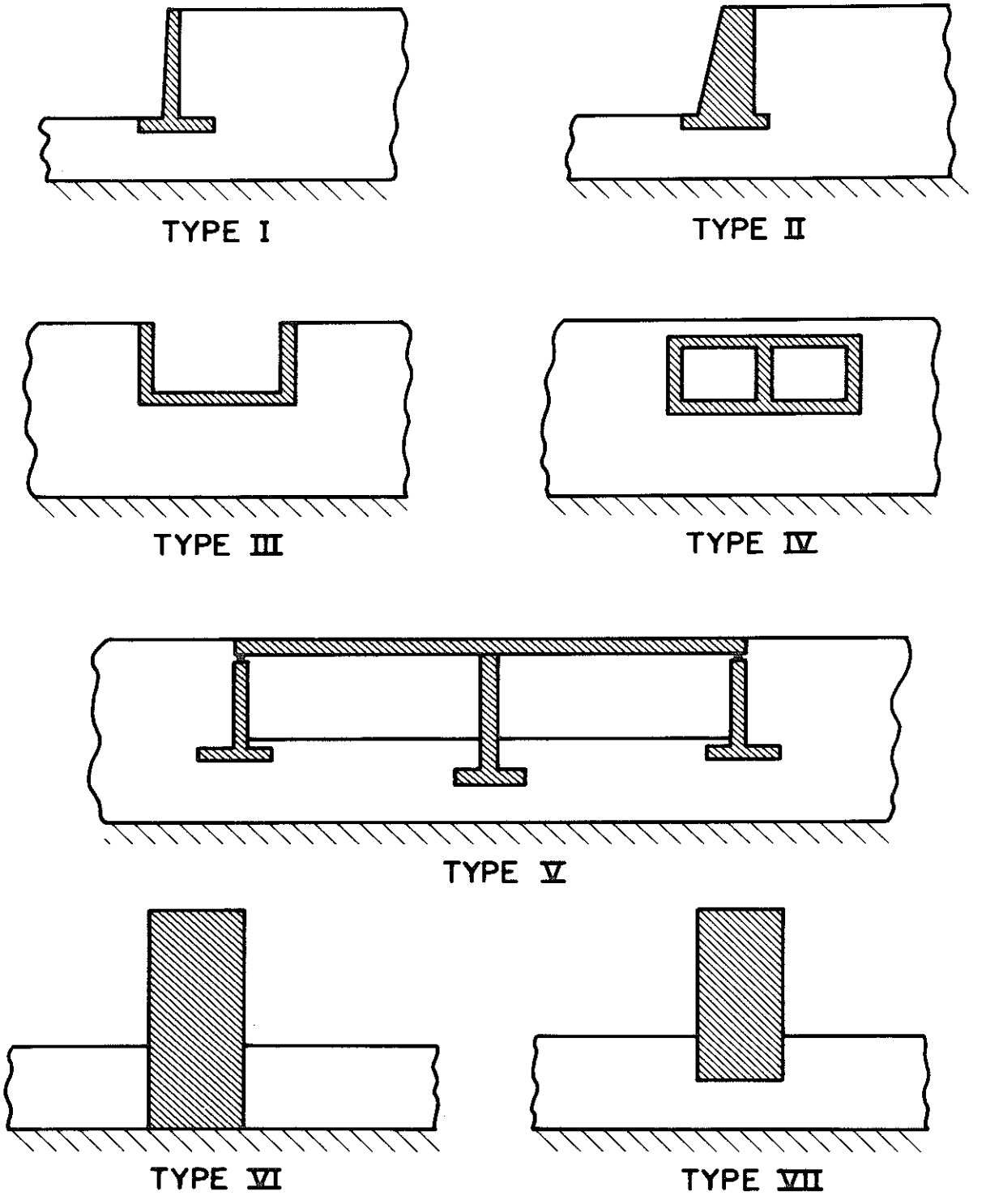

WALL TYPES

Figure 1.1

significant horizontal displacement of the wall. This displacement is primarily due to translation and rotation of the wall foundation and flexural deformation in the wall stem. The displacement of the wall is generally sufficiently large to cause the soil to have significant nonlinear properties or even to cause the development of a fully plastic state of stress in the soil mass behind the wall. To accurately determine the pressure distribution on the wall it is generally necessary to use nonlinear theory or the theory of soil plastic equilibrium.

TYPE II. Gravity or Counterfort Wall

Walls that have significantly more rigid soil-retaining elements than the simple cantilever slab may be used. Many quay walls are in this category. Under the action of gravity and earthquake loads, horizontal displacement of the wall results mainly from the rotation and translation of the foundation. Frequently the earthquake-induced displacements of relatively high structures of this type will be sufficiently large to produce significant nonlinear behavior of the soil. Because of the difficulty in performing an exact analysis for this case, a useful design approach is to evaluate pressure distribution bounds by using both elastic theory and an approximate plasticity method. Gravity type walls may have appreciable mass and if this is the case the wall inertia force should be considered in the analysis.

TYPE III. Open Hydraulic Structures

Frequently hydraulic structures associated with flood control and power generation are embedded in the soil. Lateral soil

pressures are developed on the vertical cantilever walls by gravity and earthquake loads. The walls are significantly stiffer than the conventional cantilever type wall owing to the presence of the interconnecting slab that reduces the translation and rotation at the foundation level. If the wall is relatively low the soil response may be essentially elastic and analyses based on elastic theory may often be appropriate.

TYPE IV. Closed Hydraulic Structures

In some applications hydraulic structures are covered by the construction of a slab across the tops of the vertical wall elements. Underground reservoirs are frequently of this type. The top slab imposes additional rigidity on the wall elements by preventing horizontal displacement at the top of the walls. Flexural deformations occur on the wall segments between the top and bottom slabs, but in general the displacements may be sufficiently small to enable a satisfactory analysis by elastic theory.

TYPE V. Bridge Structures

Many bridge abutment structures have soil-retaining elements. The dynamic soil pressures on the abutment walls will be strongly dependent on the type of connection made between the bridge superstructure and the abutment. If the bridge is rigidly connected to an abutment, the earthquake soil pressures will be significantly influenced by the dynamic properties of the bridge. With an unrestraining connection, the abutment wall may act in a manner similar to one of the types described above.

TYPE VI. Building on Rock Foundation

Buildings and other structures may be founded directly on a relatively rigid rock strata, and in particular this may be the case if the overlying soil layer is shallow. For large structures, such as power generation plants, extensive excavation may be undertaken to achieve a rock foundation.

Earthquake-induced inertia forces in the building produce both structural strains and foundation deformations that result in a horizontal displacement of the structure relative to the soil. The earthquake pressure distribution on the wall can be conveniently taken as the superposition of the stresses resulting from the displacement of the structure and the earthquake-generated body forces in the soil layer. Frequently the soil-retaining elements in buildings are continuous slabs stiffened by the main columns, and flexural deformation of the slab between the columns may add additional complexity to the analysis of these systems. In general, significant nonlinear behavior of the soil is unlikely for walls of this type. Most of the investigations in this study were made with this classification in mind.

TYPE VII. Building Embedded in a Soil Layer

The embedded building may be founded on piles that extend to a rock or a strong soil stratum. Alternatively the building may rest on a spread or raft foundation. In either case, if the soil is relatively soft, significant relative translation of the base of the building may occur making the analysis considerably more difficult than for the previous wall type. It is not possible to make any

general comment regarding the applicability of the elastic or plastic theory and each problem of this type requires a preliminary study to determine the most suitable method of analysis. It is important to note that if relative displacement of the foundation of the structure is sufficient to produce a plastic stress state on the walls, the maximum pressure distribution will probably be controlled by the passive earth pressure state rather than the active state normally assumed in the Mononobe-Okabe method. The forces on the wall under passive pressure conditions will be approximately 10 times greater than for the active pressure state.

1.3. EARTHQUAKE DAMAGE

Seed and Whitman[50] have presented an interesting summary of reported damage to wall structures during earthquakes. Hayashi and Katayama[13] give an account of the damage to quay wall structures in the more recent Tokachioki (1968) earthquake. From these reports it is apparent that extensive damage to quay walls has frequently occurred. Damage to soil-supporting bridge abutment structures has also been reported on a number of occasions. In general few reports exist of damage to other wall structures, although as Seed and Whitman point out, this may be because in general wall damage is often considered to be of minor significance in relation to other damage and so has not always been documented.

A number of soil-supporting structures were extensively damaged in the San Fernando, 1971, earthquake. The walls of a large reinforced concrete underground reservoir at the Balboa Water

Treatment Plant failed as a result of increased earth pressures during the earthquake. Details of the reservoir and the damage are given by Housner, Jennings and Brady in Reference (21). The reservoir was located in fairly soft filled ground. The vertical walls were approximately 20 ft high and were restrained by top and bottom slabs resulting in relatively rigid wall behavior. It is thought that the increase in pressure was mainly the result of strong ground shaking; however, permanent ground displacements were observed at the site and may have been a contributing factor.

Hradilek[18] has undertaken a comprehensive study of a number of underground reinforced concrete box-type flood control conduits extensively damaged by the earthquake. He concluded that most of the damage resulted from permanent ground displacements that generated passive soil pressures on the vertical walls considerably in excess of the active pressure state assumed in design.

Quite extensive lengths of open reinforced concrete flood control channel were also damaged and brief descriptions of some of this damage are given by Scott in Reference (21) and by Lew, Leyendecker and Dikkers[28]. Details of two of the damaged channels are given in Figs. 1.2, 1.3, 1.4 and 1.5. Complete wall failure occurred on sections of the Lopez Canyon channel but the failed sections were close to a surface expression of the faulting associated with the earthquake and probably permanent ground displacements contributed significantly to the damage. The damaged sections of the Wilson Canyon channel were close to the Olive View Hospital. It is thought that no significant permanent

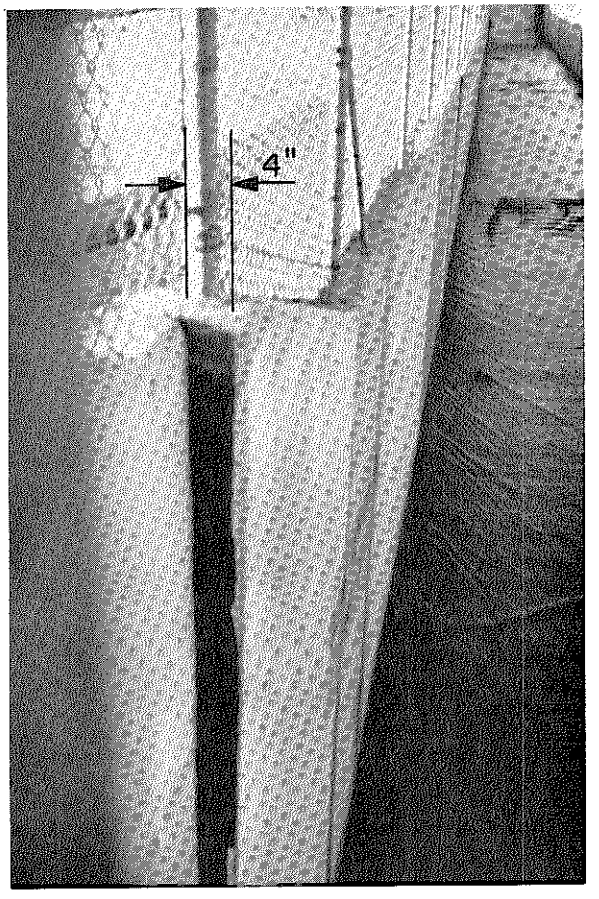

Figure 1.2 Wilson Canyon Channel. The wall top displaced 4 in with respect to bridge abutment at left.

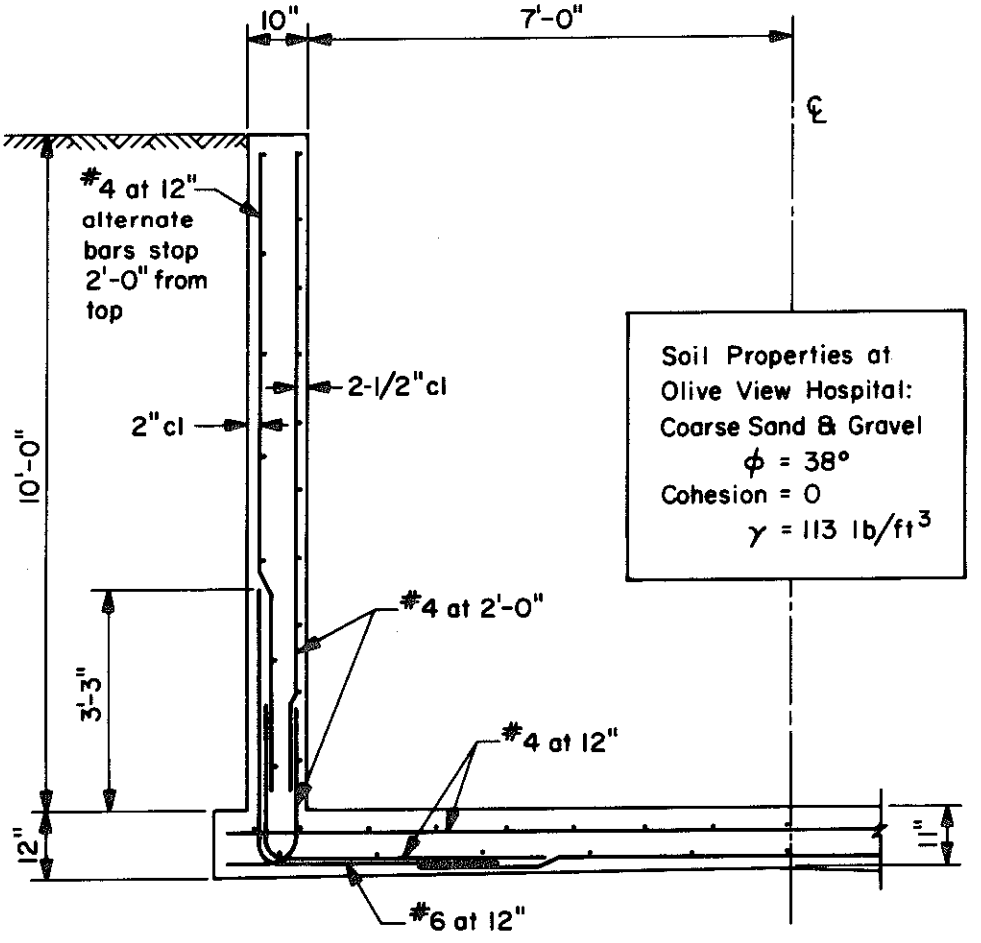

WILSON CANYON CHANNEL
Section 65' Upstream & Downstream of ℄ Olive Ave. Bridge

Figure 1.3

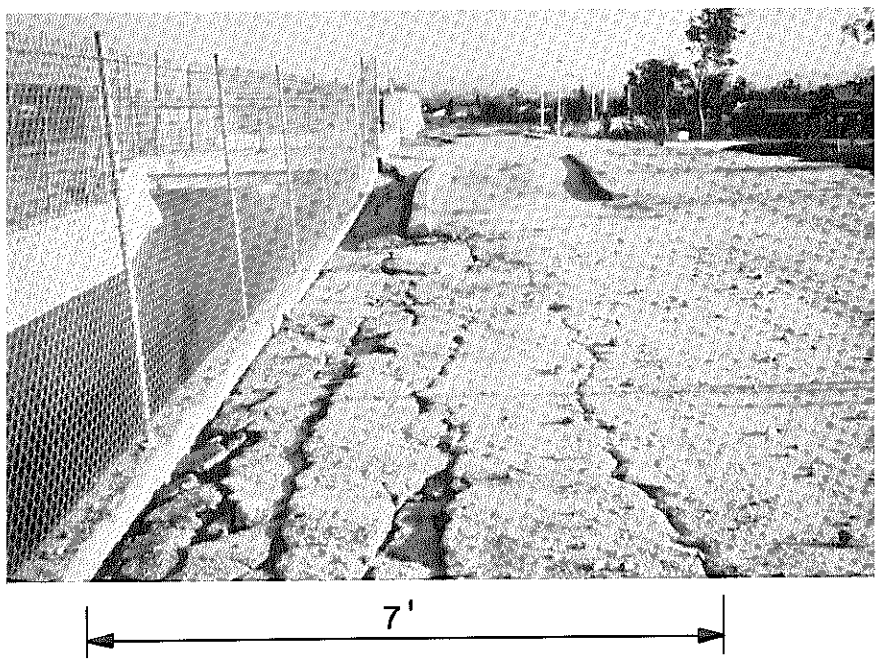

Figure 1.4 Wilson Canyon Channel. Cracking in soil as a result of wall displacements. Fine cracking was detected a distance of 15 ft behind wall.

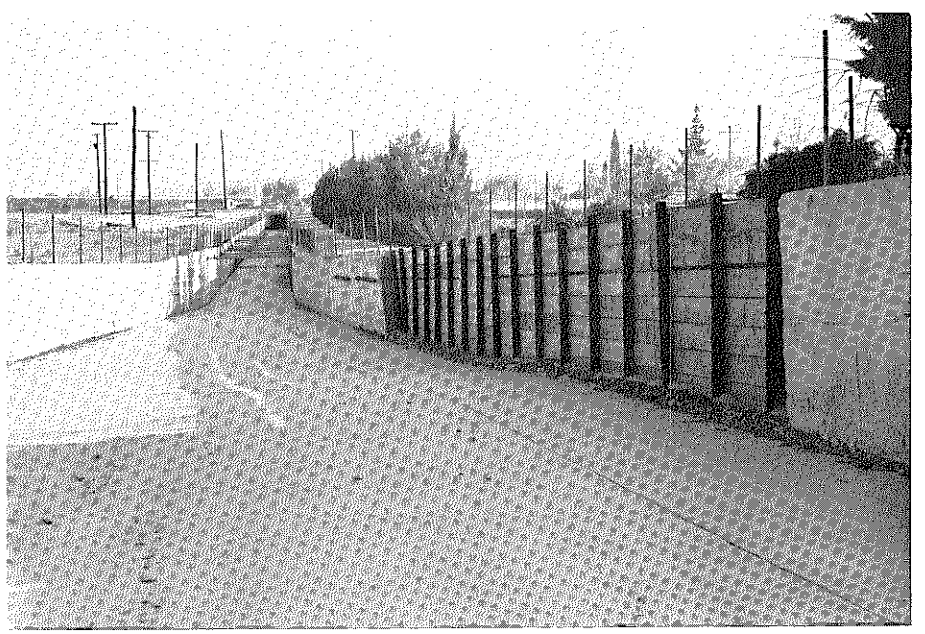

Figure 1.5 Lopez Canyon Channel. Temporary supports on failed section of wall.

ground displacements occurred in this locality and so the damage can probably be attributed to an increase of wall pressure due to the ground shaking. Inward displacement of both channel walls was observed and a maximum displacement at the wall top of about 6 in. was measured (Askilsrud[2]). The ultimate moment capacity of the channel walls was compared with an estimate of the soil-pressure moment during the earthquake. The following details summarize the basis of the comparison and the moments obtained:

Ultimate Capacity of Wall:

Steel yield stress	$f_y = 40{,}000$ lb/in^2	assumed values
Concrete compressive strength	$f'_c = 3{,}000$ lb/in^2	assumed values
Capacity reduction factor	$= 1.0$	
Ultimate Moment	$M_u = 15.1$ kip ft	

Soil Gravity Moment:

Angle of internal friction	$\phi = 35^o$
Cohesion	$= 0$
Unit weight of soil	$= 110$ lb/ft^3
Gravity Moment	$M_g = 4.5$ kip ft

Soil Earthquake Moment:

Horizontal earthquake coefficient	$k_h = 0.4$
Vertical earthquake coefficient	$k_v = 0$
Height of center of pressure above base	$= 0.6$ H
Earthquake moment	$M_E = 10.0$ kip ft

-- from Mononobe-Okabe (see Section 1.4.1)

Total Soil Moment:

$$M_g + M_E = 14.5 \text{ kip ft}$$

It is likely that in the vicinity of the Olive View Hospital a number of peaks of acceleration exceeded 0.4 g and thus on the basis of the Mononobe-Okabe method significant yielding of the wall would be expected. (Peak moments larger than the Mononobe-Okabe value would be expected when the outward movement of the top of the wall was less than about 0.5 in. This condition would exist during the early part of the earthquake.)

It is relevant to note that the failure of the flood control conduits and channels did not create any hazard to human life and since in the Los Angeles region these channels carry only very infrequent flood flows the question of the need to provide earthquake resistance arises. For these walls and similar walls of lesser importance the degree of earthquake resistance provided should be based on an economic decision involving consideration of the initial cost of earthquake resistance and the likely cost of repairs obtained from earthquake probability studies.

1.4. PREVIOUS RESEARCH

1.4.1. Mononobe-Okabe Method

Probably the earliest research related to earthquake pressures on walls was presented by Okabe (1926)[42], and Mononobe and Matsuo (1929)[37]. They developed a design method based essentially on the well known Coulomb method used to compute the approximate

magnitude of the lateral force acting on a wall as a result of gravity body forces in the soil. Much of the research undertaken following the development of what is now known as the Mononobe-Okabe method has been concerned with refinement of the method or tests of its validity by model studies. Only a few countries have building codes that specify earthquake provisions for wall structures, but in general when specified, these provisions are based on the Mononobe-Okabe method.* Even in localities where no specific code requirements exist it appears that the Mononobe-Okabe method is widely used in design.

Details of the Mononobe-Okabe method and suggestions regarding its application to design problems are given by Seed and Whitman[50]. In order to facilitate a comparison of the Mononobe-Okabe method with the work reported in this study a brief description of the method is given here. The method employs the following basic assumptions.

(1) The wall is assumed to displace laterally a sufficient amount to produce a state of plastic equilibrium behind the wall.

(2) The soil is assumed to satisfy the Mohr-Coulomb failure criterion.

(3) Failure in the soil is assumed to occur along a plane surface through the toe of the wall and inclined at some angle to the horizontal.

---

*The code requirements of countries in seismic regions are given in Reference (20).

(4) The wedge of soil between the wall and the failure plane is assumed to be in equilibrium at the point of incipient failure, under gravity, earthquake and the boundary forces along the wall and failure surface. The forces acting on the soil wedge of weight W are shown in Fig. 1.6 for the case of a cohesionless soil.

(5) The effect of the earthquake is represented by equivalent static horizontal and vertical forces $k_h W$ and $k_v W$ applied at the center of gravity of the wedge.

(6) The method gives the magnitude of the total force acting on the wall but does not give its point of application or the pressure distribution. In the initial development of the method it was apparently assumed that the total force acted at a point $\frac{1}{3}H$ above the base of the wall of height H. In view of model test results and more recent refinements of the method, Seed and Whitman[50] have recommended that the force increment on the wall due to the earthquake load be assumed to act $0.6H$ above the base.

The total active wall force (gravity and earthquake) is determined by considering the force and moment equilibrium of the soil wedge shown in Fig. 1.6. The angle of the failure plane is varied to give a maximum value of the wall force P_{AE}, and under the critical condition it can be shown that

$$P_{AE} = \frac{1}{2}\gamma H^2(1 - k_v)K_{AE} \qquad (1.1)$$

in which

$$K_{AE} = \frac{\cos^2(\phi-\theta-\beta)}{\cos\theta\cos^2\beta\cos(\delta+\beta+\theta)\left[1+\sqrt{\frac{\sin(\phi+\delta)\sin(\phi-\theta-i)}{\cos(\delta+\beta+\theta)\cos(i-\beta)}}\right]^2}$$

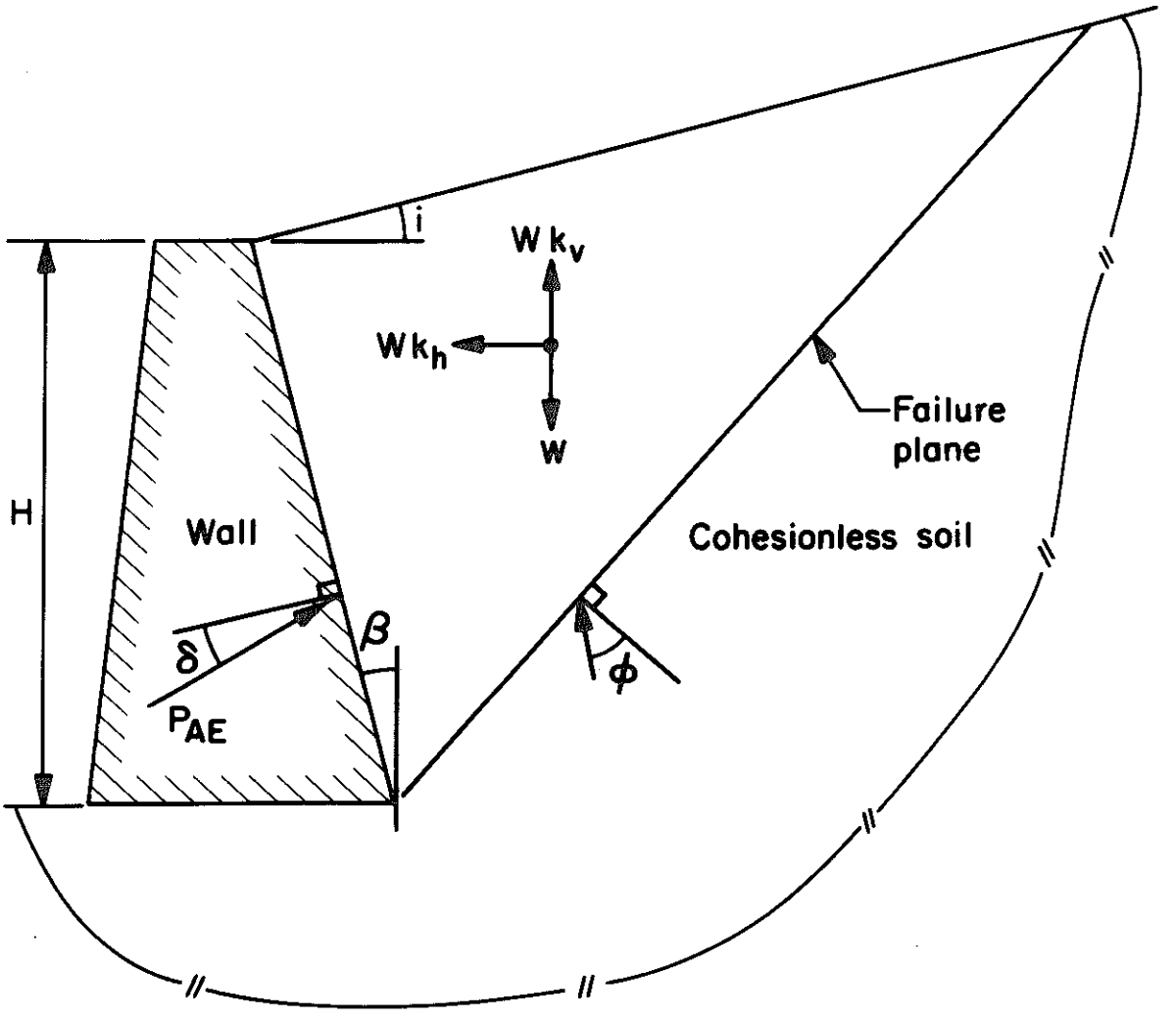

MONONOBE-OKABE ANALYSIS

Figure 1.6

$$\theta = \tan^{-1} \frac{k_h}{1 - k_v}$$

γ = unit weight of soil

ϕ = angle of internal friction of soil

δ = angle of wall friction

i = angle of soil slope (see Fig. 1.6)

β = angle of wall slope (see Fig. 1.6)

k_h = horizontal earthquake coefficient

k_v = vertical earthquake coefficient

Seed and Whitman[50] give convenient graphical solutions for expression (1.1), and give an approximate solution for zero vertical acceleration, a vertical wall, horizontal backfill slope and $\phi \approx 35^{\circ}$. Their approximation can be expressed as

$$\frac{\Delta P_{AE}}{\gamma H^2} = \frac{3}{8} k_h \qquad (1.2)$$

in which

ΔP_{AE} = active wall force increment due to horizontal earthquake load

The approximation is in close agreement with the more exact solution for $k_h < 0.35$.

The Mononobe-Okabe method can be readily extended to include soil cohesion by considering the equilibrium of the wedge with the addition of cohesive forces acting along the wall boundary and the failure surface. It is relevant to discuss here some of the limitations of the method.

(1) For a plastic state to fully develop in the soil behind the wall it is necessary for the top of the wall to deflect laterally about 0.5% of the wall height. Although this condition may be frequently satisfied by type I and II walls of Fig. 1.1 this may not be the case for types IV, VI or VII.

It is shown later that the earthquake-induced force on a relatively rigid wall computed by elastic theory is significantly greater than the force obtained by the Mononobe-Okabe method (on the assumption of a similar earthquake for each case).* Thus, if the structural elements of a relatively rigid wall structure are designed in accordance with the Mononobe-Okabe force it is likely that during peak earthquake pressures yielding of the structure will occur. As the yielding of the structural elements progresses, large strains will develop in the soil, and eventually a fully plastic stress condition may develop in the soil. With the onset of this plastic stress condition the peak forces will be reduced to approximately the Mononobe-Okabe force levels that are consistent with the peak accelerations at this stage. Further yielding will occur if these peak levels are sufficiently large. If the structural elements are insufficiently ductile to withstand the strains required to develop a fully plastic condition in the soil and any subsequent yielding, collapse of the structure may occur. Although it is common design

---

*It is assumed here that the Mononobe-Okabe force from the active pressure state would be used. The passive pressure state will give a force generally in excess of the elastic theory results; however, it is unlikely that the passive pressure state would be appropriate except for the case of a massive structure on a soft foundation.

procedure to permit yielding of structural members of building frames during strong earthquake motion it may be undesirable to design for yielding in wall systems. This is because yielding of a wall during earthquake motions tends to occur only in a direction away from the retained soil owing to the presence of the lateral gravity stresses. Uni-directional yielding during an earthquake may lead to excessive permanent displacements with severe cracking that could lead to the deterioration of the reinforcement if moisture is present. If it is considered desirable to prevent yielding in the structural elements of the wall, and if the soil does not develop a plastic state over a significant region before the onset of yielding in the structural elements, the Mononobe-Okabe method is unsuitable and wall design pressures should be computed using an elastic or nonlinear theory.

(2) Although the assumption of a plane failure surface appears reasonable, its validity has been based on a very limited number of test and field observations. For the case of vertical gravity loading, the solutions of Sokolovski[52] obtained by solving the equilibrium and failure criterion equations by numerical methods, are in good agreement with values obtained by the Coulomb plane failure surface approximation. (A comparison of wall forces obtained using both methods is given by Scott[46].) Apparently Sokolovski's method has not been applied for the case of horizontal body forces. Computer programs have been developed to evaluate solutions using this method (Ko and Scott[24]) and this approach could easily be applied to develop more exact plasticity solutions

for earthquake-induced wall pressures. Alternatively, plasticity solutions can be obtained by the finite element method. Baligh[3] has developed a suitable finite element program based on the Mohr-Coulomb criterion. More research using these numerical methods should be undertaken to check the validity of the failure surface and pressure distribution assumptions.

(3) The Mononobe-Okabe method is essentially a static method, requiring the selection of suitable earthquake coefficients k_h and k_v which are used to determine equivalent static inertia forces on the wedge. In general coefficients are chosen that are significantly less than the peak accelerations to be expected in a suitable design earthquake, apparently on the assumption that some permanent outward movement of the wall can be tolerated. There appears to be no rational basis for the magnitude of the reduction made. Reasonably exact solutions of dynamic plasticity problems are undoubtedly difficult but nevertheless it would seem desirable to improve the Mononobe-Okabe approach by accounting for dynamic effects in an approximate manner. The method used by Newmark[39] to study the stability of dams and embankments during earthquakes could be easily applied in the study of wall problems and would be a convenient way of extending the Mononobe-Okabe method to include basic plastic-dynamic behavior. In Newmark's method the sliding displacement of a soil mass resulting from peak inertia forces exceeding the sliding resistance, is computed by using a simplified form of acceleration pulse. If this approach is used the design would be based on choosing an acceptable limit for the permanent

displacement of the wall rather than the selection of an earthquake force coefficient. Newmark's results demonstrate that if the peak accelerations in the design earthquake are significantly greater than the earthquake coefficients used to compute the Mononobe-Okabe force, appreciable displacement of the wall may occur. Therefore, it is apparent that for some wall types the conventional arbitrary reduction of the Mononobe-Okabe earthquake coefficients may be undesirable. To illustrate this point it is helpful to consider an open hydraulic structure (Type III in Fig. 1.1) for which the wall is sufficiently flexible to give essentially a fully plastic stress state in the soil. For this particular example, significant displacement of the wall and the soil wedge can only occur as a result of yielding in the structure. In order to prevent significant structural yielding in this type of wall, the Mononobe-Okabe earthquake coefficients should be based on the peak accelerations in the design earthquake. In contrast to this case, the conventional cantilever, counterfort and gravity walls (Types I and II in Fig. 1.1) can displace by sliding on failure surfaces within the soil. Thus, if adequate strength is given to the structural elements, appreciable displacement can take place without damage to the wall structure. For these types the amount of sliding displacement that can be tolerated may be governed by aesthetic considerations or the clearance between the wall and adjacent structures.

(4) In the Mononobe-Okabe method no account is taken of resonance effects or the amplification of earthquake motions that might occur as the result of the propagation of the motion through

a relatively soft soil layer behind the wall. If the soil is in a plastic state this effect is difficult to consider and in fact may not be very pronounced. It is also usual in the Mononobe-Okabe method to neglect the influence of the dynamic behavior of the structure on the pressures. In contrast, the effects of ground motion amplification and the dynamic behavior of the wall structure can be readily included in the elastic theory approach and details of the influence of these effects on the wall pressure distributions are given in this study.

1.4.2. Experimental Studies

Mononobe and Matsuo(1929)[37] made an experimental study of wall pressures using a 4 ft deep, 4 ft wide and 9 ft long sand filled box subjected to horizontal harmonic forcing with a period of vibration varied between 0.42 and 0.48 sec. They measured the total end-wall forces and concluded that they were in reasonable agreement with the values computed from the Mononobe-Okabe method. The end-walls were hinged at their base and restrained by pressure measuring devices at their tops. No details were given regarding the rotational displacements of the walls during the experiments (or the characteristics of the pressure devices) but presumably the displacement was sufficient to develop a plastic stress condition.

Experimental work by Jacobsen (1939) is reported in Reference (57) prepared by the Tennessee Valley Authority. He conducted sand box tests using a shaking table and a 3 ft high layer

of sand. Details regarding the other dimensions of the box, the period of vibration and the flexibility of the wall are not given. The authors' of Reference (57) concluded that Jacobsen's experiments were in reasonable agreement with the Mononobe-Okabe force and that the dynamic force component acted at about two-thirds of the height of the sand layer above the base.

Ishii, Arai and Tsuchida[19] conducted an extensive series of tests using both a sand box with fixed and movable end-walls and model gravity walls resting on the surface of a sand layer. A 70 cm (2.3 ft) depth of sand was used behind the walls. The walls were subjected to a harmonic motion of period approximately 0.3 sec with an acceleration amplitude increased from 0.1 g to 0.7 g in 0.1 g steps. Two minutes of vibration was applied at each step. Interesting observations were made regarding sand settlements and movement, residual wall pressures and phase relationships between the wall pressures and the base motion. The type of forcing used was not representative of earthquake ground shaking, and because of this and the influence of scale effects the validity of these results for wall design is questionable. The conclusion was made by Ishii et al. that in general their results were consistent with the forces obtained by the Mononobe-Okabe method.

Matuo and Ohara[32] conducted tests on dry and water saturated sands in a harmonically forced box 40 cm (1.3 ft) deep and 100 cm long. The saturated sand study is relevant to the design of gravity type quay walls that are common in Japan. They conducted tests for both a fixed end-wall (essentially rigid) and a movable

end-wall that was permitted to rotate about its base. Harmonic forcing having a period of vibration 0.3 sec was used. Each test was run for about 24 seconds with a gradual build up and decrease of acceleration. The maximum acceleration was varied from test to test and had a range of about 0.1 - 0.4 g. Matuo and Ohara also derived analytical expressions for the fixed and rotating wall pressure distributions based on an approximate solution of the equations of elasticity. The experimental pressures for the rigid wall were significantly less than the theoretical values but Matuo and Ohara attribute this difference to the influence of the side walls of the box and the elasticity of the pressure cells. Evaluation of their theoretical solution for the rigid wall gives wall forces that are significantly higher than obtained by the Mononobe-Okabe method and also shows significant departure from the triangular pressure distribution commonly assumed.

Murphy[38] conducted dynamic tests on a 1/64 scale model gravity wall supporting a sand layer. The model was subjected to harmonic forcing having a period of 0.185 sec and a maximum acceleration of 0.25 g. Wall pressures and forces were not measured but instead the tests were conducted to determine the mode of failure. It was found that failure occurred by outward rotation of the wall about the toe, with the development of an almost plane failure surface in the soil inclined at 35° to the horizontal. This behavior is consistent with the basic assumptions made regarding the failure plane in the Mononobe-Okabe method.

Ohara[40] conducted experiments on movable walls by

harmonically forcing a sand box 30 cm (1.0 ft) deep, 56 cm wide and 100 cm long with maximum accelerations up to 0.4 g. In most of the testing various controlled displacements were given to the end-wall during the shaking. In one series of tests the wall was elastically supported and allowed to rotate about its base. Ohara concluded that his results were reasonably consistent with the wall forces computed by the Mononobe-Okabe method. However, it would appear that the procedure adopted in the controlled displacement tests did not entirely satisfy the assumptions made in the Mononobe-Okabe analysis. The controlled displacements were applied during the shaking but the dynamic pressure distributions were measured after the walls were rigidly fixed and steady-state conditions reached. Thus, the measured dynamic pressure distribution would be expected to be equal to the sum of the usual passive or active pressure distributions resulting from gravity loads, and a dynamic component that probably would be similar to the elastic pressure distribution on a rigid wall. (It is possible that some modification of the usual active and passive gravity load distributions may have occurred in these tests because of the presence of the vibrations during the wall displacement phase.)

The experimental tests described have contributed to the understanding of wall behavior during earthquakes; however, there are a number of difficulties in applying the experimental results to prototype walls and many of these details have received inadequate

attention in previous literature. The basic limitations are discussed below.

(1) In general the experimental errors that may result from the flexibility of the pressure measuring devices and from the restraining effects of the sand box side and far-end walls tend to give an underestimation of the wall force. To ensure that the box represents a long layer acting in plane strain it is probably necessary to use a box with width and length dimensions at least four times greater than the height of the soil layer. Most of the boxes used have not satisfied this requirement and in general inadequate attention appears to have been given to estimating or eliminating these errors.

(2) In all the reported tests harmonic forcing with very limited frequency ranges has been used and this type of forcing is not very representative of strong earthquake ground shaking. Even if testing were to be conducted using a variable frequency harmonic forcing or some more random motion, care would still be required to ensure that similarity relations were satisfied between the model and prototype. For an elastic soil and rigid wall the frequency similarity condition obtained on the assumption of the same Poisson's ratio in model and prototype is given by

$$\frac{f_p^2 \rho_p H_p^2}{G_p} = \frac{f_m^2 \rho_m H_m^2}{G_m} \qquad (1.3)$$

in which

f_m, f_p = frequency of vibration in model and prototype respectively

ρ_m, ρ_p = mass density in model and prototype respectively

H_m, H_p = height of model and prototype walls respectively

G_m, G_p = shear moduli of model and prototype respectively

The shear modulus of a sand material is strongly influenced by the confining pressure, the strain amplitude and the void ratio. Seed and Idriss[49] give the following relationship between the shear modulus and confining pressure

$$G = 100\, K_2 (\sigma'_m)^{1/2} \tag{1.4}$$

in which

G = shear modulus of soil

σ'_m = mean principal effective stress

K_2 = a parameter which is primarily a function of void ratio and strain amplitude

If the same horizontal accelerations are applied to both the model and prototype, then the stress similarity relation is

$$\frac{\sigma_p}{\gamma_p H_p} = \frac{\sigma_m}{\gamma_m H_m} \tag{1.5}$$

in which

σ_m, σ_p = stresses in model and prototype respectively

γ_m, γ_p = unit weight of model and prototype respectively

Equations (1.3), (1.4) and (1.5) enable the correct frequency or time scale to be computed. It is clear that if relatively low model walls are used, the frequencies in the model excitation will need to be significantly greater than in the prototype earthquake motion.

(3) The periods of vibration of the harmonic forcing have apparently always been significantly greater than the lowest natural period of the model wall-soil system and so the possibility of dynamic amplification of the base motion has not been considered in the tests. Amplification of the earthquake base motion may occur in prototype wall systems having relatively high walls supporting relatively soft soils.

(4) If the results of movable or flexible wall tests are to be applied in the design of prototype walls it is necessary to satisfy very involved similarity relationships. In addition to the parameters mentioned above, the wall flexibility and the soil failure criterion need consideration. The stress state in the soil at failure is strongly influenced by the confining pressure. In view of the difficulties in satisfying these conditions and the considerable amount of work required to undertake a comprehensive parameter study it appears that a study employing computer models would be a viable alternative for this class of wall.

1.4.3. Other Research

By considering the equilibrium of soil slices within the sliding wedge Prakash and Basavanna[44] have extended the Mononobe-

Okabe method to enable approximate wall pressure distributions to be computed. They found that the pressure distribution varied in a nonlinear manner with depth and that the point of application of the total wall force was greater than one-third the height of the wall above the base.

Tajimi[55] has used the theory of elasticity to compute the earthquake-induced soil pressures on a cylindrical structure embedded in an elastic stratum. He has also obtained a solution for the harmonically forced wall problem of Fig. 1.7 using two-dimensional elastic wave propagation theory[53,54]. Although the boundary conditions of this problem are unlikely to be encountered in practice the solution is a useful approximation for a number of dynamic wall problems. In particular the solution appears relevant for the case when a building is embedded in a relatively soft soil.

Scott[48] has used a simple one-dimensional elastic shear beam to model the soil layer in dynamic studies of both rigid and deformable walls. A Winkler spring foundation is used to connect the shear beam to the wall. Details of the model as applied to the rigid-wall problem are shown in Fig. 1.8. One advantage of this simple model approach is that closed form solutions can be obtained for certain cases that include variations of the elastic constants with depth and certain types of wall deformation. These solutions, because of their relatively simple form in comparison with more exact solutions, and because of their generality with respect to the basic soil and wall parameters, are useful for design applications.

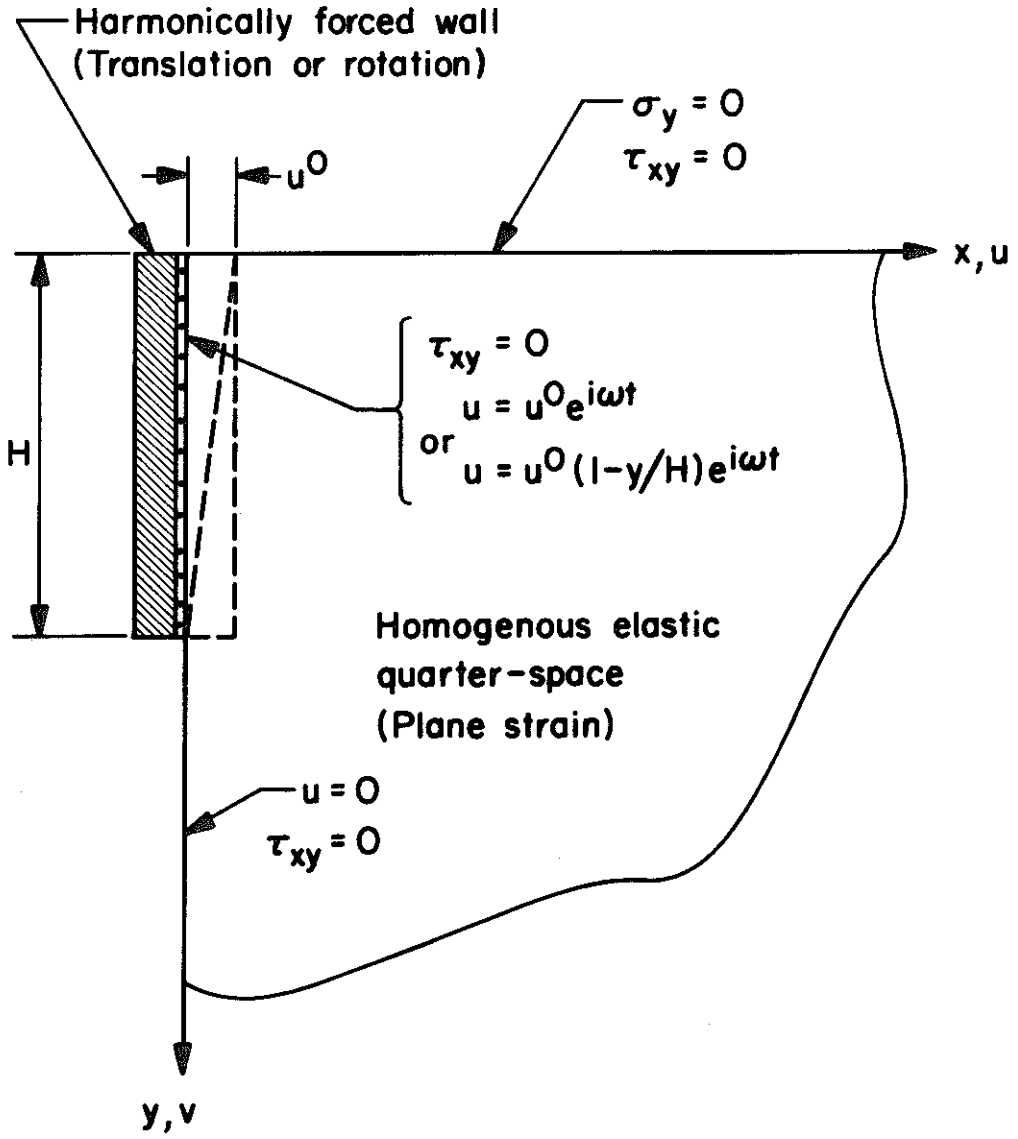

TAJIMI'S PROBLEM

Figure 1.7

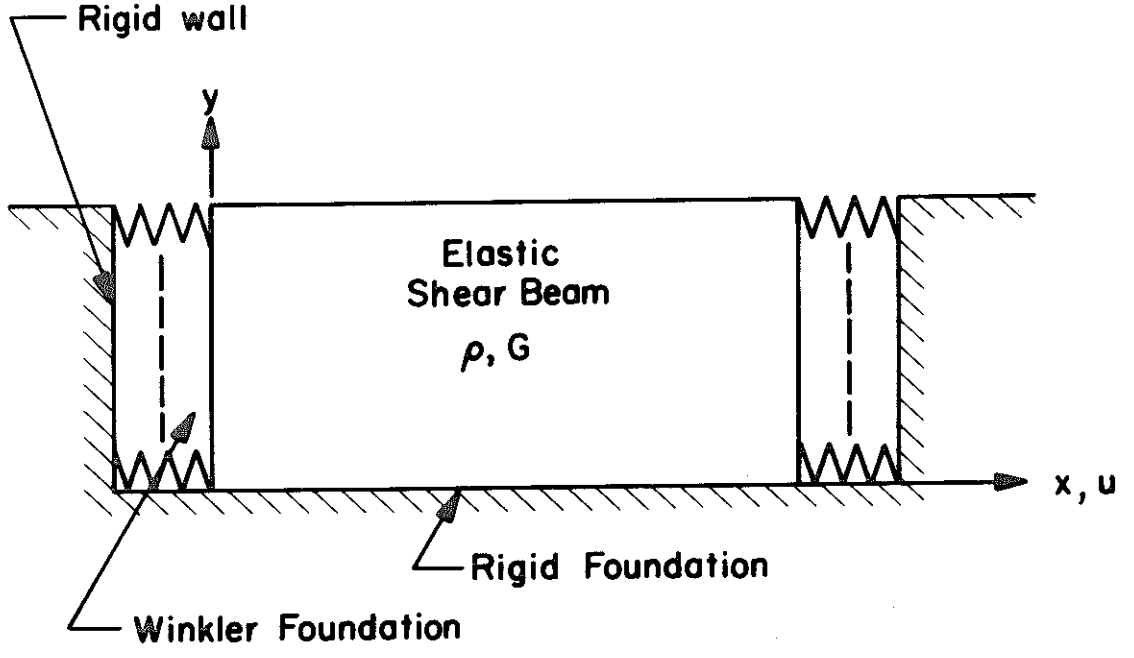

SCOTT'S MODEL

Figure 1.8

2. RIGID WALL: STATIC SOLUTIONS

2.1. ANALYTICAL SOLUTION

In this section the analytical solution of the problem shown in Fig. 2.1 is presented. The vertical end boundaries are taken to represent rigid walls and the contact between the homogeneous linearly elastic soil and the wall is assumed to be smooth; that is, the vertical boundaries are assumed to be free from shear stresses. The lower horizontal boundary represents a rigid rock layer on which no displacement is permitted. A uniform horizontal body force is assumed to act throughout the soil layer. For convenience the magnitude of this body force is taken as γ, the unit weight of the soil, and so represents the application of a static horizontal acceleration of one g. The method of solution follows the approach of Marguerre[31] and Pickett[43] who obtained solutions for an infinite elastic stratum resting on a rigid foundation with vertical loading on the surface.

Under the assumption of plane strain, the equilibrium equations for a homogeneous, linearly elastic, isotropic medium are

$$\frac{\partial \sigma_x}{\partial x} + \frac{\partial \tau_{xy}}{\partial y} + F_x = 0$$

$$\frac{\partial \sigma_y}{\partial y} + \frac{\partial \tau_{xy}}{\partial x} + F_y = 0 \qquad (2.1)$$

in which

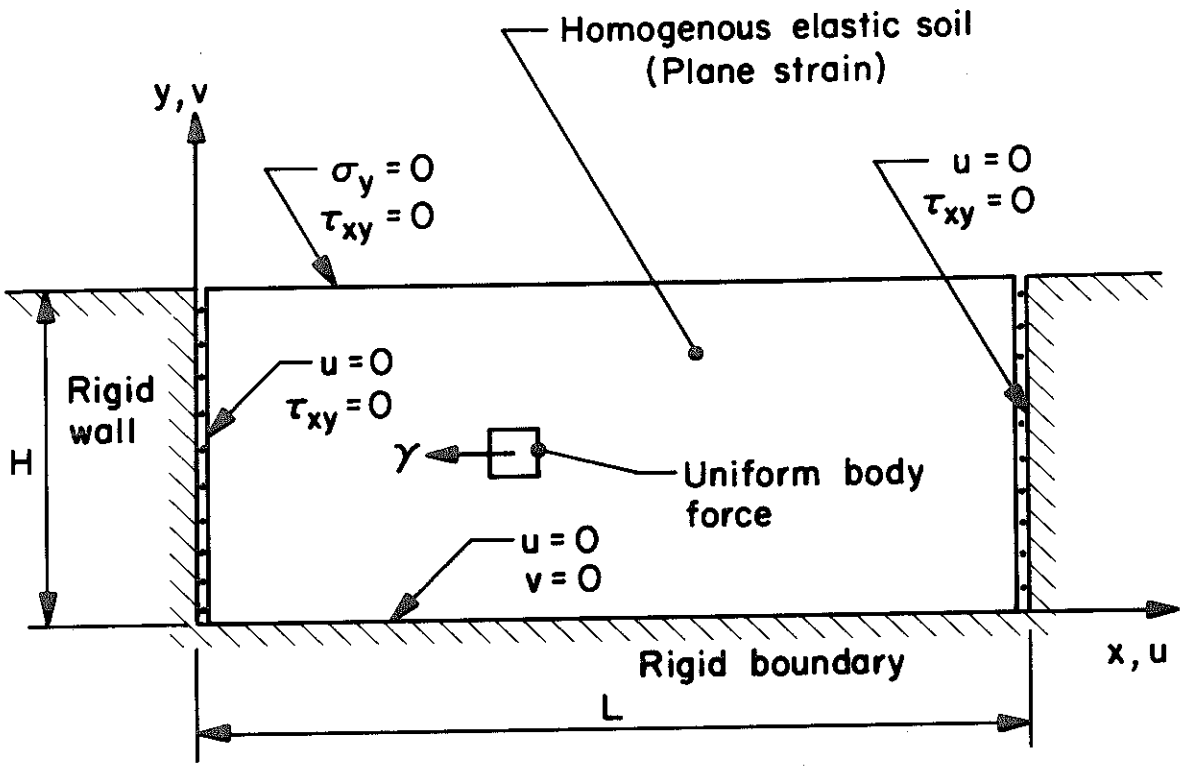

RIGID WALL PROBLEM

Figure 2.1

σ_x, σ_y = normal stresses in the x- and y-directions respectively

τ_{xy} = shear stress in the x- and y-directions

F_x, F_y = body forces per unit volume in the x- and y-directions respectively

The stress-strain relations may be expressed as

$$\frac{\sigma_x}{G} = k^2 \frac{\partial u}{\partial x} + (k^2-2) \frac{\partial v}{\partial y}$$

$$\frac{\sigma_y}{G} = (k^2-2) \frac{\partial u}{\partial x} + k^2 \frac{\partial v}{\partial y} \qquad (2.2)$$

$$\frac{\tau_{xy}}{G} = \frac{\partial u}{\partial y} + \frac{\partial v}{\partial x}$$

in which

G = shear modulus

$$k^2 = \frac{V_d^2}{V_s^2} = \frac{2(1-\nu)}{(1-2\nu)}$$

V_d = dilitational wave speed

V_s = shear wave speed

ν = Poisson's ratio

Substitution of expressions (2.2) into (2.1) gives the equilibrium equations for the problem in terms of the displacements. For the case of no vertical body force these equations are

$$k^2 \frac{\partial^2 u}{\partial x^2} + (k^2-1)\frac{\partial^2 v}{\partial x \partial y} + \frac{\partial^2 u}{\partial y^2} = \frac{\gamma}{G}$$

$$k^2 \frac{\partial^2 v}{\partial y^2} + (k^2-1)\frac{\partial^2 u}{\partial x \partial y} + \frac{\partial^2 v}{\partial x^2} = 0 \qquad (2.3)$$

for

$$0 < x < L; \qquad 0 < y < H$$

The problem boundary conditions are defined in Fig. 2.1. The constant forcing term $\frac{\gamma}{G}$ can be expanded in a Fourier series to give

$$\frac{\gamma}{G} = \sum_{n=1,3,5,\ldots}^{\infty} a_n \sin \frac{n\pi x}{L}$$

$$= \frac{\gamma}{G}\frac{4}{\pi}\left(\sin \frac{\pi x}{L} + \frac{1}{3}\sin \frac{3\pi x}{L} + \frac{1}{5}\sin \frac{5\pi x}{L} + \ldots\right) \qquad (2.4)$$

The solution of equations (2.3) can be expressed as

$$u(x,y) = \sum_{n=1,3,5,\ldots}^{\infty} \bar{u}_n(y) \sin rx$$

$$v(x,y) = \sum_{n=1,3,5,\ldots}^{\infty} \bar{v}_n(y) \cos rx \qquad (2.5)$$

in which

$$r = \frac{n\pi}{L}, \qquad n = 1,3,5,\ldots$$

A solution of this form clearly satisfies the boundary conditions at $x = 0$ and $x = L$, independently of the functions $\bar{u}_n(y)$, $\bar{v}_n(y)$.

Substitution of expressions (2.4) and (2.5) into (2.3) gives a coupled pair of equations for each of the terms in the series form of the solution. The equations for the nth term are

$$\frac{\partial^2 \bar{u}_n}{\partial y^2} - r^2 k^2 \bar{u}_n - (k^2-1) r \frac{\partial \bar{v}_n}{\partial y} = a_n$$

$$\frac{\partial^2 \bar{v}_n}{\partial y^2} - \frac{r^2}{k^2} \bar{v}_n + \frac{(k^2-1) r}{k^2} \frac{\partial \bar{u}_n}{\partial y} = 0 \qquad (2.6)$$

in which

$$a_n = \frac{4\gamma}{n\pi G} , \quad n = 1,3,5,\ldots$$

It can be shown by substitution that equations (2.6) are satisfied by the displacement functions

$$\bar{u}_n(y) = \frac{a_n}{r^2 k^2} \left\{ B_n \cosh ry + C_n (ry + k') e^{ry} + D_n (ry - k') e^{-ry} - 1 \right\} \qquad (2.7)$$

$$\bar{v}_n(y) = \frac{a_n}{r^2 k^2} \left\{ -B_n \sinh ry - C_n rye^{ry} + D_n rye^{-ry} \right\}$$

in which

$$k' = 3 - 4\nu$$

B_n, C_n, D_n = constants that can be determined by satisfying the boundary conditions at $y = 0$ and $y = H$

The condition that $\bar{v}_n = 0$ at $y = 0$ is satisfied directly by the second equation. The condition $\bar{u}_n = 0$ at $y = 0$ gives

$$B_n = k'(D_n - C_n) + 1 \tag{2.8}$$

The boundary conditions at $y = H$ are $\tau_{xy} = 0$, $\sigma_y = 0$. From equations (2.2) and (2.5) it can be shown that this stress-free surface condition is satisfied if

$$\left.\begin{aligned} \frac{\partial \bar{u}_n}{\partial y} - r\bar{v}_n &= 0 \\ (k^2-2)r\bar{u}_n + k^2 \frac{\partial \bar{v}_n}{\partial y} &= 0 \end{aligned}\right\} \text{ at } y = H \tag{2.9}$$

Substitution of equations (2.8) and (2.7) into expressions (2.9) gives the following linear algebraic equations for the constants C_n and D_n

$$\begin{aligned} &C_n[(2rH+k'+1)e^{rH} - 2k'\sinh rH] \\ &\quad + D_n[(-2rH+k'+1)e^{-rH} + 2k'\sinh rH] = -2\sinh rH \\ &C_n[(2rH+k'-1)e^{rH} - 2k'\cosh rH] \\ &\quad + D_n[(2rH-k'+1)e^{-rH} + 2k'\cosh rH] = -(k^2-2+2\cosh rH) \end{aligned} \tag{2.10}$$

Solving for C_n and D_n gives

$$\begin{aligned} C_n &= -\frac{1}{\Delta}\left[e^{-rH}\{(2rH-k'-1)(k^2-2+2\cosh rH)\right. \\ &\qquad \left. + (2rH-k'+1)(2\sinh rH)\} - 2(k^2-2)k'\sinh rH\right] \\ D_n &= -\frac{1}{\Delta}\left[e^{rH}\{(2rH+k'+1)(k^2-2+2\cosh rH)\right. \\ &\qquad \left. - (2rH+k'-1)(2\sinh rH)\} - 2(k^2-2)k'\sinh rH\right] \end{aligned} \tag{2.11}$$

in which

$$\Delta = 2\left\{1 + (2rH)^2 + k'^2 + 2k'(\sinh^2 rH + \cosh^2 rH)\right\},$$

the determinant of the coefficients of the unknowns

Hence from expression (2.8)

$$B_n = -\frac{2}{\Delta}\left[(k^2-2)k'\left\{2rH \sinh rH + (k'+1)\cosh rH\right\} - \left\{1 + (2rH)^2 - k'^2\right\}\right] \tag{2.12}$$

The complete displacement solution can be expressed in the following dimensionless form

$$\frac{uG}{\gamma H^2} = \frac{4}{\pi^3 k^2}\left(\frac{L}{H}\right)^2 \sum_{n=1,3,5,\ldots}^{\infty} \frac{1}{n^3}\left\{B_n \cosh ry + C_n(ry+k')e^{ry} + D_n(ry-k')e^{-ry} - 1\right\}\sin rx \tag{2.13}$$

$$\frac{vG}{\gamma H^2} = \frac{4}{\pi^3 k^2}\left(\frac{L}{H}\right)^2 \sum_{n=1,3,5,\ldots}^{\infty} \frac{1}{n^3}\left\{-B_n \sinh ry - C_n ry e^{ry} + D_n ry e^{-ry}\right\}\cos rx$$

in which $r = \frac{n\pi}{L}$. The complete solutions for dimensionless stresses are

$$\frac{\sigma_x}{\gamma H} = \frac{4}{\pi^2 k^2}\frac{L}{H} \sum_{n=1,3,5,\ldots}^{\infty} \frac{1}{n^2}\left\{2B_n \cosh ry + C_n(2ry+k'+3)e^{ry} + D_n(2ry-k'-3)e^{-ry} - k^2\right\}\cos rx \tag{2.14}$$

$$\frac{\sigma_y}{\gamma H} = \frac{4}{\pi^2 k^2}\frac{L}{H}\sum_{n=1,3,5,\ldots}^{\infty} -\frac{1}{n^2}\Big\{2B_n \cosh ry + C_n(2ry + k' - 1)e^{ry} + D_n(2ry - k' + 1)e^{-ry} - k^2 + 2\Big\}\cos rx \qquad (2.15)$$

$$\frac{\tau_{xy}}{\gamma H} = \frac{4}{\pi^2 k^2}\frac{L}{H}\sum_{n=1,3,5,\ldots}^{\infty} \frac{1}{n^2}\Big\{2B_n \sinh ry + C_n(2ry + k' + 1)e^{ry} + D_n(-2ry + k' + 1)e^{-ry}\Big\}\sin rx \qquad (2.16)$$

It should be noted that as $\nu \to 0.5$, $k^2 \to \infty$. The solution for $\nu = 0.5$ can be readily obtained from the above expressions by taking their limits as $k^2 \to \infty$.

The normal stress distribution on the wall boundary can be found by setting $x = 0$ in expression (2.14). The force on the wall per unit length of wall F_{sr}, and the moment on the wall about the base per unit length of wall M_{sr} are given by

$$F_{sr} = \int_0^H \sigma_x(0,y)\,dy$$
$$M_{sr} = \int_0^H y\sigma_x(0,y)\,dy \qquad (2.17)$$

Performing the integration in expressions (2.17) gives

$$\frac{F_{sr}}{\gamma H^2} = \frac{4}{\pi^3 k^2}\left(\frac{L}{H}\right)^2 \sum_{n=1,3,5,\ldots}^{\infty} \frac{1}{n^3}\Big\{2B_n \sinh rH + C_n(2rH + k' + 1)e^{rH} + D_n(-2rH + k' + 1)e^{-rH} - (C_n + D_n)(k' + 1) - k^2 rH\Big\} \qquad (2.18)$$

$$\frac{M_{sr}}{\gamma H^3} = \frac{4}{\pi^3 k^2}\left(\frac{L}{H}\right)^3 \sum_{n=1,3,5,\ldots}^{\infty} \frac{1}{n^4}\Big[\, 2B_n(rH \sinh rH - \cosh rH + 1)$$

$$+ C_n\left\{2r^2H^2 - 4rH + 4 + (rH-1)(k'+3)\right\}e^{rH}$$

$$+ D_n\left\{-2r^2H^2 - 4rH - 4 + (rH+1)(k'+3)\right\}e^{-rH}$$

$$+ (C_n - D_n)(k' - 1) - \frac{(rHk)^2}{2}\,\Big] \qquad (2.19)$$

The normal stress, force and moment on the wall were evaluated from the above solutions for a range of $\frac{L}{H}$ values between 0.5 and 10, and for ν between 0.2 and 0.5. Plots of the wall pressure distributions are given in Figs. 2.2 to 2.5 inclusive* and the wall forces and moments are shown in Fig. 2.6. The pressure and force solutions for $\frac{L}{H}$ values greater than 10 probably do not exceed the $\frac{L}{H} = 10$ solutions by more than a few percent.

Because convergence of the solutions was found to be relatively slow the presented results were numerically evaluated on the digital computer. The degree of convergence was estimated by comparing the value from the integration of the horizontal component of the boundary stress solution around the boundaries with the value of the integration of the body force over the volume. Terms in the series solutions were summed until this horizontal equilibrium check gave an error of less than 2%. For $\frac{L}{H} = 5.0$ it was found

*In the results of this study compressive pressures on the wall are plotted positively. The usual sign convention is used in the mathematical formulation of the analytical solutions; that is, a tensile stress has a positive sign and a compressive stress a negative sign.

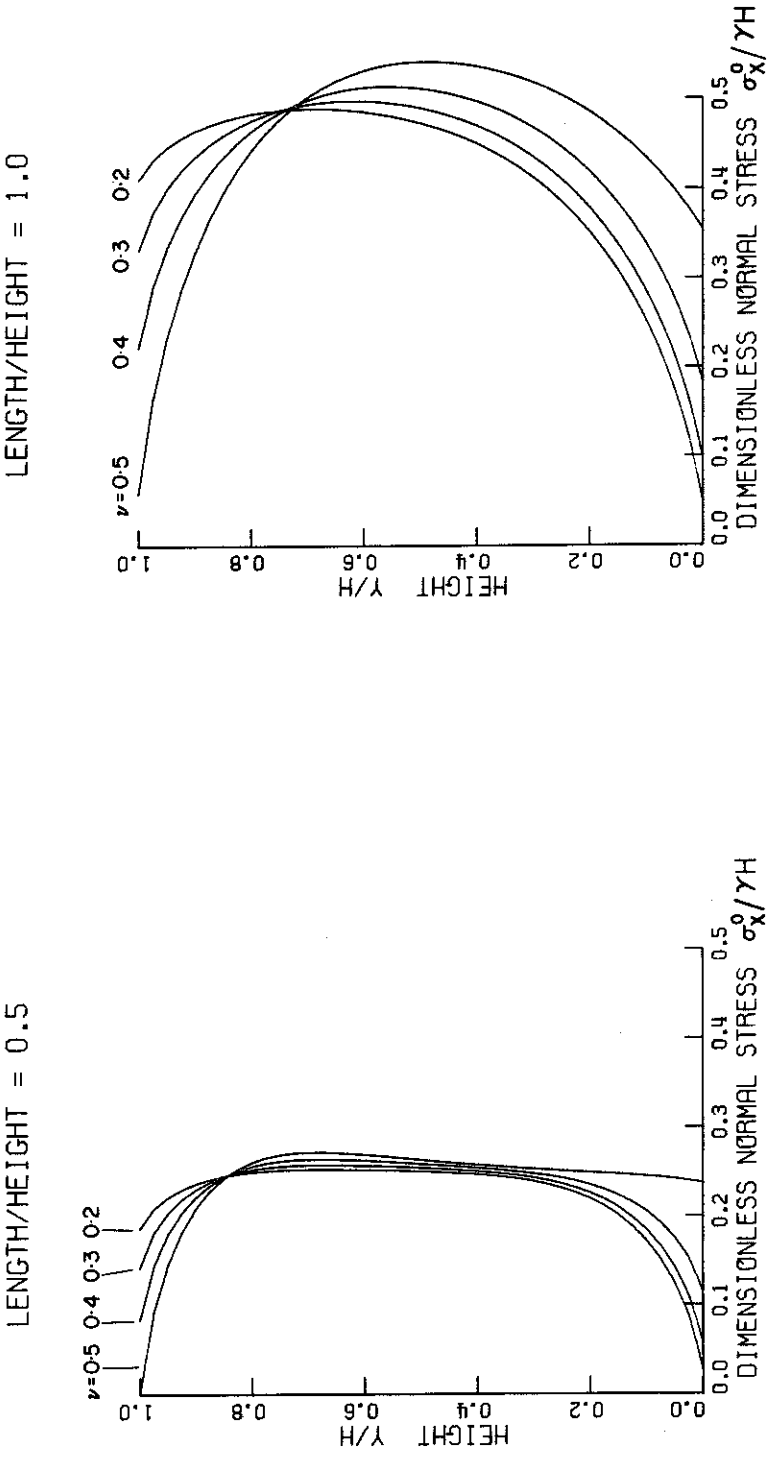

Figure 2.2 Pressure distributions on smooth rigid wall for one-g static horizontal body force.

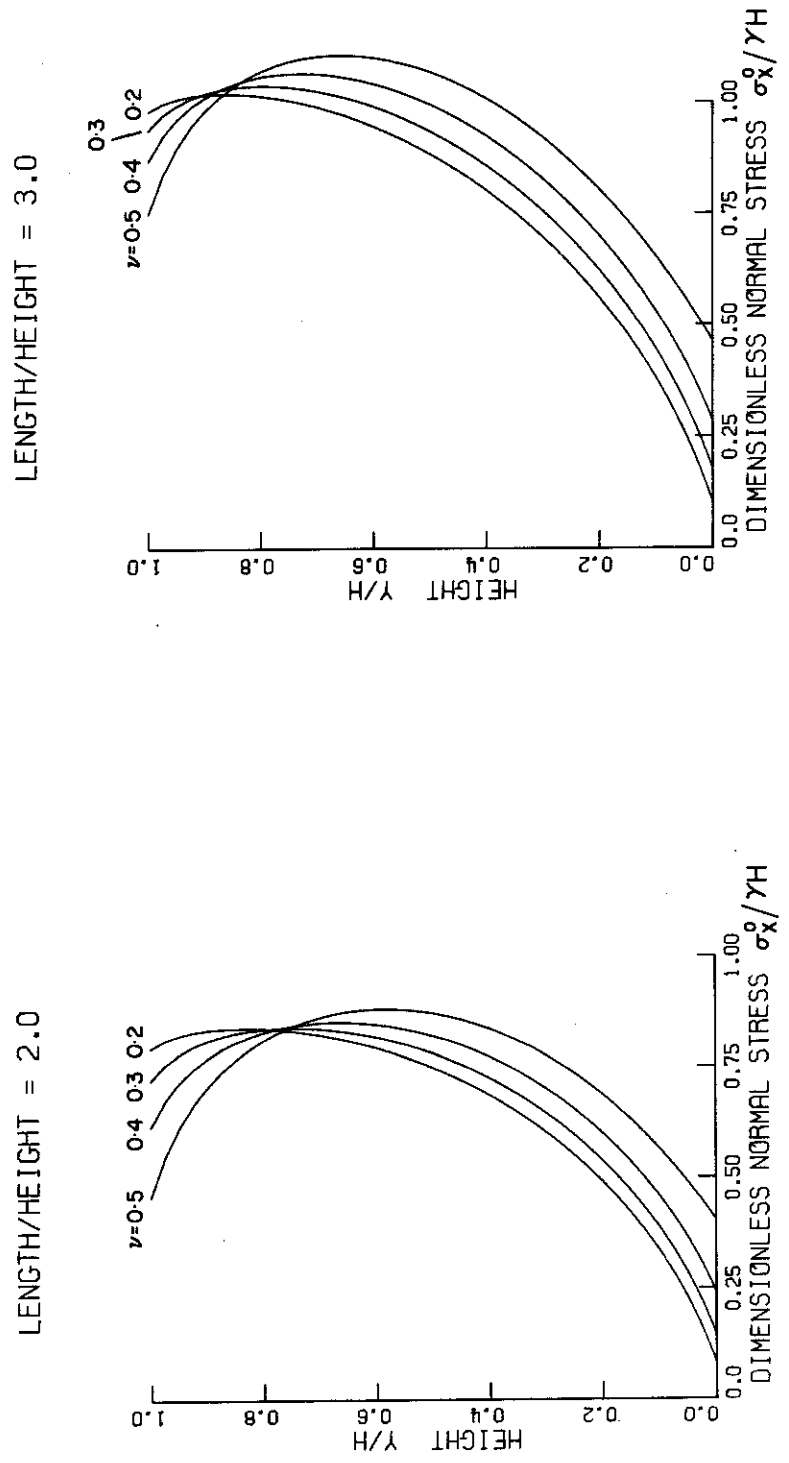

Figure 2.3 Pressure distributions on smooth rigid wall for one-g static horizontal body force.

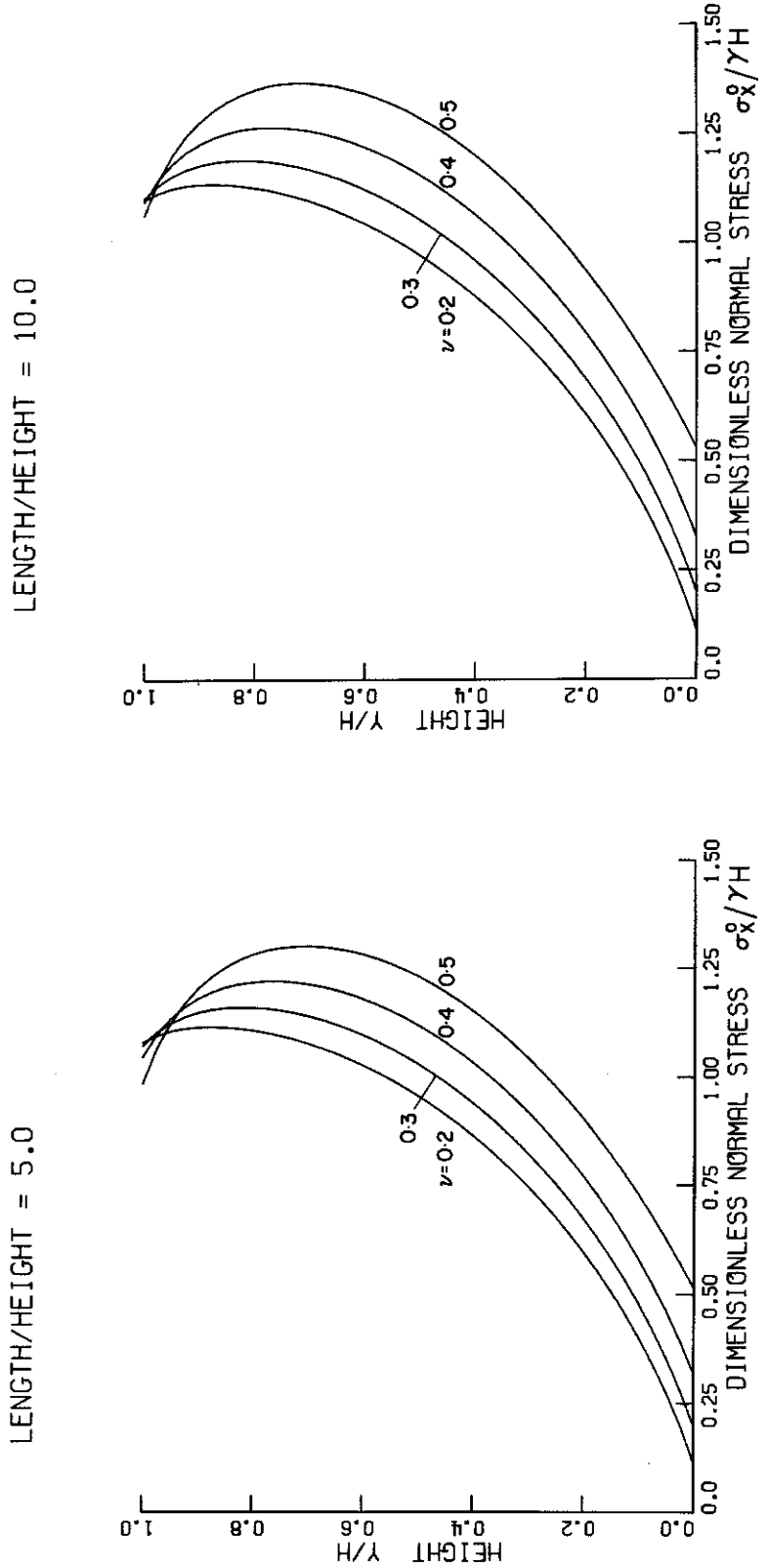

Figure 2.4 Pressure distributions on smooth rigid wall for one-g static horizontal body force.

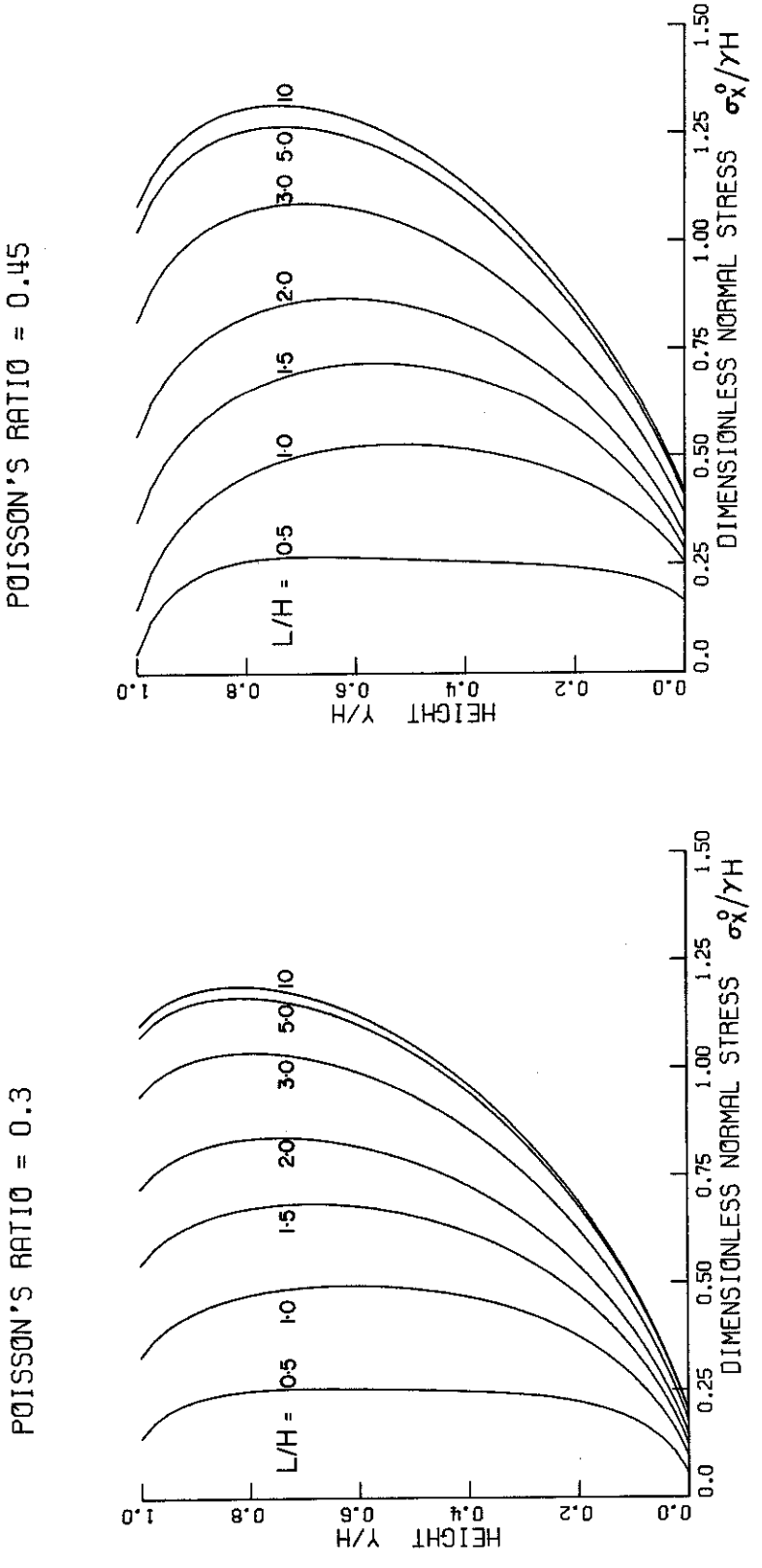

Figure 2.5 Pressure distributions on smooth rigid wall for one-g static horizontal body force.

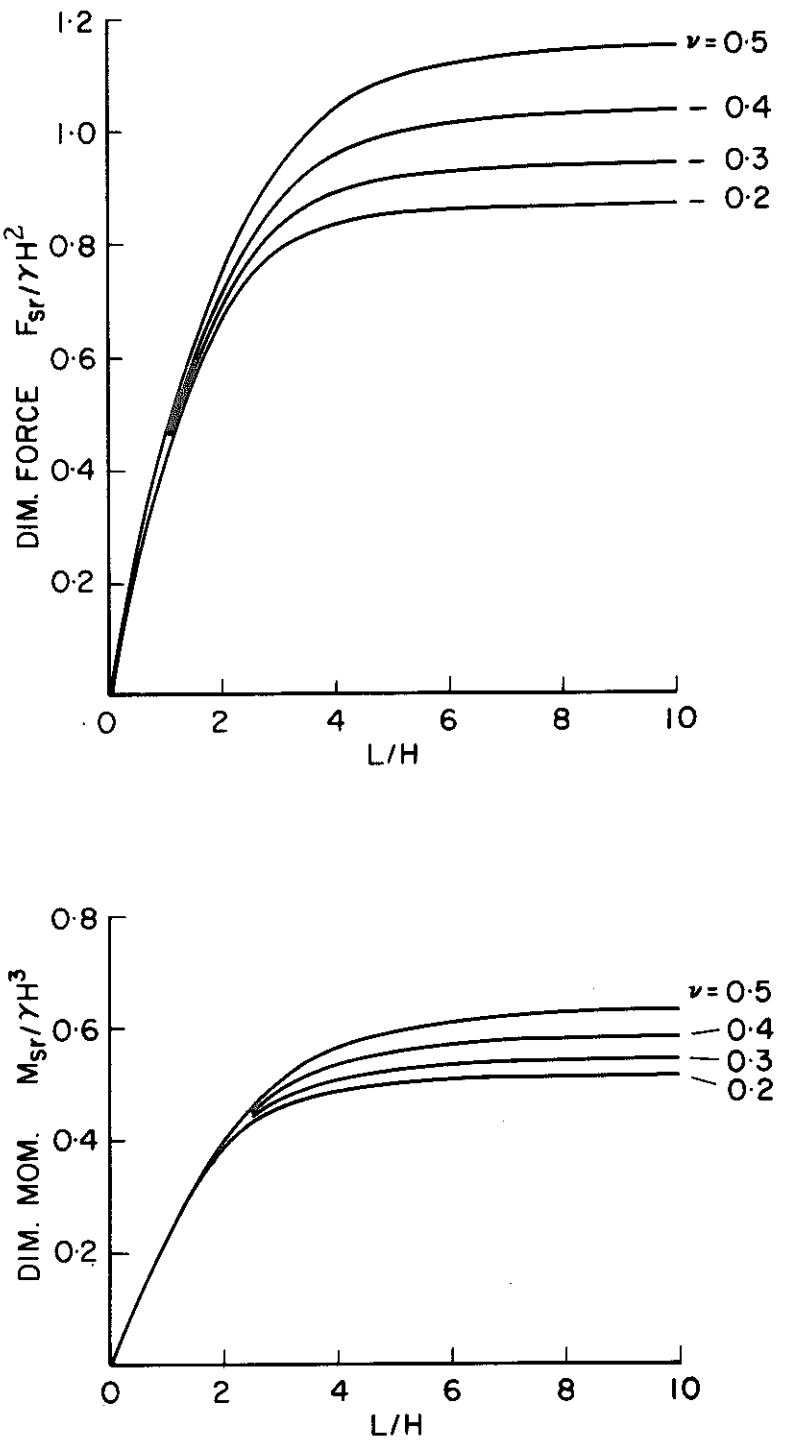

Figure 2.6 Force and moment on smooth rigid wall for one-g static horizontal body force.

necessary to sum about 20 terms to achieve this accuracy. (A smaller number of terms were required for $\frac{L}{H} < 5.0$ and a larger number for $\frac{L}{H} > 5.0$. Numerical values from one of pressure distribution solutions are compared with a finite element solution in Section 2.2.1.)

It is of interest to note that the first terms in the static series solution give a reasonably good approximation to the first mode shape and associated stress field of the equivalent free vibration problem. Details of the free vibration solution are given in Section 3.1. In both the static and free vibration solutions the displacements have the same trigonometric variations in the x-direction.

By using an approach similar to that used by Lemcoe[27] for the analysis of a horizontally layered half-space subjected to surface loads, it would be possible to extend the solution given here to the case of a horizontally layered soil. However, it would not be possible to write the solution from this method in a relatively simple form and although numerical results can be readily evaluated by solving a set of linear algebraic equations, it is doubtful whether this type of approach has any significant advantage over the more general finite element method.

2.2. FINITE ELEMENT SOLUTIONS

A comparison was made between the analytical solution of the previous section and a solution of the same problem computed by the finite element method. The finite element method was then used to compute the solutions of related problems that were not convenient-

ly handled by analytical methods. Details of the finite element method and its application to solve elasticity problems have been presented in numerous papers and texts (for example see Zienkiewicz[60], Przemieniecki[45] and Clough[61]) and there is no need to describe the method here. Two different elements, a first-order rectangle and a second-order quadrilateral were used for this investigation and details of these elements and the method used are given in Appendix II.

2.2.1. Smooth Wall

Finite element solutions were computed for the problem of the previous section (Fig. 2.1) using a number of different values of the parameters $\frac{L}{H}$ and ν. The finite element mesh used for these solutions is shown in Fig. 2.7. The antisymmetry of the problem was used to reduce the mesh length by one-half. Very good agreement was found between the finite element and the analytical solutions, and the differences in the wall pressure distributions were hardly detectable on the scale of the plots of the analytical solutions given in Section 2.1. A typical comparison of the wall pressure solutions is given in Table 2.1.

Except for a minor irregularity in the finite element solution near the bottom boundary (where the strain gradient is high), agreement between the two methods is better than 1%. Since the analytical solution is expected to have an order of accuracy of about 1%, the finite element method at this mesh size can be expected to give results to about 2% accuracy. (A mesh size of

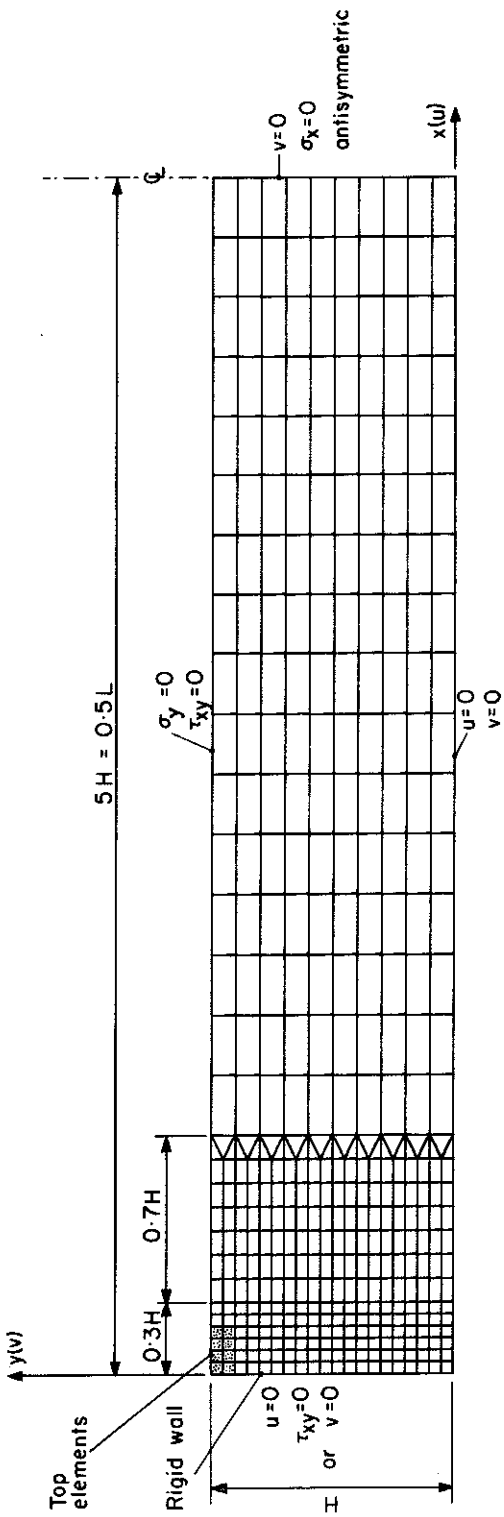

Figure 2.7 Finite element mesh for static solutions, L/H = 10. (Mesh reduced from right-hand boundary for other L/H values).

TABLE 2.1

Comparison of Analytical and Finite Element Solutions

$\frac{L}{H} = 5.0, \quad \nu = 0.3$

$\frac{y}{H}$	Dimensionless Wall Stress $\sigma_x^o/\gamma H$	
	Analytical	Finite Element
1.00	-1.076	-1.069
0.95	-1.128	-1.127
0.90	-1.154	-1.150
0.85	-1.165	-1.161
0.80	-1.166	-1.162
0.75	-1.159	-1.155
0.70	-1.146	-1.142
0.65	-1.127	-1.123
0.60	-1.102	-1.098
0.55	-1.071	-1.067
0.50	-1.035	-1.031
0.45	-0.9924	-0.9888
0.40	-0.9439	-0.9405
0.35	-0.8890	-0.8857
0.30	-0.8268	-0.8238
0.25	-0.7566	-0.7539
0.20	-0.6773	-0.6750
0.15	-0.5868	-0.5854
0.10	-0.4822	-0.4821
0.05	-0.3574	-0.3623
0.00	-0.1978	-0.1629

about twice that used here would probably be satisfactory for practical applications involving similar problems.) The finite element results given in Table 2.1 were computed using the second-order quadrilateral element. Results obtained using the first-order rectangular element were almost identical. (The quadrilateral element was preferred for subsequent work in which wall flexure was significant.)

2.2.2. Bonded Wall

In practice the boundary condition on a soil-supporting rigid wall would be expected to be between the smooth case previously analyzed and a fully bonded condition in which both components of displacement (u and v) are zero. No attempt has been made in this investigation to obtain an analytical solution for the bonded contact case but it seems likely that if a solution were possible a considerable amount of numerical work would be required for its evaluation. In view of the excellent results obtained by the finite element method for the smooth rigid-wall problem it appears reasonable to expect that this method will give satisfactory results for related problems such as the bonded-contact rigid wall.

A number of bonded contact solutions were computed for a one-g horizontal body force using essentially the same mesh (Fig. 2.7) as used previously for the smooth contact solutions. The wall boundary condition was taken as $u = 0$, $v = 0$. The solutions for the bonded-contact normal stresses are compared with the analytical smooth wall values in Fig. 2.8. For the bonded contact

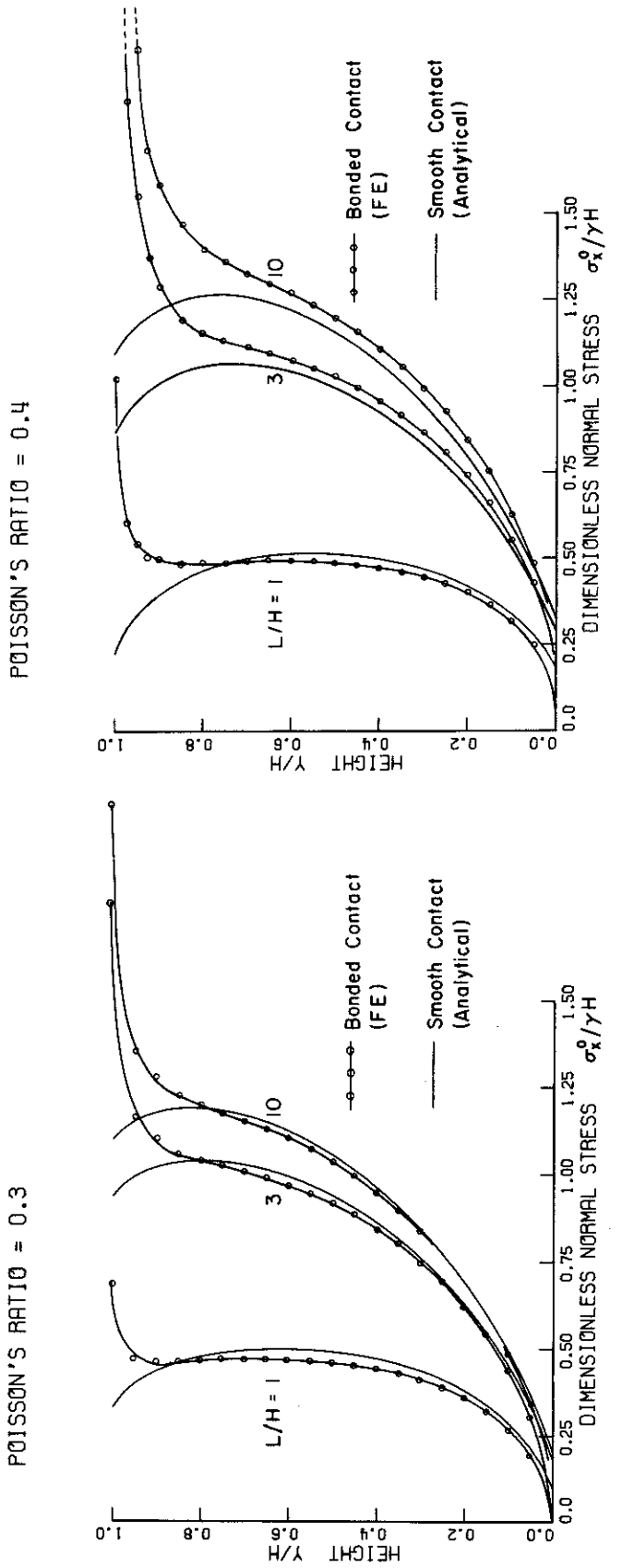

Figure 2.8 Pressure distributions on rigid wall for one-g static horizontal body force.

case a stress singularity exists at the top of the wall and in order to compute details of the singularity to a reasonable degree of accuracy the mesh was modified for some of the solutions. To compute the results shown for the $\nu = 0.4$ solutions, the elements shown as top elements in Fig. 2.7 were each horizontally subdivided into two elements.

The finite element normal and shear stresses on the bonded-contact wall boundary are given in Table 2.2 for the $\frac{L}{H} = 10$ solutions. σ_x^o and τ_{xy}^o are the normal and shear stress respectively on the wall boundary. Inspection of these stresses shows that a horizontal body force loading is unlikely to produce sliding on the rigid-wall interface, thus indicating bonded contact behavior.* (The exact nature of the stress distribution on the wall boundary for the case of vertical gravity loads is difficult to compute because the stresses are dependent on the manner in which the soil is placed behind the wall during construction. In general some slipping on the interface would be expected for this case. Clough and Duncan[7,9] have computed pressure distributions for deformable walls subjected to gravity loads by using a nonlinear finite element technique and special interface elements.)

Most unsaturated soils have a Poisson's ratio between 0.25 and 0.4 and it is evident from the wall normal stress distributions that except near the top of the wall ($\frac{y}{H} > 0.8$) quite good agreement exists between the bonded and smooth wall solutions for this range of Poisson's ratio. Solutions for Poisson's ratio greater than 0.4 have not been fully investigated, but it appears that as Poisson's

*Because of the presence of the singularity, the behavior on the contact near the top of the wall is uncertain.

TABLE 2.2

Finite Element Stresses. One-g Horizontal Body Force
Bonded Contact. $\frac{L}{H} = 10$

	$\nu = 0.3$		$\nu = 0.4$	
$\frac{y}{H}$	$\frac{\sigma_x^o}{\gamma H}$	$\frac{\tau_{xy}^o}{\gamma H}$	$\frac{\sigma_x^o}{\gamma H}$	$\frac{\tau_{xy}^o}{\gamma H}$
1.0	-2.07	0.33	-3.91	0.54
0.95	-1.35	0.30	-1.92	0.55
0.9	-1.28	0.23	-1.59	0.42
0.8	-1.20	0.13	-1.40	0.28
0.7	-1.15	0.05	-1.34	0.16
0.6	-1.10	-0.008	-1.28	0.08
0.5	-1.04	-0.05	-1.20	0.01
0.4	-0.95	-0.09	-1.11	-0.04
0.3	-0.84	-0.12	-1.00	-0.08
0.2	-0.69	-0.13	-0.85	-0.11
0.1	-0.48	-0.12	-0.63	-0.10

ratio is increased the area under the stress singularity tends to increase resulting in an increasing lack of agreement between the stress distributions for the two boundary conditions.

Because of variations in the elastic moduli near the soil surface and the relatively low stress levels at which nonlinear behavior or yield occurs in soils, the stress singularity is unlikely to develop to any appreciable degree. In a cohesionless soil, the absence of significant confining stresses near the top of the wall will result in yielding at very low stress levels. For this case the normal pressure at the top of the wall will be essentially zero irrespective of the boundary condition on the wall. The following investigations were made to establish approximately the extent to which the elastic theory pressure distributions would be modified by the nonlinear behavior of typical soils.

Cohesionless Soil. It is informative to consider the solution of a simple plasticity problem that represents approximately the stress conditions near the top of a smooth rigid wall. In Fig. 2.9 a smooth rigid wall supports a cohesionless soil which is loaded by gravity and the horizontal displacement of a smooth rigid plate. On the assumption of the Mohr-Coulomb failure criterion it is easily shown that the limiting pressure on the wall is given by

$$\frac{\sigma^{o}_{x\,max}}{\gamma H} = K_p\left(1 - \frac{y}{H}\right) \qquad (2.20)$$

in which

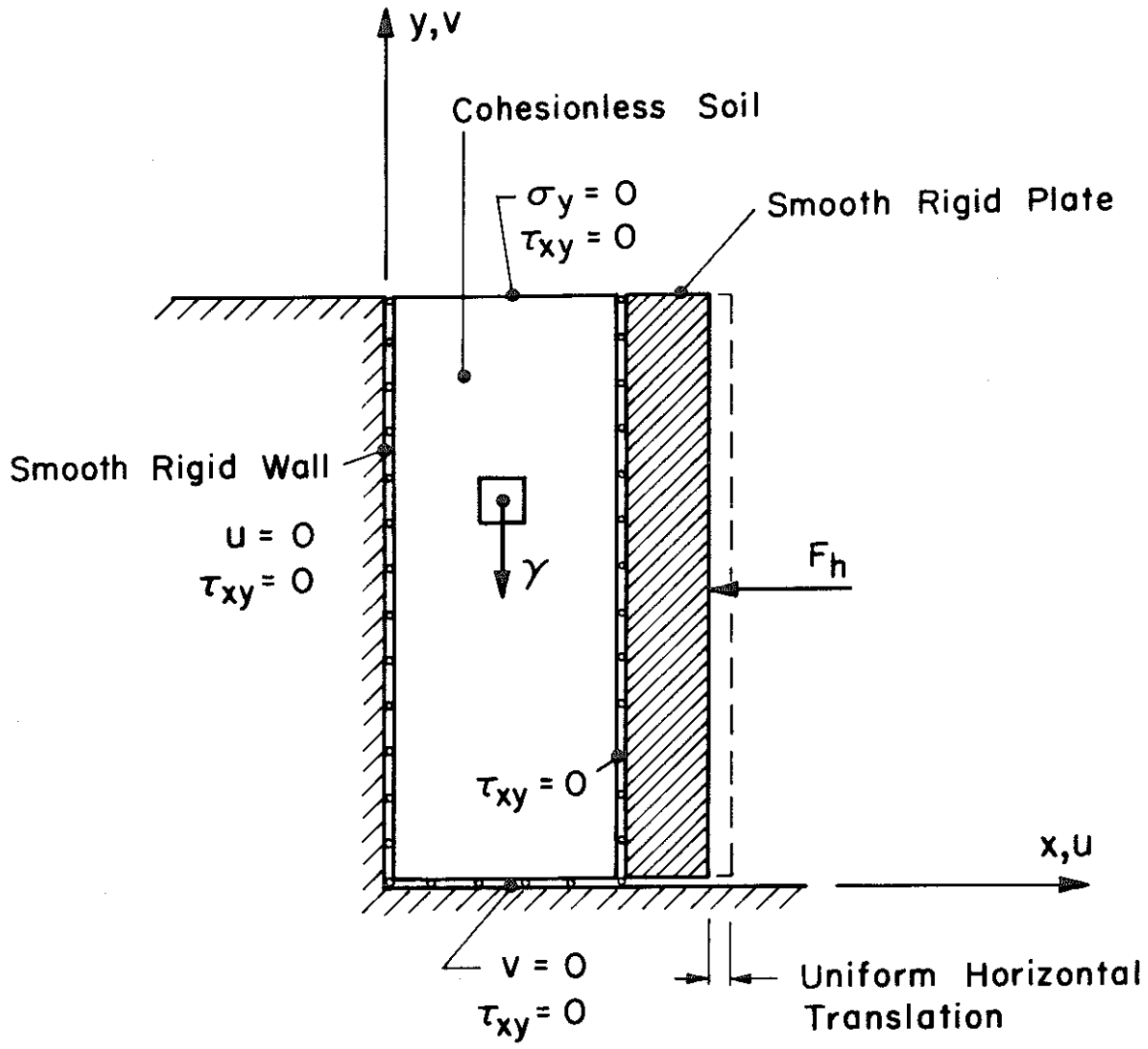
y,v
Cohesionless Soil
$\sigma_y = 0$
$\tau_{xy} = 0$
Smooth Rigid Plate
Smooth Rigid Wall
u = 0
$\tau_{xy} = 0$
γ
F_h
$\tau_{xy} = 0$
x,u
v = 0
$\tau_{xy} = 0$
Uniform Horizontal Translation

Figure 2.9

$K_p = \frac{1 + \sin \phi}{1 - \sin \phi}$, the passive earth-pressure coefficient

It is expected that expression (2.20) will give approximately the limiting pressure near the top of a smooth rigid wall supporting a cohesionless soil loaded by gravity and horizontal body forces. This result may also be a reasonable approximation for the bonded contact condition.

Expression (2.20) is superimposed in Fig. 2.10 on the wall pressure distributions computed by elastic theory for a combined vertical gravity and a one-third-g horizontal body force. It can be seen that failure of the cohesionless soil significantly reduces the elastic pressure distributions in the region $\frac{y}{H} > 0.8$. A more exact analysis of the wall problem would be required to show the influence of failure on the pressures below the region of failure; however, it appears likely that the lower pressures are increased to some extent.

Bilinear Soil. Problems involving soils with any general nonlinear stress-strain relationship can be analyzed by the finite element method. A common approach is to use an iterative technique solving successive infinitesimal elasticity problems. The full load is applied for the first solution and at each successive step the element elastic moduli are adjusted in an appropriate manner so that with successive solutions the stress-strain relationship in each element converges to the desired nonlinear behavior. (Baligh[3] has studied various methods of selecting the material properties for the successive approximations and found that to optimize the process

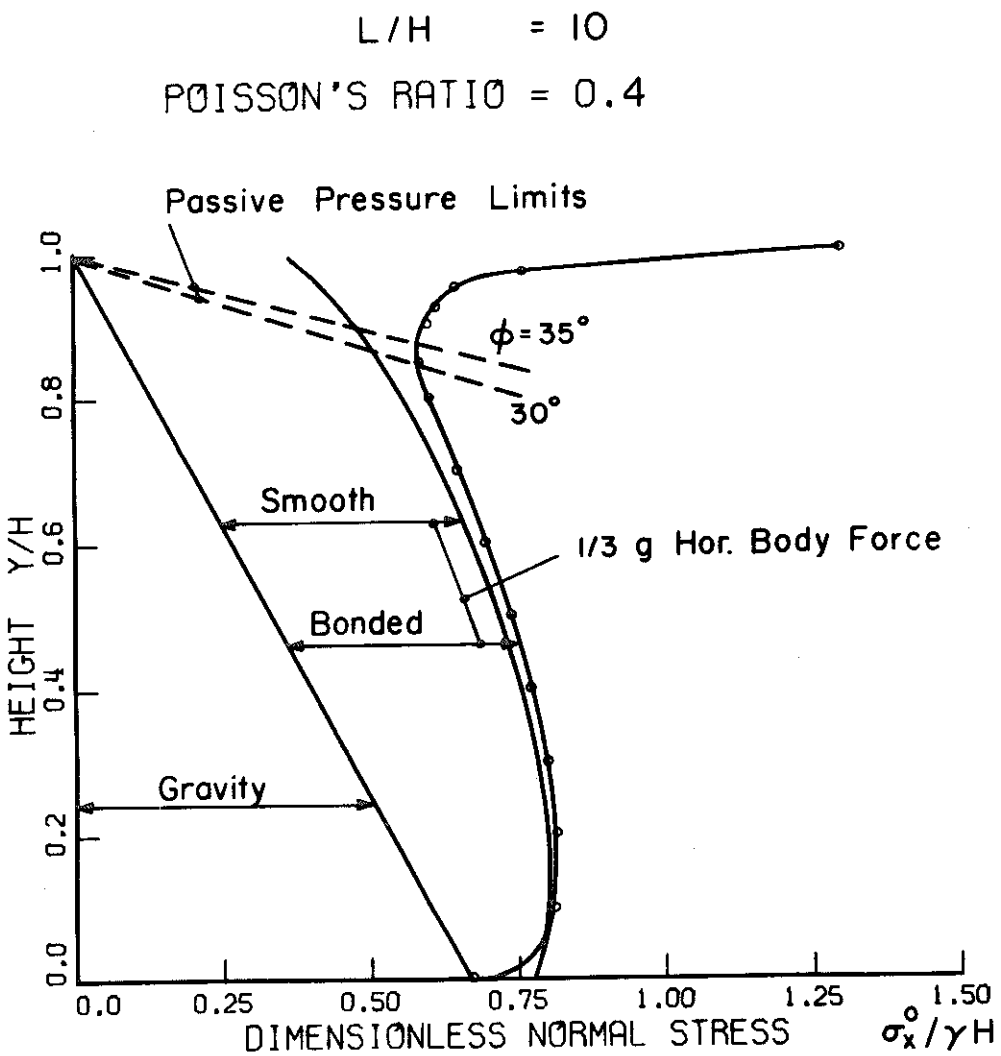

Figure 2.10 Wall pressure limits for cohesionless soil.

different methods should be used for different types of problems.)

To show the influence of nonlinear soil behavior on the stress singularity a finite element analysis was preformed for the bonded-contact rigid wall using the bilinear material properties shown in Fig. 2.11a. The soil properties are defined in terms of the deviatoric stress-strain relation. For plane strain the deviatoric stress is related to the principal stresses by

$$\tau_d = \frac{\sqrt{3}}{2}(\sigma_1 - \sigma_2) \tag{2.21}$$

in which

τ_d = deviatoric stress

σ_1, σ_2 = principal stresses in the x-y plane

The mesh and the elements described for the previous bonded contact solutions were again used. The nonlinear pressure distribution computed for a one-g horizontal body force with parameters $\frac{L}{H} = 3.0$ and $\nu = 0.4$ is compared in Fig. 2.11b with the solution for the linearly elastic soil properties. The elements that yield under the specified loading are also identified in Fig. 2.11b. It can be seen that the overall effect of the nonlinear behavior on the wall pressure distribution is not very pronounced. The stresses in the three top elements are reduced by the yielding but this reduction is offset by an increase in the stresses below the region of yield.

In the example presented here the soil has been assumed to have uniform properties. In the following section the influence of a variation of the elastic constants with depth is studied and it is

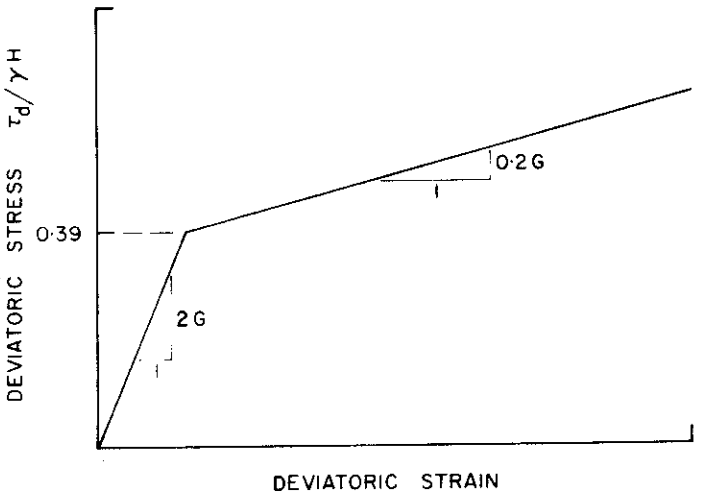

Figure 2.11a Bilinear soil properties.

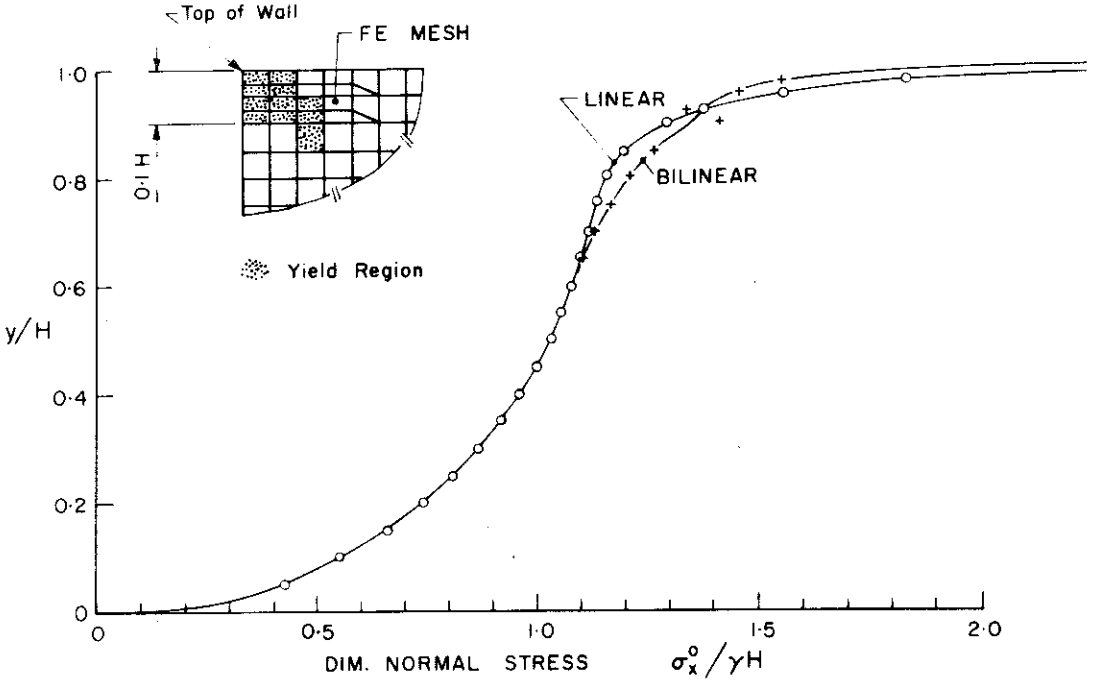

Figure 2.11b Pressure distributions on bonded rigid wall for one-g static horizontal body force. Comparison between linear and bilinear solutions.

found that this effect can produce quite a significant change in the pressure distribution. It appears that in practice the influence of both nonlinear behavior and variation of properties with depth will effectively diminish the importance of the singularity. (In theory, if the soil possesses cohesion the singularity will always be present.)

2.2.3. Nonuniform Soil

Typical soil moduli and details of the influence of various parameters on their magnitude are given in References (11, 12, 26 and 49). In a cohesionless soil, the elastic moduli (Young's modulus and the shear modulus) are strongly dependent on the confining pressure and the strain amplitude. For most soils the moduli increase with depth below the soil surface. A satisfactory approximation, suitable for practical applications, is to assume a linear increase of the moduli with depth.

Wall pressure distributions were computed by the finite element for two linear variations of Young's modulus with depth; an increase from 0.1 at the surface to 1.0 at the rigid boundary, and an increase from 0.5 to 1.0. In the finite element representation of these variations 10 equal depth homogeneous horizontal layers were used. The soil was assumed to have uniform density and Poisson's ratio. The mesh used for the previous problems was employed (Fig. 2.7). Solutions were computed for a one-g horizontal body force with the parameters $\frac{L}{H} = 10$ and $\nu = 0.3$. Both the smooth and bonded contact conditions were analyzed.

The finite element data points for the wall pressure and a hand smoothed interpretation of the results are plotted in Fig. 2.12. Lack of smoothness in the data results from high strain gradients and the discrete steps in the material properties. The smoothness of the computed values could be improved by reducing the mesh size, but since the irregularities were mainly at the top of the wall where the elastic theory is of doubtful applicability for soils, the solutions obtained were considered satisfactory. The linear variation in properties reduces the normal stresses on the top half of the wall and produces a slight increase in these stresses on the lower half. As the linear variation becomes more pronounced the bonded-contact stress singularity tends to move closer to the top of the wall with an apparently diminished contribution to the total force. Except in the region for $\frac{Y}{H} > 0.8$, good agreement is again demonstrated between the bonded and smooth contact results.

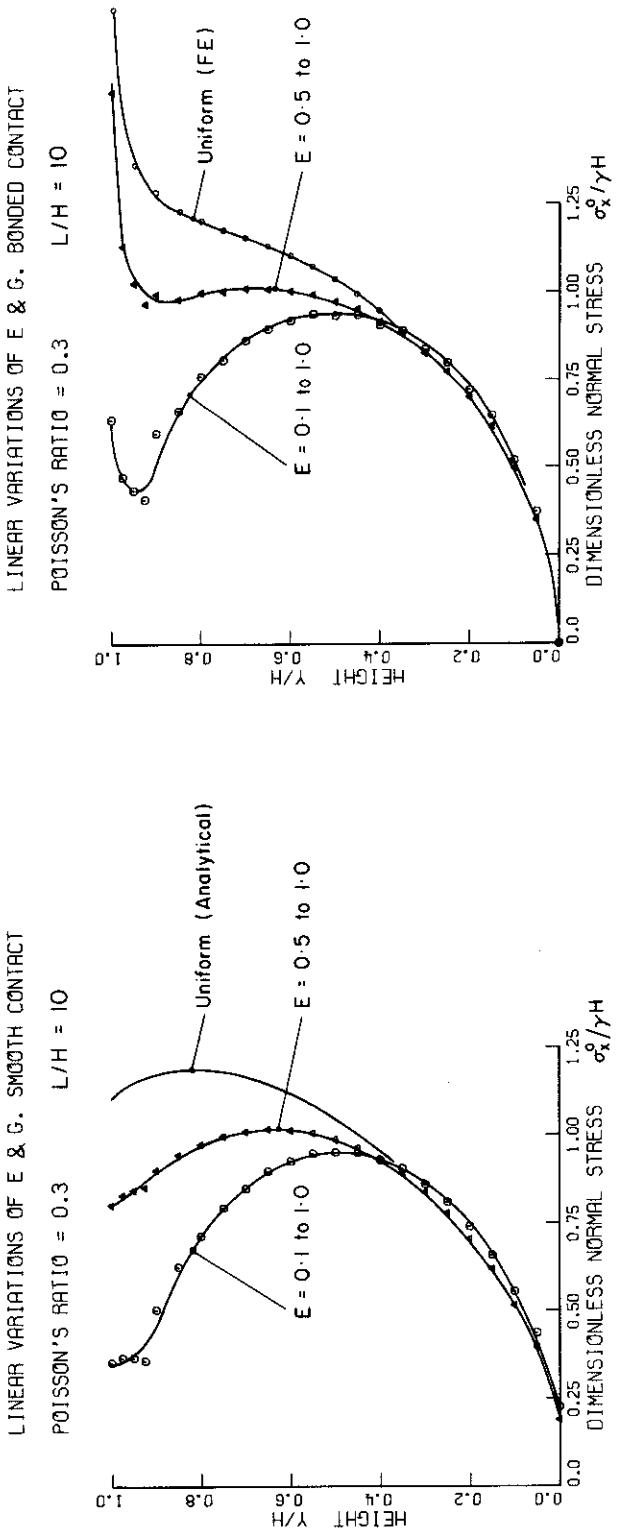

Figure 2.12 Pressure distributions on rigid wall for one-g static horizontal body force. Nonuniform soil properties.

3. RIGID WALL: DYNAMIC SOLUTIONS

3.1. ANALYTICAL SOLUTION

In this section the analytical solution is presented for the free vibrations of the homogeneous elastic solid shown in Fig. 3.1. The boundary conditions are identical with those of the static problem studied in Section 2.1 and the vertical end boundaries are again taken to represent smooth rigid walls. The free vibration solution may be used to compute the wall pressure distribution response to a time-dependent acceleration of the rigid boundaries. Details of the application of the free vibration solutions for this computation are presented in Section 3.2.

The displacement equations of motion for the homogeneous linearly elastic isotropic medium can be readily derived from the equilibrium equations and the stress-strain relations (equations (2.1) and (2.2)) by the addition of appropriate inertia terms to the equilibrium equations. Because of the linear nature of the problem the solution for static body forces may be superimposed with the dynamic solution. For the purpose of deriving the dynamic solution it is convenient to set the static body forces to zero. The displacement equations of motion for the problem can then be expressed as

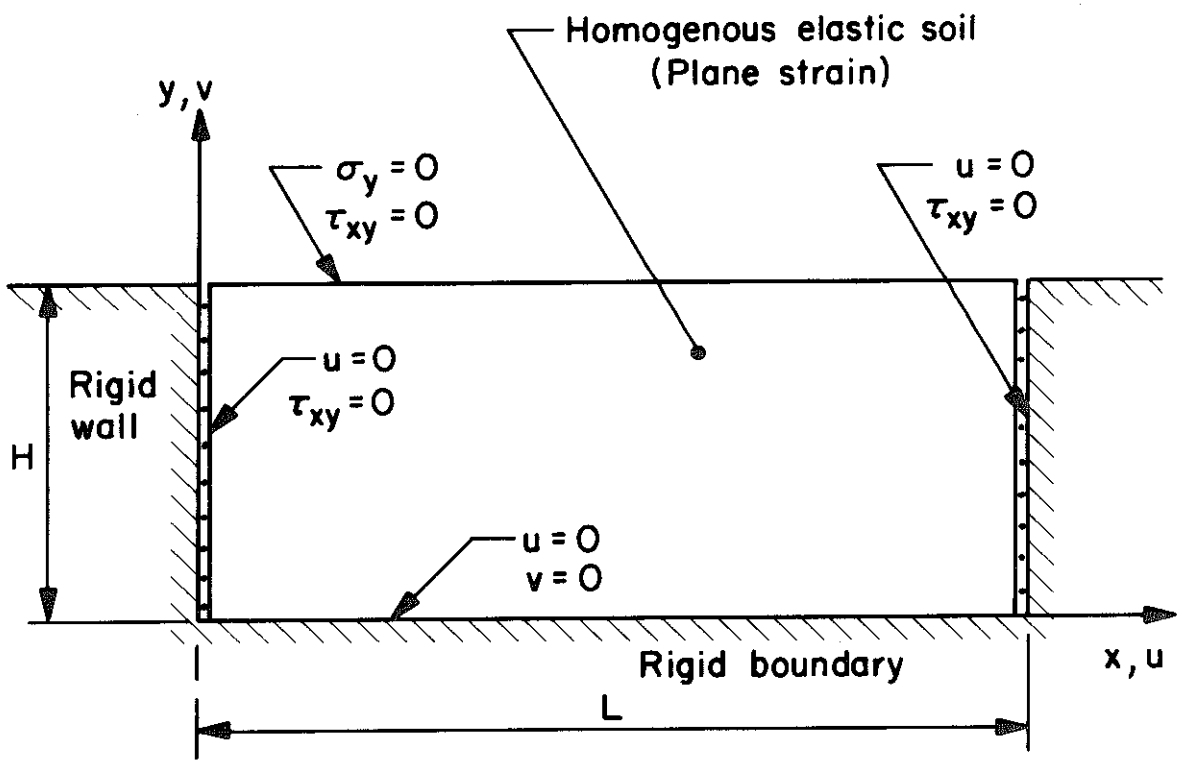

RIGID WALL PROBLEM

Figure 3.1

$$\frac{\partial^2 u(x,y,t)}{\partial x^2} + \frac{(k^2-1)}{k^2}\frac{\partial^2 v(x,y,t)}{\partial x\,\partial y} + \frac{1}{k^2}\frac{\partial^2 u(x,y,t)}{\partial y^2} = \frac{1}{V_d^2}\frac{\partial^2 u(x,y,t)}{\partial t^2}$$

$$\frac{\partial^2 v(x,y,t)}{\partial x^2} + (k^2-1)\frac{\partial^2 u(x,y,t)}{\partial x\,\partial y} + k^2\frac{\partial^2 v(x,y,t)}{\partial y^2} = \frac{1}{V_s^2}\frac{\partial^2 v(x,y,t)}{\partial t^2} \qquad (3.1)$$

$$0 < x < L\,; \qquad 0 < y < H\,; \qquad t > 0$$

in which

t = time

$$k^2 = \frac{V_d^2}{V_s^2}$$

The problem boundary conditions are shown in Fig. 3.1.

For free vibrations the solutions of equations (3.1) can be expressed as

$$u_{n,m}(x,y,t) = \sin rx\ \bar{u}(y)\, e^{i\omega_{n,m}t}$$
$$v_{n,m}(x,y,t) = \cos rx\ \bar{v}(y)\, e^{i\omega_{n,m}t} \qquad (3.2)$$

in which

$u_{n,m}$ = displacement in x-direction of mode n,m

$v_{n,m}$ = displacement in y-direction of mode n,m

$\omega_{n,m}$ = natural angular frequency of mode n,m

$r = \frac{n\pi}{L}$

n = 1,2,3,..., mode type integer

m = 1,2,3,..., mode order integer

$i = \sqrt{-1}$

By inspection it can be seen that expressions (3.2) satisfy the boundary conditions ($u = 0$, $\tau_{xy} = 0$) at $x = 0$ and $x = L$. Substitution of expressions (3.2) into (3.1) gives

$$\frac{\partial^2 \bar{u}(y)}{\partial y^2} - k^2\alpha^2\bar{u}(y) - r(k^2-1)\frac{\partial \bar{v}(y)}{\partial y} = 0$$

$$\frac{\partial^2 \bar{v}(y)}{\partial y^2} - \frac{\beta^2}{k^2}\bar{v}(y) + \frac{r(k^2-1)}{k^2}\frac{\partial \bar{u}(y)}{\partial y} = 0 \qquad (3.3)$$

in which

$$\alpha^2 = r^2 - \frac{\omega_{n,m}^2}{V_d^2}$$

$$\beta^2 = r^2 - \frac{\omega_{n,m}^2}{V_s^2}$$

(α and β have particular values for each mode.) A solution of equations (3.3) that satisfies the boundary condition at $y = 0$ ($u = 0$, $v = 0$) was found to be

$$\bar{u}(y) = C_{n,m}\left(\frac{r}{\alpha}\sinh\alpha y - \frac{\beta}{r}\sinh\beta y\right) + D_{n,m}(\cosh\alpha y - \cosh\beta y)$$

$$\bar{v}(y) = C_{n,m}(-\cosh\alpha y + \cosh\beta y) + D_{n,m}\left(-\frac{\alpha}{r}\sinh\alpha y + \frac{r}{\beta}\sinh\beta y\right) \qquad (3.4)$$

in which

$C_{n,m}, D_{n,m}$ = constants for mode n,m, that can be evaluated by satisfying the boundary conditions at y = H

From the stress-strain relations (equations (2.2))

$$\frac{\tau_{xy}}{G} = \frac{\partial u}{\partial y} + \frac{\partial v}{\partial x}$$

$$\frac{\sigma_y}{G} = (k^2-2)\frac{\partial u}{\partial x} + k^2 \frac{\partial v}{\partial y}$$

Thus, the boundary conditions at y = H require that

$$\left.\begin{aligned} \frac{\partial \bar{u}}{\partial y} - r\bar{v} &= 0 \\ r(k^2-2)\bar{u} + k^2 \frac{\partial \bar{v}}{\partial y} &= 0 \end{aligned}\right\} \text{ at } y = H \qquad (3.5)$$

Substitution of expressions (3.4) into (3.5) gives

$$\begin{aligned} &C_{n,m}\left\{2\cosh \alpha H - \left(1 + \frac{\beta^2}{r^2}\right)\cosh \beta H\right\} \\ &\quad + D_{n,m}\left\{2\frac{\alpha}{r}\sinh \alpha H - \left(\frac{\beta}{r} + \frac{r}{\beta}\right)\sinh \beta H\right\} = 0 \\ &C_{n,m}\left\{\left(\frac{r}{\alpha}(k^2-2) - \frac{\alpha k^2}{r}\right)\sinh \alpha H + 2\frac{\beta}{r}\sinh \beta H\right\} \\ &\quad + D_{n,m}\left\{\left((k^2-2) - \frac{\alpha^2 k^2}{r^2}\right)\cosh \alpha H + 2\cosh \beta H\right\} = 0 \end{aligned} \qquad (3.6)$$

For non-trivial solutions of equations (3.6) the determinant of the coefficients of $C_{n,m}$ and $D_{n,m}$ must vanish. Evaluating the determinant and equating it to zero gives

$$\left\{4\beta\alpha + \frac{(r^2+\beta^2)^2}{\alpha\beta}\right\} \sinh \alpha H \sinh \beta H$$

$$- \left\{4r^2 + \frac{(r^2+\beta^2)^2}{r^2}\right\} \cosh \alpha H \cosh \beta H + 4(r^2+\beta^2) = 0 \quad (3.7)$$

Equation (3.7) is the frequency equation for the problem.* This equation was derived by Bycroft[5] in a study of the forced vibrations of a rigid disc resting on an infinite elastic stratum but was not used in the development of his main results and apparently has not been previously evaluated.

The solutions of the frequency equation give the natural frequencies of the system. The ratio of the constants $C_{n,m}$ and $D_{n,m}$ can be found from equations (3.6) for each frequency equation solution and thus the modal displacement functions, expressions (3.4), can be determined to within an arbitrary constant.

A degenerate form of the solution exists which has displacements constant with respect to the x-direction. This solution represents the pure vertical-dilitation modes.

The degenerate solution is of the form

$$u_{0,m}(y,t) = 0$$

$$v_{0,m}(y,t) = A_{0,m} \sin \frac{\omega_{0,m}\, y}{V_d}\; e^{i\omega_{0,m} t} \quad (3.8)$$

*It is readily shown that this equation is the frequency equation for elastic wave propagation in an infinite elastic stratum bonded to a rigid foundation. The equation is analogous to the well known Rayleigh-Lamb frequency equation for plates. In a form used by Miklowitz[36], the Rayleigh-Lamb equation for a plate of thickness 2h is

$$(r^2+\beta^2)^2 \cosh \alpha h \sinh \beta h - 4r^2 \alpha\beta \cosh \beta h \sinh \alpha h = 0$$

in which

$A_{0,m}$ is a constant for mode $0,m$

Expressions (3.8) satisfy the boundary conditions at $x = 0$, $x = L$, and at $y = 0$. To satisfy the boundary conditions at $y = H$ it is necessary that

$$\omega_{0,m} = \frac{(2m-1)\pi V_d}{2H} , \quad m = 1,2,3,... \tag{3.9}$$

Equation (3.9) gives the natural frequencies for this form of the solution. The modal displacements can be expressed as

$$\begin{aligned} u_{0,m} &= 0 \\ v_{0,m} &= A_{0,m} \sin \frac{(2m-1)\pi y}{2H} \; e^{i\omega_{0,m}t} \end{aligned} \tag{3.10}$$

The complete set of natural frequencies for the problem are given by the solutions of expressions (3.7) and (3.9) and the corresponding mode shapes are given by the appropriate evaluations of expressions (3.2) and (3.10).

3.1.1. Numerical Evaluation of Solution

The frequency equation, (3.7), and the displacement functions, (3.4), are even in α and β and so it is immaterial whether these parameters are assigned the positive or negative root. α and β can be either real or imaginary, and thus to facilitate the numerical solution of the frequency equation and the numerical evaluation of the mode shapes, it is convenient for cases when the hyperbolic functions have imaginary arguments to express them as

trigonometric functions, and to write the frequency equation and the displacement solutions in three different forms. It is also convenient to express the solutions in terms of the following dimensionless parameters,

$$R = \frac{n\pi H}{L}$$

$$\Omega_{n,m} = \frac{\omega_{n,m}}{\omega_s} \quad \text{, dimensionless natural frequency for mode } n,m$$

where

$$\omega_s = \frac{\pi V_s}{2H} \quad \text{, natural angular frequency of the fundamental horizontal-shear mode of an infinite elastic stratum}$$

$$\alpha' = \pi \sqrt{\left| \left(\frac{nH}{L}\right)^2 - \frac{\Omega_{n,m}^2}{4k^2} \right|}$$

$$\beta' = \pi \sqrt{\left| \left(\frac{nH}{L}\right)^2 - \frac{\Omega_{n,m}^2}{4} \right|}$$

The displacement solutions and the frequency equation can then be expressed in the following forms:

for $\left(\frac{nH}{L}\right)^2 > \frac{\Omega_{n,m}^2}{4}$

$$u_{n,m} = \sin \frac{n\pi x}{L} \left\{ C_{n,m} \left(\frac{R}{\alpha'} \sinh \frac{\alpha' y}{H} - \frac{\beta'}{R} \sinh \frac{\beta' y}{H} \right) + D_{n,m} \left(\cosh \frac{\alpha' y}{H} - \cosh \frac{\beta' y}{H} \right) \right\} e^{i\omega_{n,m} t} \qquad (3.11)$$

$$v_{n,m} = \cos\frac{n\pi x}{L}\left\{C_{n,m}\left(-\cosh\frac{\alpha' y}{H} + \cosh\frac{\beta' y}{H}\right)\right.$$

$$\left. + D_{n,m}\left(-\frac{\alpha'}{R}\sinh\frac{\alpha' y}{H} + \frac{R}{\beta'}\sinh\frac{\beta' y}{H}\right)\right\} e^{i\omega_{n,m}t}$$

frequency equation:

$$\left\{4\beta'\alpha' + \frac{(R^2+\beta'^2)^2}{\alpha'\beta'}\right\}\sinh\alpha'\sinh\beta'$$

$$- \left\{4R^2 + \frac{(R^2+\beta'^2)^2}{R^2}\right\}\cosh\alpha'\cosh\beta' + 4(R^2+\beta'^2) = 0 \qquad (3.12)$$

for $\dfrac{\Omega_{n,m}^2}{4} > \left(\dfrac{nH}{L}\right)^2 > \dfrac{\Omega_{n,m}^2}{4k^2}$

$$u_{n,m} = \sin\frac{n\pi x}{L}\left\{C_{n,m}\left(\frac{R}{\alpha'}\sinh\frac{\alpha' y}{H} + \frac{\beta'}{R}\sin\frac{\beta' y}{H}\right)\right.$$

$$\left. + D_{n,m}\left(\cosh\frac{\alpha' y}{H} - \cos\frac{\beta' y}{H}\right)\right\} e^{i\omega_{n,m}t} \qquad (3.13)$$

$$v_{n,m} = \cos\frac{n\pi x}{L}\left\{C_{n,m}\left(-\cosh\frac{\alpha' y}{H} + \cos\frac{\beta' y}{H}\right)\right.$$

$$\left. + D_{n,m}\left(-\frac{\alpha'}{R}\sinh\frac{\alpha' y}{H} + \frac{R}{\beta'}\sin\frac{\beta' y}{H}\right)\right\} e^{i\omega_{n,m}t}$$

frequency equation:

$$\left\{-4\beta'\alpha' + \frac{(R^2-\beta'^2)^2}{\alpha'\beta'}\right\}\sinh\alpha'\sin\beta'$$

$$- \left\{4R^2 + \frac{(R^2-\beta'^2)^2}{R^2}\right\}\cosh\alpha'\cos\beta' + 4(R^2-\beta'^2) = 0 \qquad (3.14)$$

for $\dfrac{\Omega_{n,m}^2}{4k^2} > \left(\dfrac{nH}{L}\right)^2$

$$u_{n,m} = \sin\frac{n\pi x}{L}\left\{C_{n,m}\left(\frac{R}{\alpha'}\sin\frac{\alpha' y}{H} + \frac{\beta'}{R}\sin\frac{\beta' y}{H}\right)\right.$$
$$\left. + D_{n,m}\left(\cos\frac{\alpha' y}{H} - \cos\frac{\beta' y}{H}\right)\right\} e^{i\omega_{n,m}t}$$

$$v_{n,m} = \cos\frac{n\pi x}{L}\left\{C_{n,m}\left(-\cos\frac{\alpha' y}{H} + \cos\frac{\beta' y}{H}\right)\right.$$
$$\left. + D_{n,m}\left(\frac{\alpha'}{R}\sin\frac{\alpha' y}{H} + \frac{R}{\beta'}\sin\frac{\beta' y}{H}\right)\right\} e^{i\omega_{n,m}t} \qquad (3.15)$$

frequency equation:

$$\left\{4\beta'\alpha' + \frac{(R^2-\beta'^2)^2}{\alpha'\beta'}\right\}\sin\alpha'\sin\beta'$$
$$-\left\{4R^2 + \frac{(R^2-\beta'^2)^2}{R^2}\right\}\cos\alpha'\cos\beta' + 4(R^2-\beta'^2) = 0 \qquad (3.16)$$

The special cases of $\alpha' = 0$ and $\beta' = 0$ (that is, $(nH/L)^2 = \Omega_{n,m}^2/4k^2$, and $(nH/L)^2 = \Omega_{n,m}^2/4$) can be readily derived from the above expressions by taking the limits, $\alpha' \to 0$ and $\beta' \to 0$.

Recalling that $k^2 = \dfrac{2(1-\nu)}{(1-2\nu)}$, it can be seen that the frequency equation, written in terms of the dimensionless parameters, has solutions dependent on the value of Poisson's ratio ν and independent of the other elastic constants. (The natural frequencies, expressed in dimensional form, depend on E or G because of the dependence of ω_s on E or G.) The roots of the frequency equations (3.12), (3.14) and (3.16) were numerically evaluated

using Newton's method on the digital computer. The method was applied by selecting a particular value of the parameter $\frac{L}{nH}$ and incrementing the dimensionless frequency through the range 1.0 to 12.0, iteratively computing the roots indicated by sign changes in the frequency equations.

Plots of the frequency equation solutions for a range of Poisson's ratio between 0.2 and 0.5 are presented in Figs 3.2, 3.3 and 3.4. As the parameter $\frac{L}{nH} \rightarrow \infty$, the dimensionless frequencies $\Omega_{n,m}$ become asymptotic to the pure horizontal-shear and vertical-dilitation frequencies of the infinite elastic stratum. That is, $\Omega_{n,m}$ is asymptotic to the values 1, 3, 5,..., and k(1,3,5,...). Numerical values of the frequencies of typical modes, computed for a range of $\frac{L}{H}$ and ν parameters, are given in Appendices III and VI. Details of typical mode shapes are tabulated and plotted in Appendix III. (Also see Fig. 3.15.)

3.2. HORIZONTAL FORCING

The analytical normal mode solution given in the previous section can be conveniently used to compute the wall pressure distribution and force responses to an arbitrarily time-varying horizontal acceleration of the rigid boundaries. The forced boundary problem is shown in Fig. 3.5. It is convenient to approach this problem by using d'Alembert's principle to replace the boundary forcing by a uniform horizontal time-varying body force within the elastic soil. With the addition of the d'Alembert forcing, the equations of motion become

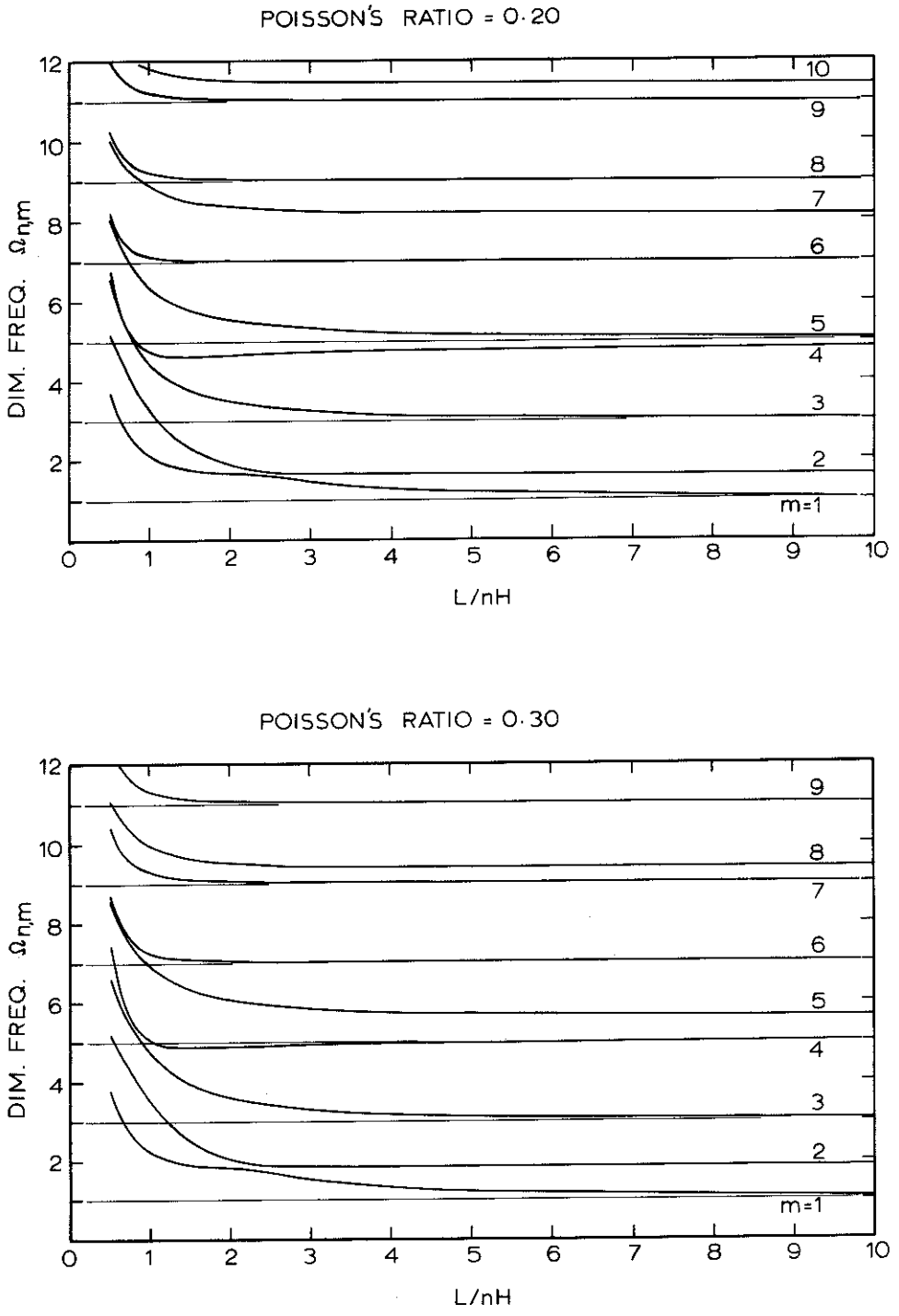

Figure 3.2 Frequency equation solution.

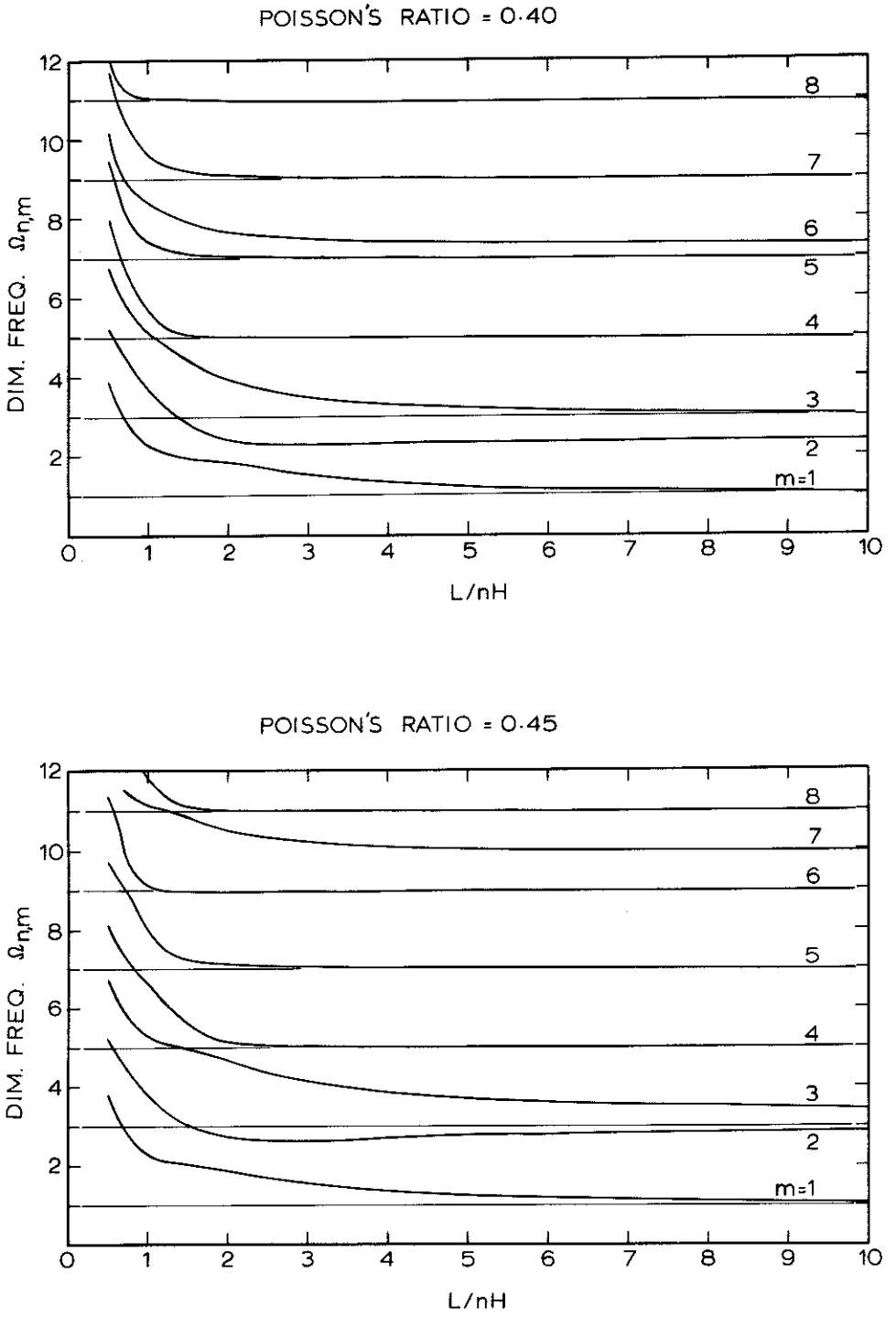

Figure 3.3 Frequency equation solution.

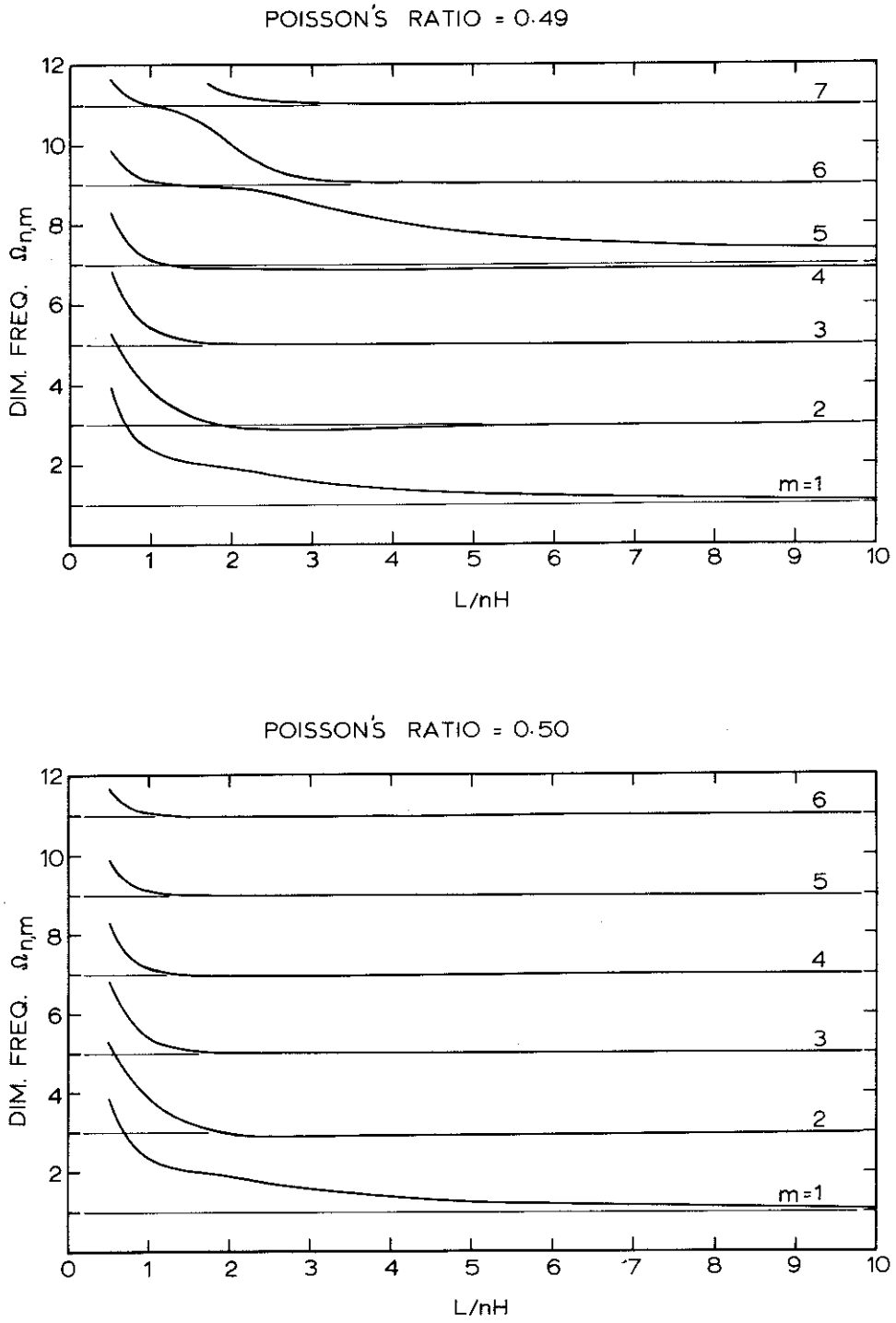

Figure 3.4 Frequency equation solution.

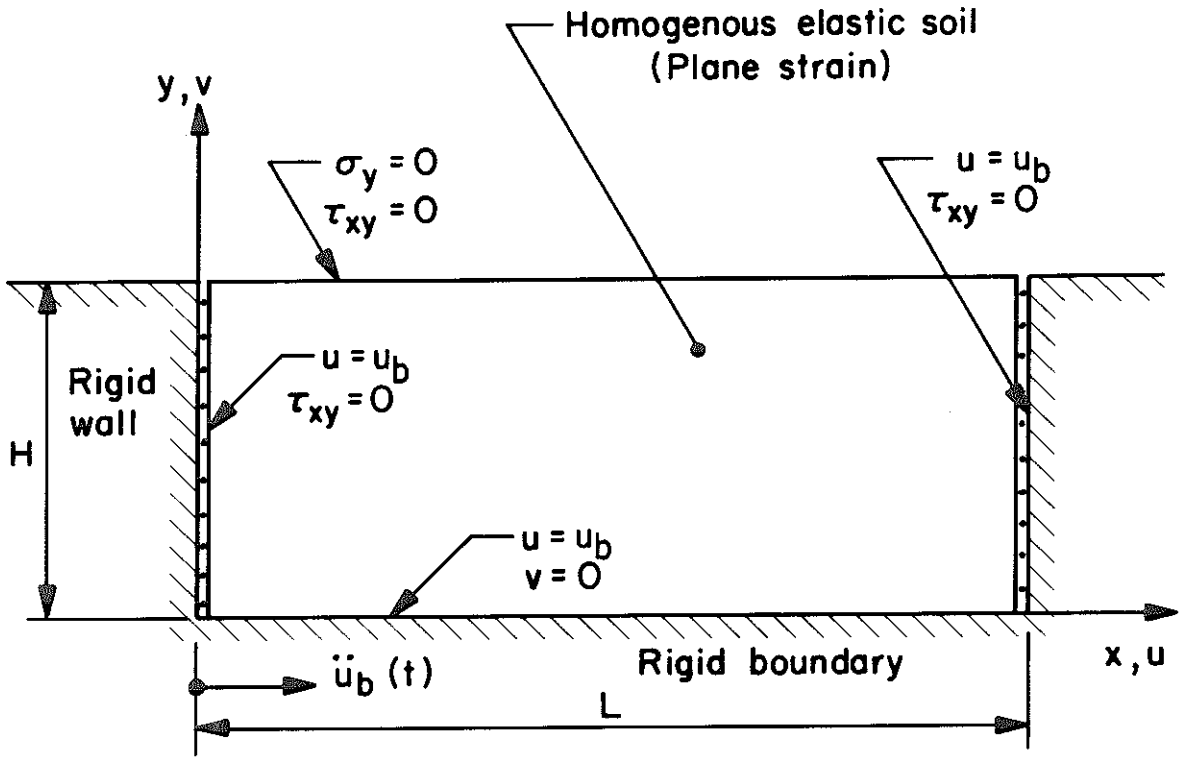

RIGID WALL PROBLEM

Figure 3.5 Horizontal forcing on rigid boundaries.

$$G\left\{k^2 \frac{\partial^2 u(x,y,t)}{\partial x^2} + (k^2-1) \frac{\partial^2 v(x,y,t)}{\partial x \partial y} + \frac{\partial^2 u(x,y,t)}{\partial y^2}\right\}$$

$$= \rho \frac{\partial^2 u(x,y,t)}{\partial t^2} + \rho \frac{\partial^2 u_b(t)}{\partial t^2}$$

$$G\left\{\frac{\partial^2 v(x,y,t)}{\partial x^2} + (k^2-1) \frac{\partial^2 u(x,y,t)}{\partial x \partial y} + k^2 \frac{\partial^2 v(x,y,t)}{\partial y^2}\right\} \qquad (3.17)$$

$$= \rho \frac{\partial^2 v(x,y,t)}{\partial t^2}$$

in which

ρ = mass density of soil

$u_b(t)$ = displacement in x-direction of rigid boundary

The effects of dissipation within the system can be approximated by the addition of viscous damping terms in the analysis. Dissipation will result from nonlinear behavior within the soil structure and from the radiation of energy from the system owing to the fact that in general the boundaries are not perfectly rigid. Damping within the soil structure probably results mainly from sliding at the points of contact of the soil grains. Discussions of this type of damping and experimentally determined values are given by Seed and Idriss[49], Kovacs, Seed and Chan[26], and Hardin and Drnevich[11,12]. Further research regarding the most appropriate mathematical formulation of the total damping is required but it appears reasonable to expect that the method of representing the dissipation will not have a significant influence on the results presented here.

With the addition of viscous damping terms, the equations of motion may be written in vector form as

$$L\underline{u}(x,y,t) = \rho\ddot{\underline{u}}(x,y,t) + c\dot{\underline{u}}(x,y,t) + \rho\ddot{\underline{u}}_b(t) \tag{3.18}$$

in which

L = linear operator with respect to the spatial coordinates

$\underline{u}(x,y,t) = \begin{Bmatrix} u(x,y,t) \\ v(x,y,t) \end{Bmatrix}$, vector of the displacement components u and v

$\underline{u}_b(t) = \begin{Bmatrix} u_b(t) \\ 0 \end{Bmatrix}$, vector of displacements on the rigid boundary

c = damping coefficient

The dots above the symbols denote differentiation with respect to time.

Equations (3.18) may be solved by the standard normal mode expansion technique.* Because the normal modes form a complete set of functions, the solution can be expressed as

$$\underline{u}(x,y,t) = \sum_{\substack{n=1 \\ m=1}}^{\infty} Q_{n,m}(t)\, \underline{\phi}_{n,m}(x,y) \tag{3.19}$$

in which

$Q_{n,m}(t)$ = participation coefficient for mode n,m

$\underline{\phi}_{n,m}(x,y)$ = mode shape for mode n,m

*Frazier and Roberts[10] give a detailed account of the application of this method in a study of the dynamics of soil layers.

Substitution of expression (3.19) into (3.18) gives

$$\sum_{\substack{n=1\\m=1}}^{\infty} Q_{n,m}(t) L\underline{\phi}_{n,m}(x,y) = \sum_{\substack{n=1\\m=1}}^{\infty} \left\{ \rho \ddot{Q}_{n,m}(t) + c\dot{Q}_{n,m}(t) \right\} \underline{\phi}_{n,m}(x,y) + \rho \ddot{\underline{u}}_b(t) \quad (3.20)$$

From the equations of motion for free undamped vibrations

$$L\underline{\phi}_{n,m}(x,y) = - \rho \omega^2_{n,m} \underline{\phi}_{n,m}(x,y) \quad (3.21)$$

For convenience let the damping coefficient be expressed as

$$c = 2\rho \omega_{n,m} \zeta_{n,m} \quad (3.22)$$

in which

$\zeta_{n,m}$ = fraction of critical damping in mode n,m

Substitution of expressions (3.21) and (3.22) into (3.20) gives

$$-\rho \sum_{\substack{n=1\\m=1}}^{\infty} \left\{ \ddot{Q}_{n,m}(t) + 2\omega_{n,m}\zeta_{n,m}\dot{Q}_{n,m}(t) + \omega^2_{n,m} Q_{n,m}(t) \right\} \underline{\phi}_{n,m}(x,y) = \rho \ddot{\underline{u}}_b(t) \quad (3.23)$$

The uncoupled equation of motion for each of the modal participitation coefficients can be derived by forming the dot product of equation (3.23) with a particular mode, integrating over the volume and employing the orthogonal property of the modes. On the assumption of

uniform soil density these equations of motion can be expressed as

$$\ddot{Q}_{n,m}(t) + 2\omega_{n,m}\zeta_{n,m}\dot{Q}_{n,m}(t) + \omega^2_{n,m}Q_{n,m}(t)$$

$$= \frac{-\ddot{u}_b(t)\int_V u_{n,m}(x,y)\, dV}{\int_V \underline{\phi}_{n,m}(x,y)\cdot\underline{\phi}_{n,m}(x,y)\, dV} \qquad (3.24)$$

in which

$u_{n,m}(x,y)$ = displacement component in x-direction of mode $\underline{\phi}_{n,m}$

V = volume

The solution of equation (3.24) for zero initial conditions is given by

$$Q_{n,m}(t) = \frac{-\int_V u_{n,m}(x,y)\, dV}{\int_V \underline{\phi}_{n,m}\cdot\underline{\phi}_{n,m}\, dV}$$

$$x \frac{\int_0^t \ddot{u}_b(\tau)\, e^{-\zeta_{n,m}\omega_{n,m}(t-\tau)} \sin\omega_{n,m}\sqrt{1-\zeta^2_{n,m}}(t-\tau)\, d\tau}{\omega_{n,m}\sqrt{1-\zeta^2_{n,m}}} \qquad (3.25)$$

Let

$$P_{n,m} = \frac{-g}{\omega^2_{n,m}} \frac{\int_V u_{n,m}\, dV}{\int_V \underline{\phi}_{n,m}\cdot\underline{\phi}_{n,m}\, dV} \qquad (3.26)$$

$P_{n,m}$ is called "the static-one-g modal participation factor for mode n,m." Let

$$PA_{n,m}(t) = \omega^2_{n,m}D_{n,m}(t) \qquad (3.27)$$

in which

$$D_{n,m}(t) = \frac{1}{\omega_{n,m}\sqrt{1-\zeta_{n,m}^2}} \int_0^t \frac{\ddot{u}_b(\tau)}{g} e^{-\zeta_{n,m}\omega_{n,m}(t-\tau)} \times \sin \omega_{n,m}\sqrt{1-\zeta_{n,m}^2}(t-\tau)\, d\tau,$$

the relative displacement response of a single degree-of-freedom oscillator, with undamped natural angular frequency $\omega_{n,m}$ and fraction of critical damping $\zeta_{n,m}$, to a base excitation $\ddot{u}_b(t)/g$

$PA_{n,m}(t)$ is called "the pseudo-acceleration response for mode n,m." Thus, the complete solution of equation (3.18) can be expressed as

$$\underline{u}(x,y,t) = \sum_{\substack{n=1 \\ m=1}}^{\infty} P_{n,m} PA_{n,m}(t)\, \underline{\phi}_{n,m}(x,y) \tag{3.28}$$

From the stress-strain relations (equations (2.2)) the normal stress on the wall can be expressed as

$$\sigma_x(0,y,t) = L_p \underline{u}(x,y,t) \tag{3.29}$$

in which

L_p = a linear operator with respect to the spatial coordinates

Thus the normal pressure distribution on the wall, resulting from an arbitrarily time-varying horizontal acceleration of the rigid boundaries, can be expressed as

$$\sigma_x(0,y,t) = \sum_{\substack{n=1 \\ m=1}}^{\infty} p_{n,m}(y) PA_{n,m}(t) \qquad (3.30)$$

in which

$$p_{n,m}(y) = P_{n,m} L_{p\phi_{n,m}}(x,y),$$

the static-one-g modal wall pressure distribution for mode n,m

$P_{n,m}$ can be readily evaluated from the modal displacement functions, expressions (3.11), (3.13) and (3.15), by performing the appropriate volume integrations indicated in expression (3.26). It is possible to express the required integrations in closed form and details of these expressions are given in Appendix IV. The operations, $L_{p\phi_{n,m}}(x,y)$, can be readily evaluated by the appropriate differentiations of the modal displacement functions. The expressions obtained are given in Appendix V. It is of interest to note that for either horizontal or vertical forcing of the rigid boundaries the participation factors, $P_{n,m}$, are zero for the symmetrical modes, that is for even values of n. The pure vertical-dilitation modes, represented by n = 0, have zero participation for horizontal forcing of the rigid boundaries but have significant contribution in the response to vertical forcing.

The evaluation of expression (3.30) can be carried out by computing by numerical methods the time-history of the modal pseudo-accelerations for each significant mode and performing the required summation at suitable time intervals. In view

of the uncertainties inherent in the estimation of earthquake-induced pressures on walls, computation of the response time-history is probably not warranted and approximate evaluations of expression (3.30) may often be satisfactory. The Response Spectrum method of obtaining approximate values of the maximum response is discussed in Section 3.7.

The static solution of the problem studied in Section 2.1 can be represented in a different form by using a modal expansion technique similar to the method used here for the forced dynamic solution. It is informative to show the relationship between this representation of the static solution and the forced dynamic solution. Equations (2.3) can be written as

$$L\underline{u}(x,y) + \underline{F} = \underline{0} \tag{3.31}$$

in which

$$\underline{F} = \begin{Bmatrix} F_x \\ F_y \end{Bmatrix} = \begin{Bmatrix} -\gamma \\ 0 \end{Bmatrix} \text{ , the body force vector}$$

The solution of equation (3.31) can be expressed as

$$\underline{u}(x,y) = \sum_{\substack{n=1 \\ m=1}}^{\infty} Q'_{n,m} \underline{\phi}_{n,m}(x,y) \tag{3.32}$$

in which

$Q'_{n,m}$ = static participation coefficient for mode n,m

Substitution of expression (3.32) into (3.31), and elimination of the spatial operator L by use of expression (3.21) gives

$$\rho \sum_{\substack{n=1 \\ m=1}}^{\infty} Q'_{n,m} \omega^2_{n,m} \underline{\phi}_{n,m}(x,y) = \underline{F} \tag{3.33}$$

By forming the dot product of equation (3.33) with a particular mode, integrating over the volume and employing the orthogonal property of the modes, the expressions for the participation coefficients are found to be

$$Q'_{n,m} = \frac{-\gamma}{\omega^2_{n,m}} \quad \frac{\int_V \underline{u}_{n,m}(x,y)\, dV}{\int_V \rho \underline{\phi}_{n,m}(x,y) \cdot \underline{\phi}_{n,m}(x,y)\, dV} \tag{3.34}$$

Thus for uniform soil density, the static displacement solution can be expressed as

$$\underline{u}(x,y) = \sum_{\substack{n=1 \\ m=1}}^{\infty} P_{n,m} \underline{\phi}_{n,m}(x,y) \tag{3.35}$$

The normal stress on the wall for the one-g static horizontal body force can hence be expressed as

$$\sigma_x(0,y) = \sum_{\substack{n=1 \\ m=1}}^{\infty} p_{n,m}(y) \tag{3.36}$$

The simple relationship between the dynamic pressure distribution and the static solution can be seen by comparison of expressions (3.30) and (3.36). The modal pressure distribution, $p_{n,m}(y)$, is called in this study "the static-one-g modal pressure distribution for mode n,m."

The modal summation method of computing the static solution was used as a method of checking the analytical normal mode solution. Although this approach provided a convenient check it was found that for $\frac{L}{H}$ values greater than 5,convergence was relatively poor. Static solutions solved by this method require considerably more computation time than solutions obtained using the Fourier expansion method presented in Section 2.1.

3.3. STATIC-ONE-g MODAL PRESSURES

Static-one-g modal pressure distributions were evaluated for the smooth rigid wall using the analytical expressions given in Appendix V. Results were computed for a range of $\frac{L}{H}$ and ν values, and typical static-one-g modal pressures are compared with the analytical static solutions for a one-g horizontal body force in Figs. 3.6 to 3.12 inclusive. The pressure distributions are plotted for all the modes that have force contributions greater than 7% of the static force and in a number of cases modes with a smaller contribution are shown. In some of the unplotted higher modes, particularly for ν values 0.45 and 0.5, relatively large pressure values occur but sign changes in the pressure distributions result in a low force contribution. The algebraic sums of the plotted modal pressure contributions are shown, and it can be seen that for each case the modes plotted (five or less) contribute at least 60% of the total static force. For $\frac{L}{H}$ values greater than 10 the number of modes required to give a force summation in reasonable agreement with the static solution increases roughly in proportion to the $\frac{L}{H}$

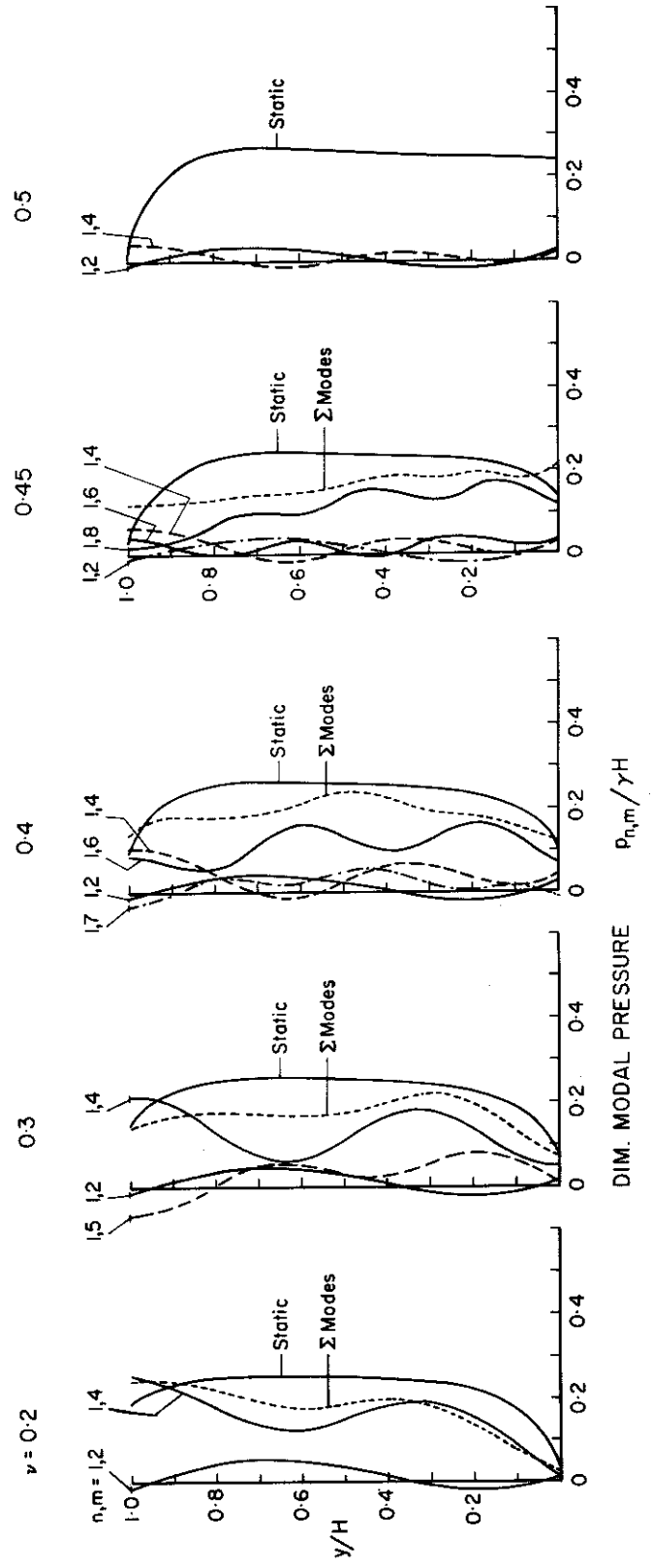

Figure 3.6 Static-one-g modal pressure distributions on smooth rigid wall.

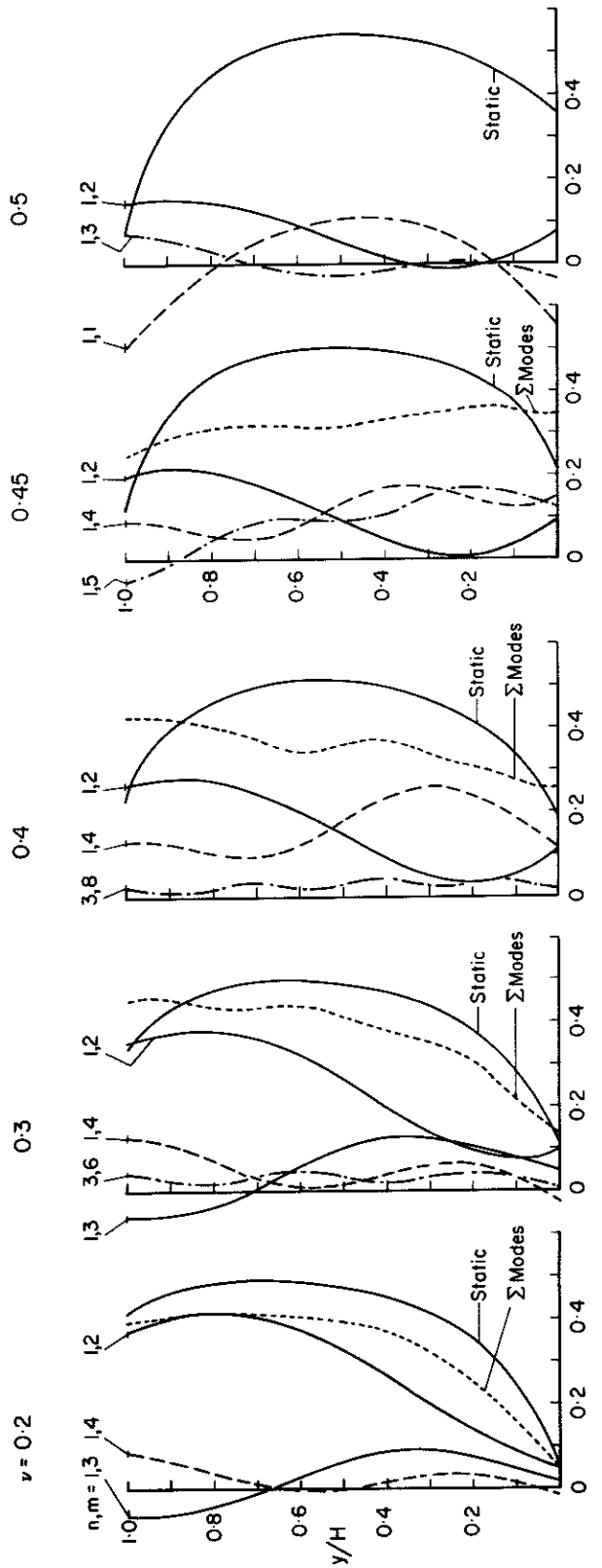

Figure 3.7 Static-one-g modal pressure distributions on smooth rigid wall.

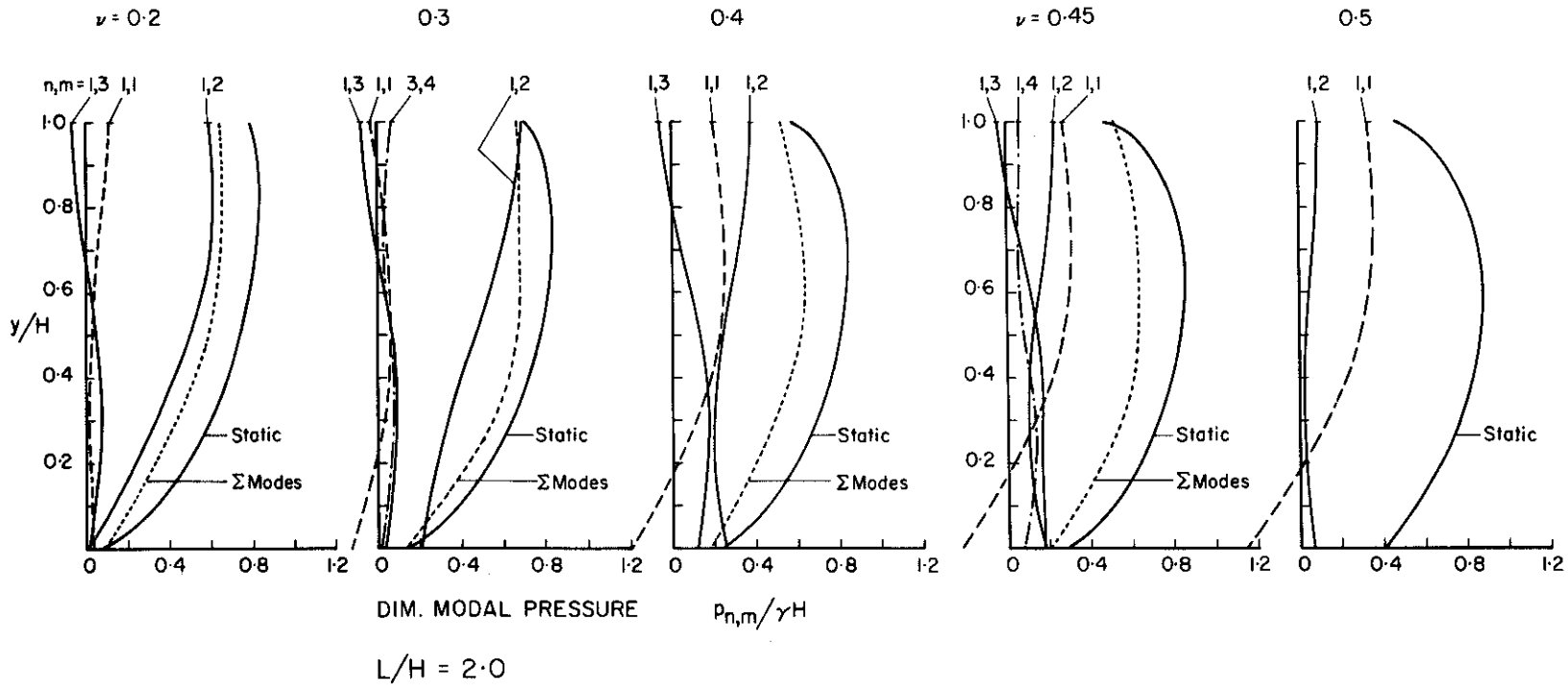

Figure 3.8 Static-one-g modal pressure distributions on smooth rigid wall.

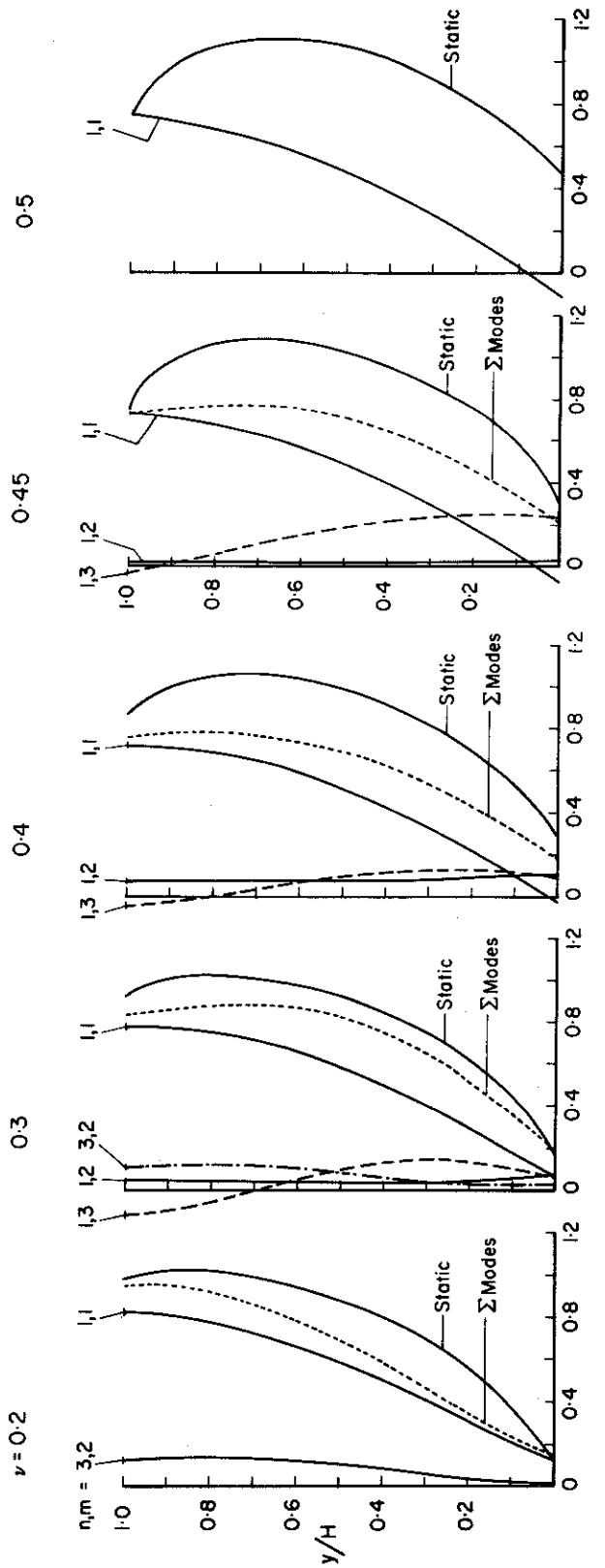

Figure 3.9 Static-one-g modal pressure distributions on smooth rigid wall.

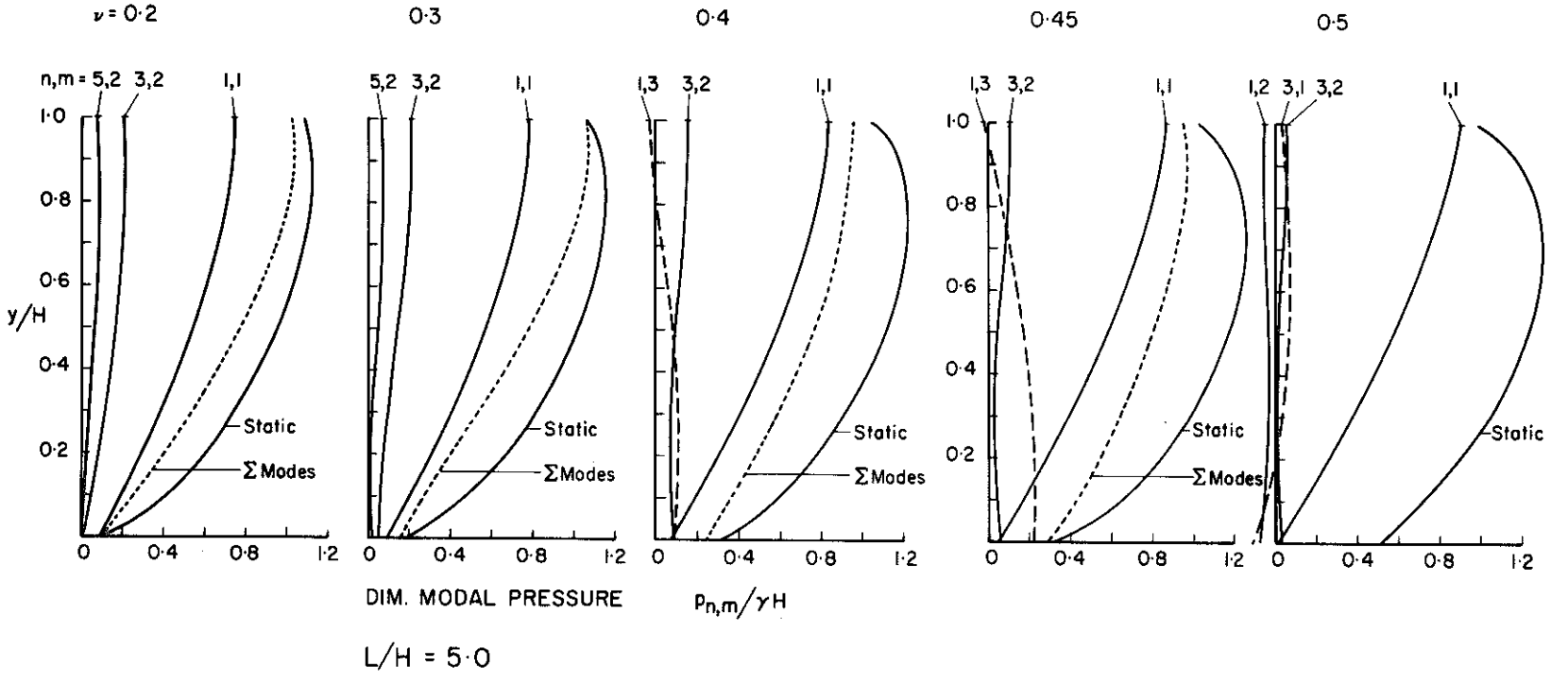

Figure 3.10 Static-one-g modal pressure distributions on smooth rigid wall.

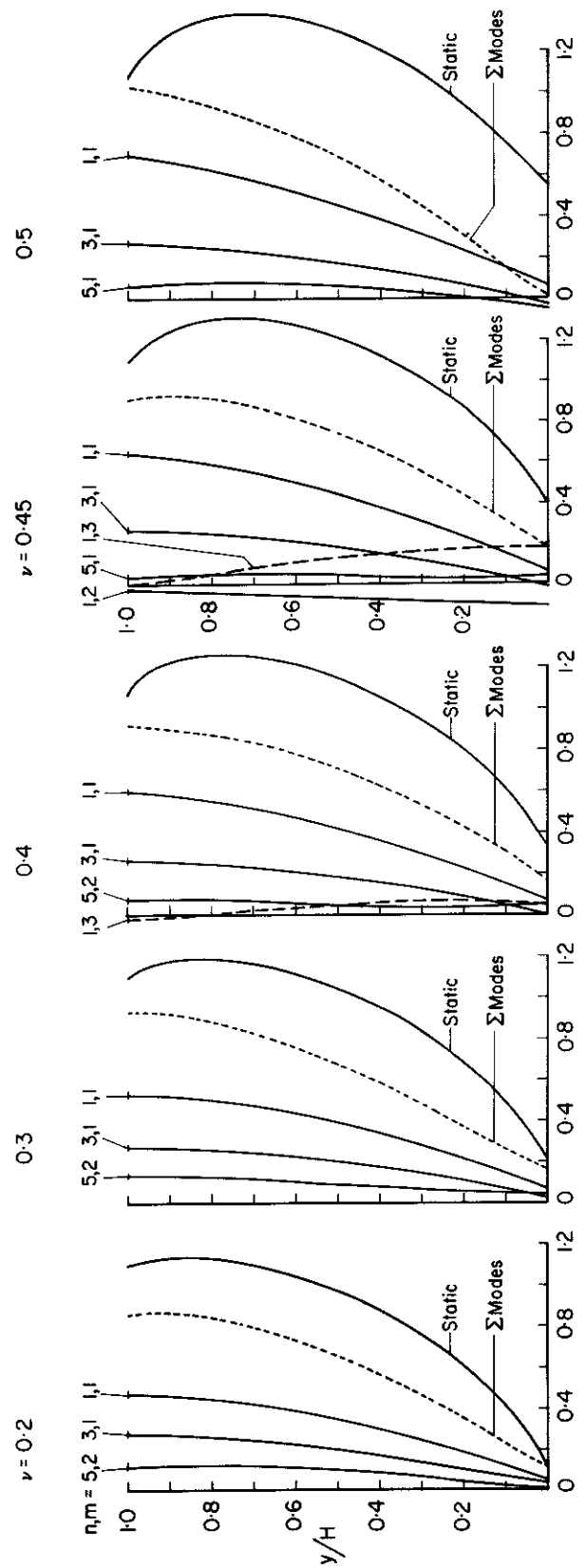

Figure 3.11 Static-one-g modal pressure distributions on smooth rigid wall.

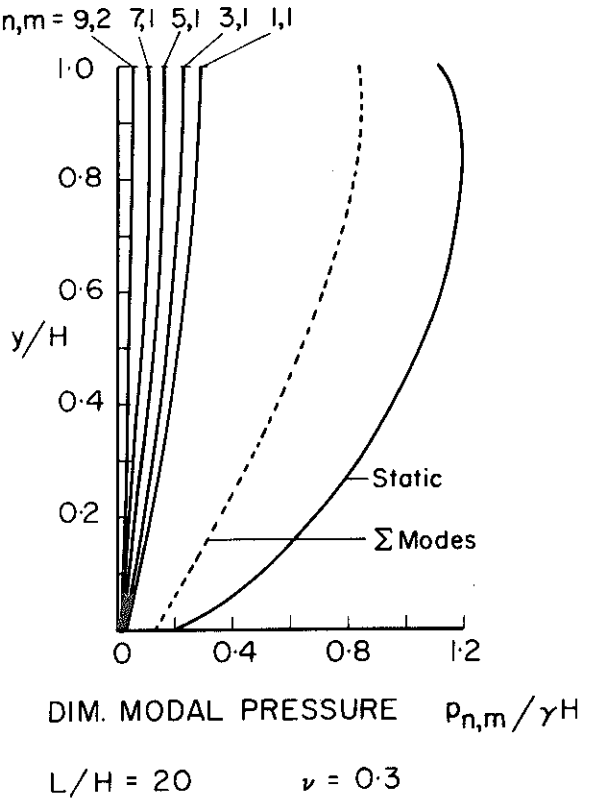

Figure 3.12 Static-one-g modal pressure distributions on smooth rigid wall.

value. Although this would tend to indicate difficulty in computing the dynamic response for large $\frac{L}{H}$ values, a simplifying approximation is presented in Section 3.5 that alleviates this difficulty. For Poisson's ratio equal to 0.5 and for $\frac{L}{H}$ values less than 2 the lower mode force contributions are small. Apparently for these cases a large number of modes contribute to the total static pressure response and a satisfactory approximation for the earthquake-induced pressures can presumably be obtained by using the static solution. The dimensionless natural frequencies, static-one-g modal forces and moments for the plotted pressure distributions and for some of the higher mode distributions are given in Appendix VI.

3.4. STATIC-ONE-g MODAL FORCES

The static-one-g modal force per unit length $F_{n,m}$, and the static-one-g modal moment per unit length $M_{n,m}$ are defined by

$$F_{n,m} = \int_0^H p_{n,m}(y)\, dy$$
$$M_{n,m} = \int_0^H y p_{n,m}(y)\, dy \qquad (3.37)$$

Expressions (3.37) were evaluated for values of Poisson's ratio between 0.3 and 0.5. The static-one-g modal force, expressed in the dimensionless form $\frac{nF_{n,m}}{\gamma H^2}$, is plotted versus the geometric parameter $\frac{L}{nH}$ in Figs. 3.13 and 3.14. For comparison the static force solution is also plotted. The mode type integer n is included

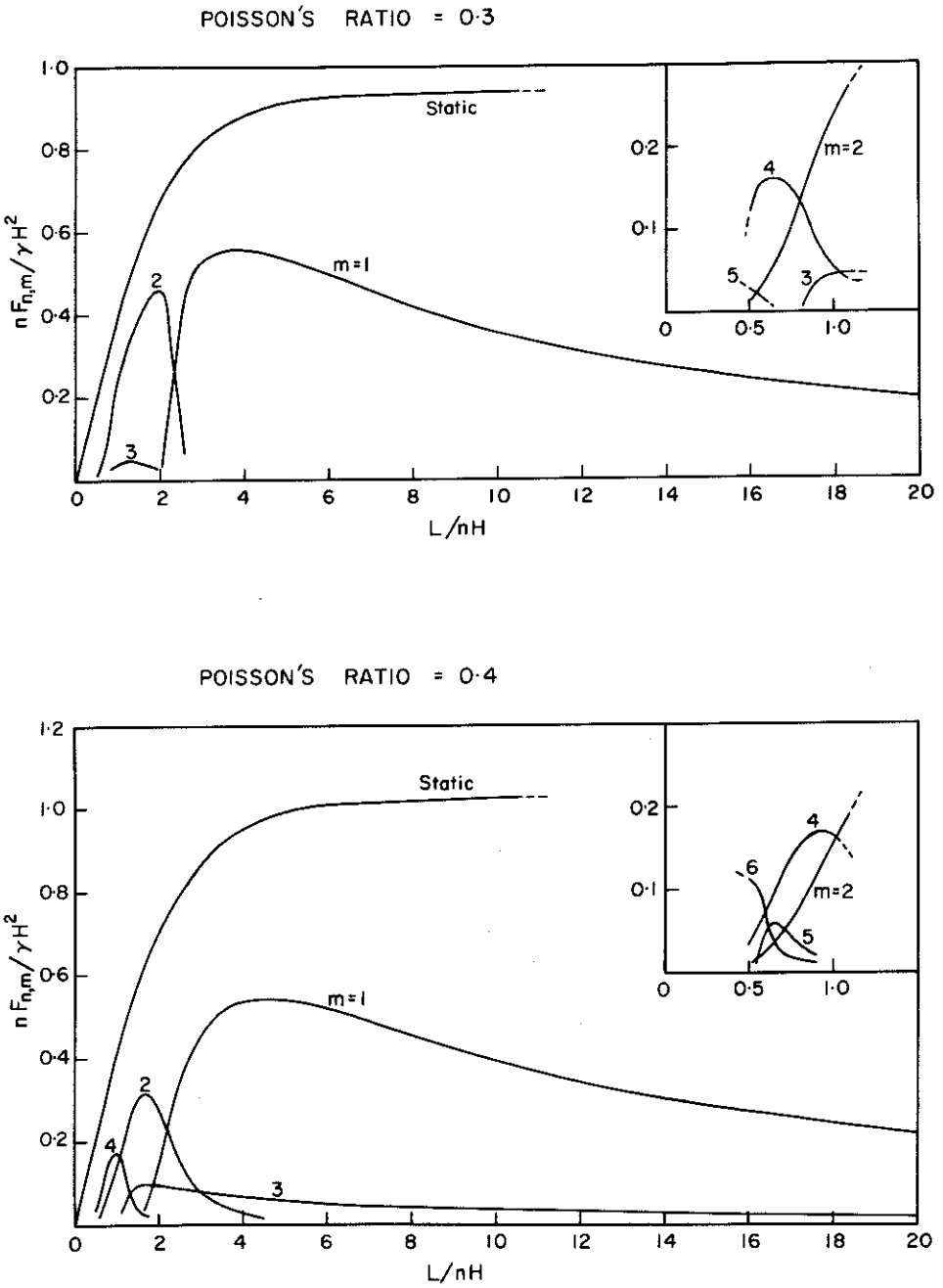

Figure 3.13 Static-one-g modal forces on smooth rigid wall. (Definitions adopted give net compressive forces).

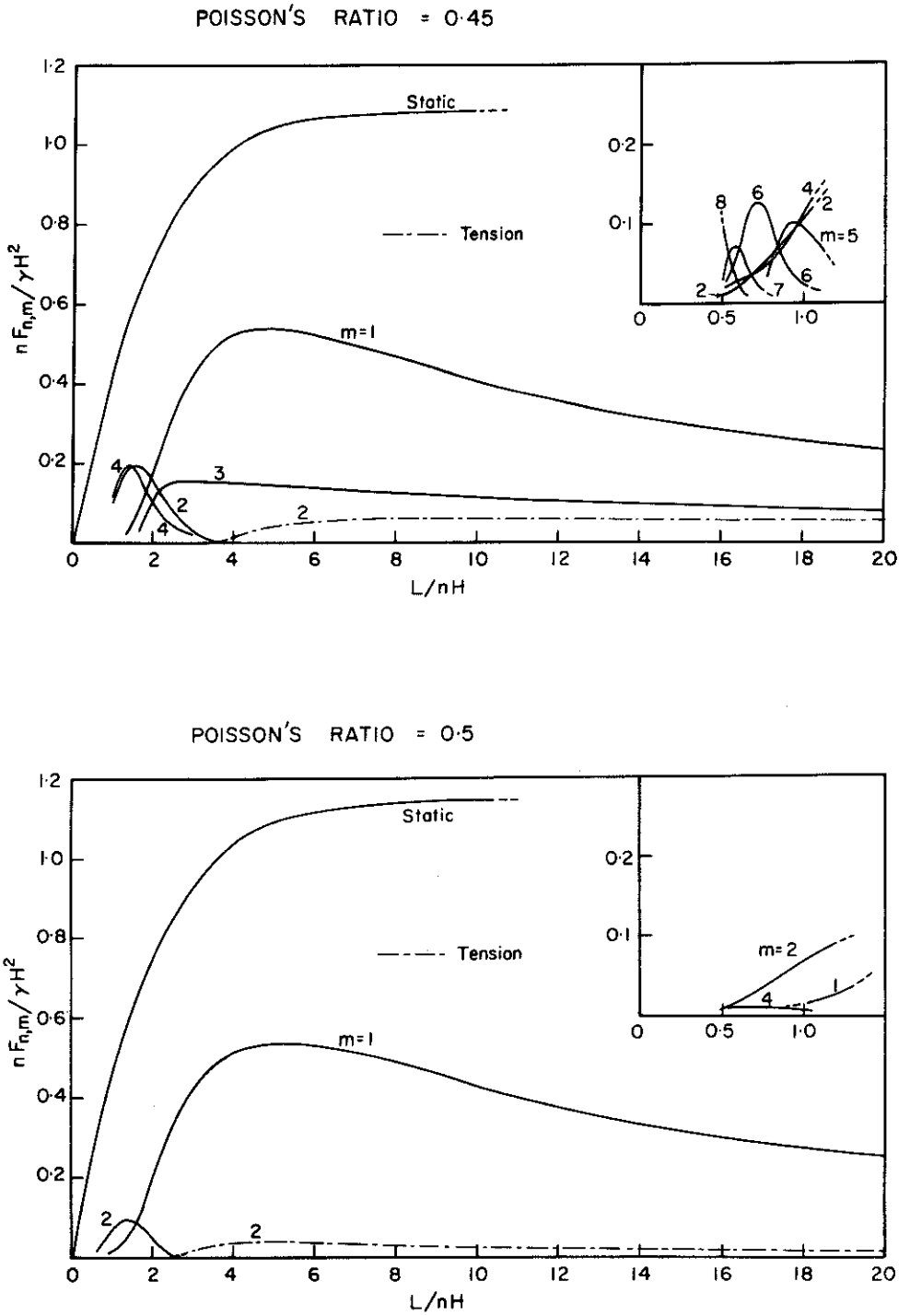

Figure 3.14 Static-one-g modal forces on smooth rigid wall. (Definitions adopted give net compressive forces except as indicated).

in the dimensionless plot ordinates to indicate that a simple relationship exists between the modal forces of modes having a particular m value and any odd value of n. This is best illustrated by stating the following relationship:

$$[\text{Static-one-g modal force for } \frac{L}{H} = a;\ n = b;\ m = c]$$

$$= \frac{1}{b}[\text{Static-one-g modal force for } \frac{L}{H} = \frac{a}{b};\ n = 1;\ m = c]$$

In general the plots show only the modal force values that exceed 5% of the static wall force for the $n = 1$ case. For $\frac{L}{nH}$ values less than 2 the forces exhibit a complex behavior that is sensitive to changes in both Poisson's ratio and $\frac{L}{H}$. The influence of this behavior on the earthquake-induced wall force is more clearly demonstrated by the steady-state solutions for harmonic forcing given in the next section. A feature of interest in the plots is the crossing point between the $m = 1$ and the $m = 2$ modes in the vicinity of $\frac{L}{nH} = 2.0$. Near this point both these modes have relatively similar natural frequencies and so will probably give approximately equal contributions to the total earthquake-induced wall force. In the vicinity of the crossing point the character of the two modes is interchanged, with a conversion between a basically vertical-dilitation and a basically horizontal-shear character. This behavior is illustrated by the mode shapes plotted in Fig. 3.15.

Figs. 3.16 and 3.17 show the variation in the location of the centers of pressure of the modal pressure distributions and can be used to compute the static-one-g modal moments. These

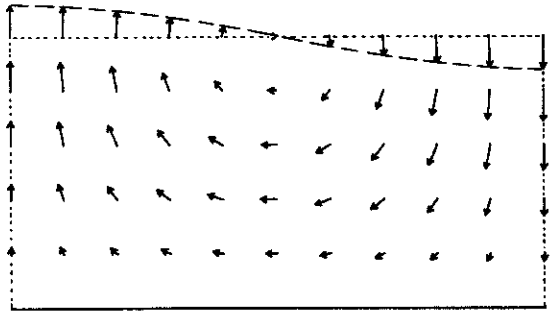

MODE 1,1 L/H = 2.0

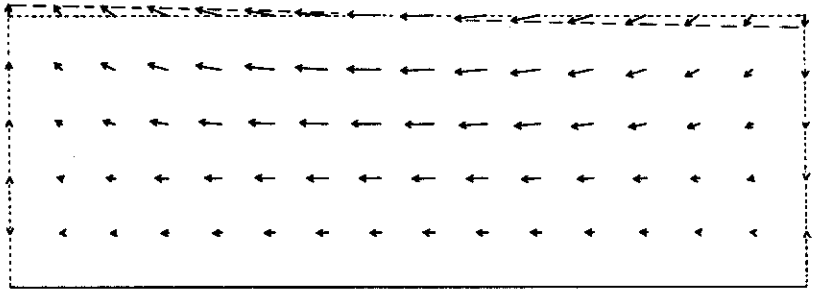

MODE 1,1 L/H = 3.0

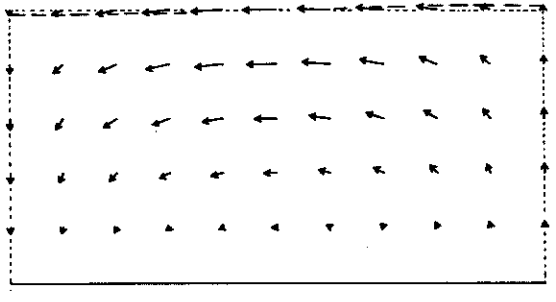

MODE 1,2 L/H = 2.0

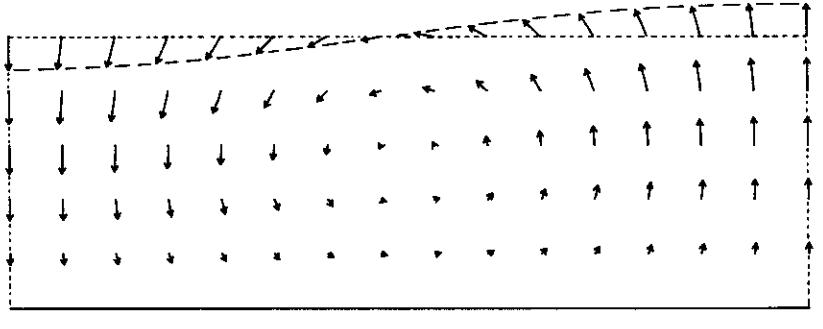

MODE 1,2 L/H = 3.0

Figure 3.15 Mode shapes. L/H = 2.0 and 3.0.
Poisson's ratio = 0.3.

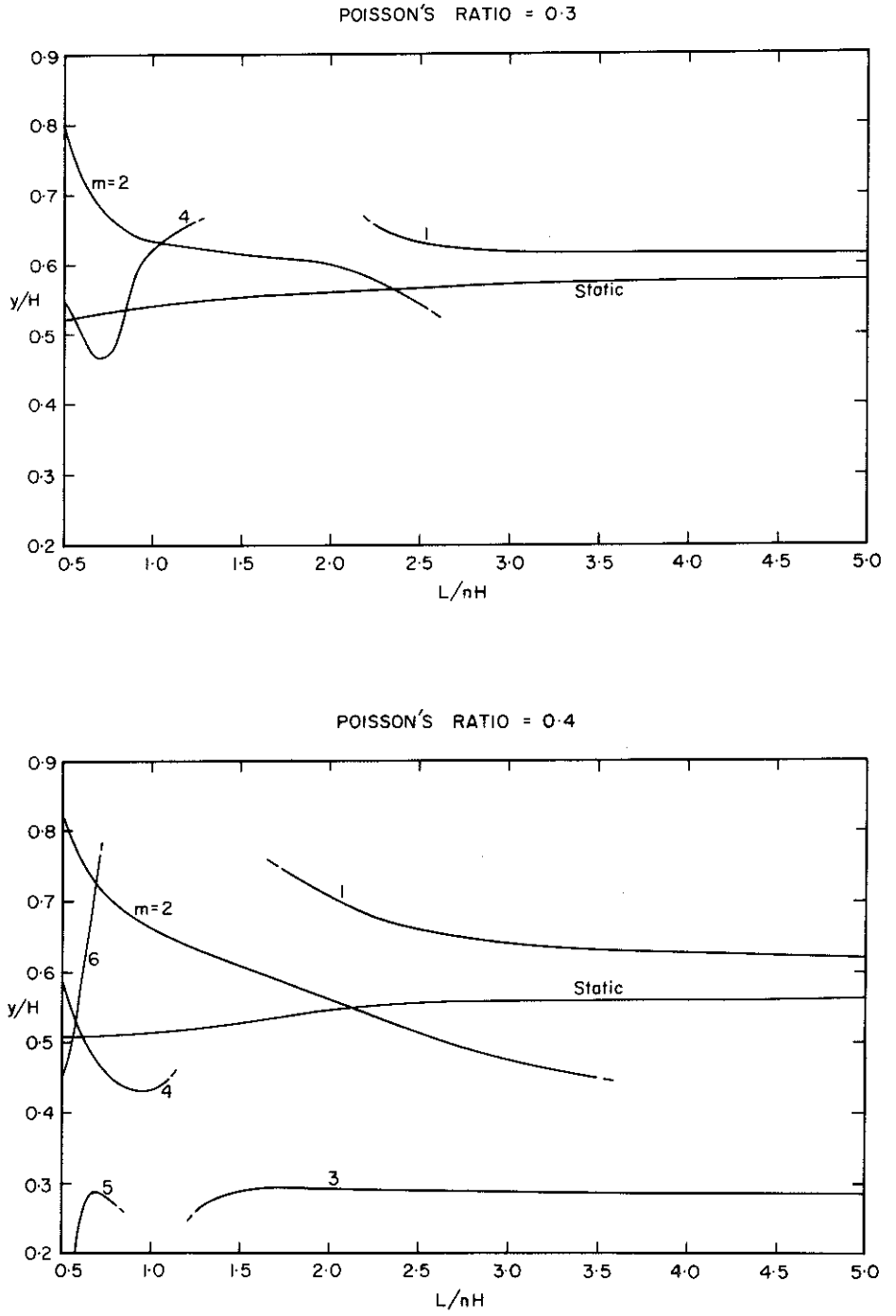

Figure 3.16 Centers of pressure of modal pressure distributions on smooth rigid wall.

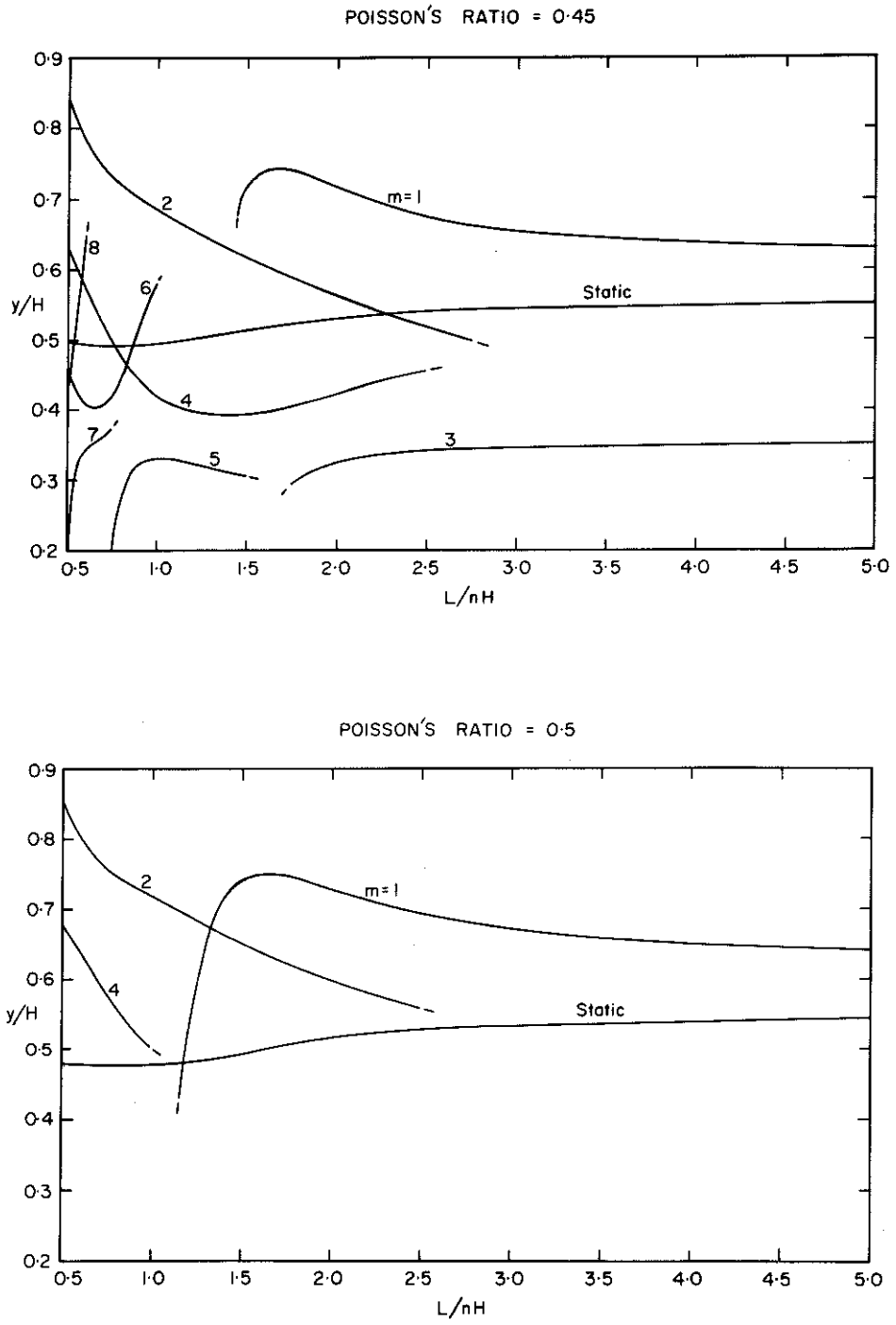

Figure 3.17 Centers of pressure of modal pressure distributions on smooth rigid wall.

curves show only the modes that were previously found to produce at least 5% of the static force on the wall for the $n = 1$ case. By the appropriate choice of n in the parameter $\frac{L}{nH}$, the curves can be used to obtain the centers of pressure for a mode having a plotted m value and any odd n value.

3.5. HARMONIC FORCING

In this section the steady-state solutions are presented for horizontal harmonic forcing of the rigid boundaries of the previously studied smooth rigid-wall problem (Fig. 3.5). These solutions are required in the method used in Section 7.2 to evaluate dynamic solutions for deformable-wall structures. They also give further insight into the dynamic behavior of the rigid-wall problem. A study of the steady-state solutions enabled a convenient two-mode approximation to be formulated for $\frac{L}{H}$ values greater than 10. These cases were previously found to have a relatively large number of modes participating with significant wall force contributions.

For harmonic forcing $\ddot{u}_b e^{i\omega t}$ on the rigid boundaries, the equations of motion governing the modal participation coefficients are found from equation (3.24) to be

$$\ddot{Q}_{n,m}(t) + 2\zeta_{n,m}\omega_{n,m}\dot{Q}_{n,m}(t) + \omega^2_{n,m}Q_{n,m}(t) = \frac{\omega^2_{n,m}P_{n,m}\ddot{u}_b e^{i\omega t}}{g} \qquad (3.38)$$

The steady-state solution of equation (3.38) is given by

$$Q_{n,m}(t) = \frac{P_{n,m}\ddot{u}_b e^{i\omega t}}{g\left\{1 - \frac{\omega^2}{\omega_{n,m}^2} + 2i\zeta_{n,m}\frac{\omega}{\omega_{n,m}}\right\}} \tag{3.39}$$

Substitution of expression (3.39) into (3.19) gives the steady-state displacement response to harmonic forcing as

$$\underline{u}(x,y,t) = \frac{\ddot{u}_b}{g}\sum_{\substack{n=1\\m=1}}^{\infty} \frac{P_{n,m}\underline{\phi}_{n,m}(x,y)e^{i\omega t}}{\left\{\left(1 - \frac{\omega^2}{\omega_{n,m}^2}\right) + 2i\zeta_{n,m}\frac{\omega}{\omega_{n,m}}\right\}} \tag{3.40}$$

The wall pressure distribution response is given by

$$\sigma_x(0,y,t) = \frac{\ddot{u}_b}{g}\sum_{\substack{n=1\\m=1}}^{\infty} \frac{p_{n,m}(y)e^{i\omega t}}{\left\{\left(1 - \frac{\omega^2}{\omega_{n,m}^2}\right) + 2i\zeta_{n,m}\frac{\omega}{\omega_{n,m}}\right\}} \tag{3.41}$$

The complex-amplitudes of steady-state wall force and moment for a one-g-amplitude harmonic base forcing, $\bar{F}'_r(\omega)$ and $\bar{M}'_r(\omega)$, can be expressed in dimensionless form as

$$\frac{\bar{F}'_r(\omega)}{F_{sr}} = \sum_{\substack{n=1\\m=1}}^{\infty} \frac{F_{n,m}/F_{sr}}{\left\{\left(1 - \frac{\omega^2}{\omega_{n,m}^2}\right) + 2i\zeta_{n,m}\frac{\omega}{\omega_{n,m}}\right\}}$$

$$\frac{\bar{M}'_r(\omega)}{M_{sr}} = \sum_{\substack{n=1\\m=1}}^{\infty} \frac{M_{n,m}/M_{sr}}{\left\{\left(1 - \frac{\omega^2}{\omega_{n,m}^2}\right) + 2i\zeta_{n,m}\frac{\omega}{\omega_{n,m}}\right\}} \tag{3.42}$$

in which

F_{sr}, M_{sr} = force and moment respectively on rigid wall for one-g static horizontal loading

Plots of the complex-amplitude ratios, expressions (3.42), are shown in Figs. 3.18 to 3.23 inclusive for $\frac{L}{H}$ values between 1.0 and 50. The real and imaginary parts, and the moduli of both the force and moment ratios are plotted against the dimensionless frequency $\Omega = \frac{\omega}{\omega_s}$. All the modes satisfying the bounds, $\Omega_{n,m} < 10$ and $\frac{L}{nH} \geq 0.333$, were included in the computation of the complex-amplitudes. These bounds gave all the modes with a dimensionless frequency less than 10 that produced a significant contribution to the wall force. Only about 20% of the modes used added significant contributions to the forces and moments; however, it was computationally convenient to include all modes within the specified bounds. The modal forces were summed for each of the solutions and in all cases presented this sum exceeded 90% of the static force. For $\frac{L}{H}$ values less than 10 the sum was about 95% of the static force. A correction to account for this discrepancy was applied by taking the difference between the summations of the modal forces and moments and the respective static solutions, and assuming that this difference acted as a "rigid" mode. The "rigid" mode was assumed to have a natural frequency large in comparison to the maximum forcing frequency. The validity of this correction can be seen by inspection of expressions (3.42) for the case when $\omega_{n,m} >> \omega$. The solutions presented were evaluated using a 10% damping ratio for

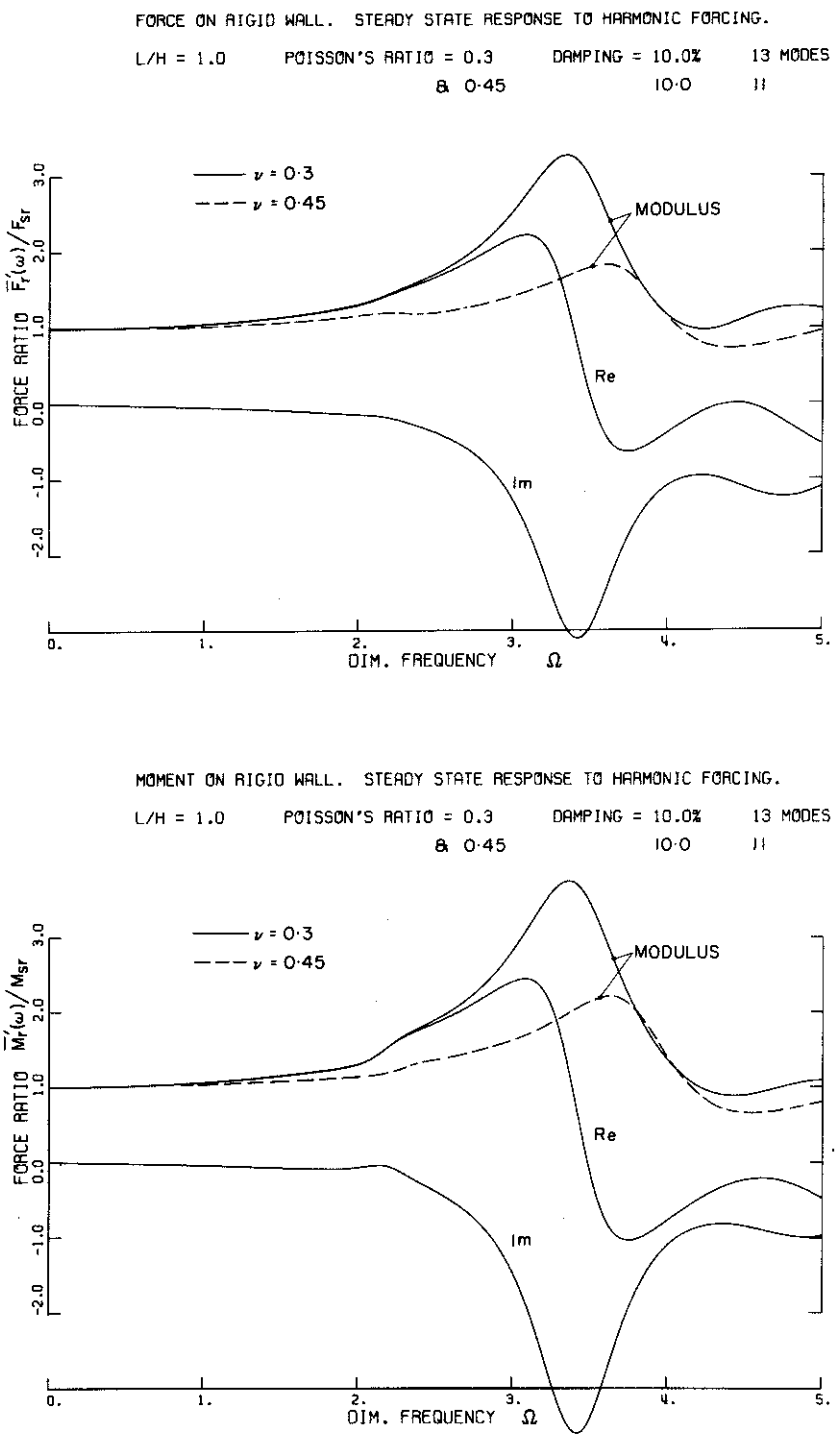

Figure 3.18 Complex-amplitudes of force ratio and moment ratio on smooth rigid wall. L/H = 1.0.

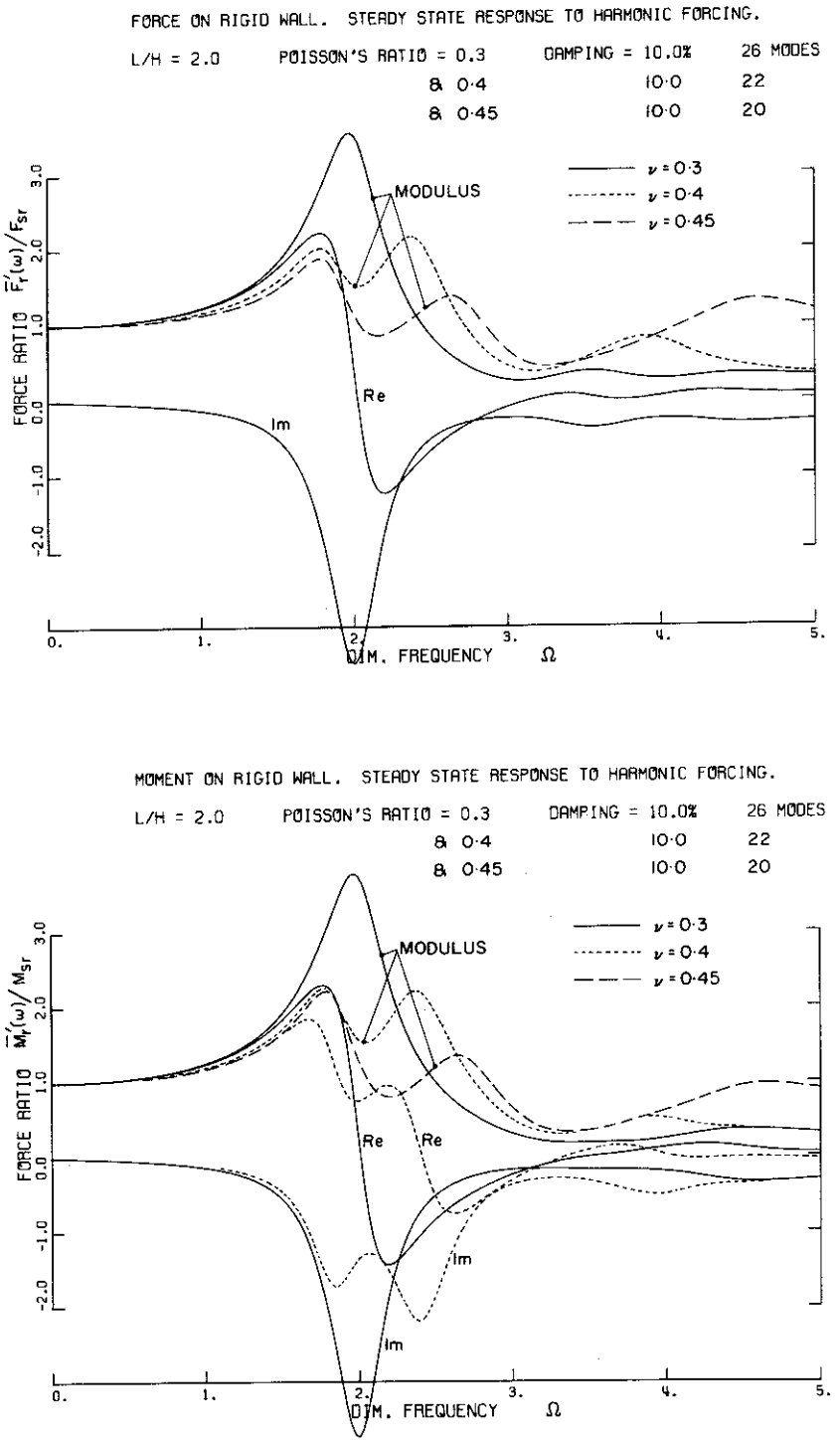

Figure 3.19 Complex-amplitudes of force ratio and moment ratio on smooth rigid wall. L/H = 2.0.

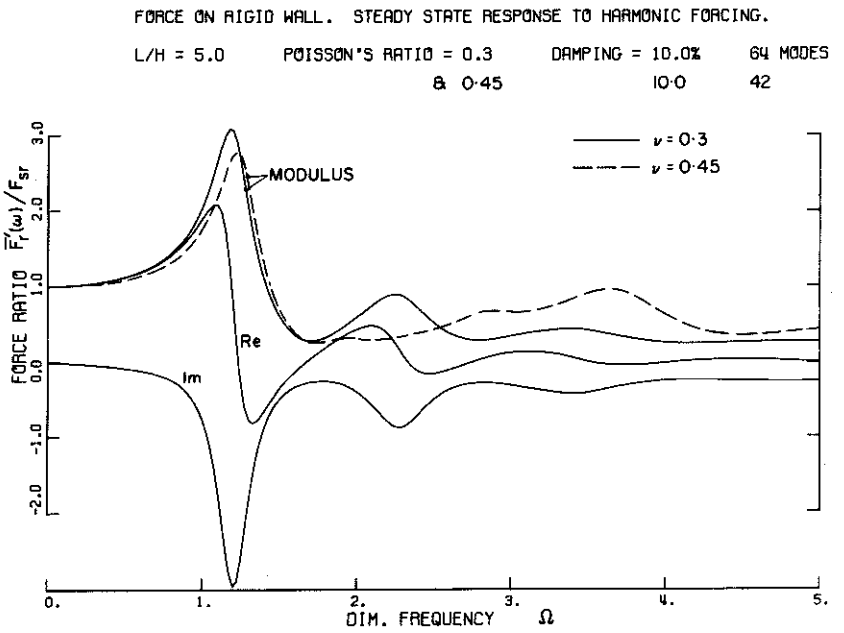

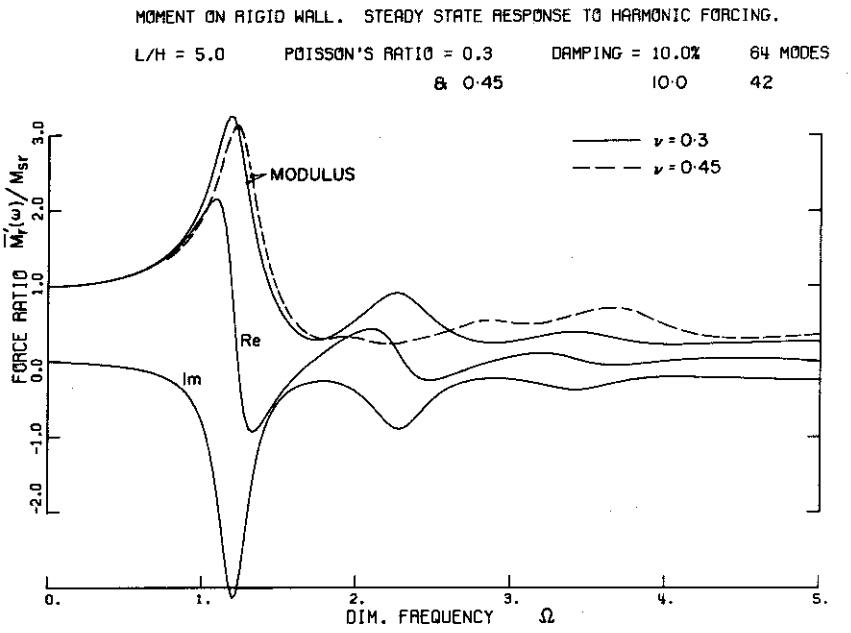

Figure 3.20 Complex-amplitudes of force ratio and moment ratio on smooth rigid wall. L/H = 5.0.

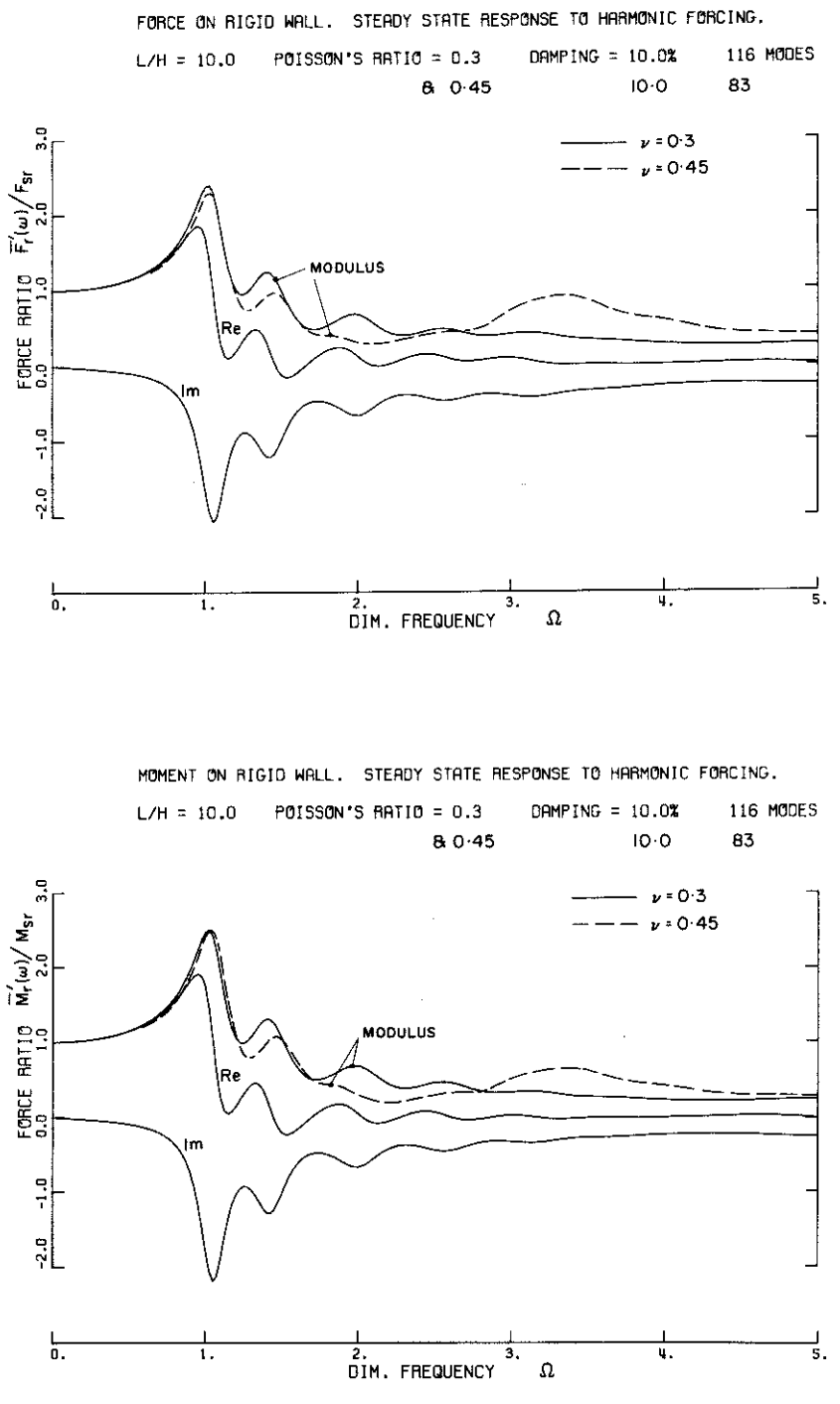

Figure 3.21 Complex-amplitudes of force ratio and moment ratio on smooth rigid wall. L/H = 10.

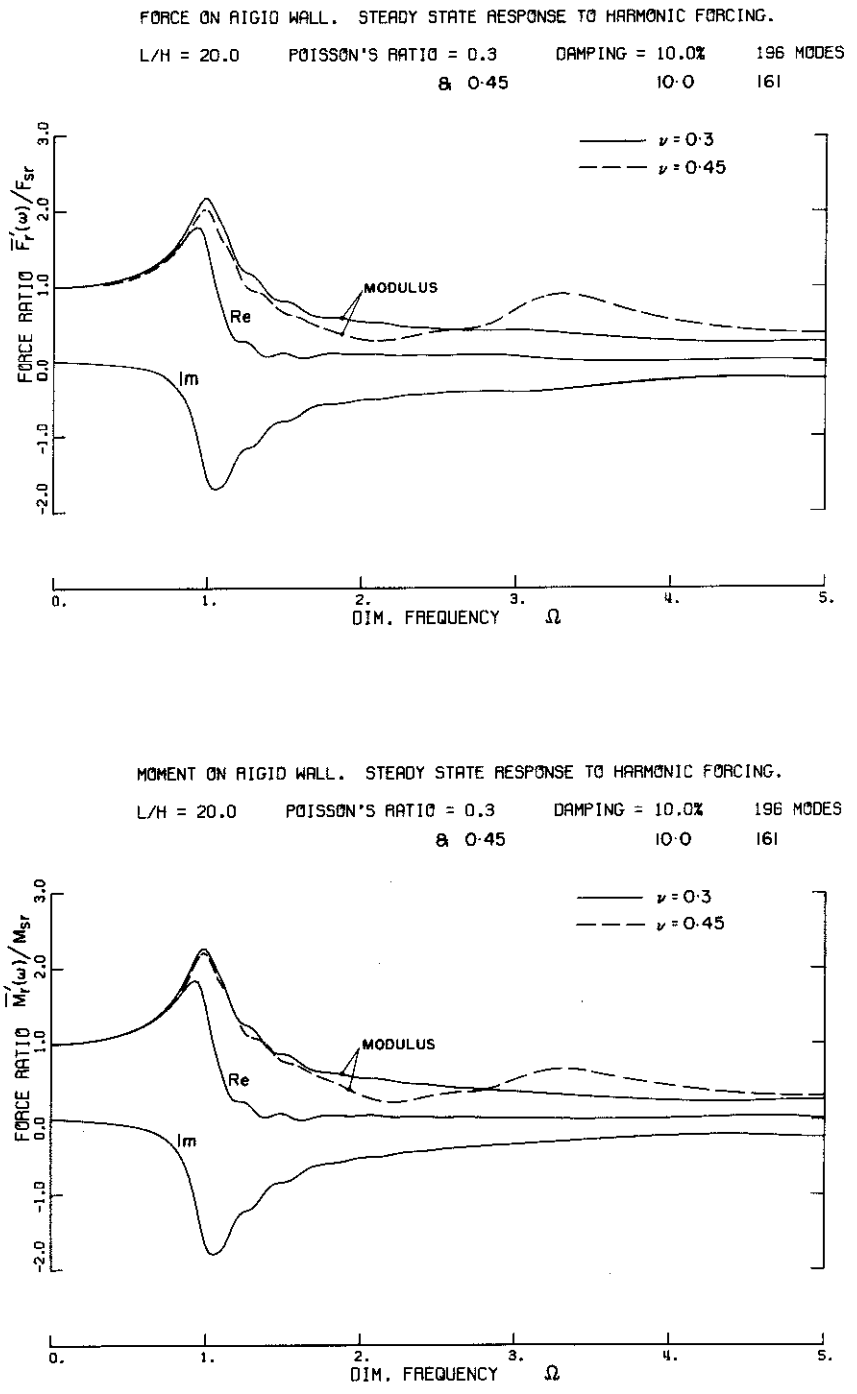

Figure 3.22 Complex-amplitudes of force ratio and moment ratio on smooth rigid wall. L/H = 20.

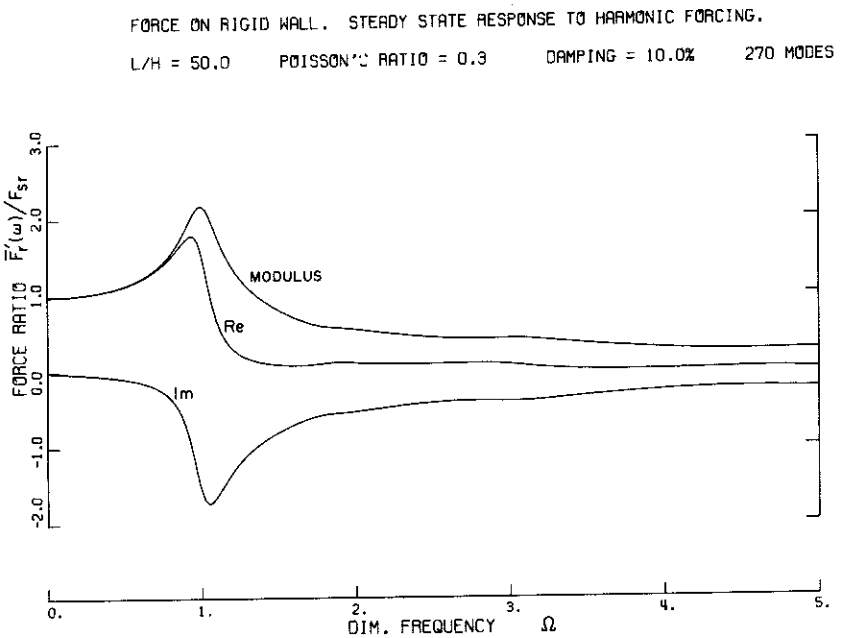

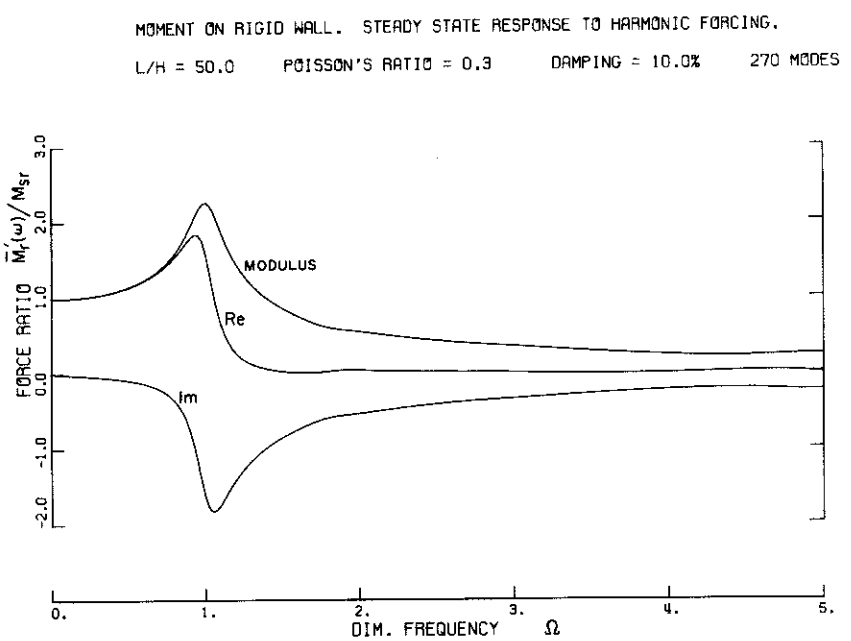

Figure 3.23 Complex-amplitudes of force ratio and moment ratio on smooth rigid wall. L/H = 50.

each mode.* A limited study on the effects of varying the damping was made and typical solutions for 5% damping in all modes are compared with the 10% damping solutions in Fig. 3.24.

For $\frac{L}{H}$ values less than 5 it can be seen that the force and moment solutions become quite sensitive to changes in Poisson's ratio. It is also of interest to note that the character of both the force and moment solutions are very similar, which suggests that the shape of the pressure distribution does not vary significantly with changes in frequency.

From an inspection of the plotted solutions it is apparent that for $\frac{L}{H}$ values greater than 10 the dynamic behavior of the wall force and moment can be represented to a good degree of approximation by an equivalent two-mode system with a higher modal damping than in the basic system. The following equivalent parameters were found suitable for Poisson's ratio between 0.3 and 0.4:

	Mode 1	Mode 2
Dimensionless frequency	1.1	3.0
Damping ratio	18%	18%
Static-one-g modal force	$0.85\ F_{sr}$	$0.15\ F_{sr}$
Static-one-g modal moment	$0.85\ M_{sr}$	$0.15\ M_{sr}$

The complex-amplitude of force and moment for this two-mode system are compared with the exact solutions for $\frac{L}{H} = 10$ and 20, $\nu = 0.3$ and a 10% modal damping in Fig. 3.25.

---

*This assumption is in contradiction with the form of damping chosen in expression (3.22) to satisfy the conditions for existence of classical normal modes. However, practical experience with dynamic systems suggests that it is reasonable to assume that the modal damping ratios have the same values.

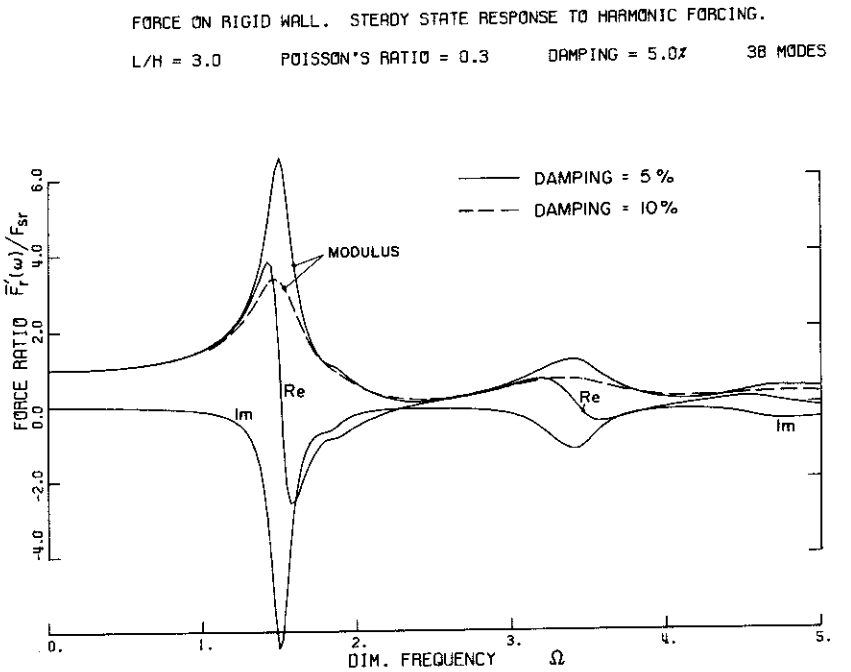

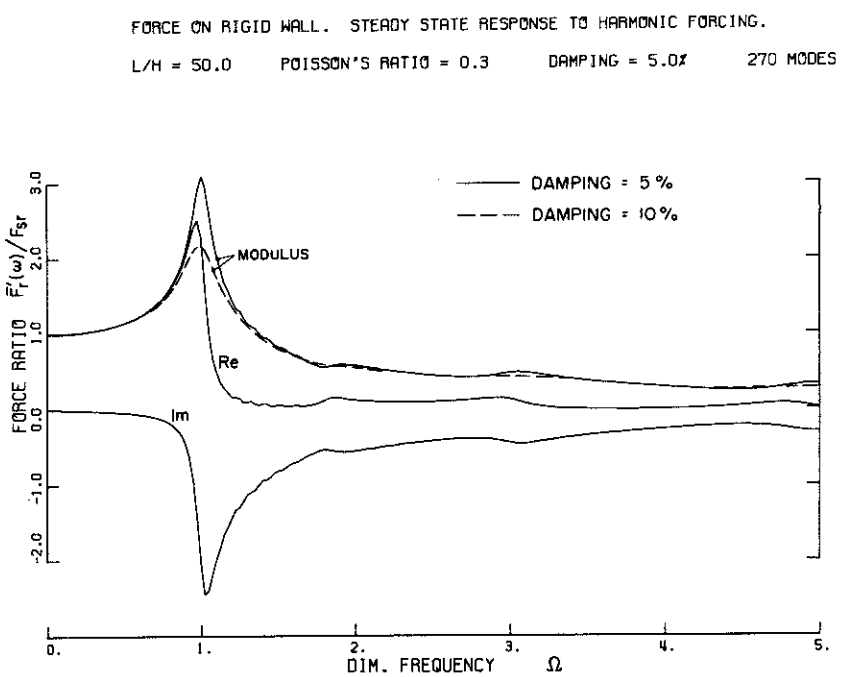

Figure 3.24 Complex-amplitude of force ratio on smooth rigid wall. Comparison between 5% and 10% damping.

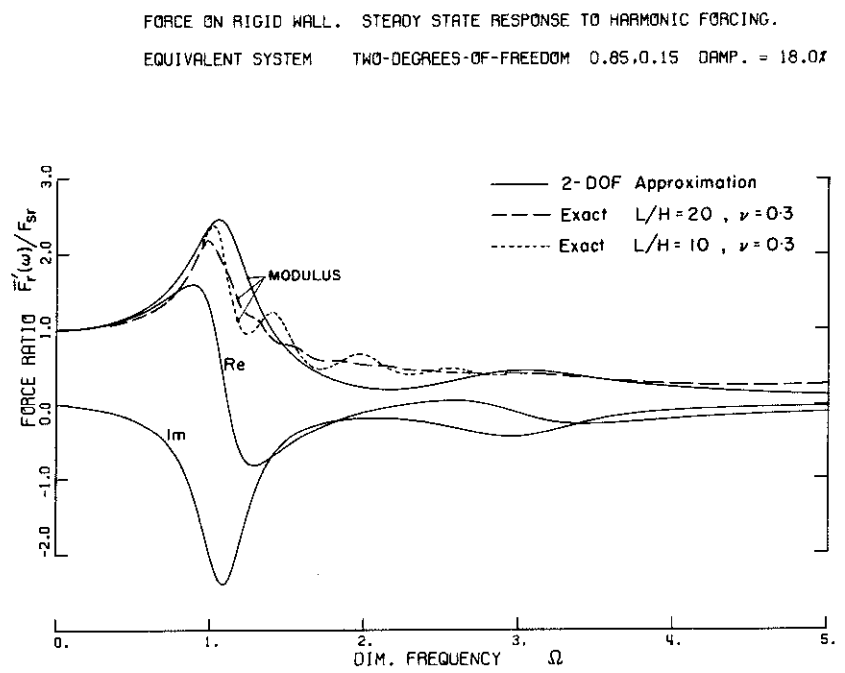

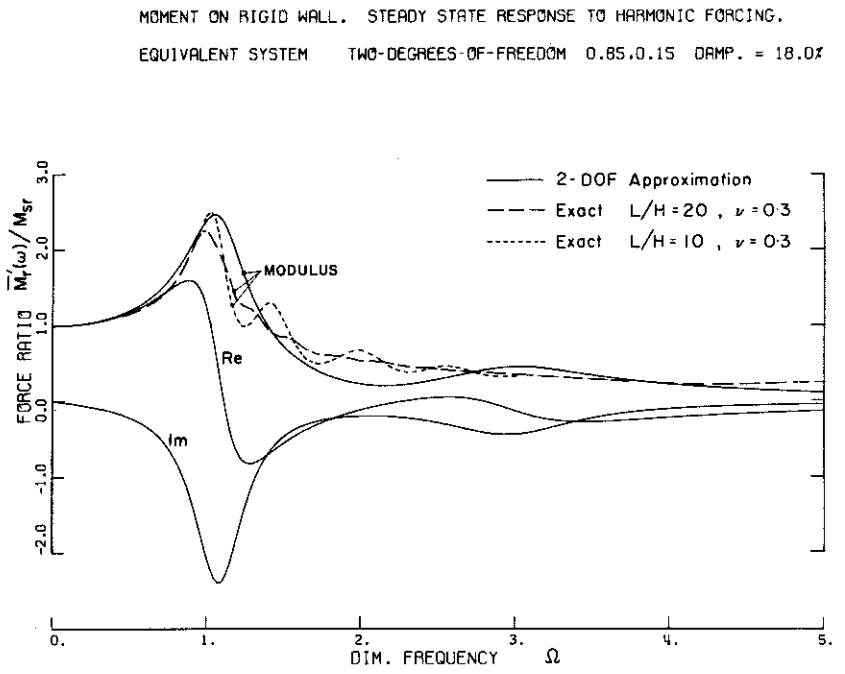

Figure 3.25 Complex-amplitude of force ratio and moment ratio on smooth rigid wall. Comparison between exact and equivalent two-mode system.

3.6. SPRING-MASS-DASHPOT ANALOGY

From the steady-state solutions for the wall force and moment (expressions (3.42)) it can be easily shown that the rigid-wall problem for either static or dynamic forcing can be represented by a simple spring-mass-dashpot analogy. Each of the modes that contribute significantly to the wall force are represented by a spring-mass-dashpot unit, and the higher modes that contribute less significantly are represented by a single mass rigidly attached to the wall.* This analogy is shown in Fig. 3.26. The analogue parameters can be related to the previously defined prototype modal parameters by the following expressions:

$$m_{n,m} = \frac{F_{n,m}}{g}$$
$$m_{n,m} h_{n,m} = \frac{M_{n,m}}{g} \tag{3.43}$$

$$m_r = \frac{1}{g}\left(F_{sr} - \sum^{N} F_{n,m}\right)$$
$$m_r h_r = \frac{1}{g}\left(M_{sr} - \sum^{N} M_{n,m}\right) \tag{3.44}$$

in which $\sum^{N}$ represents the sum over the N significant modes.

$$\frac{k_{n,m}}{m_{n,m}} = \omega_{n,m}^2$$
$$\frac{c_{n,m}}{m_{n,m}} = 2\omega_{n,m}\zeta_{n,m} \tag{3.45}$$

*The analogy is essentially equivalent to the one used by Housner[16] in a study of dynamic pressures on liquid containers.

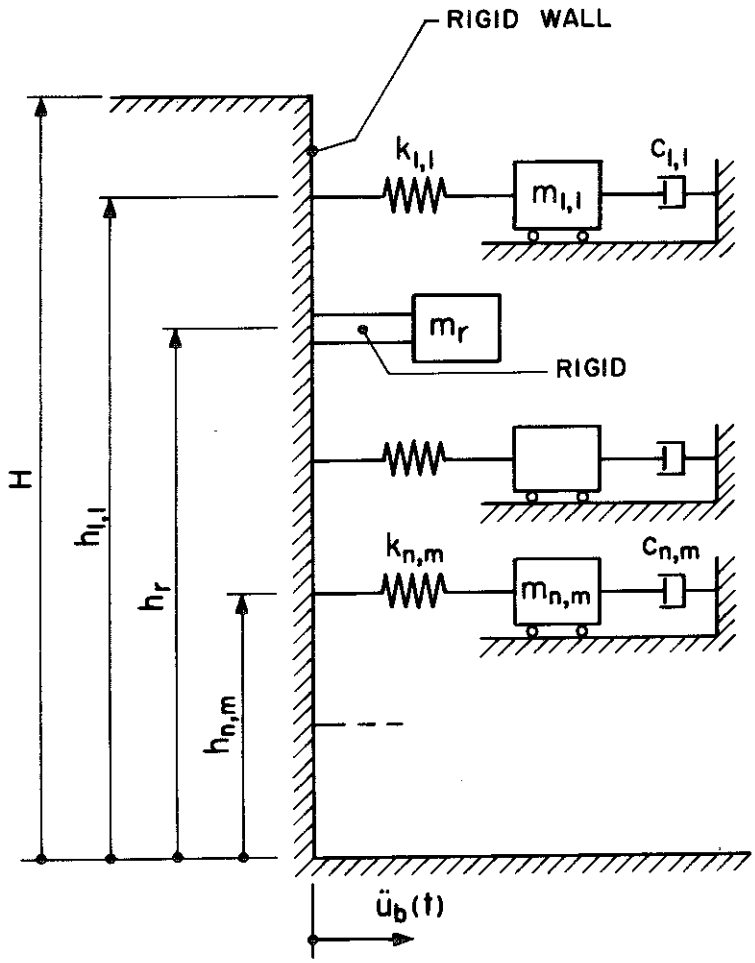

RIGID WALL : SPRING-MASS-DASHPOT ANALOGY

Figure 3.26

Equations (3.45) express the equivalence between the natural frequencies and damping factors of the analogue spring-mass-dashpot units and the prototype modes which they represent.

In most applications the dynamic wall forces and moments can be computed directly from the natural frequencies, modal forces and modal moments, and no purpose is served by evaluating the analogue parameters. The analogue is merely used to illustrate the physical interpretation of the previous solutions.

3.7. RESPONSE SPECTRUM METHOD

The number of modes required to give a good dynamic representation of the rigid-wall systems depends on a number of factors including the relationship between the modal natural frequencies and the range of predominant frequencies in the forcing. To determine this relationship for typical earthquake ground motion it is necessary to know the geometric and material properties of the wall system. Thus in each application, the degree of exactness achieved by using a limited number of modes will vary. However, from the results presented in the foregoing sections it can be seen that in general a moderately good dynamic representation of the rigid-wall systems can be achieved with five or less modes.

In view of the uncertainties involved in the estimation of earthquake-induced wall pressures and the fact that a satisfactory dynamic representation of the rigid-wall system can be achieved with a limited number of modes, the well known Response Spectrum method of evaluating the total earthquake response from the modal

properties appears suitable for relatively rigid walls. In the application of this method the earthquake responses of the individual modes are computed from the modal properties and an earthquake response spectrum. The total earthquake response is found by combining the individual responses by some approximate method.

Smoothed earthquake response spectra, suitable for design applications, have been presented by Housner[14,15] and Skinner[51]. Housner's spectra are reproduced in Appendix VIII. The generally accepted method of combining the individual modal responses for building design is to use the root-mean-square sum. A discussion of the errors involved in the application of this approximation to buildings and possible refinements of the method have been presented by Merchant and Hudson[35]. From the results of the previous sections it was found that in general there is a reasonably good similarity between the characteristics of the modal pressure distributions and modal force distributions in buildings. Hence, it appears reasonable to expect that the rms method will be satisfactory for many wall problems. There are two wall cases for which the rms approach may need some modification. One particular difficulty arises when two modes that have significant pressure contributions have nearly the same frequencies. Since the rms method is based on the assumption that the individual modal responses are independent random variables there remains some question about the validity of the method for this case. A further difficulty arises when two modes have nearly equal contributions. For this case the rms sum is significantly less than the absolute or algebraic sums,

and so if a design is based on the rms sum there exists the possibility (although at low probability) that the design values will be exceeded by a considerable margin. For these two cases a reasonable design approach is to use pressures or forces computed from an average of the rms sum and the algebraic sum. Skinner[51] has computed earthquake response spectra for two-mode systems. Although these have been prepared with the design of buildings in mind they can be applied to give additional refinement to wall problems. Informative estimates of the likely errors arising from the rms method for the case of two modes with relatively close frequencies can be made from Skinner's spectra.

The application of the Response Spectrum method to compute an earthquake-induced pressure distribution is illustrated by the example studied in Chapter 5. Modal frequencies, pressure distributions, forces and moments for the rigid wall can be obtained from the plots given in the foregoing sections or read from the tables in Appendix VI. A rapid application of the Response Spectrum method can be made by using only the modal wall forces and assuming that the dynamic pressure distribution has similar shape to the static solution or the largest modal contribution. In applying the results given in this study it is recommended that the static solutions be used to compute a "rigid" mode to represent the effect of the higher modes that are not otherwise included. The properties of this "rigid" mode are defined for the spring-mass-dashpot analogue described in the previous section.

3.8. RANDOM EXCITATION

Housner and Jennings[17] have shown that the important properties of recorded strong-motion earthquake accelerograms can be modelled with sections of a stationary, Gaussian, random process having a power spectral density found from the averaged undamped velocity spectrum. (More recently Jennings, Housner and Tsai[22] have refined this model by using an envelope function to introduce the changing intensity at the beginning and end of an accelerogram.) The earthquake power spectral density given by Housner and Jennings[17] is plotted in Fig. 3.27 and expressed by

$$G(\omega) = \frac{0.01238\left(1 + \frac{\omega^2}{147.8}\right)}{\left(1 - \frac{\omega^2}{242}\right)^2 + \frac{\omega^2}{147.8}} \quad \frac{(\text{ft/sec}^2)^2}{(\text{rad/sec})} \tag{3.46}$$

Their relationship between the relative velocity response spectra and the power spectral density is expressed by

$$S_V = 1.796 \sqrt{\frac{\pi G(\omega)}{2\zeta\omega}\left(1 - e^{-2\zeta\omega T/2.44}\right)} \tag{3.47}$$

in which

S_V = relative velocity response spectrum

$G(\omega)$ = power spectral density of earthquake

ω = angular frequency

ζ = damping ratio

T = accelerogram duration

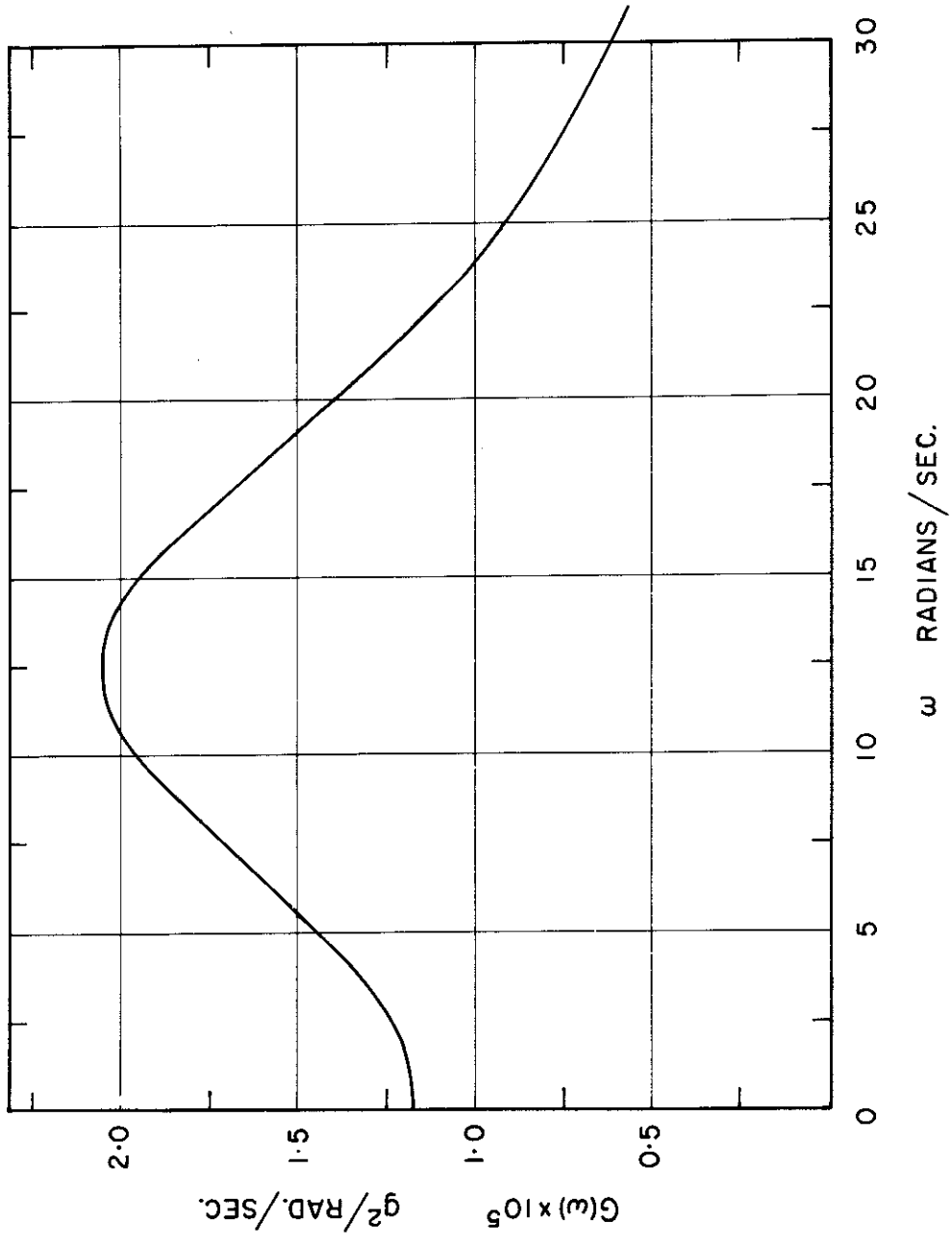

Figure 3.27 Power spectral density of strong-motion earthquake acceleration.

If $T = 18.6$ and $\zeta = 0$, then S_V is approximately equal to 1.0 for a 3.0 sec period oscillator. This approximate relationship may be used to scale $G(\omega)$ to the correct value for different velocity spectra.

Statistical estimates of the earthquake wall forces and moments can be computed from the earthquake power spectral density and the steady-state solutions for harmonic forcing by using some of the basic results of random vibration theory. The mean-square-response $E[y^2]$ of a linear system to random excitation is given by

$$E[y^2] = \int_0^\infty |H(\omega)|^2 G_x(\omega)\, d\omega \tag{3.48}$$

in which

$H(\omega)$ = system transfer function

$G_x(\omega)$ = power spectral density of input ($\omega = 0$ to ∞)

If the input is normally distributed with zero mean the output will also be normally distributed with zero mean. Assuming zero mean for the earthquake input and expressing (3.48) in terms of the wall problem parameters gives

$$\begin{aligned} s_F^2 &= \int_0^\infty |\overline{F}_r'(\omega)|^2 G(\omega)\, d\omega \\ s_M^2 &= \int_0^\infty |\overline{M}_r'(\omega)|^2 G(\omega)\, d\omega \end{aligned} \tag{3.49}$$

in which

s_F^2 = variance of wall force

s_M^2 = variance of wall moment

$G(\omega)$ = power spectral density of earthquake

$\overline{F}'_r(\omega)$ and $\overline{M}'_r(\omega)$ are defined in dimensionless form by expressions (3.42). Expressions (3.49) can be numerically evaluated by using expressions (3.42) and the analytical expression for the power spectral density; alternatively, an approximate evaluation can be made by using the simple graphical interpretation of expressions (3.49) and the plots given for $|\overline{F}'_r(\omega)|/F_{sr}$, $|\overline{M}'_r(\omega)|/M_{sr}$ and $G(\omega)$. Statistical estimates of the maximum forces and moments can be found from the mean-square responses by using the properties of the normal distribution curve. An example of the application of this method is given in Chapter 5.

Although not widely used the random vibration approach has general applicability to many earthquake engineering problems. Details of the application of this method to the estimation of responses of buildings to earthquakes are given by Tajimi[54]. The method has particular advantage if the system transfer function can be readily derived and if classical normal modes do not exist or are difficult to evaluate. This is frequently the case for many soil-structure interaction problems and in particular the random vibration approach was found to be a convenient method for computing the response of the deformable-wall structures analyzed in Chapter 7.

3.9. FINITE ELEMENT SOLUTIONS

The finite element method was used to compute normal mode solutions for a number of rigid-wall problems. The purpose of this study was to check the accuracy of the finite element method for this type of problem by a comparison with the analytical solution for the smooth wall, and to investigate the effect of the wall-soil contact assumption on the dynamic behavior.

The normal modes were computed using the second-order quadrilateral element and a consistent mass matrix (see Archer[1]). Details of this element and the finite element formulation used are given in Appendix II. Solutions were computed for $\frac{L}{H}$ equal to 1.0 and 3.0 with a Poisson's ratio of 0.3 for each case. Two different meshs were used for each case and these are shown in Fig. 3.28. Both the smooth and bonded contact boundary conditions were analyzed. For the smooth wall problem the boundary conditions were taken to be the same as used previously for the analytical solution (Fig. 3.1). The bonded wall problems were identical in detail to their smooth wall counterparts except that the boundary condition on the end walls was taken as $u = 0$ and $v = 0$.

Solutions for the natural frequencies of the lower anti-symmetric modes are compared in Tables 3.1, 3.2, 3.3 and 3.4 below. The solutions for the static-one-g modal wall pressure distributions that contribute significantly to the static wall forces are shown in Figs. 3.29 and 3.30.

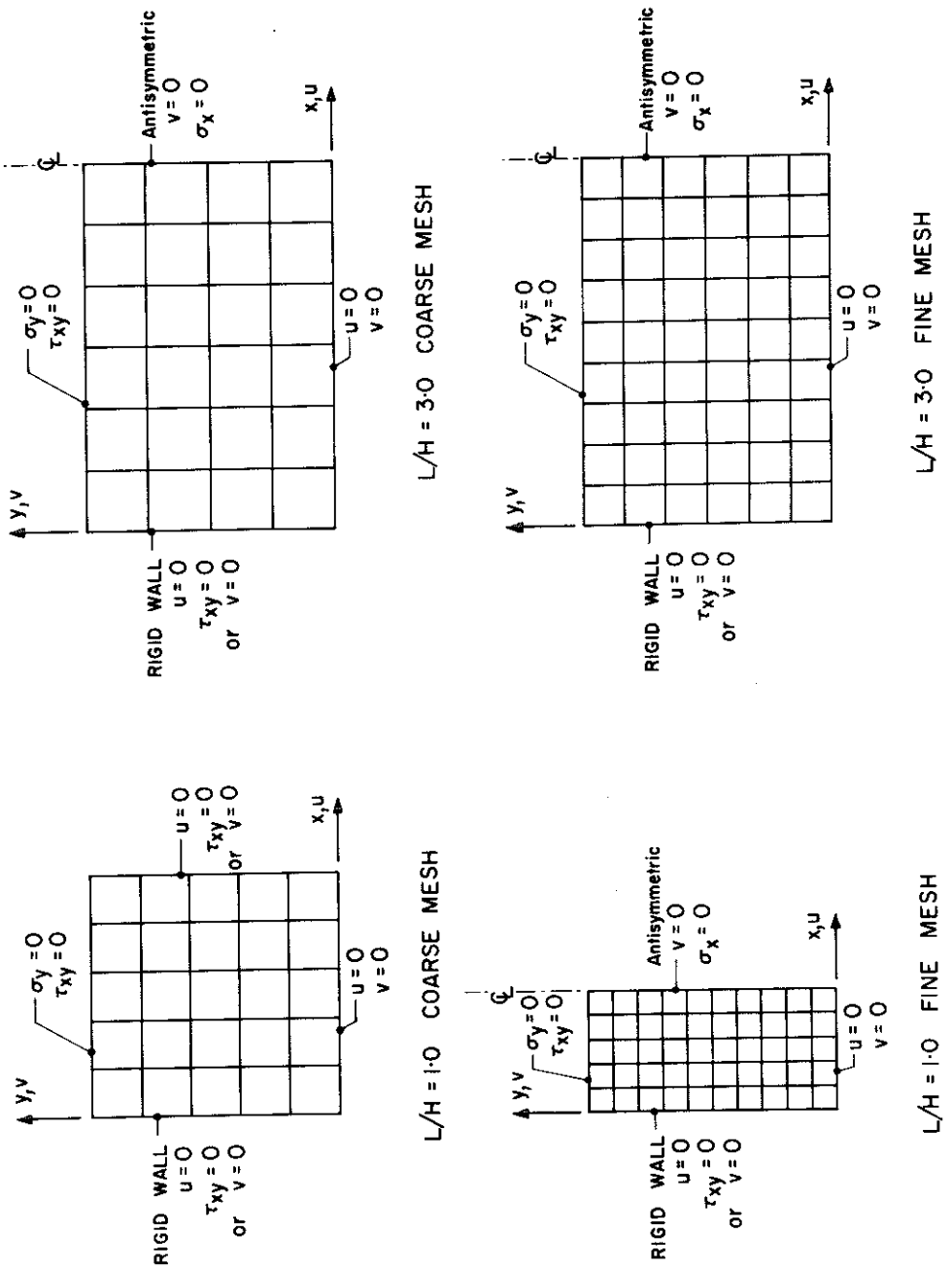

Figure 3.28 Finite element meshes for normal mode analyses.

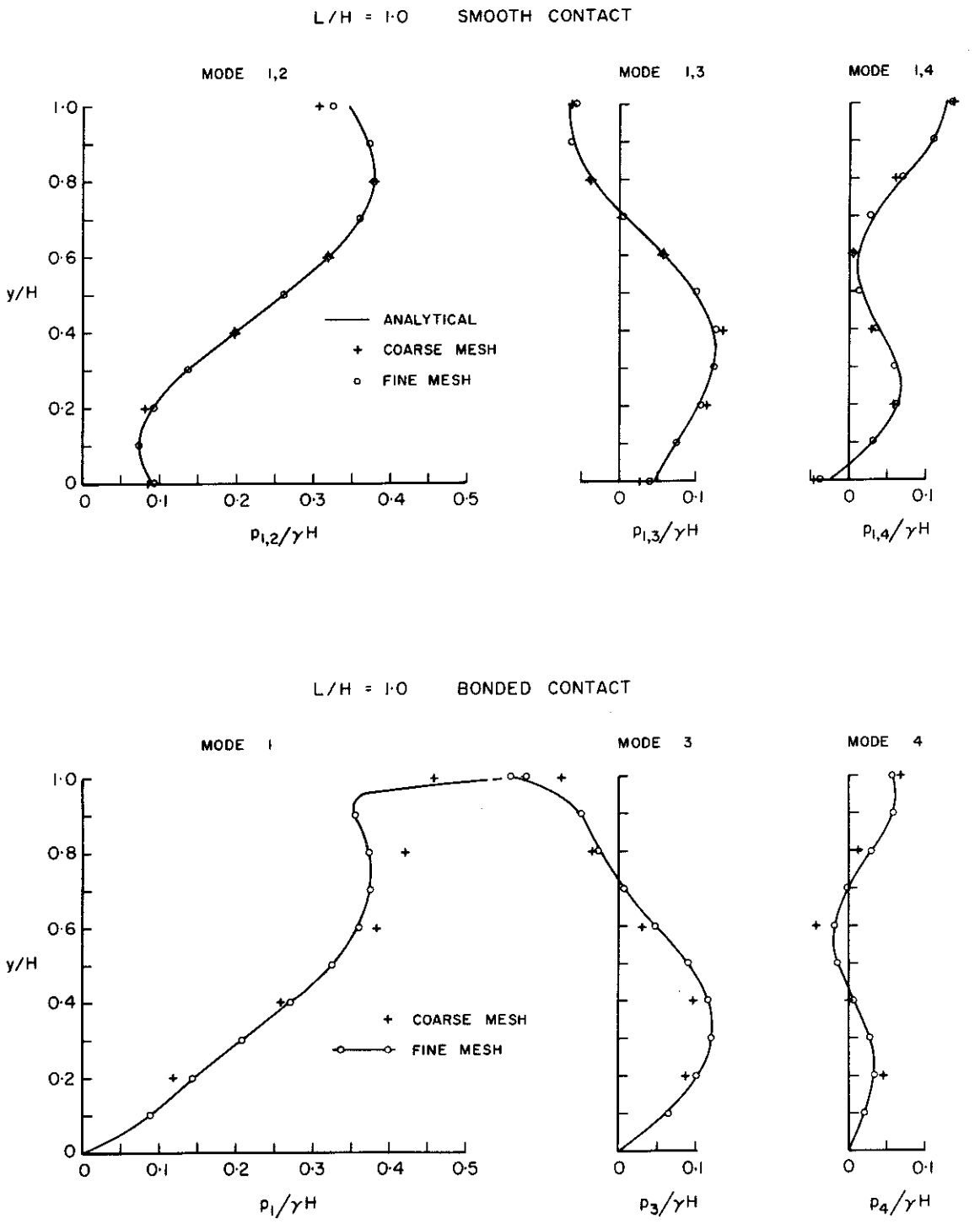

Figure 3.29 Static-one-g modal pressure distributions. Smooth and bonded rigid wall. L/H = 1.0.

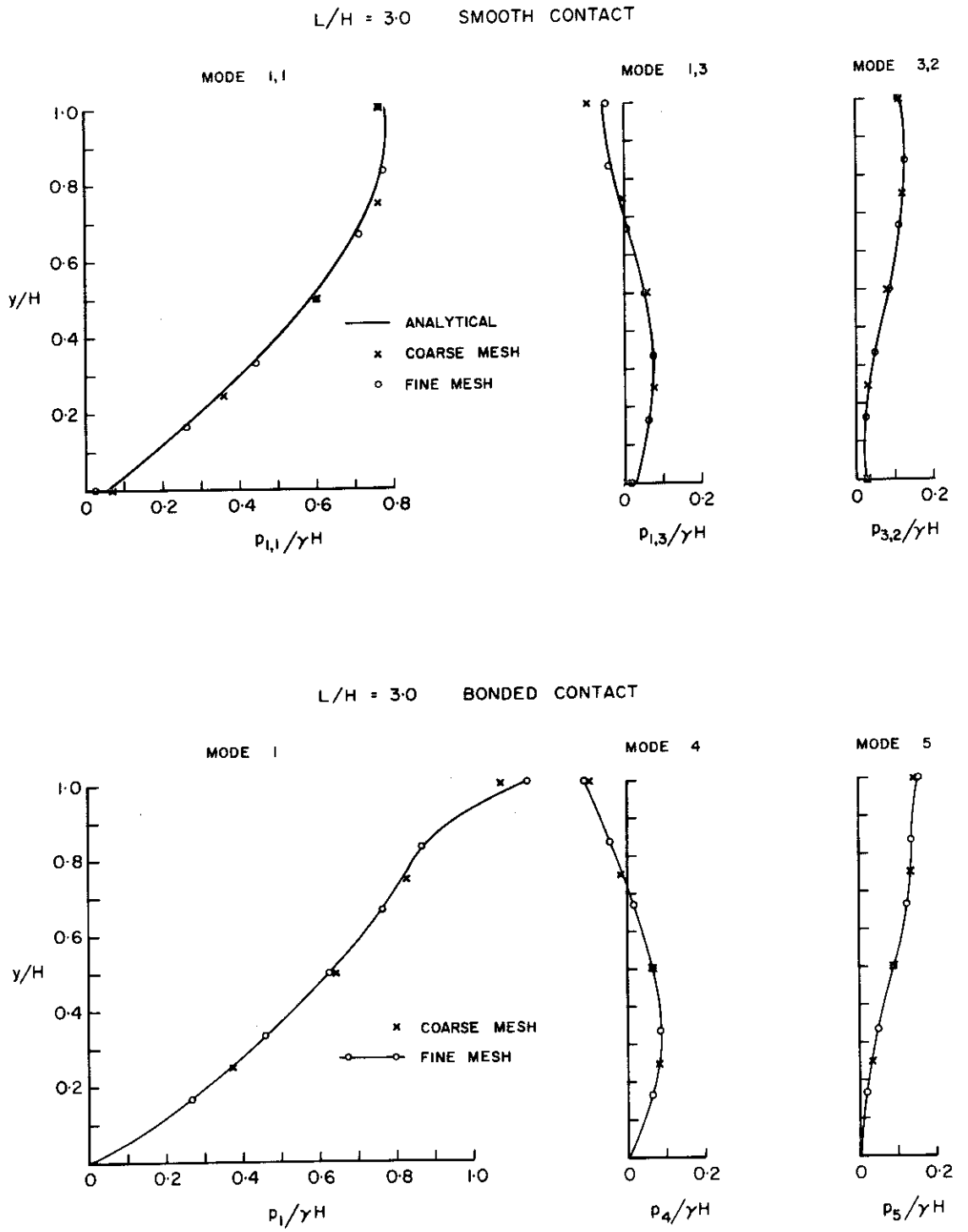

Figure 3.30 Static-one-g modal pressure distributions. Smooth and bonded rigid wall. L/H = 3.0.

TABLE 3.1

Natural Frequencies, Smooth Contact $\frac{L}{H} = 1.0$

Mode Type, Order	Dimensionless Natural Frequency $\Omega_{n,m}$		
	Coarse Mesh	Fine Mesh	Analytical
1,1	2.23	2.19	2.18
1,2 *	3.51	3.45	3.44
1,3 *	4.81	4.71	4.67
1,4 *	5.33	5.09	5.01
3,1	6.65	5.85	5.57
3,2	7.62	6.94	6.72

TABLE 3.2

Natural Frequencies, Bonded Contact $\frac{L}{H} = 1.0$

Mode Type, Order	Dim. Natural Fre. $\Omega_{n,m}$	
	Coarse Mesh	Fine Mesh
1 *	3.70	3.63
2	3.98	3.79
3 *	5.07	4.89
4 *	5.82	5.50
5	7.37	6.96
6	8.51	7.62

*These modes contribute significantly to the static wall force.

TABLE 3.3

Natural Frequencies, Smooth Contact $\frac{L}{H} = 3.0$

Mode Type, Order	Dimensionless Natural Frequency $\Omega_{n,m}$		
	Coarse Mesh	Fine Mesh	Analytical
1,1 *	1.521	1.518	1.510
1,2	1.852	1.844	1.836
3,1	2.24	2.21	2.18
5,1	3.45	3.33	3.17
1,3 *	3.46	3.36	3.28
3,2 *	3.55	3.49	3.44
3,3	4.89	4.77	4.67
5,2	5.12	4.80	4.74

TABLE 3.4

Natural Frequencies, Bonded Contact $\frac{L}{H} = 3.0$

Mode Type, Order	Dim. Natural Fre. $\Omega_{n,m}$	
	Coarse Mesh	Fine Mesh
1 *	1.537	1.532
2	2.03	2.01
3	2.85	2.78
4 *	3.45	3.36
5 *	3.61	3.56
6	4.27	4.06
7	4.92	4.80
8	5.24	5.02

*These modes contribute significantly to the static wall force.

The analytical and the fine mesh finite element results, for both the frequencies and the pressure distributions, show agreement to within 5%. (Agreement for the lowest mode frequencies is better than 1%.) Agreement between the fine and coarse mesh results is generally to about 10%. Thus the coarse mesh would be satisfactory for most applications. From these solutions it would appear that satisfactory results can be obtained for modes that have at least four elements within the modal wave length. It is of interest to note that when the $\frac{L}{H} = 3.0$ coarse and fine meshes were used in a static finite element analysis for horizontal body force they gave pressure distributions within 10% and 7% respectively of the static analytical results.

Quite good agreement can be seen between the equivalent frequencies and modal pressure distributions of the smooth and bonded contact cases. Thus it is unlikely that the wall-soil interface condition will have a significant influence on the earthquake-induced pressures.

3.10. NONUNIFORM SOIL

The effect on the normal mode solutions of a linear increase with depth of the soil elastic constants (E and G) was investigated using both analytical and finite element methods.

3.10.1. Analytical Solution for Infinite Stratum

It is possible to derive analytical solutions for the pure horizontal-shear and vertical-dilitation modes of an infinite elastic

stratum having certain variations of the shear modulus G (or Young's modulus) with depth. From the frequency equation solutions given in Figs. 3.2, 3.3 and 3.4 it can be seen that for $\frac{L}{H}$ values greater than 5 all the n = 1 modes have frequencies within 25% of the infinite stratum pure horizontal-shear and vertical dilitation frequencies. Hence the natural frequencies of the nonuniform infinite layer can be expected to be reasonably good approximations for the frequencies of the low n modes of the nonuniform bounded problem with relatively large $\frac{L}{H}$ values. In view of this approximation it was considered informative to present the frequency solution for an infinite stratum which has a linear increase of shear modulus with depth. The density and Poisson's ratio are assumed to be uniform.

Details of the problem and the coordinate system adopted are shown in Fig. 3.31. On the assumption of plane strain and no variation in the x-direction of the displacements, substitution of the stress-strain relations into the equilibrium equations gives the equations of motion as

$$\frac{\partial}{\partial y}\left\{G\frac{\partial u(y,t)}{\partial y}\right\} = \rho\frac{\partial^2 u(y,t)}{\partial t^2}$$

$$\frac{\partial}{\partial y}\left\{k^2 G\frac{\partial v(y,t)}{\partial y}\right\} = \rho\frac{\partial^2 v(y,t)}{\partial t^2} \qquad (3.50)$$

These equations are uncoupled and clearly the solution of the second can be obtained directly from the first. The linear variation of the shear modulus G can be expressed as

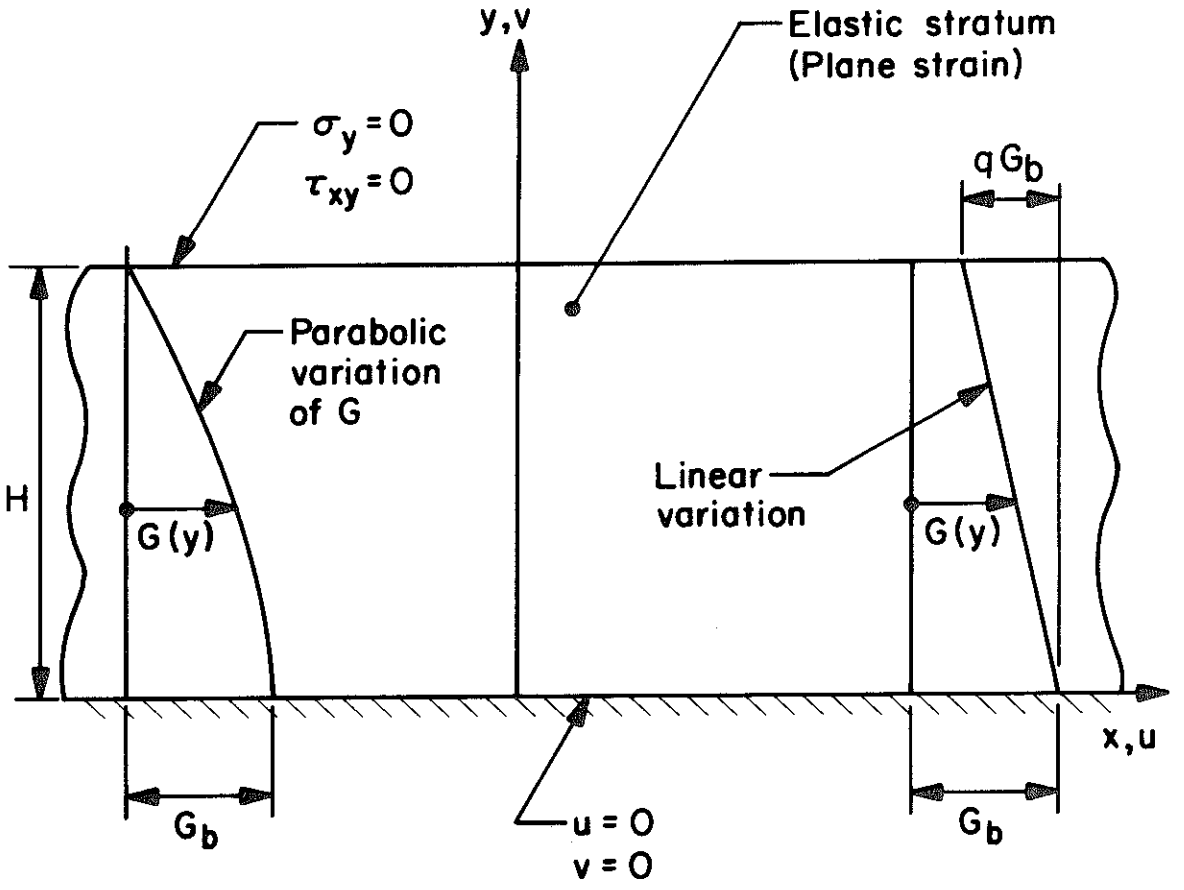

NONUNIFORM STRATUM

Figure 3.31

$$G(y) = G_b\left(1 - \frac{qy}{H}\right) \qquad 0 < q \leq 1 \tag{3.51}$$

in which

G_b = shear modulus of soil at bottom of stratum

q = soil modulus parameter, defined in Fig. 3.31

By assuming a solution of the form

$$u(y,t) = \bar{u}(y)e^{i\omega_m t}$$

in which ω_m is the natural angular frequency of mode m, the first of equations (3.50) gives

$$G_b\left(1 - \frac{qy}{H}\right)\frac{\partial^2 \bar{u}}{\partial y^2} - G_b \frac{q}{H}\frac{\partial \bar{u}}{\partial y} + \rho\omega_m^2 \bar{u} = 0 \tag{3.52}$$

Let $\bar{y} = \left(1 - \frac{qy}{H}\right)$, then equation (3.52) can be written as

$$\bar{y}^2 \frac{\partial^2 \bar{u}(\bar{y})}{\partial \bar{y}^2} + \bar{y}\frac{\partial \bar{u}(\bar{y})}{\partial \bar{y}} + \left(\frac{H}{q}\right)^2 \frac{\rho\omega_m^2}{G_b}\bar{y}\,\bar{u}(\bar{y}) = 0 \tag{3.53}$$

Expression (3.53) is a standard form of Bessel's equation and has the solution

$$\bar{u}(\bar{y}) = AJ_0(\tilde{\beta}\sqrt{\bar{y}}) + BY_0(\tilde{\beta}\sqrt{\bar{y}}) \tag{3.54}$$

in which

A, B = constants

$$\tilde{\beta} = \frac{2H\omega_m}{q}\sqrt{\frac{\rho}{G_b}}$$

J_0, Y_0 = the zero-order Bessel functions of the first and second kind respectively.

The solution in terms of the variable y is

$$\bar{u}(y) = AJ_0\left(\tilde{\beta}\sqrt{1 - \frac{qy}{H}}\right) + BY_0\left(\tilde{\beta}\sqrt{1 - \frac{qy}{H}}\right) \tag{3.55}$$

The ratio of the constants A and B can be found from the following boundary conditions,

$$\text{at } y = 0\,, \quad \bar{u}(y) = 0$$

$$\text{at } y = H\,, \quad \frac{\partial \bar{u}(y)}{\partial y} = 0$$

For the special case $q = 1$, B must be set to zero because of the unboundedness of $Y_0(0)$. For $0 < q < 1$ the boundary conditions require that

$$AJ_1(\tilde{\beta}\sqrt{1-q}) + BY_1(\tilde{\beta}\sqrt{1-q})$$

$$AJ_0(\tilde{\beta}) + BY_0(\tilde{\beta}) = 0 \tag{3.56}$$

use having been made of the relations $dJ_0/dy = -J_1$; $dY_0/dy = -Y_1$.

Setting the determinant of the coefficients of A and B in expression (3.56) to zero gives the frequency equation

$$J_1(\tilde{\beta}\sqrt{1-q})Y_0(\tilde{\beta}) - J_0(\tilde{\beta})Y_1(\tilde{\beta}\sqrt{1-q}) = 0 \tag{3.57}$$

$$0 < q < 1$$

For $q = 1$ the frequency equation is

$$J_0(\tilde{\beta}) = 0 \tag{3.58}$$

The roots $\tilde{\beta}_m$, $m = 1,2,3,\ldots$ of equations (3.57) and (3.58) give the natural angular frequencies ω_m of the shear modes of the stratum. The roots of equation (3.57) for q varied from 0 to 1.0, were evaluated by an iterative procedure on the digital computer. The dimensionless natural frequencies of the lowest four modes are plotted versus the parameter q in Fig. 3.32. The dimensionless frequency used here is defined by

$$\Omega_m = \frac{\omega_m}{\omega_{s,m}} \tag{3.59}$$

in which

$$\omega_{s,m} = \frac{(2m-1)\pi}{2H}\sqrt{\frac{G_a}{\rho}} \quad , \quad m = 1,2,3,\ldots$$

the natural angular frequency of mode m of a uniform infinite elastic stratum with shear modulus equal to the average of the nonuniform stratum

$$G_a = G_b\left(1 - \frac{q}{2}\right),$$

the average shear modulus of the nonuniform stratum

Bielak[4] has shown that the normal modes of a cantilever shear beam, having a parabolic distribution of shear rigidity, are governed by Legendre's equation. From Bielak's solution the natural frequencies of a stratum with the parabolic distribution of shear modulus shown in Fig. 3.31 are given by

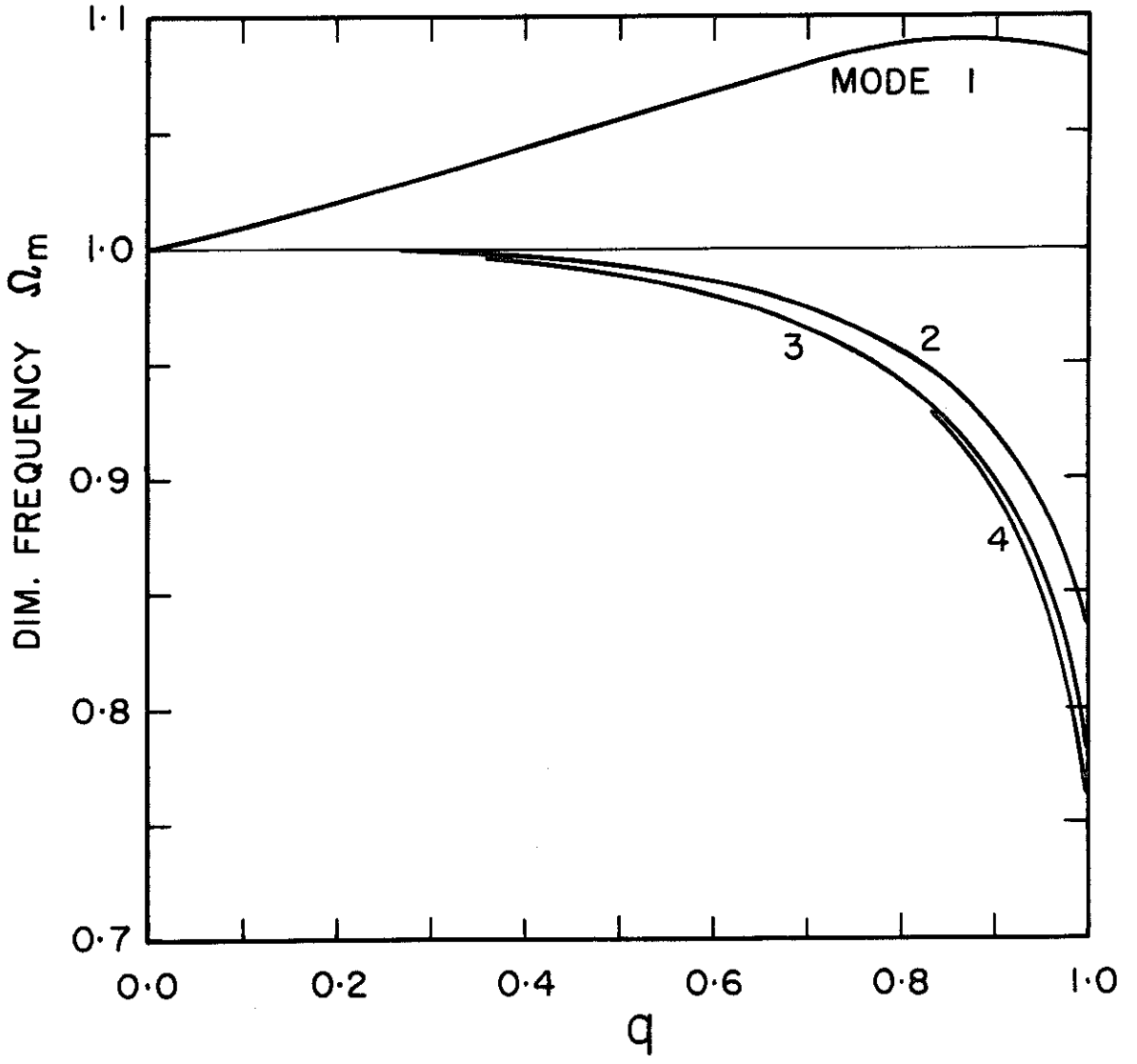

Figure 3.32 Frequency equation solution for infinite stratum with linear increase of elastic moduli with depth.

$$\frac{\omega_m}{\omega_{s,m}} \text{ (for } m = 1,2,3,4) = 1.10,\ 0.901,\ 0.853,\ 0.832$$

(For the parabolic distribution G_a was taken to be $\frac{2}{3} G_b$.)

3.10.2. Finite Element Solutions

Finite element normal mode solutions were computed for two smooth wall problems with linear variations in Young's modulus (and the shear modulus) between a value of 0.1 at the top to 1.0 at the bottom of the soil layer. The two cases analyzed were for $\frac{L}{H} = 1.0$ and $\frac{L}{H} = 3.0$ and a uniform soil density.

The natural frequencies of the six lowest antisymmetric modes (in order given by the finite element analyses) are given in Tables 3.5 and 3.6. The frequencies have been converted to dimensionless form by dividing by the finite element frequency of the same mode of the equivalent uniform soil problem. The equivalent uniform soil problem was taken to have the average of the Young's modulus of the nonuniform problem. The significant modal pressure contributions are compared with the finite element solutions for the equivalent uniform soil problems in Fig. 3.33.

In Table 3.6 the dimensionless natural frequencies of the $n = 1$ modes for $\frac{L}{H} = 3.0$ are compared with the dimensionless natural frequencies of the nonuniform infinite layer (linear variation, $q = 0.9$). It is clear that at $\frac{L}{H}$ values as low as 3.0 the end boundaries have a significant influence on most of the relevant natural frequencies. The end boundaries produce only a relatively small change in the

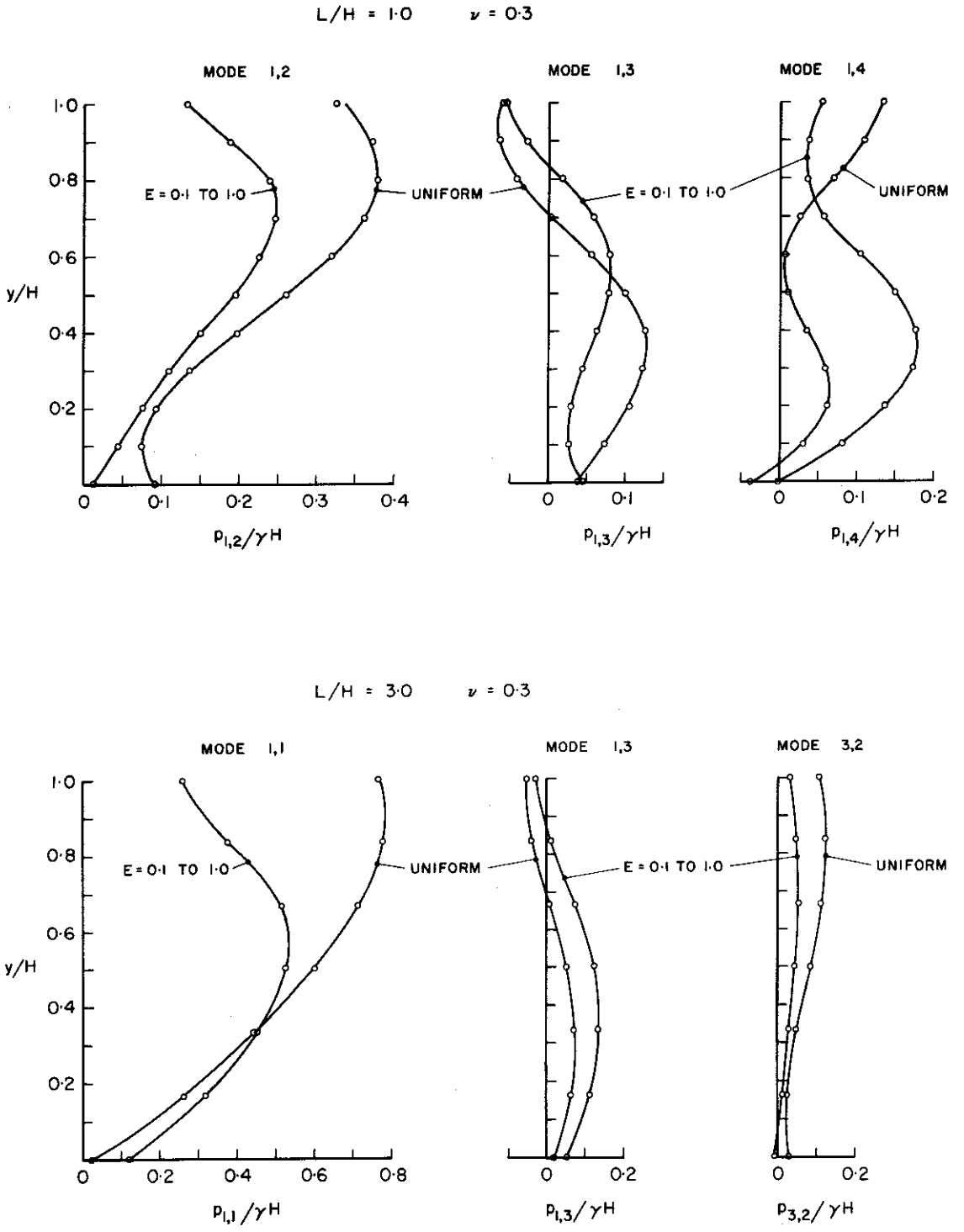

Figure 3.33 Static-one-g modal pressure distributions on smooth rigid wall. Comparison between uniform and nonuniform soil.

TABLE 3.5

Natural Frequencies, Linear Variation of E, $\frac{L}{H} = 1.0$

Mode Type, Order	Dim. Natural Freq. *
1,1	0.96
1,2 **	0.72
3,1	0.68
1,3 **	0.85
1,4 **	0.93
3,2	0.76

TABLE 3.6

Natural Frequencies, Linear Variation of E, $\frac{L}{H} = 3.0$

Mode Type, Order	Dim. Natural Freq. *	Dim. Freq. Nonunif. Inf. Layer, Ω_m
1,1 **	0.89	1.09
1,2	1.07	1.09
3,1	0.94	
3,2 **	0.68	
5,1	0.80	
1,3 **	0.85	0.90

---

*See definition given in text above.

**These modes contribute significantly to the static wall force.

mode 1,2 frequency and this is because this mode is basically a vertical-dilitation type. The dimensionless frequencies of the tabulated modes are lower than the infinite layer counterparts, which indicates that for these modes the boundaries have a greater influence on the uniform problem frequencies than on the nonuniform problem values.

For applications in which precise variations of the soil properties with depth are unknown it appears satisfactory to estimate the natural frequencies from the uniform soil solutions using average soil properties. If average properties are used to compute the natural frequencies, the wall pressures should also be computed using the uniform soil pressure solutions. Using this approach, the uncertainty in the frequencies is to some extent compensated for by the fact that if a decrease of soil moduli with depth does exist the modal pressure distributions will tend to be overestimated. In cases where variations in soil properties with depth have been well established a satisfactory analysis can probably be undertaken by using the uniform soil solutions and applying corrections to the frequencies and pressure distributions in accordance with the results of this and the preceeding section.

4. RIGID WALL: COMPARISON WITH OTHER RESEARCH

4.1. v = 0 Approximate Solutions

Matuo and Ohara[32] have presented an analytical solution for the harmonically forced rigid-wall semi-infinite soil layer problem shown in Fig. 4.1. They assume that the vertical displacement is zero throughout the soil layer and so their solution is based on an approximate formulation of the equations of elasticity.

The addition of time-dependent body force terms to the plane strain equations of motion given by expressions (3.1) yields

$$k^2 \frac{\partial^2 u(x,y,t)}{\partial x^2} + (k^2-1) \frac{\partial^2 v(x,y,t)}{\partial x \partial y} + \frac{\partial^2 u(x,y,t)}{\partial y^2} + \frac{F_x(x,y,t)}{G} = \frac{1}{V_s^2} \frac{\partial^2 u(x,y,t)}{\partial t^2}$$

$$\frac{\partial^2 v(x,y,t)}{\partial x^2} + (k^2-1) \frac{\partial^2 u(x,y,t)}{\partial x \partial y} + k^2 \frac{\partial^2 v(x,y,t)}{\partial y^2} + \frac{F_y(x,y,t)}{G} = \frac{1}{V_s^2} \frac{\partial^2 v(x,y,t)}{\partial t^2} \qquad (4.1)$$

By assuming v and F_x are zero, expressions (4.1) reduce to

$$k^2 \frac{\partial^2 u(x,y,t)}{\partial x^2} + \frac{\partial^2 u(x,y,t)}{\partial y^2} = \frac{1}{V_s^2} \frac{\partial^2 u(x,y,t)}{\partial t^2}$$

$$(k^2-1) \frac{\partial^2 u(x,y,t)}{\partial x \partial y} + \frac{F_y(x,y,t)}{G} = 0 \qquad (4.2)$$

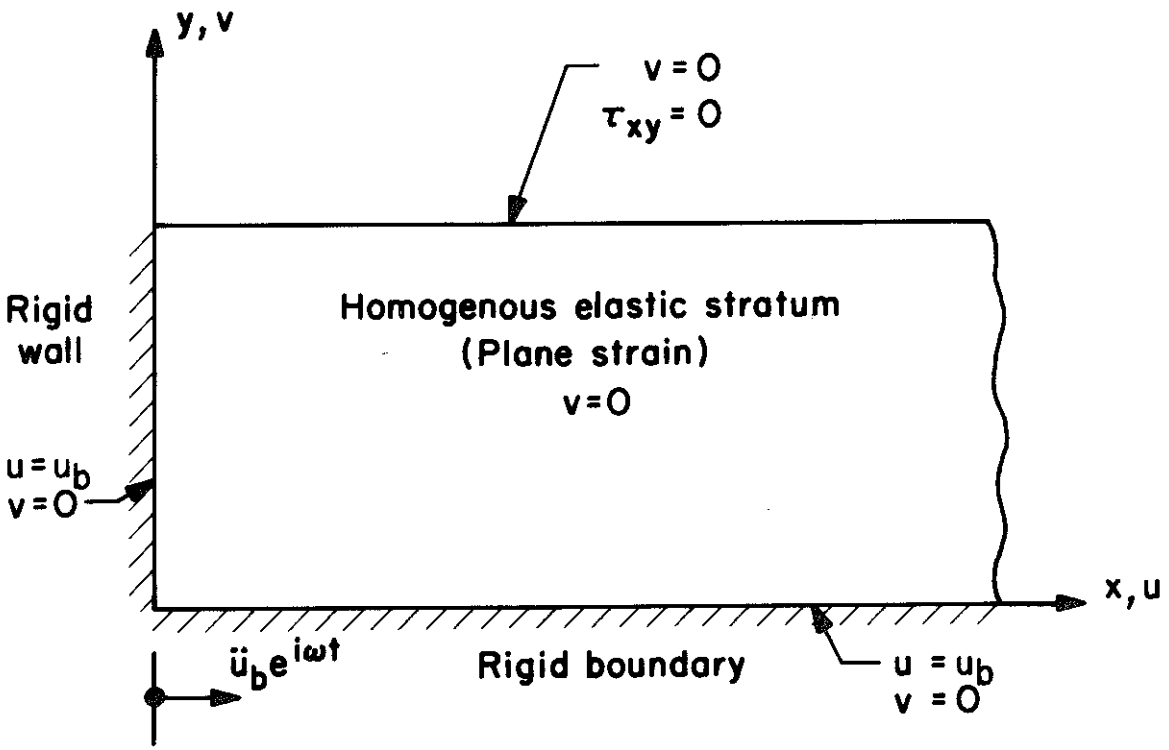
y, v
v = 0
τ_{xy} = 0
Rigid wall
Homogenous elastic stratum
(Plane strain)
v=0
u = u_b
v = 0
x, u
$\ddot{u}_b e^{i\omega t}$
Rigid boundary
u = u_b
v = 0
RIGID WALL v = 0

Figure 4.1

Only the first of equations (4.2) is used in Matuo and Ohara's solution and so in effect this approximation is equivalent to the imposition of a vertical body force given by

$$F_y(x,y,t) = - G(k^2-1) \frac{\partial^2 u(x,y,t)}{\partial x \, \partial y} \qquad (4.3)$$

Although this interpretation is informative it appears difficult to estimate, without a detailed analysis, the magnitude of the error introduced to the wall pressure distribution by the approximation. A check on the accuracy of the $v = 0$ approximation was made by comparing the static solution derived from this approximation with the exact static solution for the smooth rigid wall. The static pressure distribution on the wall of the problem shown in Fig. 4.1 can be readily derived by taking the limit of Matuo and Ohara's solution as the forcing frequency goes to zero or alternatively by expanding the static body force in a Fourier series in the y-direction. The pressure distribution for a uniform one-g static body force in the negative x-direction is given by

$$\frac{\sigma_x(0,y)}{\gamma H} = - \frac{8k}{\pi^2} \sum_{n=1}^{\infty} \frac{1}{(2n-1)^2} \sin \frac{(2n-1)\pi y}{2H} \qquad (4.4)$$

$$n = 1,2,3,\ldots$$

Expression 4.4 was evaluated for a Poisson's ratio of 0.3 and is compared with the exact smooth rigid-wall static solution for $\frac{L}{H} = 10.0$ and $\nu = 0.3$ in Fig. 4.2.

The dynamic solution for the $v = 0$ problem has not been

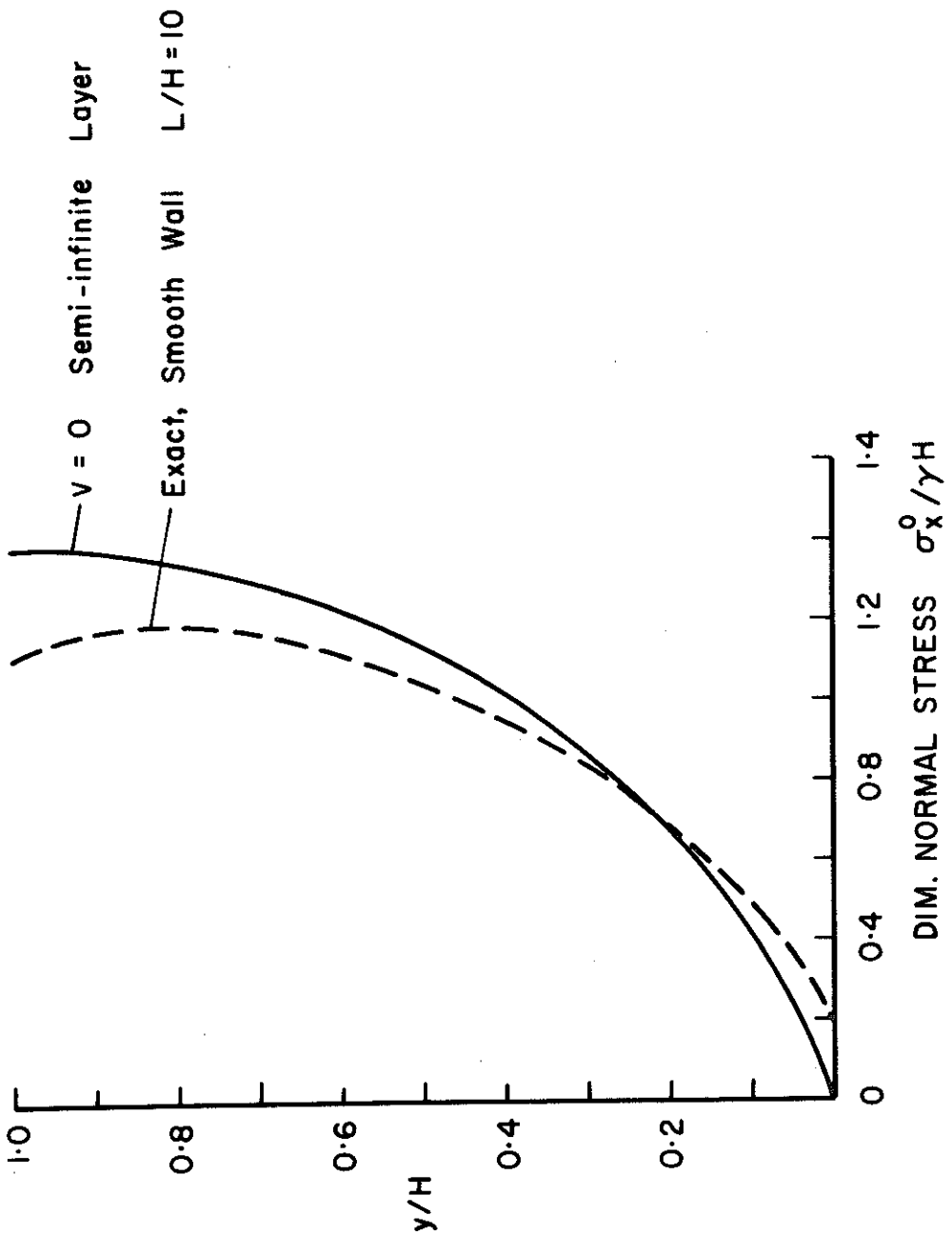

Figure 4.2 Pressure distributions on rigid wall for one-g static horizontal body force.

studied in detail but it seems reasonable to expect that it would also give a satisfactory approximation for the wall pressures over the frequency range of interest in this study. (The $v = 0$ assumption eliminates one set of characteristic mode types.)

The normal mode solution for the rigid-wall problem presented in Section 3.1 can be simplified by using the $v = 0$ approximation. Application of the $v = 0$ assumption to this problem gives in effect a bounded soil-layer version of Matuo and Ohara's problem. The simplified bounded problem is of interest because it is a simple two-dimensional refinement of Scott's shear beam model described in Section 1.4.3. This refinement enables the effects of the significant higher modes to be conveniently included in the solution. The $v = 0$ bounded problem is also of interest because it can probably be used to derive analytical solutions for cases when the elastic properties are variable with depth and when rotational deformation of the wall occurs. Further study of these cases is required.

The $v = 0$ bounded problem is shown in Fig. 4.3. The equation of motion for this problem is given by the first of equations (4.2). A solution for the natural frequencies and mode shapes was obtained by applying the standard separation of variables method. The mode shapes are given by

$$u_{n,m}(x,y) = A_{n,m} \sin \frac{n\pi x}{L} \sin \frac{(2m-1)\pi y}{2H} \qquad (4.5)$$

in which

$n = 1,2,3,\ldots,$ the mode type

$m = 1,2,3,\ldots,$ the mode order

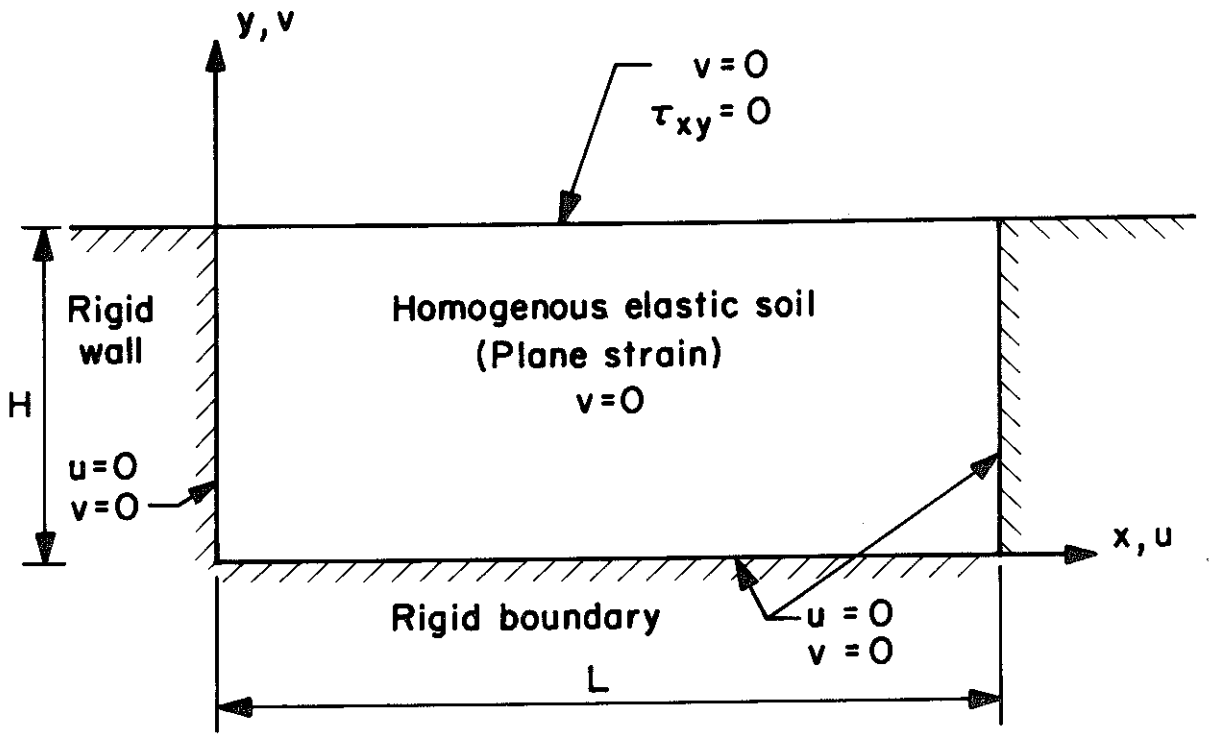
y, v
v = 0
τ_{xy} = 0
Rigid wall
Homogenous elastic soil
(Plane strain)
v = 0
H
u = 0
v = 0
x, u
Rigid boundary
u = 0
v = 0
L
RIGID WALL v = 0

Figure 4.3

$A_{n,m}$ = a constant for mode n,m

The dimensionless natural frequencies are given by

$$\Omega_{n,m} = \frac{\omega_{n,m}}{\omega_s} = \sqrt{\left(\frac{2knH}{L}\right)^2 + (2m-1)^2} \qquad (4.6)^*$$

(in which $k = V_d/V_s$; $\omega_s = \pi V_s/2H$). The dimensionless static-one-g modal wall pressure distributions are given by

$$\frac{p_{n,m}(y)}{\gamma H} = -\frac{64}{\pi^3}\frac{H}{L}\frac{k^2}{\Omega_{n,m}^2}\frac{1}{(2m-1)}\sin\frac{(2m-1)\pi y}{2H} \qquad (4.7)^*$$

In expression (4.7) n should be restricted to the odd values since only the antisymmetric modes participate under horizontal forcing of the rigid boundaries.

The frequency equation (4.6) was numerically evaluated for Poisson's ratio equal to 0.3 and the results are compared in Fig. 4.4 with the exact solution computed from the frequency equations of Section 3.1. Static-one-g modal pressure distributions evaluated from expression (4.7) are compared with some of the exact smooth wall counterparts in Fig. 4.5.

The steady-state solutions for horizontal harmonic forcing of the rigid boundaries of the $v = 0$ problem were computed in a manner similar to that described for the exact problem in Section 3.5. Typical comparisons of the $v = 0$ and the exact smooth wall complex-amplitudes of wall force are shown in Fig. 4.6. The $v = 0$

*These solutions are singular for $\nu = 0.5$.

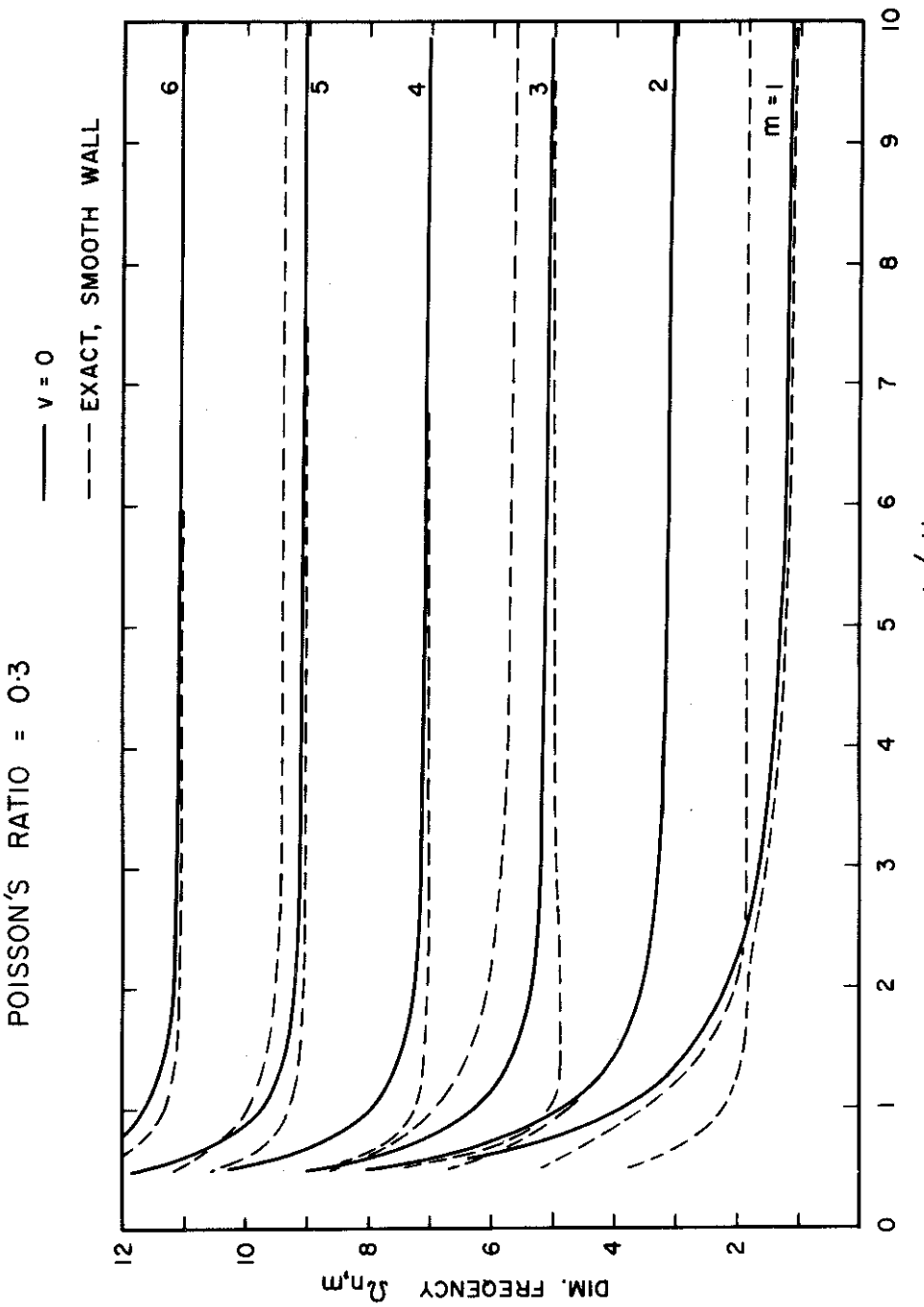

Figure 4.4 Frequency equation solutions. Comparison between exact smooth wall solution and approximate v = 0 analysis. Note that the modes which for large L/nH values have frequencies that approach the vertical-dilitation frequencies of the infinite stratum, do not exist in the v = 0 solution.

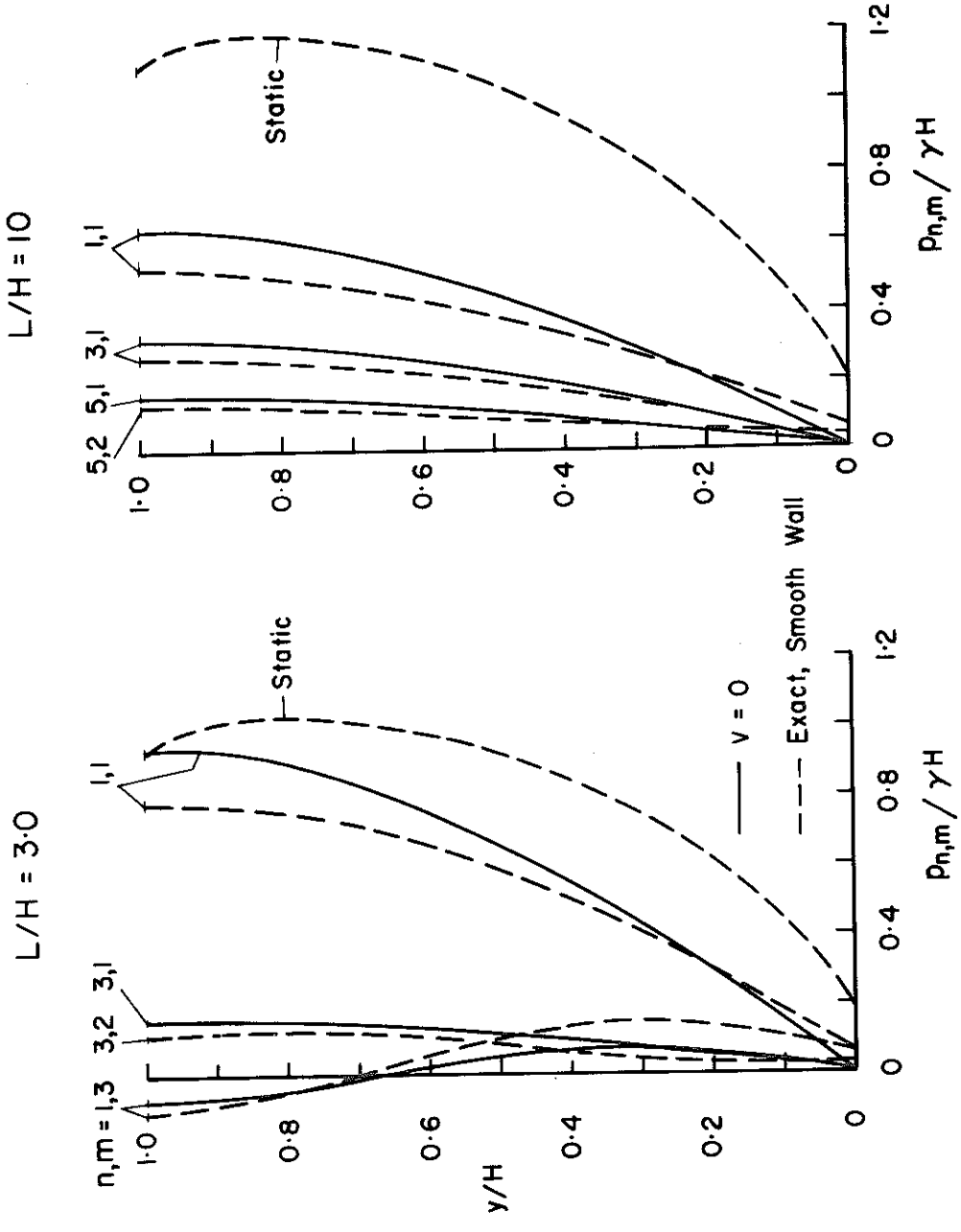

Figure 4.5 Static-one-g modal pressure distributions. Comparison between exact smooth wall solution and approximate $\nu = 0$ analysis.

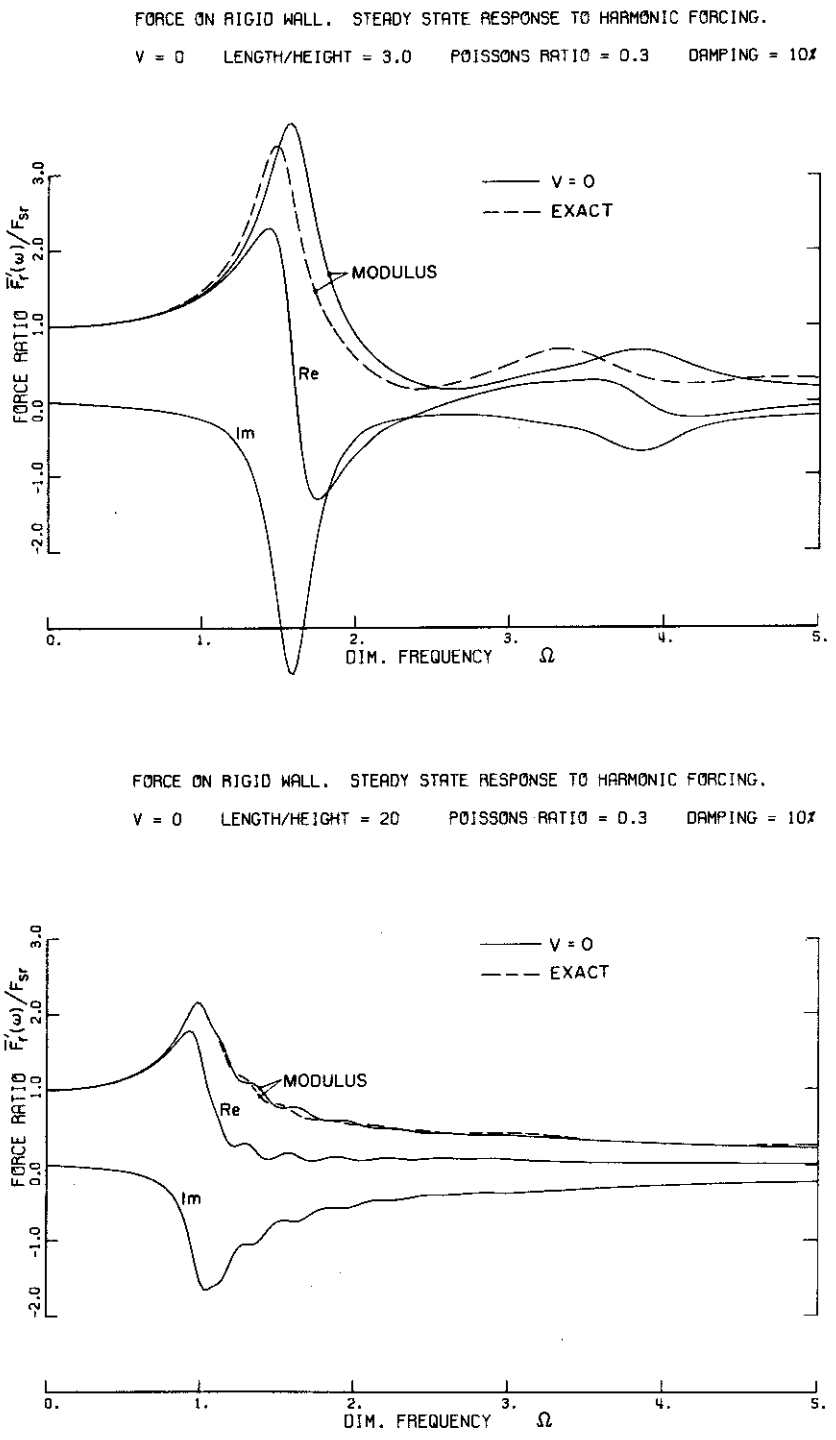

Figure 4.6 Complex-amplitude of force ratio. Comparison between exact smooth wall solutions and approximate $v = 0$ solutions.

approximation tends to increase the natural frequencies, and the shift of the response peaks produced by this effect can be seen in the $\frac{L}{H} = 3.0$ solution. Satisfactory agreement was found between the approximate and exact complex-amplitudes for $\frac{L}{H}$ values greater than 2.0. This agreement improves with increasing $\frac{L}{H}$ values.

4.2. Mononobe-Okabe Method

Although the Mononobe-Okabe method and the theory of elasticity approach should in general be applied to different types of problems, it is of interest to make a comparison between the wall pressures and forces given by both methods. The Mononobe-Okabe pressure distribution, computed using Seed and Whitman's approximation (equation (1.2)), is compared in Fig. 4.7 with pressures from the static elastic theory solutions for the smooth wall with $\frac{L}{H} = 10$. As well as the analytical rigid-wall elastic theory solutions for horizontal body force loading, two plots are shown to illustrate the effects of wall rotation on the rigid-wall pressures. Pressures are shown for both an 0.2% and an 0.4% rotational displacement of the wall. These pressures are the total pressures resulting from both the horizontal body force and the wall rotation. The pressures resulting from wall rotation were taken from finite element solutions described later in this study. In contrast to the rigid-wall case, deformable wall pressures are dependent on the value of Young's modulus (or the shear modulus). The rotating wall solutions presented in Fig. 4.7 were computed using an E value of 10^6 lb/ft^2. For convenience both the elastic solutions and the Mononobe-Okabe pressures are

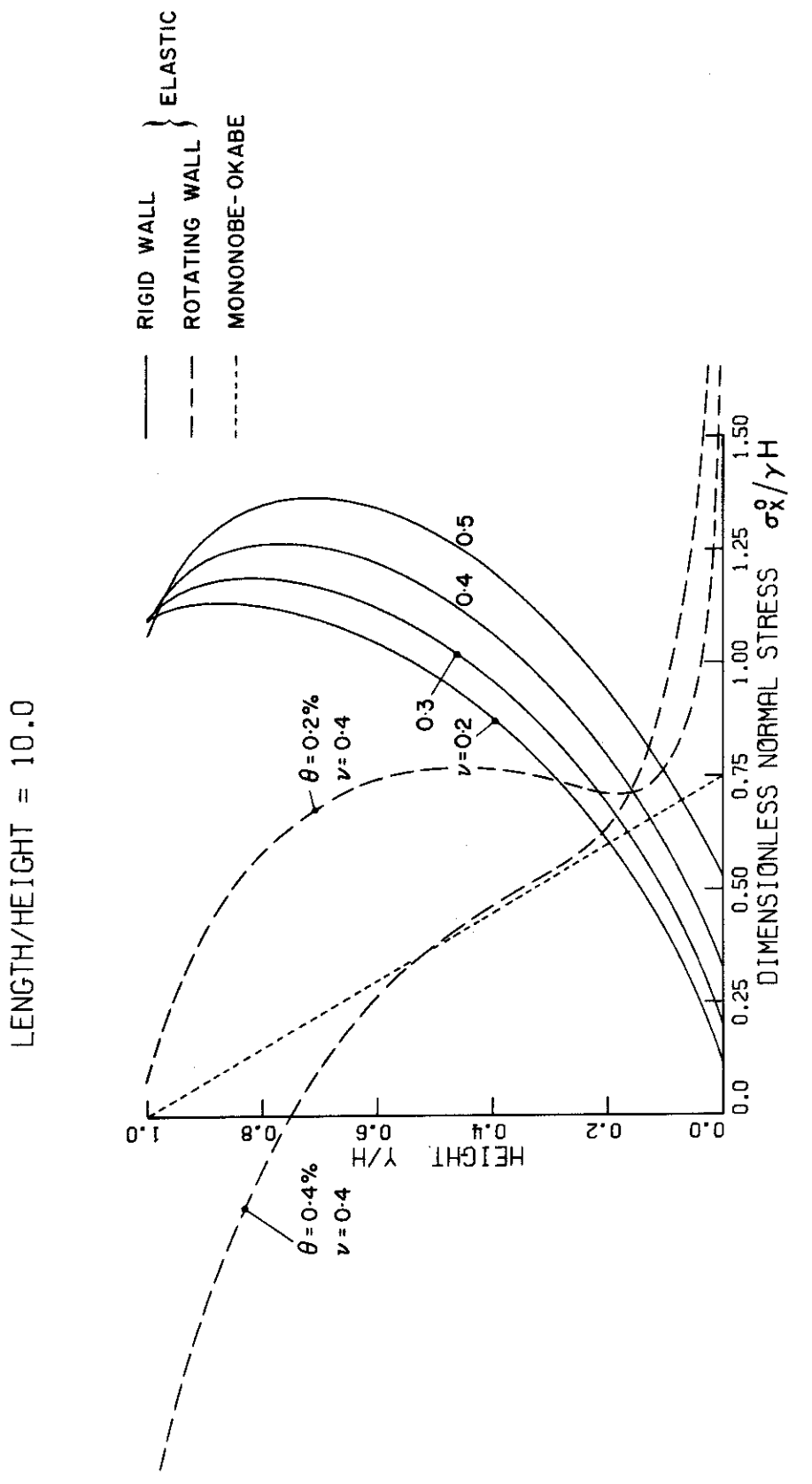

Figure 4.7 Pressure distributions for one-g static horizontal body force. Comparison between elastic theory and Mononobe-Okabe method.

shown for a one-g horizontal body force. For the purpose of the comparison, the Mononobe-Okabe force was assumed to have a triangular pressure distribution with the maximum pressure at the base of the wall. However, it should be kept in mind that the Mononobe-Okabe force is generally assumed to act at a higher center of pressure than indicated by the triangular distribution.

For rigid or almost rigid walls the pressure distributions given in Fig. 4.7 show that the Mononobe-Okabe wall force will be less than one-half of the elastic theory force. The comparison given here has been made on the basis of the static elastic theory solutions. From experience it is found that the static pressures are often good approximations to the maximum earthquake-induced dynamic elastic theory pressures. The following general remarks can be made regarding static approximations for dynamic wall pressures:

(a) static solutions are good approximations for low walls (less than 20 ft) and relatively firm soils;

(b) for damping ratios of 10% or higher in the wall-soil system, dynamic amplification under earthquake forcing will not be pronounced, and in general a static solution will give a conservative estimate of the maximum dynamic pressures.

Wall deformation has a significant influence on the elastic pressure distributions; for an E value less than used here (that is a softer soil) the effect is less pronounced.

5. RIGID WALL: CASTAIC POWER STATION

To illustrate the application of some of the foregoing solutions, the earthquake-induced soil pressures were computed for a soil retaining wall which forms part of the main structure of the Castaic power-generating station.* The Castaic power plant is a 1,250,000 kilowatt reversible-turbine hydro-electric facility located approximately 45 miles northwest of downtown Los Angeles and about 11 miles from the San Andreas fault. A typical cross-section of the powerhouse, which shows the extent of the soil retaining function of one face of the structure, is shown in Fig. 5.1. Photographs in Figs. 5.2 and 5.3 show details of the structure and the soil being placed alongside the building during construction.

Because of the rock foundation and the rigid nature of the structure, a moderately good approximation for the earthquake pressures can be obtained by assuming rigid-wall behavior. The influence of the dynamics of the structure and the displacement of the wall have been investigated and are discussed in Chapter 8. For the purpose of the following illustrative example the wall was assumed rigid.

The earthquake-induced wall pressures were computed using the static finite element method, the normal mode finite element method and the exact analytical normal mode solution for the smooth rigid wall. In the finite element analyses both smooth and bonded

---

*The Castaic power-generating station, which is at the present time under construction, is a joint venture of the City of Los Angeles, Department of Water and Power and the California State Department of Water Resources.

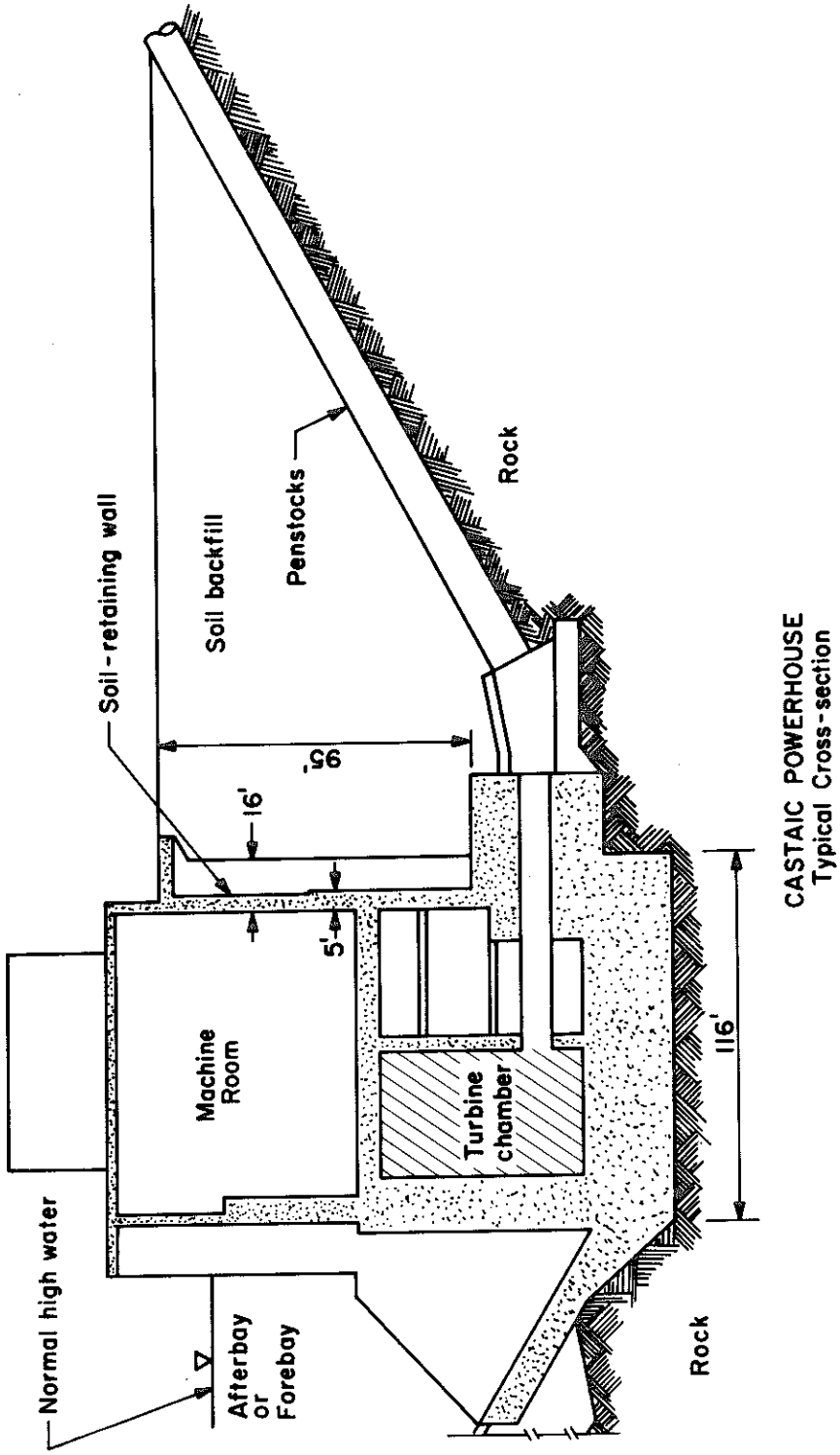
Soil - retaining wall
Soil backfill
Penstocks
Rock
95'
16'
5'
Machine Room
Turbine chamber
116'
Normal high water
Afterbay or Forebay
Rock
CASTAIC POWERHOUSE
Typical Cross-section

Figure 5.1

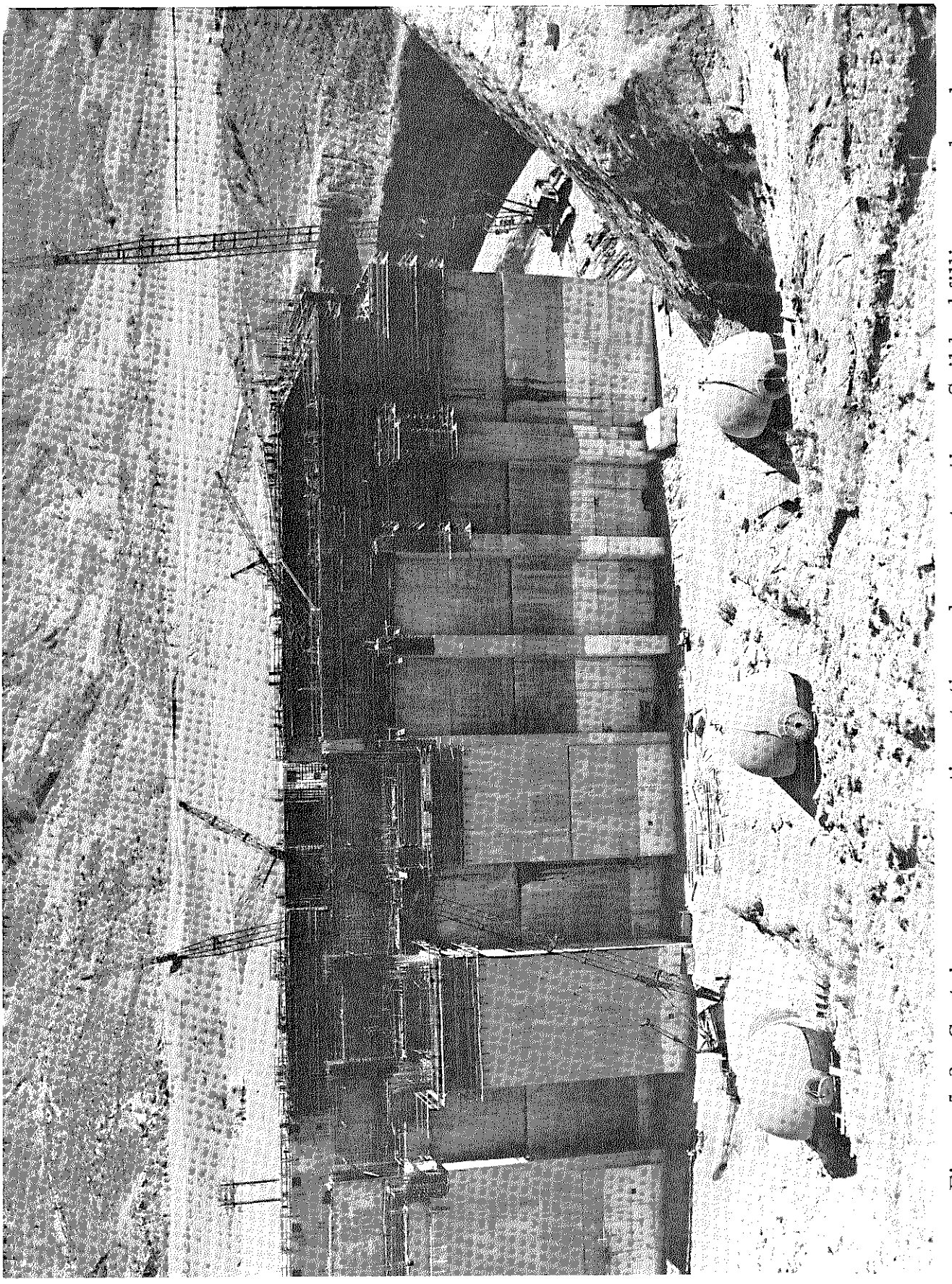

Figure 5.2 Castaic power-generating station under construction. Soil backfilling was placed between the wall in view and the penstock slope in the foreground.

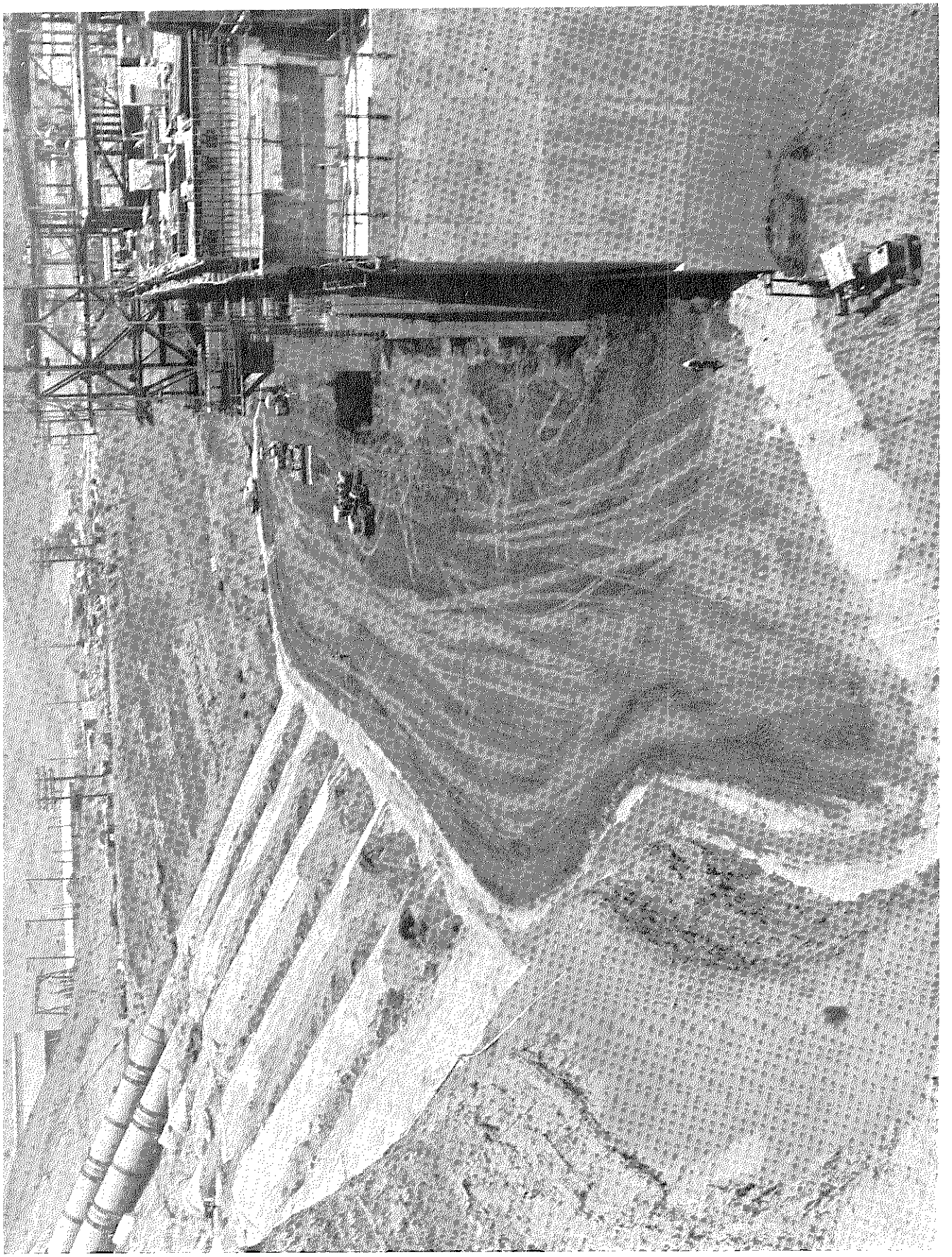

Figure 5.3 Castaic power-generating station under construction. Soil backfilling being placed against wall of structure.

wall contacts were used. The other boundary conditions and the mesh for the dynamic solutions are shown in Fig. 5.4. A mesh with 5 ft × 5 ft elements in the vicinity of the wall was used for the static solutions. In the application of the analytical solution the soil body was represented by an equivalent rectangle having $\frac{L}{H} = 1.67$. The following soil properties (from Scott[47]) were used:

Young's modulus	$E = 10^6$ lb/ft^2
Poisson's ratio	$\nu = 0.4$
unit weight	$\gamma = 120$ lb/ft^2

The static pressure distributions for a one-g horizontal body force and the significant static-one-g modal pressure contributions are plotted in Fig. 5.5a. (Gravity pressures are not included in these results.) The natural frequencies of the modes that gave significant contribution to the wall pressure distributions are given in Table 5.1.

TABLE 5.1

Natural Frequencies

F.E. Bonded		F.E. Smooth		Analytical	
Mode*	Freq. hz	Mode*	Freq. hz	Mode	Freq. hz
1	1.82	1	1.68	1,1	1.58
6	3.68	2	2.00	1,2	2.14
		7	3.85	1,3	3.42

*Mode number in order of increasing frequency as given by the finite element analyses.

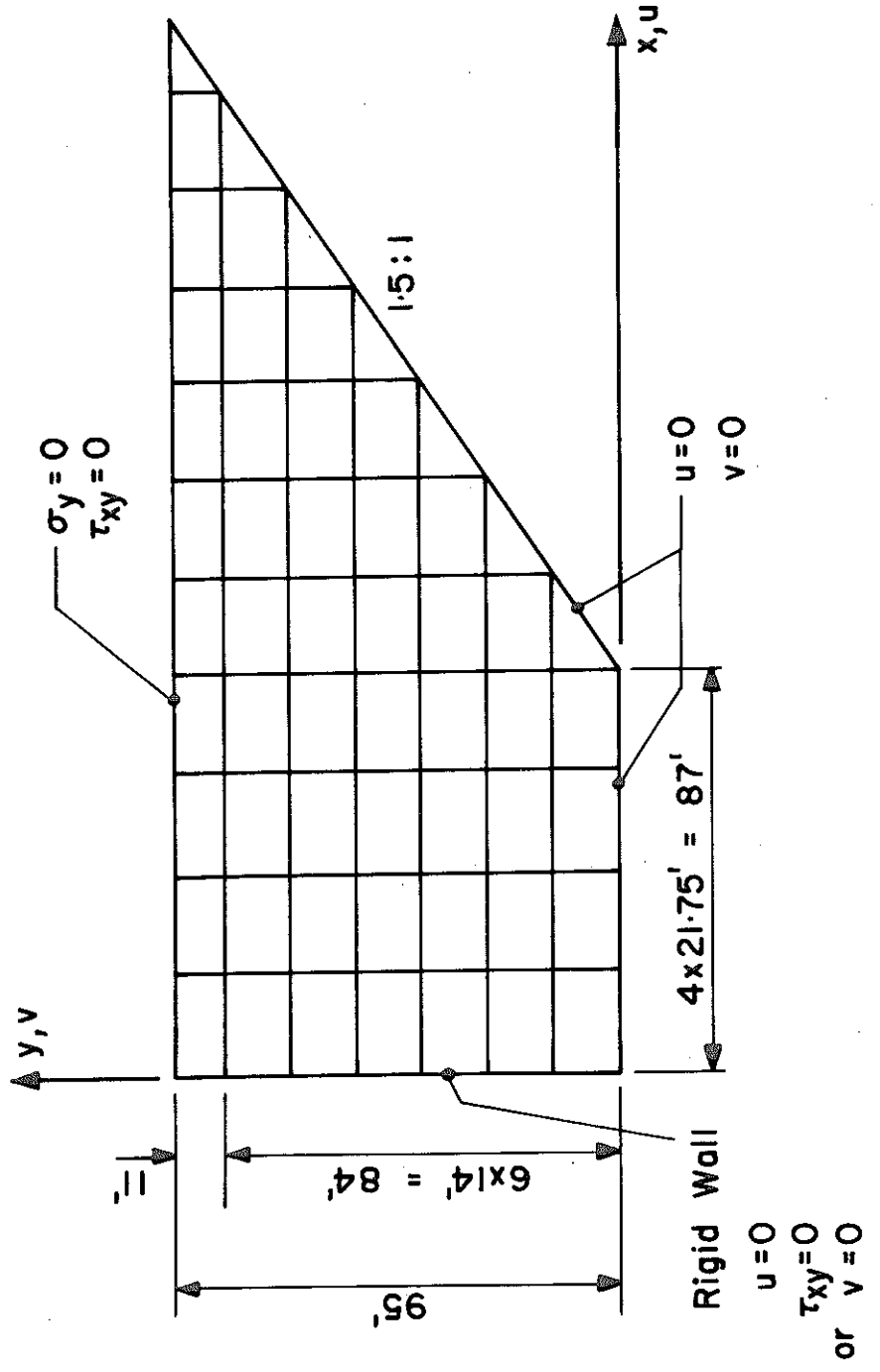

CASTIC PROBLEM. MESH FOR NORMAL MODES.

Figure 5.4

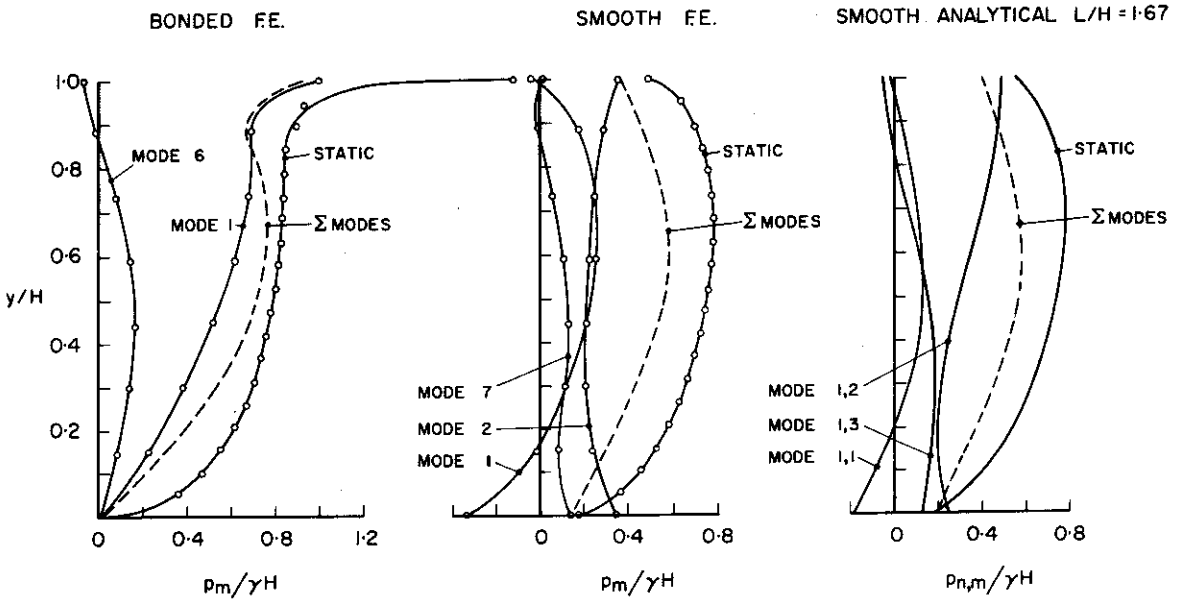

Figure 5.5a Castaic example. Static-one-g modal pressure distributions.

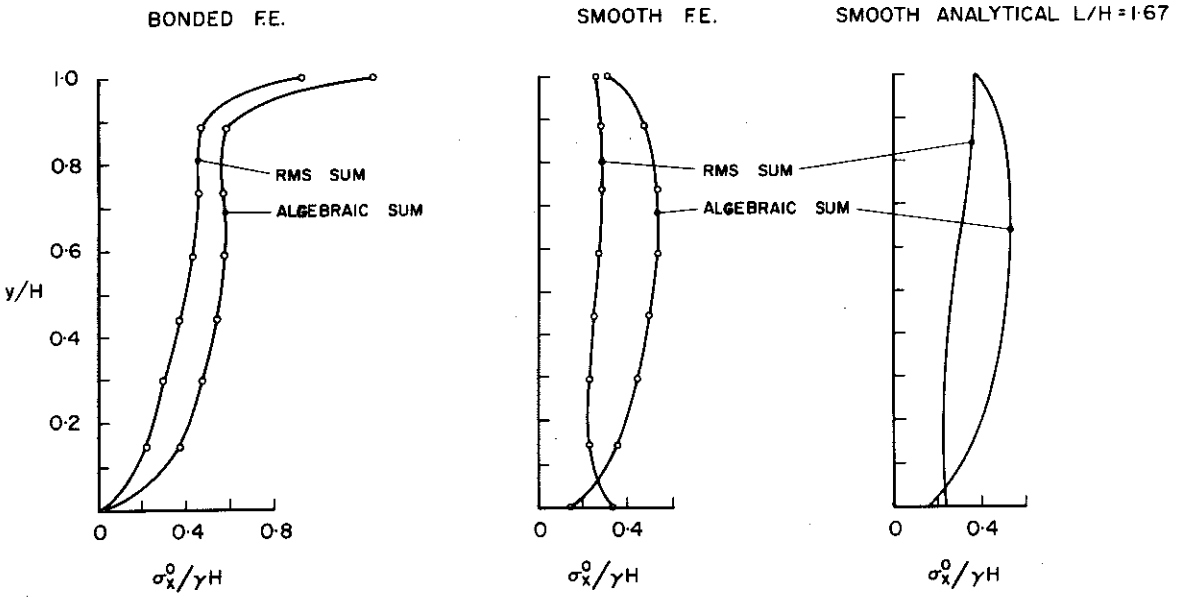

Figure 5.5b Castaic example. Estimates of maximum earthquake-induced pressures.

Maximum earthquake-induced pressure distributions were computed using the Response Spectrum method, and the 10% damped velocity spectrum given in Appendix VIII.* The effects of the higher modes were included by using a "rigid" mode having a pressure distribution the difference between the appropriate static solution and the sum of the two modal contributions for the bonded wall and the three contributions for both the smooth wall solutions. This "rigid" mode distribution was assumed to contribute at an acceleration of 0.33 g (that is the peak ground acceleration). Plots of the pressure distributions obtained by taking the root-mean-square sums and the algebraic sums of the modal contributions (including the "rigid" mode) are given in Fig. 5.5b. The large difference between the rms and the algebraic sums of the modal pressures for the smooth wall cases is due to the relatively similar magnitude of two of the modal contributions. In the bonded contact case most of the pressure distribution comes from a single mode and thus the difference between the pressures summed by the two methods is relatively small. Near $\frac{L}{H}$ values of 2.0 it was previously found that the relative magnitude of the modal pressure contributions of the analytical solution were quite sensitive to the value of the $\frac{L}{H}$ parameter. This type of effect is probably the reason for the difference in character of the bonded and smooth contact modal solutions of this problem. For cases in which a significant difference occurs between

*Because of the closeness of this facility to the San Andreas fault a response spectrum of higher intensity was used for design.

the rms and algebraic sum it would appear reasonable to use for design a pressure distribution intermediate between the two results or to at least consider the consequence of an unfavorable combination of the modes.

In general the agreement between the three different solutions is relatively good. Better agreement between the bonded and the smooth contact solutions would be expected for values of equivalent $\frac{L}{H}$ greater than 2.5 and for equivalent $\frac{L}{H}$ values between 0.5 and 1.5. In these ranges the relative participation of the modal contributions becomes less sensitive to changes in the geometry and boundary conditions.

The random vibration theory method, outlined in Section 3.8, was used to compute statistical estimates of the earthquake-induced maximum wall force and moment. To obtain approximate equivalence with the velocity response spectra given in Appendix VIII, the power spectral density shown in Fig. 3.27 was increased by a factor of 8.0. (Further study is required to establish a more exact equivalence.) Mean-square forces and moments were computed using this increased power spectral density function and the complex-amplitude response functions given in Fig. 3.19 for the $\frac{L}{H} = 2.0$, $\nu = 0.4$ case. (A $\frac{L}{H}$ value of 2.0 was used for this illustration because the complex-amplitude responses had been previously computed for this case.) From the properties of the normal distribution curve, a value 2.5 times greater than the mean will not be exceeded at a probability of 0.988. The $P = 0.988$ values of wall force and moment are given in Table 5.2 below. For comparison the earthquake-induced force and

moment were evaluated using the Response Spectrum method. The method was applied by using the three largest modal contributions from the analytical solution for $\frac{L}{H} = 2.0$ and $\nu = 0.4$ (tabulated in Appendix VI), and a "rigid" mode that was chosen to give a modal summation equal to the static solutions. The earthquake modal responses were computed from the 10% damped velocity spectrum given in Appendix VIII. Absolute and rms sums of the modal responses are given in Table 5.2. The static elastic theory (analytical) force and moment, the Mononobe-Okabe force and moment and vertical gravity values are also given in Table 5.2.

The vertical gravity force and moment were computed from the analytical expression for the normal stress on a smooth rigid wall given by

$$\frac{\sigma_x(0,y)}{\gamma H} = \frac{\nu}{1-\nu}\left(1 - \frac{y}{H}\right) \qquad (5.1)$$

where the origin of the coordinate system is assumed at the base of the wall.

The Mononobe-Okabe force and moment are significantly less than the values computed by the other methods. Because the soil is expected to remain essentially elastic for this problem, the Mononobe-Okabe method is not really applicable; however, the values from this method are given to show the error that might result if the method is used. The force and moment obtained from the static theory of elasticity solution are probably conservative and this approach appears likely to give a good first approximation for

many rigid wall structures.

TABLE 5.2

Castaic Forces and Moments
Rigid wall, Smooth Contact, $\frac{L}{H} = 2.0$, $\nu = 0.4$

Method of Computation	Force/γH^2	Moment/γH^3
Random Vibration	0.140	0.076
Response Spectrum, $\zeta = 10\%$ rms sum	0.130	0.071
Response Spectrum, $\zeta = 10\%$ absolute sum	0.245	0.130
Static Solution for $k_h = 0.33$ g (elastic, analytical)	0.235	0.128
Mononobe-Okabe for $k_h = 0.33$ g (triangular pressure distribution)	0.124	0.041
Vertical Gravity (elastic, analytical)	0.333	0.111

6. FORCED WALL

It is convenient to evaluate the earthquake-induced pressures on deformable wall structures by obtaining the solution in two parts; a rigid-wall solution for soil body forcing, and a solution for displacement forcing on the wall boundary. If the wall-soil system is assumed to be linear, the principle of superposition can be applied to combine these two solutions to give the total earthquake-induced pressures. To obtain an essentially exact solution it is necessary to perform the superposition in the frequency domain using the harmonically forced steady-state solutions for the two cases. In this chapter solutions are presented for both static and harmonic displacement forcing on the wall boundary. In Chapter 7 these solutions are superimposed with the rigid-wall solutions to give total earthquake forces and moments on the deformable wall.

In Section 1.2 wall types and their basic deformational behavior under horizontal earthquake loads were discussed. It is clearly not possible to consider all types of wall deformation in a general investigation and in this study only a rotational deformation of the wall about its base is considered in detail. This type of wall displacement will probably be a relatively good approximation for many cases. The methods used for the rotational deformation can be extended to analyze other forms of wall displacement.

6.1. STATIC ANALYTICAL SOLUTION

An analytical solution is presented in this section for the pressures on a smooth wall resulting from a static rotational displacement. The soil is once again assumed to be a homogeneous linearly elastic medium. The problem and the boundary conditions are shown in Fig. 6.1. From the equilibrium equations and the stress-strain relations (expressions (2.1) and (2.2))

$$k^2 \frac{\partial^2 u}{\partial x^2} + (k^2-1) \frac{\partial^2 v}{\partial x \partial y} + \frac{\partial^2 u}{\partial y^2} = 0$$

$$k^2 \frac{\partial^2 v}{\partial y^2} + (k^2-1) \frac{\partial^2 u}{\partial x \partial y} + \frac{\partial^2 v}{\partial x^2} = 0 \qquad (6.1)$$

for $\quad 0 < x < L \; ; \quad 0 < y < H$

The solution of equations (6.1) can be expressed in the following form:

$$u(x,y) = \frac{u^o y}{H} \cos px + \sum_{n=0}^{\infty} \bar{u}_n(y) \sin rx$$

$$v(x,y) = -\frac{u^o}{Hp} \sin px + \sum_{n=0}^{\infty} \bar{v}_n(y) \cos rx \qquad (6.2)$$

in which

$$r = \frac{n\pi}{L} \; , \quad n = 0,1,2,\ldots$$

$$p = \frac{\pi}{2L}$$

u^o = displacement in the x-direction at the top of the wall

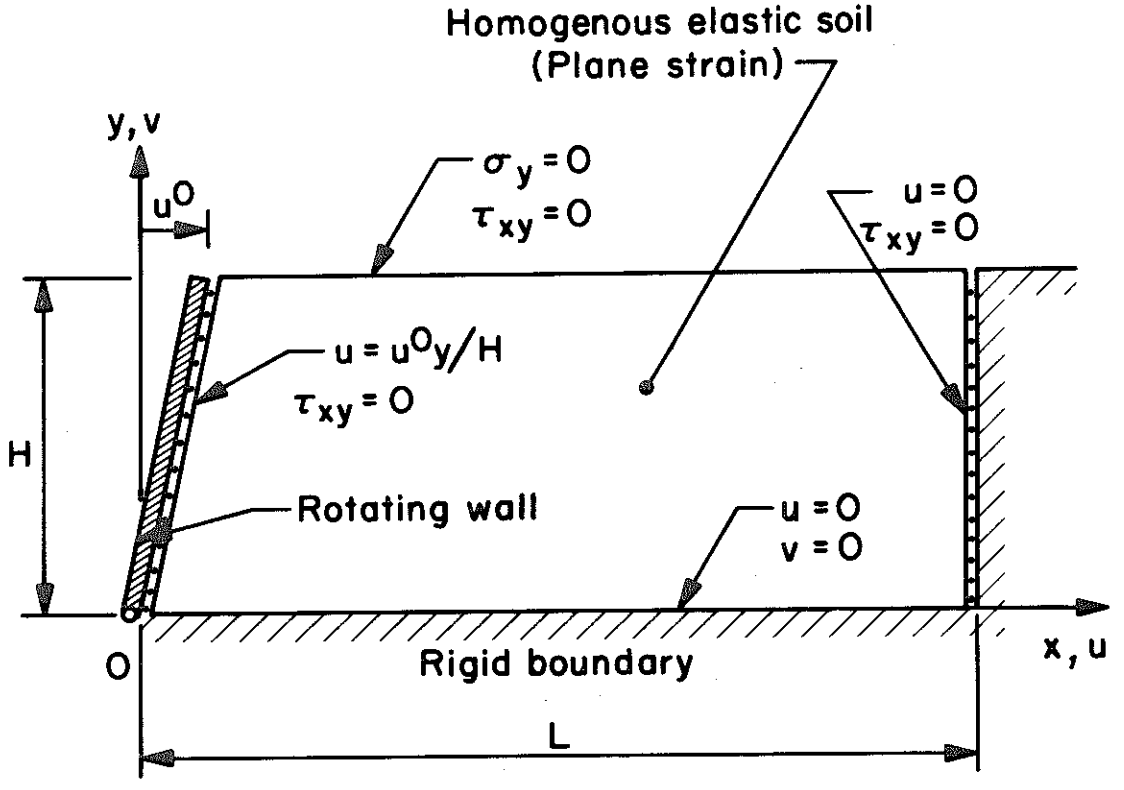

DISPLACEMENT FORCING OF WALL

Figure 6.1

In this form the solution clearly satisfies the displacement boundary conditions at $x = 0$ and $x = L$. Substitution of expressions (6.2) into the stress-strain relation for shear stress gives

$$\frac{\tau_{xy}}{G} = \sum_{n=0}^{\infty} \left\{ \frac{\partial \bar{u}_n(y)}{\partial y} - r\bar{v}_n(y) \right\} \sin rx \tag{6.3}$$

From expression (6.3) it is evident that the stress boundary condition ($\tau_{xy} = 0$) at $x = 0$ and $x = L$ is also satisfied by the assumed solution. Substitution of equations (6.2) into equations (6.1) gives

$$\sum_{n=0}^{\infty} \left\{ \frac{\partial^2 \bar{u}_n}{\partial y^2} - r^2 k^2 \bar{u}_n - (k^2-1) r \frac{\partial \bar{v}_n}{\partial y} \right\} \sin rx = \frac{u^o k^2 p^2 y}{H} \cos px$$

$$\sum_{n=0}^{\infty} \left\{ \frac{\partial^2 \bar{v}_n}{\partial y^2} - \frac{r^2}{k^2} \bar{v}_n + \frac{(k^2-1) r}{k^2} \frac{\partial \bar{u}_n}{\partial y} \right\} \cos rx = \frac{u^o (k^2-2) p}{H k^2} \sin px \tag{6.4}$$

Fourier series expansions can be written for $\sin px$ and $\cos px$ as follows

$$\sin px = a_0 + \sum_{n=1}^{\infty} a_n \cos \frac{n\pi x}{L}$$

$$\cos px = \sum_{n=1}^{\infty} b_n \sin \frac{n\pi x}{L} \tag{6.5}$$

in which

$$a_0 = \frac{2}{\pi}$$

$$a_n = -\frac{4}{\pi} \frac{1}{(4n^2-1)} \quad , \quad n = 1, 2, 3, \ldots$$

$$b_n = \frac{4}{\pi} \frac{n}{(4n^2-1)} \quad , \quad n = 1,2,3,\ldots$$

Hence for a particular value of n (except the special case of $n = 0$ which is treated later) equations (6.4) give

$$\frac{\partial^2 \bar{u}_n}{\partial y^2} - r^2 k^2 \bar{u}_n - (k^2-1) r \frac{\partial \bar{v}_n}{\partial y} = \frac{u^o b_n k^2 p^2 y}{H}$$

$$\frac{\partial^2 \bar{v}_n}{\partial y^2} - \frac{r^2}{k^2} \bar{v}_n + \frac{(k^2-1) r}{k^2} \frac{\partial \bar{u}_n}{\partial y} = \frac{u^o a_n (k^2-2) p}{H k^2} \qquad (6.6)$$

It can be shown by substitution that a general form of the solution of equations (6.6) is

$$\bar{u}_n(y) = \frac{u^o a_n}{Hp} \left[B_n \sinh ry + C_n ry e^{ry} + D_n ry e^{-ry} + \frac{np^3 y}{r^2} \right]$$

$$\bar{v}_n(y) = \frac{u^o a_n}{Hp} \Big[-B_n \cosh ry - C_n (ry - k') e^{ry} + D_n (ry + k') e^{-ry} \qquad (6.7)$$

$$- \left(\frac{p}{r}\right)^2 \left\{ (k^2-2) - \frac{np}{r} (k^2-1) \right\} \Big]$$

in which

$$k' = 3 - 4\nu$$

B_n, C_n, D_n = constants determined by the boundary conditions at $y = 0$ and $y = H$

The boundary conditions at $y = 0$ are $u = 0$ and $v = 0$. Hence from expressions (6.2)

$$\left.\begin{aligned} \bar{u}_n(0) &= 0 \\ \bar{v}_n(0) &= \frac{u^o a_n}{Hp} \end{aligned}\right\} \text{ at } y = 0 \qquad (6.8)$$

At $y = H$, $\sigma_y = 0$ and $\tau_{xy} = 0$. From the stress-strain relations and expressions (6.2) it is readily shown that these boundary conditions require

$$\left.\begin{aligned} \left(\frac{\partial \bar{u}_n}{\partial y} - r\bar{v}_n\right)\sin rx &= 0 \\ k^2 \frac{\partial \bar{v}_n}{\partial y} + (k^2-2)r\bar{u}_n &= u^0(k^2-2)pa_n \end{aligned}\right\} \text{ at } y = H \qquad (6.9)$$

The first equation of expressions (6.8) is satisfied directly by expressions (6.7). From the second equations of expressions (6.7) and (6.8)

$$B_n = k'(C_n + D_n) - \left[\left(\frac{p}{r}\right)^2\left\{(k^2-2) - \frac{np}{r}(k^2-1)\right\} + 1\right] \qquad (6.10)$$

Substitution of expressions (6.7) and (6.10) into (6.9) gives

$$\begin{aligned} &C_n[(2rH-k'+1)e^{rH} + 2k'\cosh rH] + D_n[(-2rH-k'+1)e^{-rH} + 2k'\cosh rH] \\ &\qquad = 2d_n \cosh rH - f_n \\ &C_n[(2rH-k'-1)e^{rH} + 2k'\sinh rH] + D_n[(2rH+k'+1)e^{-rH} + 2k'\sinh rH] \\ &\qquad = 2d_n \sinh rH - rHf_n \end{aligned} \qquad (6.11)$$

in which

$$d_n = \left(\frac{p}{r}\right)^2 \left\{(k^2-2) - \frac{np}{r}(k^2-1)\right\} + 1$$

$$f_n = \left(\frac{p}{r}\right)^2 (k^2-2)\left(1 - \frac{np}{r}\right)$$

Solution of the linear algebraic equations (6.11) gives

$$C_n = \frac{1}{\Delta}\left[e^{-rH}\left\{(2rH+k'+1)(2d_n\cosh rH - f_n)\right.\right.$$
$$\left.\left. - (2rH+k'-1)(2d_n\sinh rH - rHf_n)\right\} - 2k'f_n(\sinh rH - rH\cosh rH)\right]$$

(6.12)

$$D_n = \frac{1}{\Delta}\left[e^{rH}\left\{(2rH-k'+1)(2d_n\sinh rH - rHf_n)\right.\right.$$
$$\left.\left. + (2rH-k'-1)(2d_n\cosh rH - f_n)\right\} + 2k'f_n(\sinh rH - rH\cosh rH)\right]$$

in which

$$\Delta = 2\left\{1 + (2rH)^2 + k'^2 + 2k'(\sinh^2 rH + \cosh^2 rH)\right\}$$

For the special case of $n = 0$ the partial differential equations reduce to a single equation given by

$$\frac{\partial^2 \bar{v}_0}{\partial y^2} = \frac{u^o a_0 p(k^2-2)}{Hk^2} \tag{6.13}$$

A solution of equation (6.13) that satisfies the appropriate boundary conditions at $y = 0$ and $y = H$ is

$$\bar{v}_0 = \frac{u^o a_0}{Hp}\left[H^2p^2\,\frac{(k^2-2)}{k^2}\,\frac{y^2}{2H^2} + 1\right] \tag{6.14}$$

The complete displacement solution can be expressed in the

following dimensionless form,

$$\frac{u(x,y)}{u^o} = \frac{y}{H}\cos px + \frac{1}{Hp}\sum_{n=1}^{\infty} a_n\Big\{B_n \sinh ry + C_n ry e^{ry} + D_n ry e^{-ry} + \frac{np^3 y}{r^2}\Big\}\sin rx \tag{6.15}$$

$$\frac{v(x,y)}{u^o} = -\frac{1}{Hp}\sin px + \frac{a_o}{Hp}\left[H^2p^2\frac{(k^2-2)}{k^2}\frac{y^2}{2H^2}+1\right] + \frac{1}{Hp}\sum_{n=1}^{\infty} a_n\Big[-B_n\cosh ry - C_n(ry-k')e^{ry} + D_n(ry+k')e^{-ry} - \left(\frac{p}{r}\right)^2\Big\{(k^2-2) - \frac{np}{r}(k^2-1)\Big\}\Big]\cos rx$$

(in which $r = n\pi/L$, $p = \pi/2L$).

The normal stress on the wall $\sigma_x^o(y)$ is readily derived from the displacement solution and the stress-strain relations, and can be expressed as

$$\frac{\sigma_x^o(y)H}{Gu^o} = a_o Hp\frac{(k^2-2)}{k^2}\frac{y}{H} + \sum_{n=1}^{\infty}\frac{a_n r}{p}\Big\{2B_n\sinh ry + C_n(2ry-k'+3)e^{ry} + D_n(2ry+k'-3)e^{-ry} + \frac{k^2 np^3 y}{r^2}\Big\} \tag{6.16}$$

The above solution has not been numerically evaluated; however, it is expected that this can be performed with the aid of a simple digital computer program similar to that used in Section 2.1

for the rigid-wall problem.

Inspection of expression (6.16) shows that the wall pressures for this problem are singular for Poisson's ratio equal to 0.5. It is of interest to note that the formal solution for the case $L \rightarrow \infty$ is readily derived by taking Fourier transforms of equations(6.1) with respect to x. The sine transform is used for the first equation, the cosine for the second, and in principle the solution is obtained in a manner similar to the bounded problem. It does not appear possible to express the Fourier integral of the formal solution in analytical form; however, approximate expressions and numerical methods can be applied to give solutions.

Solutions for forcing by a higher-order displacement function on the wall boundary can be evaluated by assuming a solution of the form

$$u(x,y) = \frac{u^o y^m}{H} \cos px + \sum_{n=0}^{\infty} \bar{u}_n(y) \sin rx$$

$$v(x,y) = -\frac{u^o y^{(m-1)}}{mHp} \sin px + \sum_{n=0}^{\infty} \bar{v}_n(y) \cos rx \qquad (6.17)$$

in which $m = 2,3,4,\ldots$.

6.2. STATIC FINITE ELEMENT SOLUTIONS

Pressures on the statically rotated wall of the problem shown in Fig. 6.1 and studied in the previous section were evaluated using the finite element method. The second-order quadrilateral element and the mesh described previously for the rigid-wall solutions

(Fig. 2.7) were used. (The previously used antisymmetry is not applicable for this problem and so a mesh extending the full length of the problem was used.)

The wall pressures computed for various values of $\frac{L}{H}$ and Poisson's ratio are shown in Figs. 6.2 and 6.3*. The wall forces and moments (about the base of the wall) were computed by numerical integration of the finite element pressure distributions and are plotted in Fig. 6.4. The wall pressures, forces and moments are dependent on the soil elastic moduli (E or G) and the magnitude of the rotation θ. Consequently these variables appear in the dimensionless parameters used in the pressure and force plots. (In contrast the rigid-wall pressures and forces are independent of the soil moduli.)

The effect of assuming a bonded contact on the wall boundary was investigated by computing solutions with the wall boundary conditions taken as $u = \frac{u^o y}{H}$ and $v = 0$. The bonded contact pressures for $\frac{L}{H} = 5.0$ and Poisson's ratio values of 0.3 and 0.4 are compared with the smooth wall counterparts in Fig. 6.5. Except in the region at the top of the wall $(\frac{y}{H} > 0.8)$, where the bonded wall stresses become singular, agreement between the smooth and bonded pressure distributions is moderately good. In view of the fact that the development of the singularity will be limited by the nonuniform and nonlinear properties of a typical soil, the difference between the results for the two contact assumptions is unlikely to be of practical significance.

*The pressure distributions shown in this section do not include stresses resulting from gravity forces in the soil.

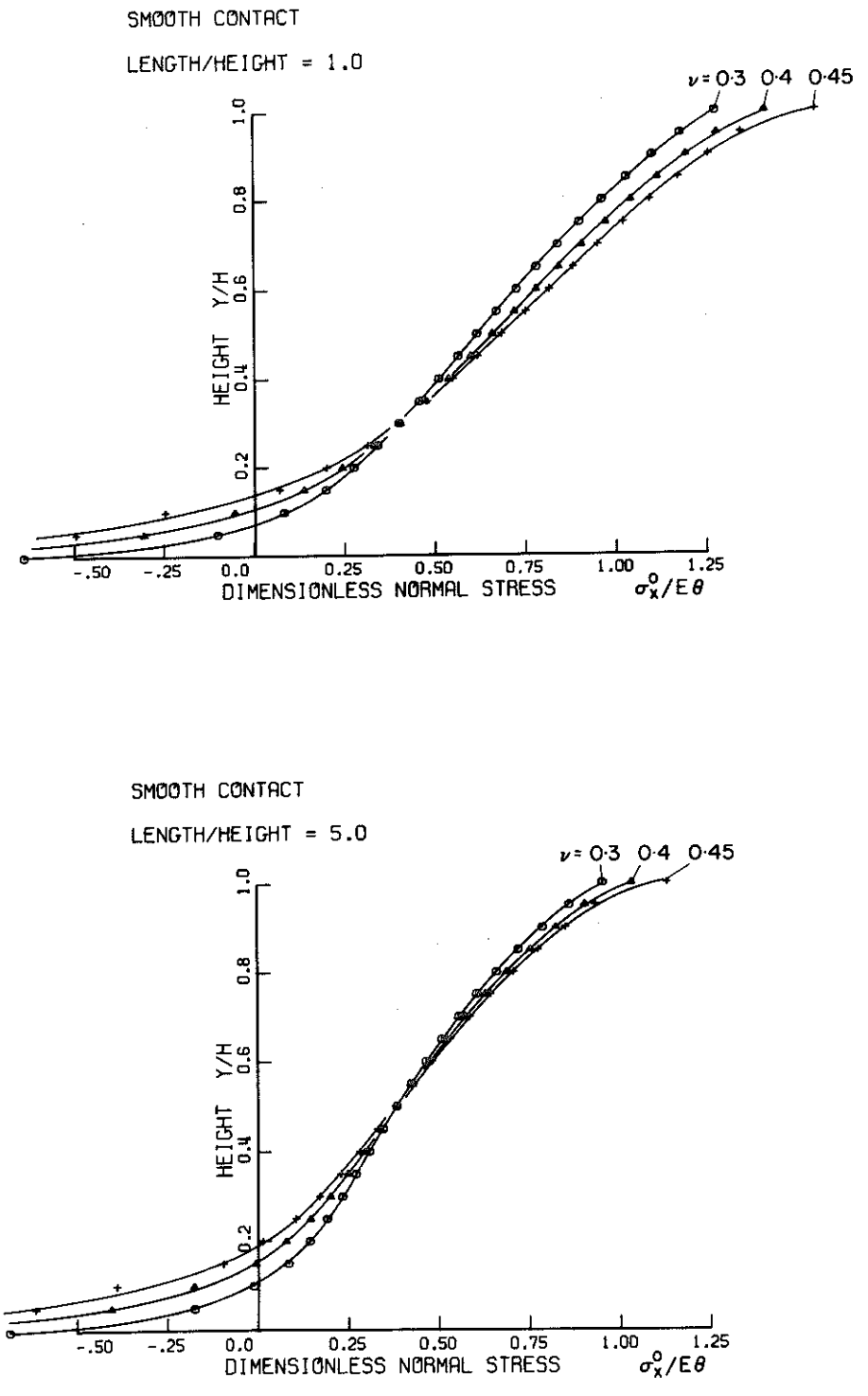

Figure 6.2 Pressure distributions on statically forced smooth rotating wall.

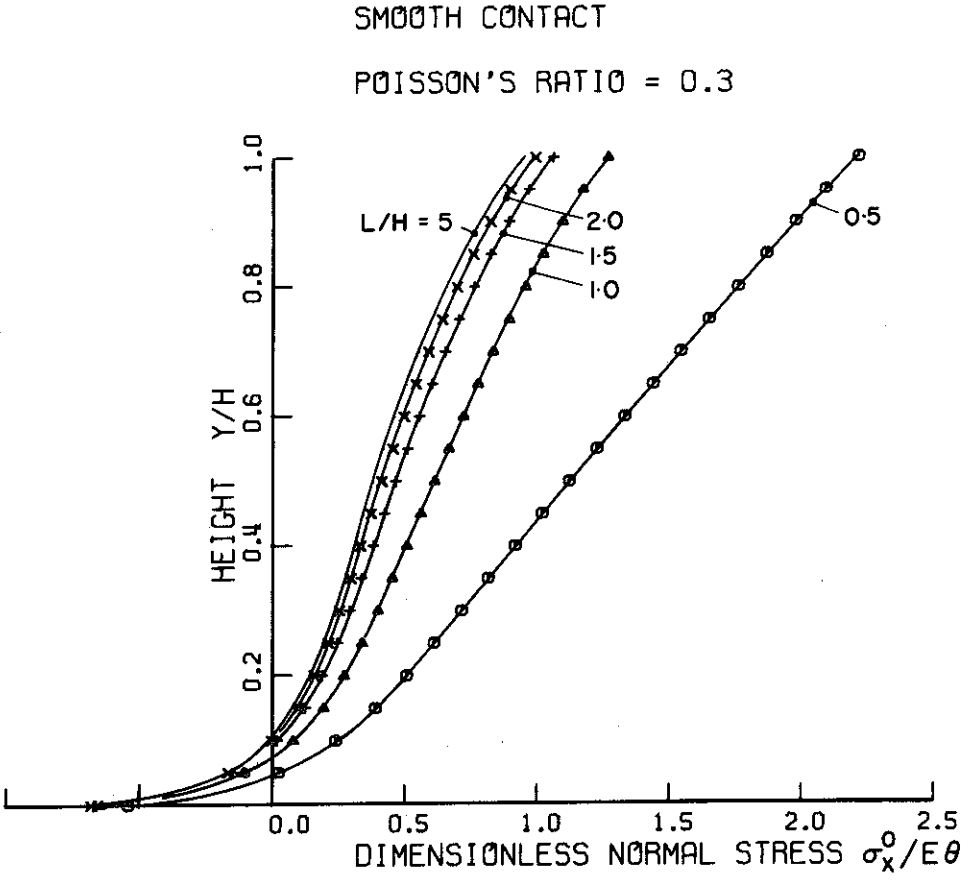

Figure 6.3 Pressure distributions on statically forced smooth rotating wall.

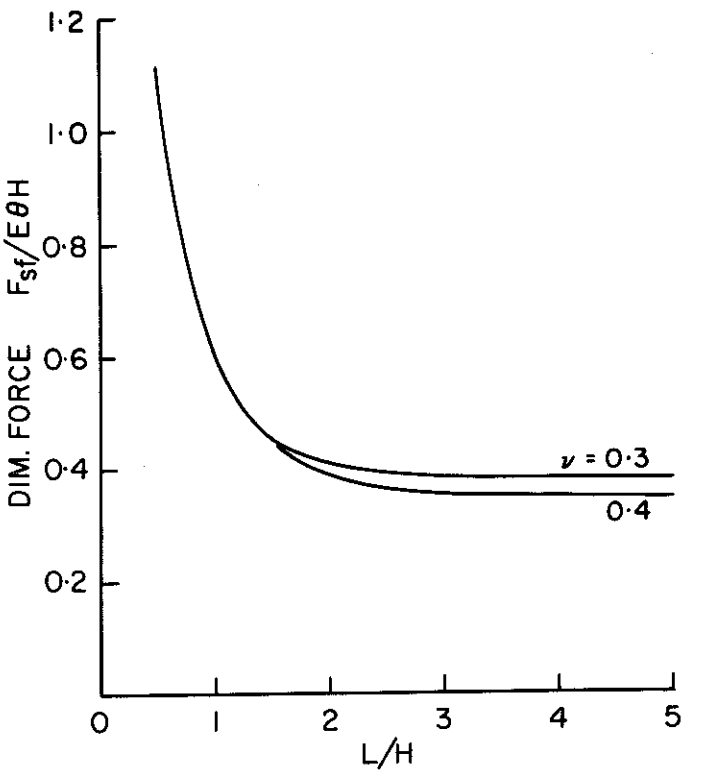

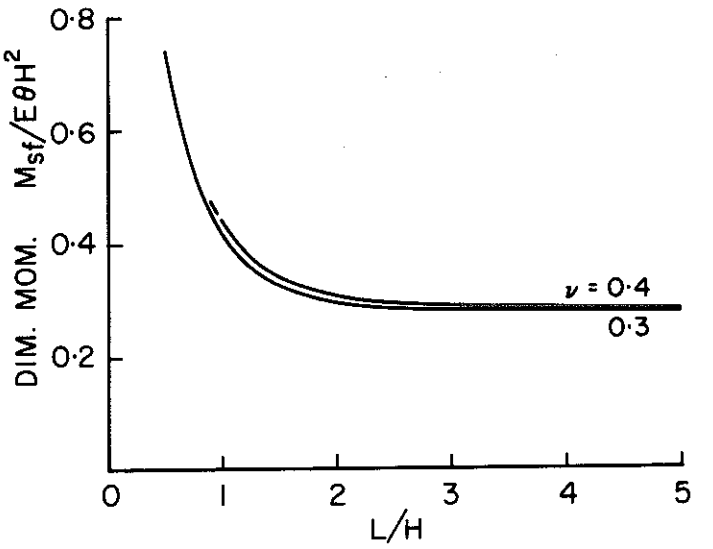

Figure 6.4 Force and moment on statically forced smooth rotating wall.

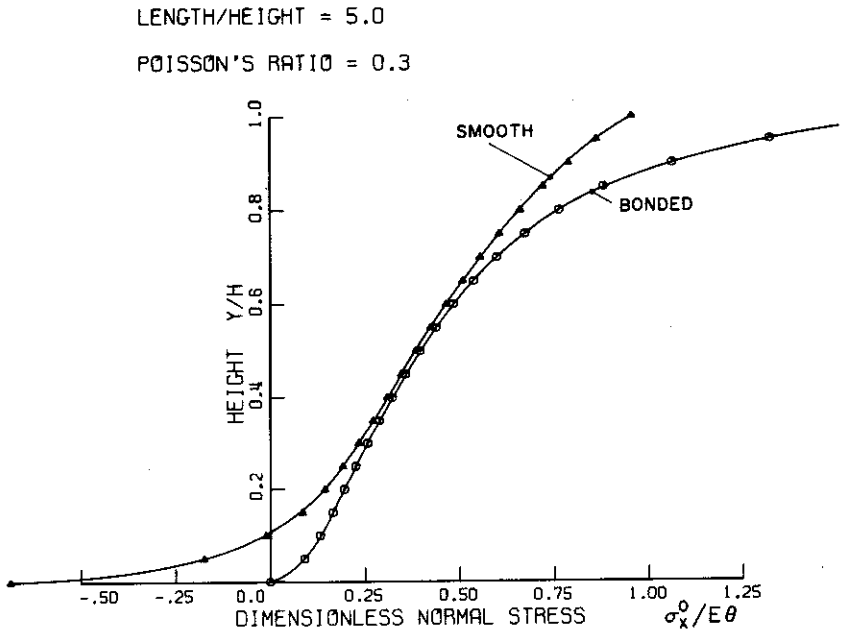

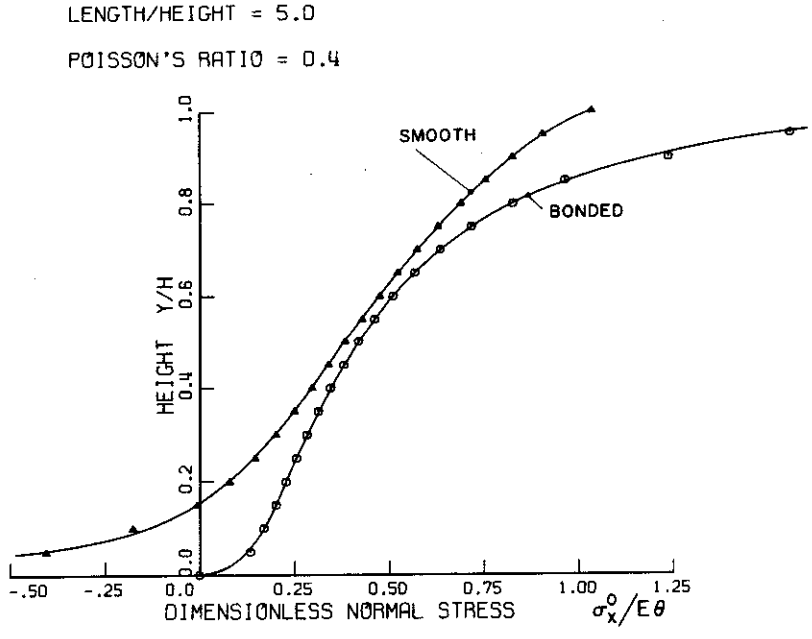

Figure 6.5 Pressure distributions on statically forced rotating walls. Comparison between smooth and bonded contacts.

The finite element results for the normal and shear stresses on the bonded contact wall boundary are given in Table 6.1. To determine whether sliding will occur on the wall-soil interface when the wall undergoes rotational deformation it is necessary to consider the superposition of the stresses given in Table 6.1 with the stresses induced by gravity and horizontal body forces (see Table 2.2).

The influence on the pressure distributions of a variation of the soil elastic moduli (E or G) with depth was investigated by computing solutions for the smooth wall case with E varied linearly from 0.1 at the surface to 1.0 at the base and for E varied linearly from 0.5 to 1.0. In the finite element representation of these variations 10 equal depth homogeneous horizontal layers were used. The mesh used for the uniform soil solutions was again employed. The wall pressures for the nonuniform soil, computed for $\frac{L}{H} = 5.0$ and $\nu = 0.3$, are compared with the uniform soil counterparts in Fig. 6.6.

Solutions for any form of the wall displacement function can be conveniently computed by the finite element method. Two further cases of practical interest, $u(0,y) = u^o$ (wall translation), and $u(0,y) = u^o(y/H)^2$ (parabolic displacement), were analyzed using the smooth contact assumption, and the solutions for the wall pressure distributions are shown in Fig. 6.7.

TABLE 6.1

Finite Element Stresses on Wall Boundary
Bonded Contact $\frac{L}{H} = 5.0$

$\frac{y}{H}$	$\nu = 0.3$		$\nu = 0.4$	
	$\frac{\sigma_x^o}{E\theta}$	$\frac{\tau_{xy}^o}{E\theta}$	$\frac{\sigma_x^o}{E\theta}$	$\frac{\tau_{xy}^o}{E\theta}$
1.0	-2.44	0.39	-3.68	0.56
0.95	-1.32	0.38	-1.56	0.52
0.9	-1.06	0.34	-1.24	0.43
0.8	-0.76	0.29	-0.83	0.34
0.7	-0.60	0.28	-0.64	0.30
0.6	-0.49	0.27	-0.51	0.28
0.5	-0.40	0.28	-0.42	0.28
0.4	-0.32	0.29	-0.35	0.28
0.3	-0.26	0.30	-0.28	0.29
0.2	-0.20	0.31	-0.23	0.30
0.1	-0.13	0.34	-0.17	0.32

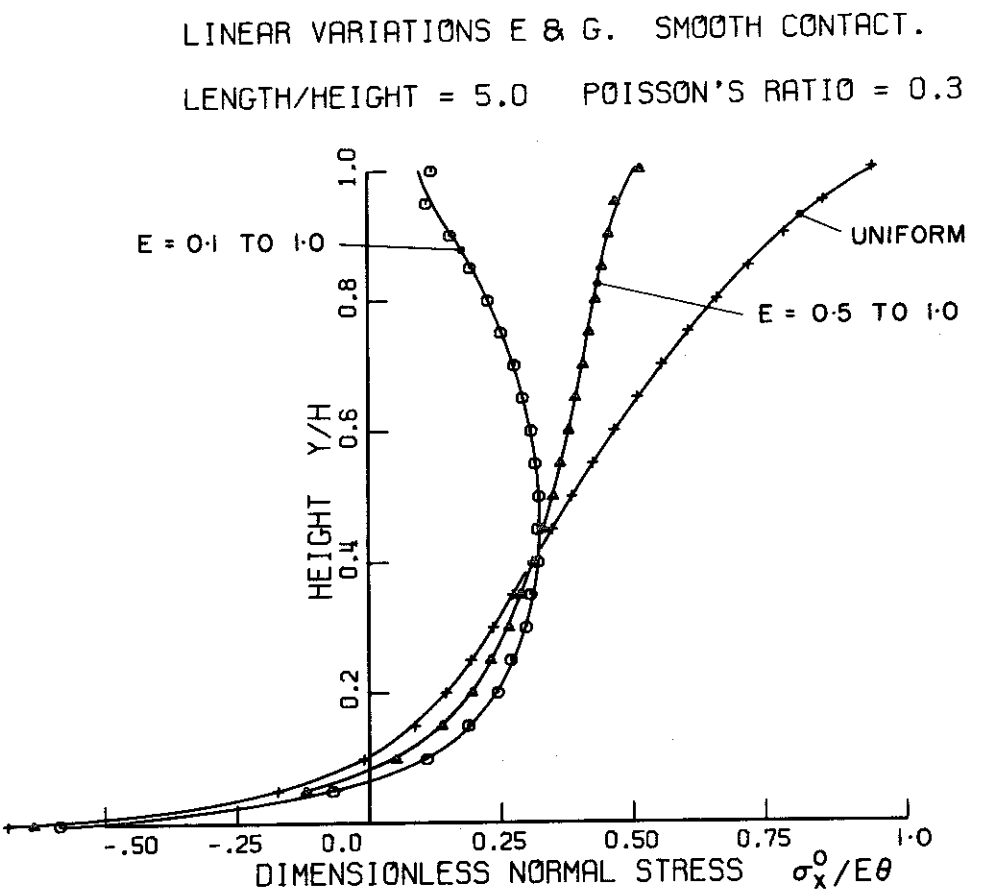

Figure 6.6 Pressure distributions on statically forced smooth rotating walls. Comparison between uniform and nonuniform soils.

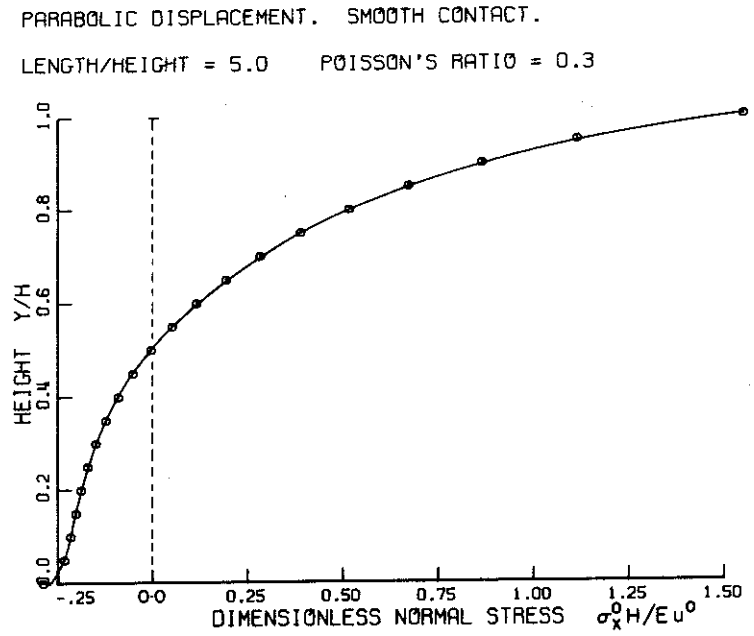

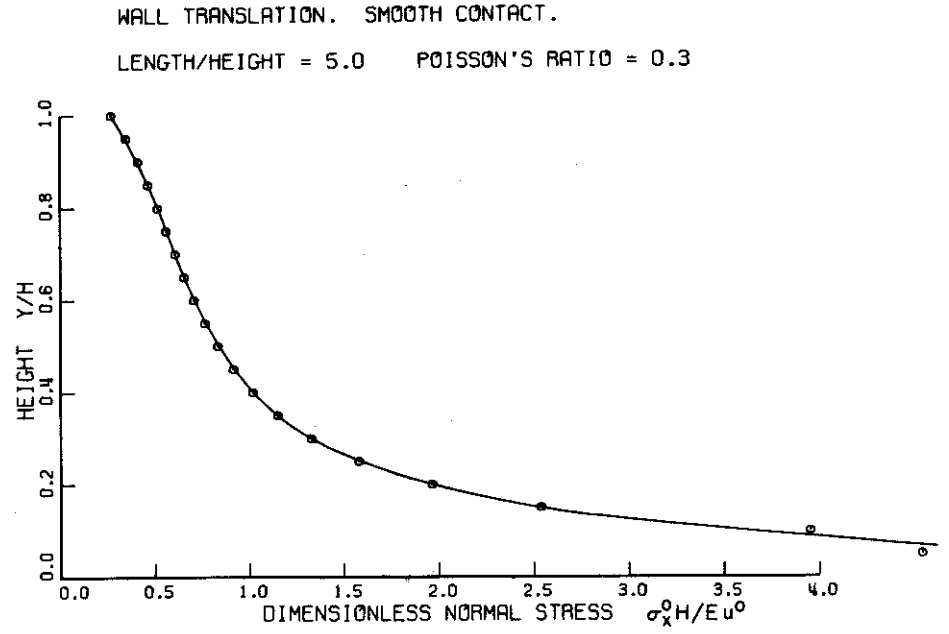

Figure 6.7 Pressure distributions on statically forced walls. Parabolic displacement and uniform translation.

6.3. HARMONIC FORCING: ANALYTICAL SOLUTION

An outline is presented in this section of an analytical solution for the steady-state response of a homogeneous linearly elastic soil body forced by a harmonically rotated smooth wall. The problem and the assumed boundary conditions are shown in Fig. 6.8. The method of solution is analogous to the approach used for the statically rotated wall. The dynamic solution is of greater complexity than the static solution and appears to be more difficult to evaluate numerically.

The time-varying rotational displacement of the wall can be written as

$$u(0,y,t) = \frac{u^o y e^{i\omega t}}{H} \tag{6.18}$$

in which

u^o = the amplitude at the top of the wall

ω = angular frequency of the harmonic forcing

The displacement equations of motion can be expressed as

$$\frac{\partial^2 u(x,y,t)}{\partial x^2} + \frac{(k^2-1)}{k^2}\frac{\partial^2 v(x,y,t)}{\partial x \partial y} + \frac{1}{k^2}\frac{\partial^2 u(x,y,t)}{\partial y^2} = \frac{1}{V_d^2}\frac{\partial^2 u(x,y,t)}{\partial t^2}$$

$$\frac{\partial^2 v(x,y,t)}{\partial x^2} + (k^2-1)\frac{\partial^2 u(x,y,t)}{\partial x \partial y} + k^2\frac{\partial^2 v(x,y,t)}{\partial y^2} = \frac{1}{V_s^2}\frac{\partial^2 v(x,y,t)}{\partial t^2} \tag{6.19}$$

$$0 < x < L\ ;\quad 0 < y < H\ ;\quad t > 0$$

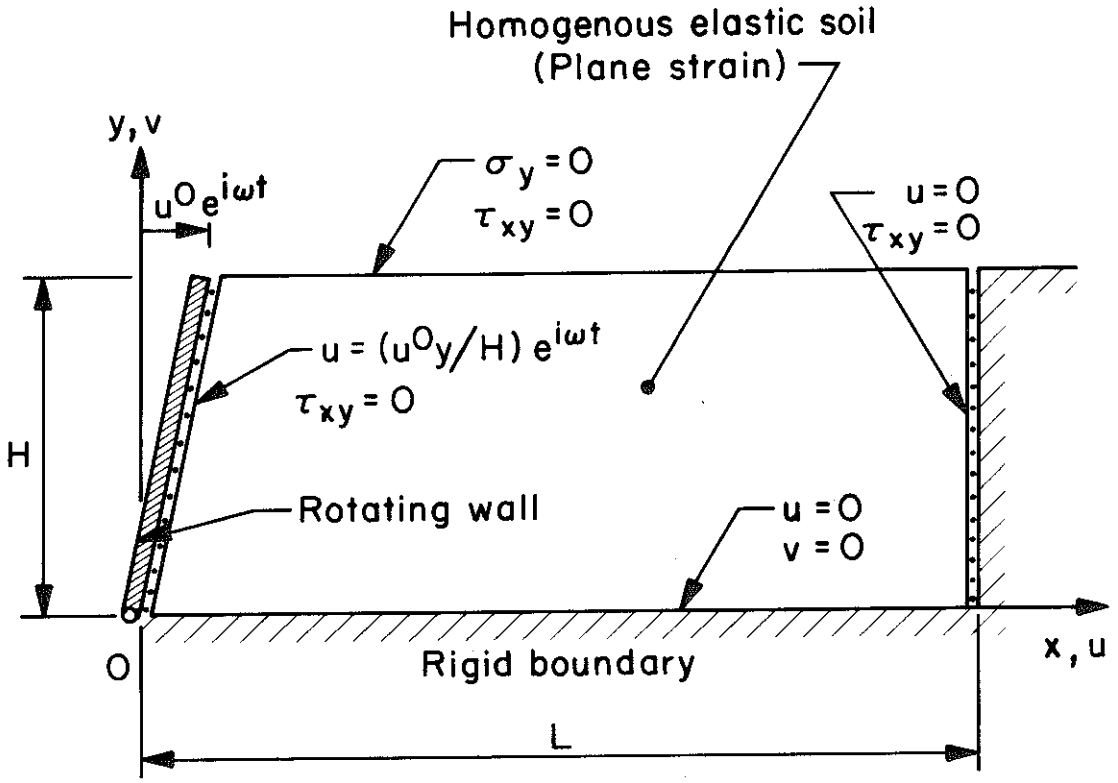

DISPLACEMENT FORCING OF WALL

Figure 6.8

The steady-state solution of equations (6.19) is of the form

$$u(x,y,t) = \bar{u}(x,y)e^{i\omega t}$$
$$v(x,y,t) = \bar{v}(x,y)e^{i\omega t} \tag{6.20}$$

The following expressions for the displacement functions $\bar{u}(x,y)$ and $\bar{v}(x,y)$ satisfy the displacement and stress boundary conditions at $x = 0$ and $x = L$,

$$\bar{u}(x,y) = \frac{u^o y}{H}\cos px + \sum_{n=0}^{\infty} \tilde{u}_n(y) \sin rx$$
$$\bar{v}(x,y) = -\frac{u^o}{Hp}\sin px + \sum_{n=0}^{\infty} \tilde{v}_n(y) \cos rx \tag{6.21}$$

in which

$$r = \frac{n\pi}{L} \qquad n = 0,1,2,\ldots$$
$$p = \frac{\pi}{2L}$$

Substitution of expressions (6.20) and (6.21) into (6.19) gives

$$\sum_{n=0}^{\infty} \left\{ \frac{\partial^2 \tilde{u}_n(y)}{\partial y^2} - k^2\alpha^2 \tilde{u}_n(y) - r(k^2-1)\frac{\partial \tilde{v}_n(y)}{\partial y} \right\} \sin rx$$
$$= \frac{u^o y k^2}{H}\left(p^2 - \frac{\omega^2}{V_d^2}\right)\cos px$$
$$\sum_{n=0}^{\infty} \left\{ \frac{\partial^2 \tilde{v}_n(y)}{\partial y^2} - \frac{\beta^2 \tilde{v}_n(y)}{k^2} + \frac{r(k^2-1)}{k^2}\frac{\partial \tilde{u}_n(y)}{\partial y} \right\} \cos rx \tag{6.22}$$
$$= \frac{u^o}{pHk^2}\left\{(k^2-2)p^2 + \frac{\omega^2}{V_s^2}\right\}\sin px$$

in which

$$\alpha^2 = \left(r^2 - \frac{\omega^2}{V_d^2}\right)$$

$$\beta^2 = \left(r^2 - \frac{\omega^2}{V_s^2}\right)$$

The functions sin px and cos px in equations (6.22) can be expanded in the Fourier series given by expressions (6.5). Hence for a particular value of n (except the special case of n = 0 which is treated later) equations (6.22) can be expressed as

$$\frac{\partial^2 \tilde{u}_n(y)}{\partial y^2} - k^2\alpha^2 \tilde{u}_n(y) - r(k^2-1)\frac{\partial \tilde{v}_n}{\partial y} = \frac{u^o y k^2}{H}\left\{p^2 - \frac{\omega^2}{V_d^2}\right\} b_n$$

$$\frac{\partial^2 \tilde{v}_n(y)}{\partial y^2} - \frac{\beta^2 \tilde{v}_n(y)}{k^2} + \frac{r(k^2-1)}{k^2}\frac{\partial \tilde{u}_n}{\partial y} = \frac{u^o}{pHk^2}\left\{(k^2-2)p^2 + \frac{\omega^2}{V_s^2}\right\} a_n \qquad (6.23)$$

Let

$$\tilde{u}_n = \tilde{u}_{n,h} + \tilde{u}_{n,p}$$

$$\tilde{v}_n = \tilde{v}_{n,h} + \tilde{v}_{n,p} \qquad (6.24)$$

in which

$\tilde{v}_{n,h}$ = solution of the homogeneous equations; that is, the solution of equations (6.23) with the right-hand side set to zero

By inspection the particular integrals of equations (6.23) are

$$\tilde{u}_{n,p} = \frac{u^o a_n y}{H} \left\{ \frac{n}{\alpha^2} \left(p^2 - \frac{\omega^2}{V_d^2}\right)\right\}$$

$$\tilde{v}_{n,p} = - \frac{u^o a_n}{p+1} \frac{1}{\beta^2}\left[\left\{(k^2-2)p^2 + \frac{\omega^2}{V_s^2}\right\} - \frac{nrp}{\alpha^2}\left(p^2 - \frac{\omega^2}{V_d^2}\right)(k^2-1)\right] \tag{6.25}$$

The solution of the homogeneous equations may be expressed in the general form

$$\tilde{u}_{n,h} = A_n e^{\alpha y} + B_n e^{\beta y} + C_n e^{-\alpha y} + D_n e^{-\beta y}$$

$$\tilde{v}_{n,h} = -A_n \frac{\alpha}{r} e^{\alpha y} - B_n \frac{r}{\beta} e^{\beta y} + C_n \frac{\alpha}{r} e^{-\alpha y} + D_n \frac{r}{\beta} e^{-\beta y} \tag{6.26}$$

The constants A_n, B_n, C_n and D_n are determined by satisfying the boundary conditions at $y = 0$ and $y = H$. To satisfy these conditions it is necessary to satisfy equations identical to expressions (6.8) and (6.9) given for the static problem. The expressions for the constants cannot be written in a compact form and so they are not presented here. The constants have as denominator a determinant that has zeros corresponding to the natural frequencies of the soil body and consequently the displacements have an infinite number of singularities. (The zeros of the determinant correspond to the zeros of the frequency equation (3.7).)

For the special case of $n = 0$ equations (6.23) reduce to the single equation

$$\frac{\partial^2 \tilde{v}_0}{\partial y^2} + \frac{\omega^2 \tilde{v}_0}{V_d^2} = \frac{u^o a_0}{pHk^2}\left\{(k^2-2)p^2 + \frac{\omega^2}{V_s^2}\right\} \qquad (6.27)$$

The solution of equation (6.27) can be written as

$$\tilde{v}_0 = A_0 \sin\frac{\omega y}{V_d} + B_0 \cos\frac{\omega y}{V_d} + \frac{u^o a_0}{pH}\left\{(k^2-2)\frac{p^2 V_s^2}{\omega^2} + 1\right\} \qquad (6.28)$$

A_0 and B_0 can be determined from the boundary conditions at $y = 0$ and $y = H$. Satisfying the appropriate conditions gives

$$A_0 = \frac{B_0 \sin\frac{\omega H}{V_d} + u^0 a_0 \frac{(k^2-2)p}{k^2}\frac{V_d}{\omega}}{\cos\frac{\omega H}{V_d}}$$

$$B_0 = -\frac{u^o a_0}{H}(k^2-2)p\frac{V_s^2}{\omega^2} \qquad (6.29)$$

The general displacement solution is given by substitution of expressions (6.25), (6.26), (6.28) and (6.29) into equations (6.21).

The case $L \to \infty$ can be solved by taking the Fourier sine transform of the first of equations (6.19) and the Fourier cosine of the second. The formal solution is readily derived from the transformed equations by following much the same method as given for the bounded problem above. Numerical evaluation of the Fourier integral of the formal solution appears difficult and has not been fully investigated. The solution of this semi-infinite stratum problem is however of interest since it can be used to show the influence of energy propagating out of the system.

6.4. HARMONIC FORCING: ANALYTICAL SOLUTION USING STATIC SOLUTION

A solution for the problem of the previous section can be derived from the solution for the equivalent static problem and the properties of the normal modes of the smooth rigid-wall problem. Details of this method and typical numerical results evaluated from the solution are given in this section.

The problem and the boundary conditions are taken to be identical to the problem and boundary conditions of the previous section (Fig. 6.8). In the solution presented here it is convenient to introduce dissipation by the inclusion of a viscous damping term in the equations of motion. Thus, the displacement equations of motion for the homogeneous linearly elastic soil can be expressed in vector form as

$$L\underline{u}(x,y,t) = \rho\ddot{\underline{u}}(x,y,t) + c\dot{\underline{u}}(x,y,t) \tag{6.30}$$

The solution technique developed here is applicable for a general form of the horizontal displacement forcing applied at the wall boundary. It is informative to firstly consider the general case before evaluating the solution for the particular case of harmonic rotational forcing of the wall. Consider the wall boundary to be forced by a time-varying function satisfying

$$\begin{aligned} u(0,y,t) &= f^{o}(y)g^{o}(t) \\ \tau_{xy}(0,y,t) &= 0 \end{aligned} \tag{6.31}$$

in which

$f^o(y)$ = wall displacement function such that $f^o(H) = 1$

The solution of equation (6.30) for this form of boundary forcing can be expressed as

$$\underline{u}(x,y,t) = u_1(x,y,t) + \underline{u}_{sf}(x,y)g^o(t) \tag{6.32}$$

in which

$\underline{u}_{sf}(x,y)$ = solution for static wall-forcing given by

$$\begin{aligned} u(0,y) &= f^o(y) \\ \tau_{xy}(0,y) &= 0 \end{aligned} \tag{6.33}$$

It can be readily seen that the component of the solution given by $\underline{u}_1(x,y,t)$ must satisfy all the boundary conditions of Fig. 6.8 except the wall displacement boundary condition. On the wall boundary it is necessary that $\underline{u}_1(0,y,t) = 0$. Substitution of equation (6.32) into (6.30) gives

$$\begin{aligned} L\underline{u}_1(x,y,t) = \rho\ddot{\underline{u}}_1(x,y,t) + c\dot{\underline{u}}_1(x,y,t) \\ + \underline{u}_{sf}(x,y)\left\{\rho\ddot{g}^o(t) + c\dot{g}^o(t)\right\} \end{aligned} \tag{6.34}$$

Equation (6.34) is similar in form to equation (3.18) which described the forced vibrations of the rigid-wall problem. (In equation (6.34) the forcing term $\underline{u}_{sf}(x,y)\left\{\rho\ddot{g}^o(t) + c\dot{g}^o(t)\right\}$ is spatially variable whereas the equivalent forcing term in equation (3.18) $\rho\ddot{u}_b(t)$ is constant with respect to the spatial coordinates.) The boundary conditions to be satisfied by the solution $\underline{u}_1(x,y,t)$ of equation (6.34) are identical to the boundary conditions of the smooth rigid-wall problem. Thus the solution of equation (6.34) may be obtained

directly from the solutions given in Sections 3.2 and 3.5. For the case of harmonic wall-forcing given by $u(0,y,t) = f^{o}(y)e^{i\omega t}$, the complete displacement solution of equation (6.30) can be written as

$$\underline{u}(x,y,t) = \left\{ \underline{u}_{sf}(x,y) + \sum_{\substack{n=1 \\ m=1}}^{\infty} \underline{\phi}_{n,m} \frac{\left(\frac{\omega^2}{\omega_{n,m}^2} - 2i\zeta_{n,m} \frac{\omega}{\omega_{n,m}} \right)}{\left(1 - \frac{\omega^2}{\omega_{n,m}^2} + 2i\zeta_{n,m} \frac{\omega}{\omega_{n,m}} \right)} \times \frac{\int_V \underline{u}_{sf}(x,y) \cdot \underline{\phi}_{n,m} \, dV}{\int_V \underline{\phi}_{n,m} \cdot \underline{\phi}_{n,m} \, dV} \right\} e^{i\omega t} \quad (6.35)$$

The normal stress on the wall is given by

$$\sigma_x(0,y,t) = L_p \underline{u}(x,y,t) \quad (6.36)$$

(in which L_p = linear operator with respect to the spatial coordinates.) The complex-amplitudes of the steady-state wall force and moment for a forcing of unit displacement amplitude at the top of the wall, $\overline{F}_f'(\omega)$ and $\overline{M}_f'(\omega)$, can be expressed as

$$\frac{\overline{F}_f'(\omega)}{F_{sf}} = 1 - \sum_{\substack{n=1 \\ m=1}}^{\infty} \frac{\left(\frac{\omega^2}{\omega_{n,m}^2} - 2i\zeta_{n,m} \frac{\omega}{\omega_{n,m}} \right)}{\left(1 - \frac{\omega^2}{\omega_{n,m}^2} + 2i\zeta_{n,m} \frac{\omega}{\omega_{n,m}} \right)} \frac{k_{n,m}}{F_{sf}}$$

$$\frac{\overline{M}_f'(\omega)}{M_{sf}} = 1 - \sum_{\substack{n=1 \\ m=1}}^{\infty} \frac{\left(\frac{\omega^2}{\omega_{n,m}^2} - 2i\zeta_{n,m} \frac{\omega}{\omega_{n,m}} \right)}{\left(1 - \frac{\omega^2}{\omega_{n,m}^2} + 2i\zeta_{n,m} \frac{\omega}{\omega_{n,m}} \right)} \frac{k_{n,m} h_{n,m}}{M_{sf}} \quad (6.37)$$

in which

$$F_{sf} = \int_0^H L_p \underline{u}_{sf}(x,y)\, dy, \text{ force on statically forced wall for unit displacement at wall top}$$

$$M_{sf} = \int_0^H y L_p \underline{u}_{sf}(x,y)\, dy, \text{ moment on statically forced wall for unit displacement at wall top}$$

$$k_{n,m} = P^s_{n,m} \int_0^H L_p \underline{\phi}_{n,m}(x,y)\, dy, \text{ analogous spring constant for mode } n,m$$

$$k_{n,m} h_{n,m} = P^s_{n,m} \int_0^H y L_p \underline{\phi}_{n,m}(x,y)\, dy$$

$h_{n,m}$ = height of center of pressure for mode n,m

$$P^s_{n,m} = - \frac{\int_V \underline{u}_{sf} \cdot \underline{\phi}_{n,m}\, dV}{\int_V \underline{\phi}_{n,m} \cdot \underline{\phi}_{n,m}\, dV}$$

From an inspection of the complex-amplitude solutions for the wall force and moment it is evident that the forced-wall problem can be represented by the spring-mass-dashpot analogy shown in Fig. 6.9. The equivalence can be readily shown by deriving the wall force and moment responses of the analogue to harmonic forcing. From expressions (6.37) it can be seen that modes having natural frequencies such that $\omega_{n,m} >> \omega$, produce no significant contribution to the total wall force or moment.

The main computational effort in numerically evaluating expressions (6.37) is devoted to the evaluation of the integrals in the expression for $P^s_{n,m}$. The denominator of the expression was

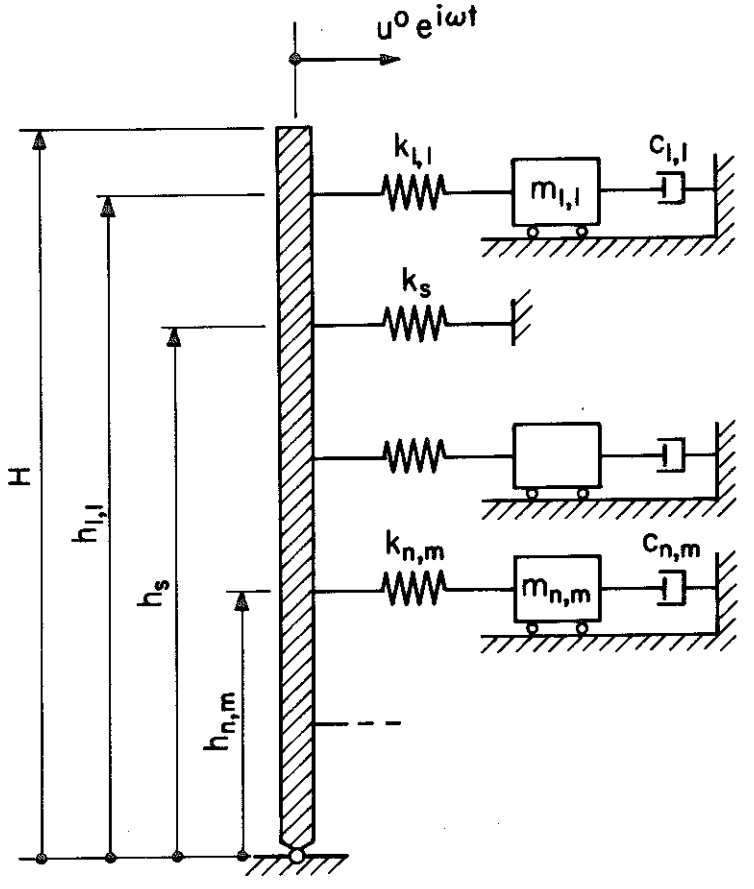

DISPLACEMENT FORCING : SPRING-MASS-DASHPOT ANALOGY

Figure 6.9

previously evaluated in the derivation of the modal participation factors for the rigid-wall case and the analytical expressions obtained are given in Appendix IV. To evaluate the numerator of expression (6.37) it is necessary to integrate the dot product of the static displacement field and the mode shapes over the volume. For the rotating wall problem this can be readily accomplished by using the analytical static solution given by expressions (6.15) and the mode shapes given by expressions (3.10), (3.11), (3.13) and (3.15). The dot product of the static solution and the mode shapes produces a number of elementary functions which can be integrated exactly. In this study the numerator product was evaluated using the static displacements computed from finite element analyses and the analytical mode shapes. The finite element displacements and the product function were evaluated at each of the nodal points of the finite element mesh and the integration was performed numerically using a double Simpson's rule technique over these points. The mesh used for the previous finite element solutions and shown in Fig. 2.7 was again employed. In the computation of solutions by this method the maximum frequency of forcing for which a reliable solution can be computed is limited by the finite element mesh size. The mesh adopted was found to be adequate for the frequency range of interest in this study.

Numerical solutions of expressions (6.37) were computed for the smooth rotating wall and typical plots of the results for a range of the $\frac{L}{H}$ and ν parameters are shown in Figs. 6.10 to 6.14 inclusive. The real parts, imaginary parts and moduli of the complex-

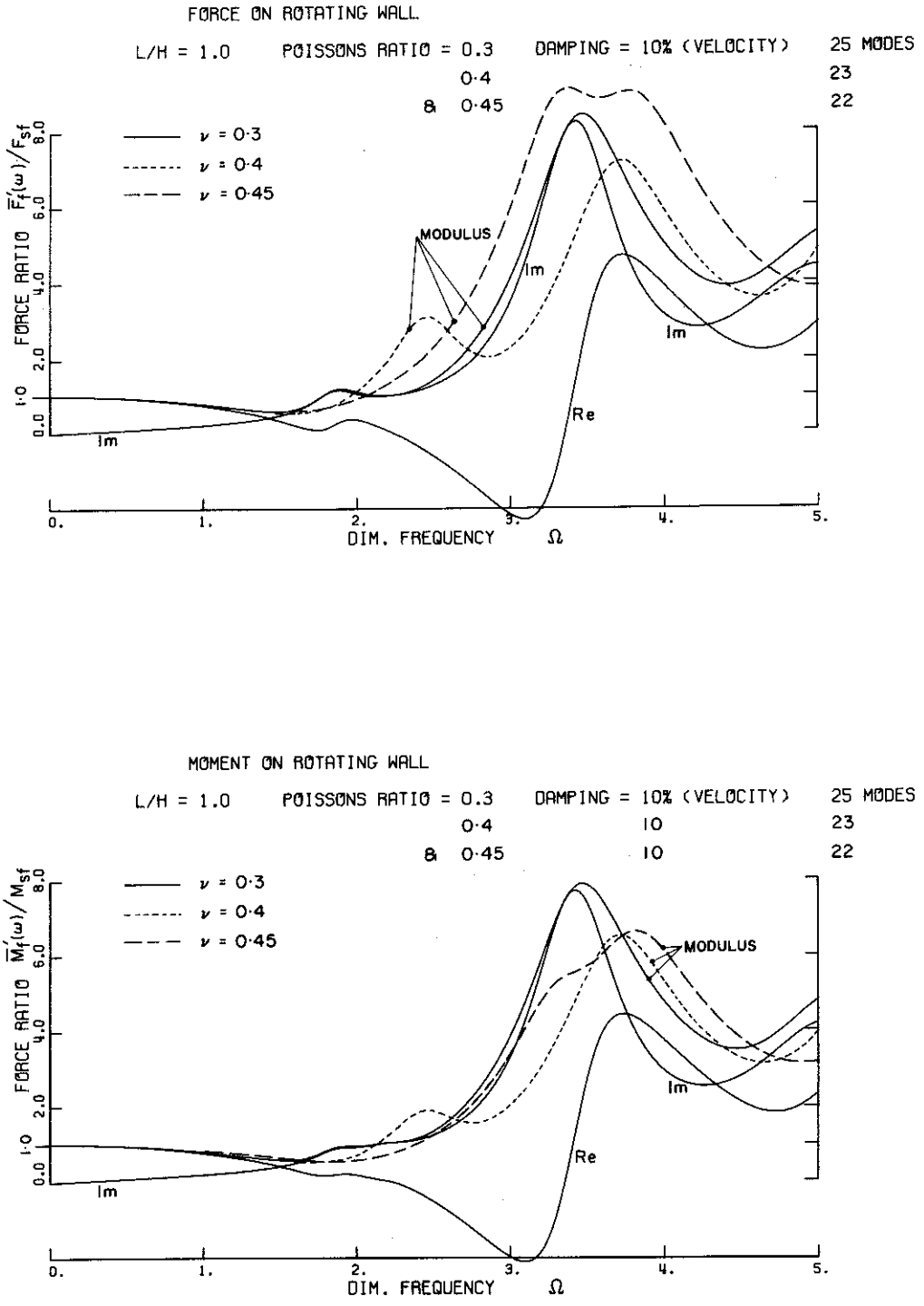

Figure 6.10 Complex-amplitudes of force ratio and moment ratio on harmonically forced smooth rotating wall. L/H = 1.0.

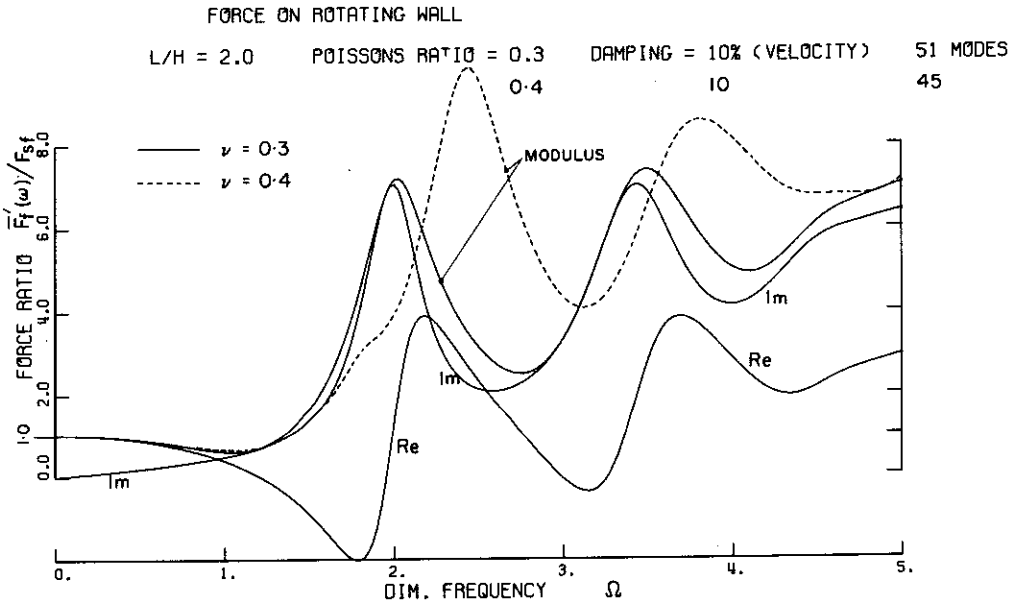

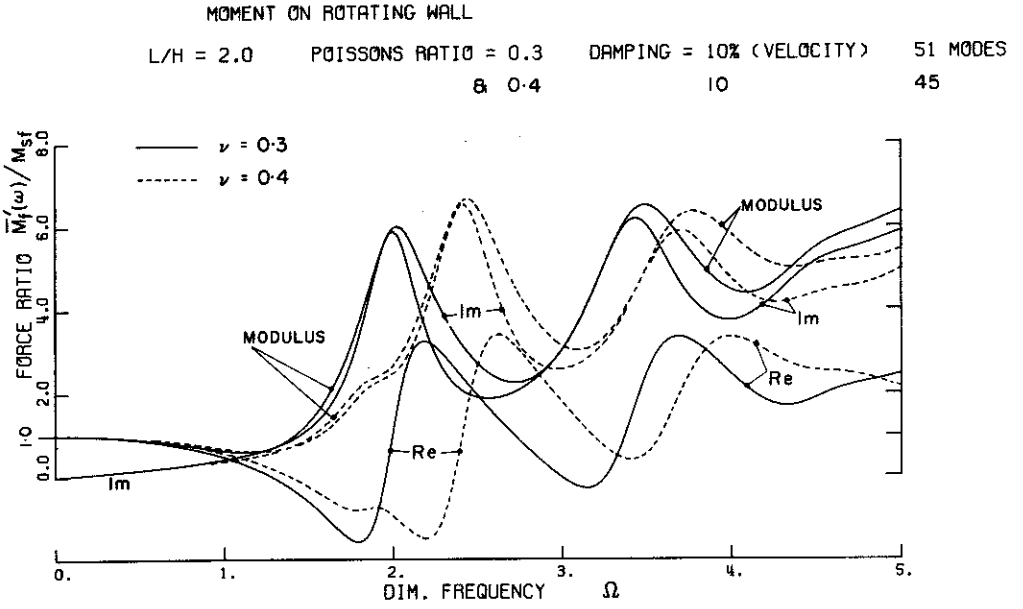

Figure 6.11 Complex-amplitudes of force ratio and moment ratio on harmonically forced smooth rotating wall. L/H = 2.0.

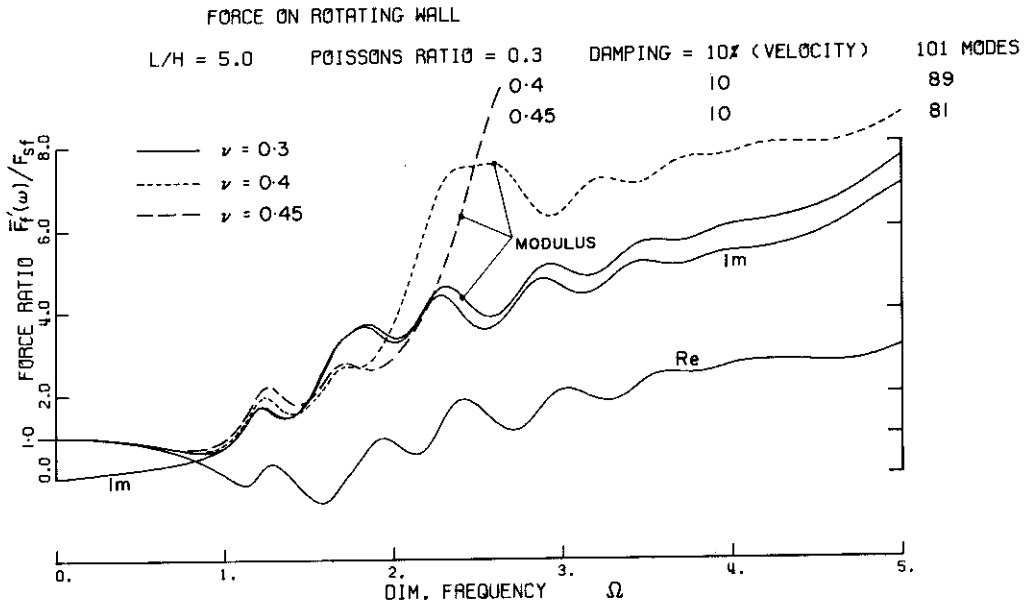

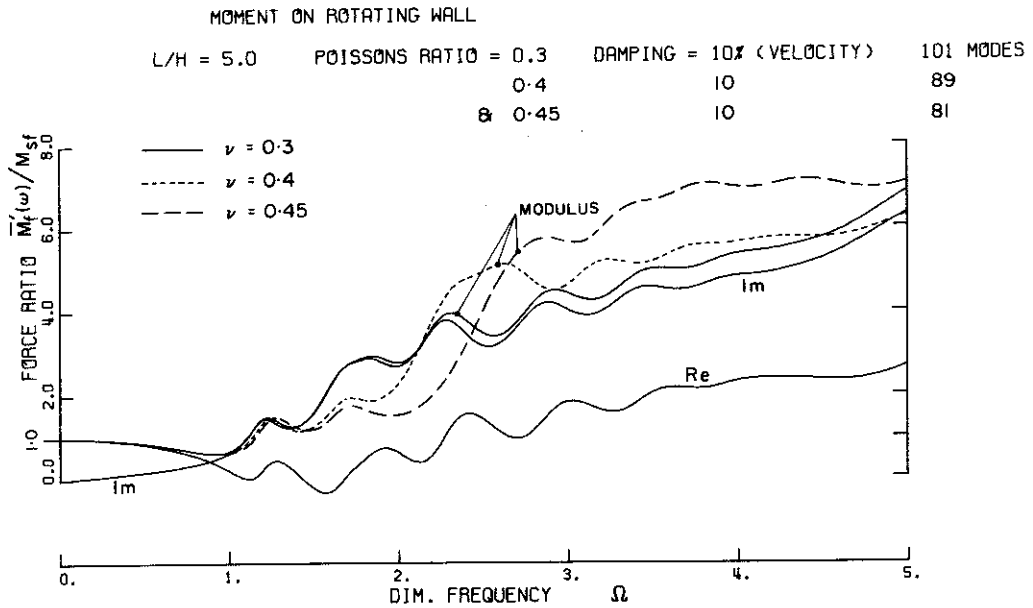

Figure 6.12 Complex-amplitudes of force ratio and moment ratio on harmonically forced smooth rotating wall. L/H = 5.0.

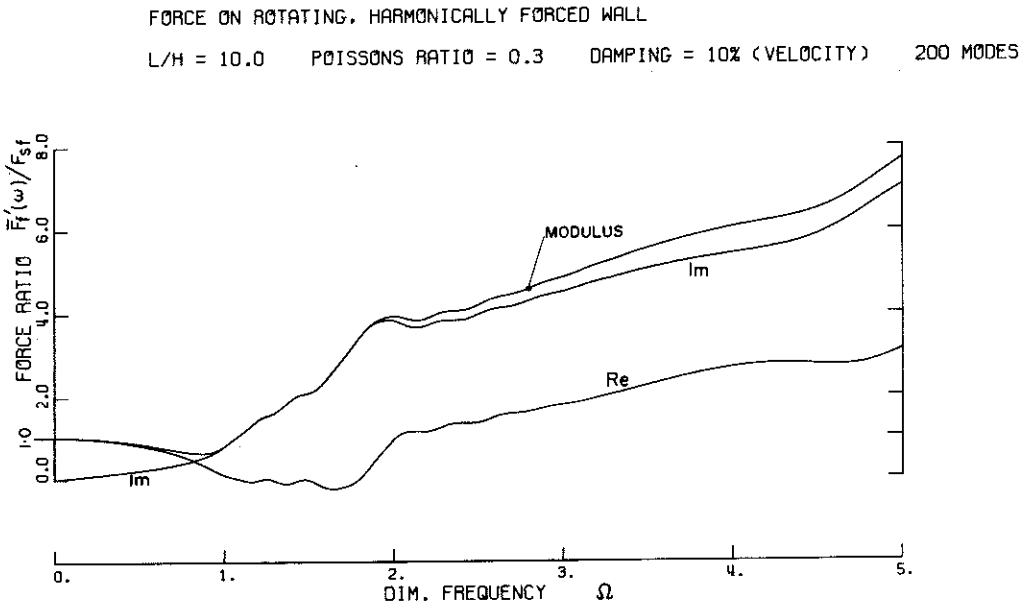

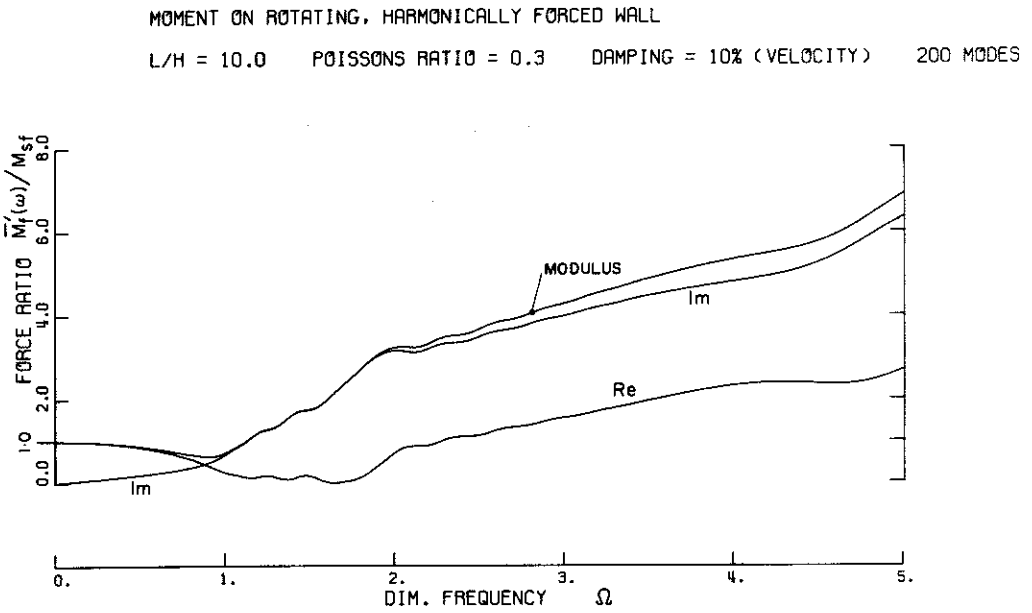

Figure 6.13 Complex-amplitudes of force ratio and moment ratio on harmonically forced smooth rotating wall. L/H = 10.

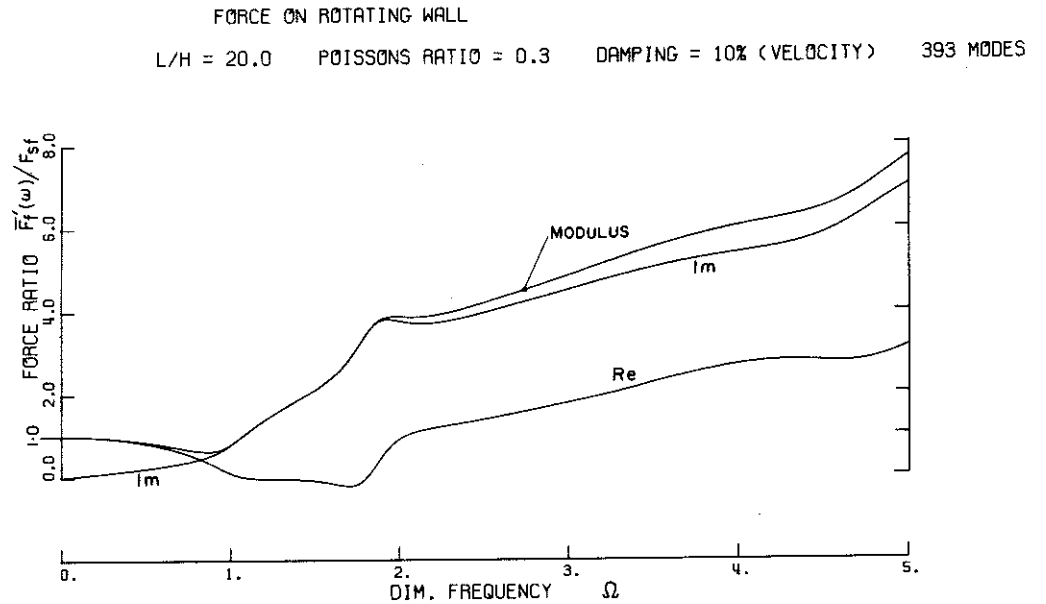

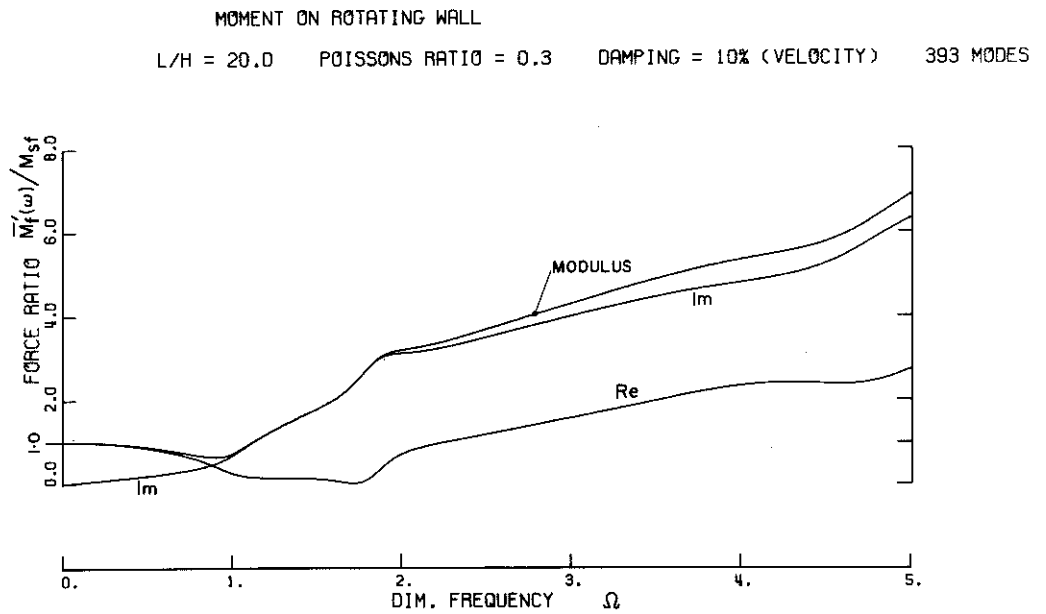

Figure 6.14 Complex-amplitudes of force ratio and moment ratio on harmonically forced smooth rotating wall. L/H = 20.

amplitudes of the dimensionless wall forces and moments are plotted against the forcing frequency which has been converted to dimensionless form by dividing by the lowest horizontal-shear mode frequency of the infinite elastic stratum. Wall pressure distributions were also evaluated for a number of values of the dimensionless forcing frequency and typical plots of the real parts, imaginary parts and moduli of these distributions are shown in Figs. 6.15 to 6.18 inclusive. In computing the force, moment and pressure solutions all the normal modes satisfying the bounds, $\Omega_{n,m} < 10$ and $\frac{L}{nH} \geq 0.333$, were included. The bound chosen for $\frac{L}{nH}$ was found to include all the modes at a dimensionless frequency less than 10 that gave a significant contribution to the wall force. It is of interest to note that the degenerate modes (n = 0), symmetric modes (n even) and the antisymmetric modes all participate in the solution. The solutions shown in Figs. 6.10 to 6.18 inclusive were computed using a 10% damping ratio for all modes. The effect on the complex-amplitude of wall force of reducing the modal damping ratios to 5% is shown in Fig. 6.19 for the two cases of $\frac{L}{H} = 3.0$ and 20 with $\nu = 0.3$.

From the plotted solutions it can be seen that the moduli of the wall forces and moments decrease from the static values at zero frequency to about 60% of the static values at a dimensionless forcing frequency of 1.0. As the forcing frequency is increased beyond the fundamental frequency of the soil body, the moduli increase significantly with the force modulus reaching about eight times the static value at a dimensionless forcing frequency of 5.0. For $\frac{L}{H}$ values less than 5.0, and between dimensionless frequencies 1.0 and 5.0

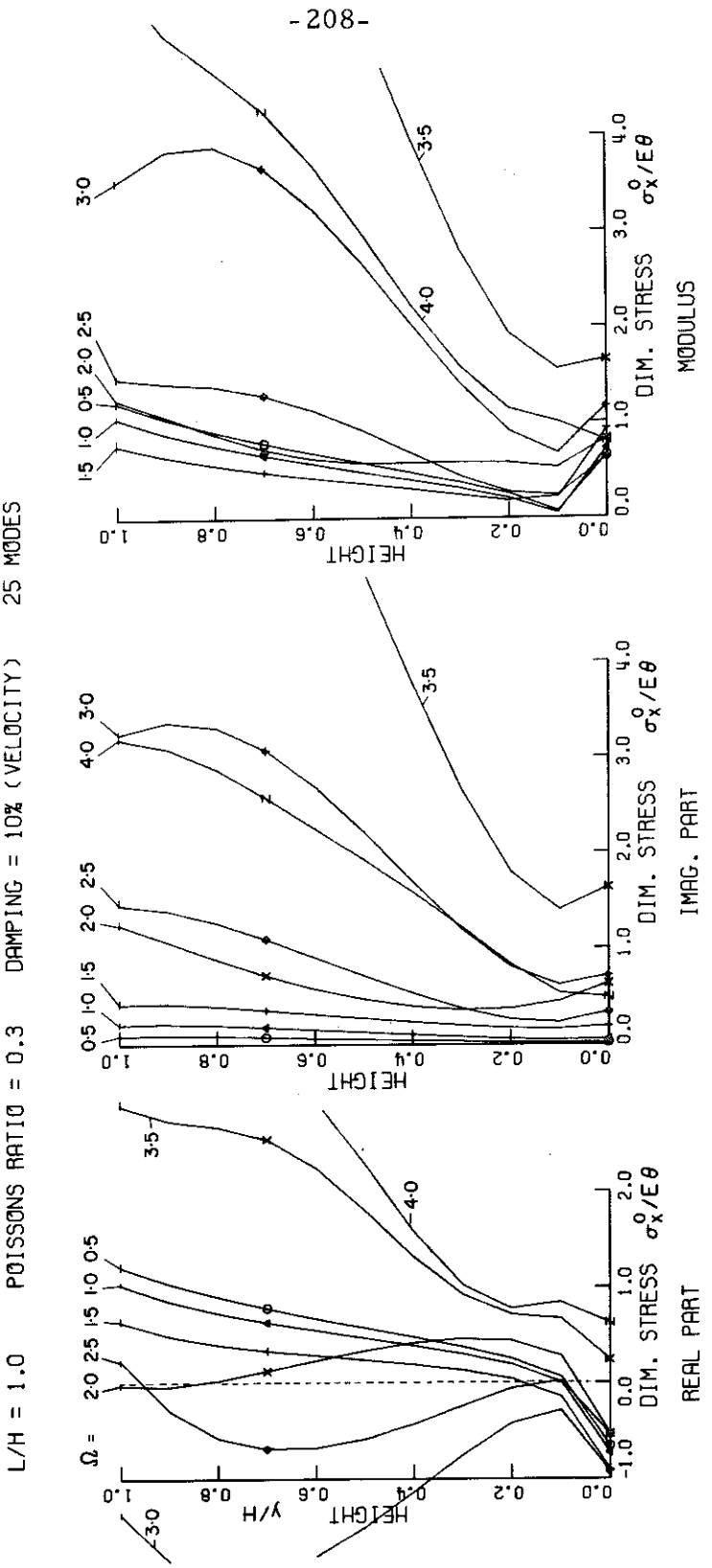

Figure 6.15 Pressure distributions on harmonically forced smooth rotating wall. L/H = 1.0.

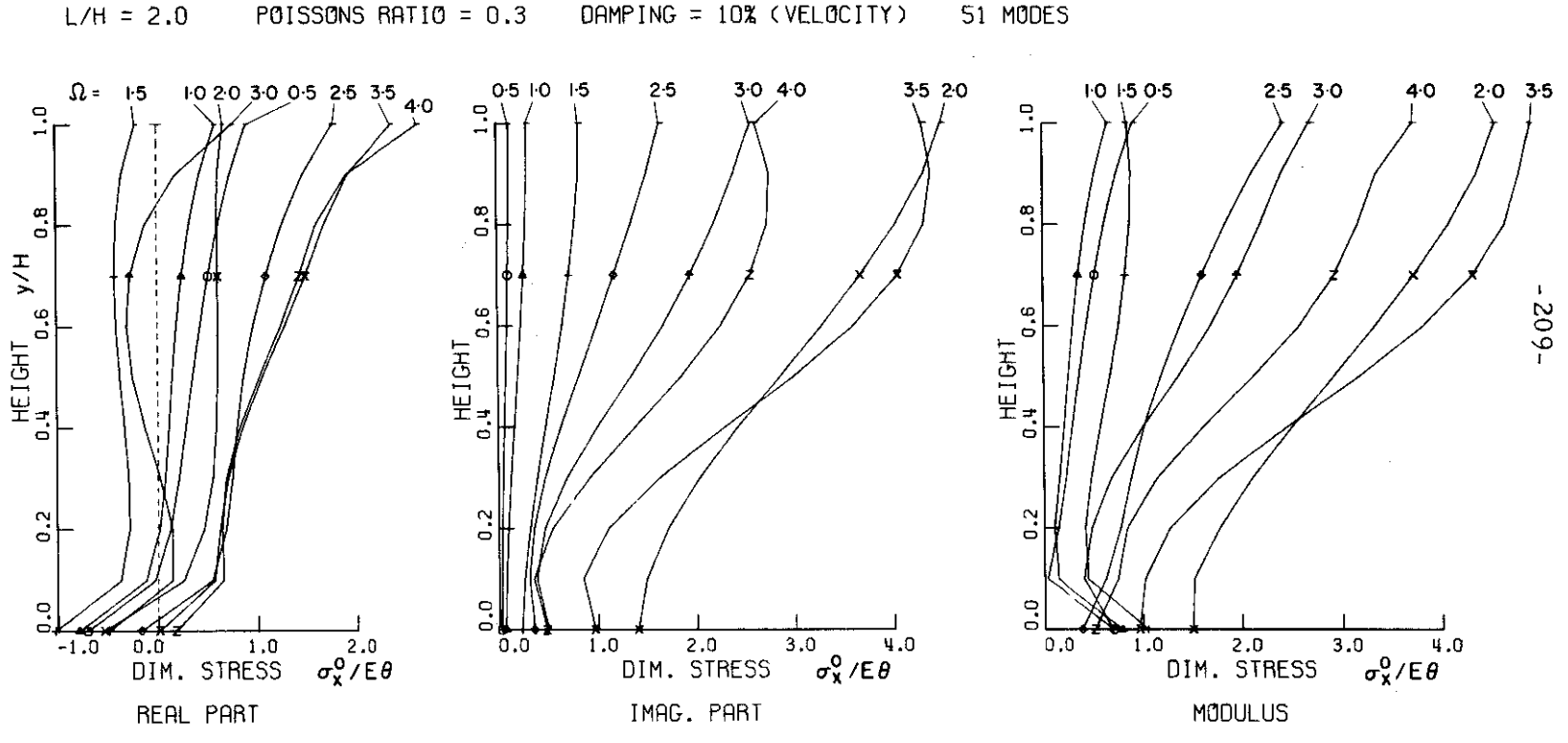

Figure 6.16 Pressure distributions on harmonically forced smooth rotating wall. L/H = 2.0.

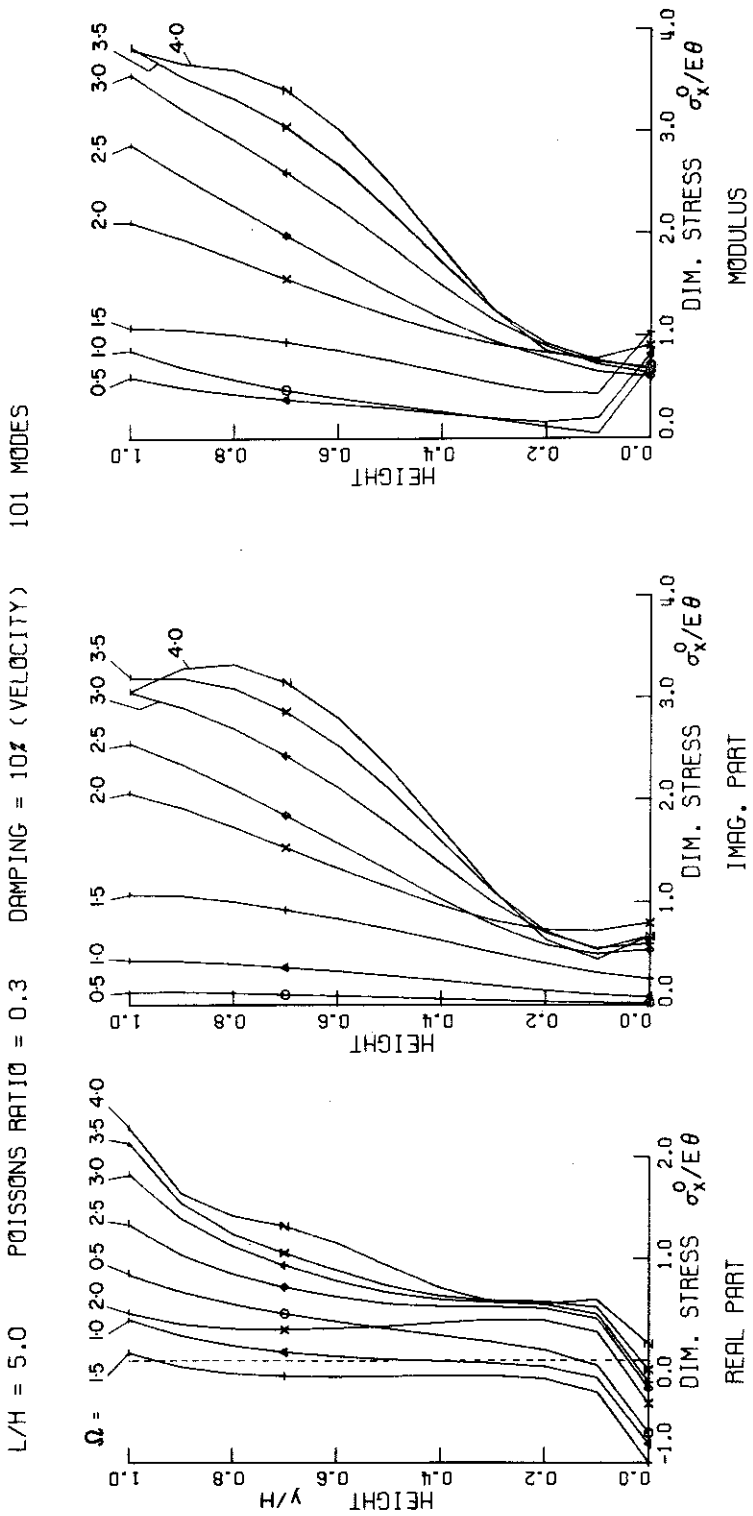

Figure 6.17 Pressure distributions on harmonically forced smooth rotating wall. L/H = 5.0.

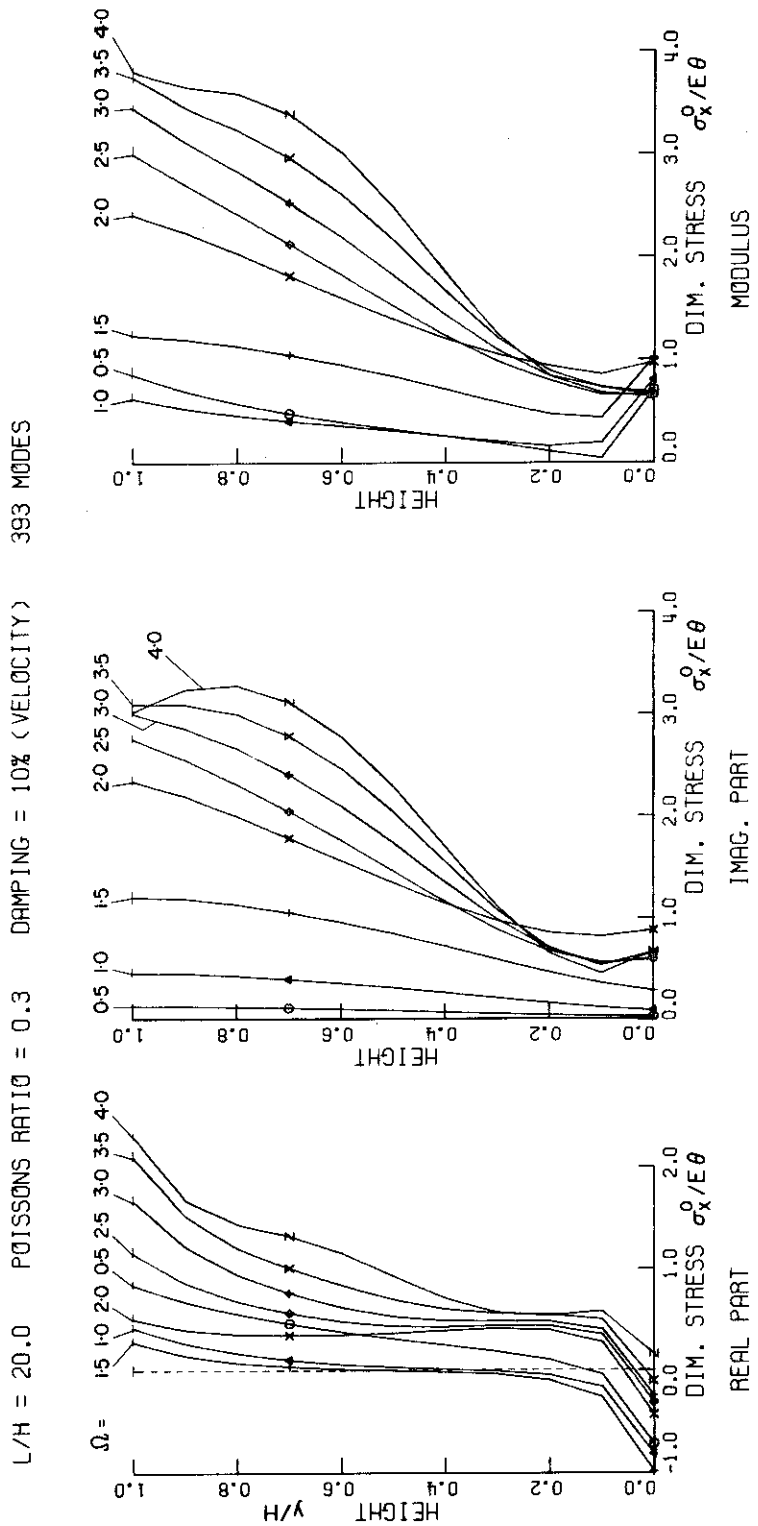

Figure 6.18 Pressure distributions on harmonically forced smooth rotating wall. L/H = 20.

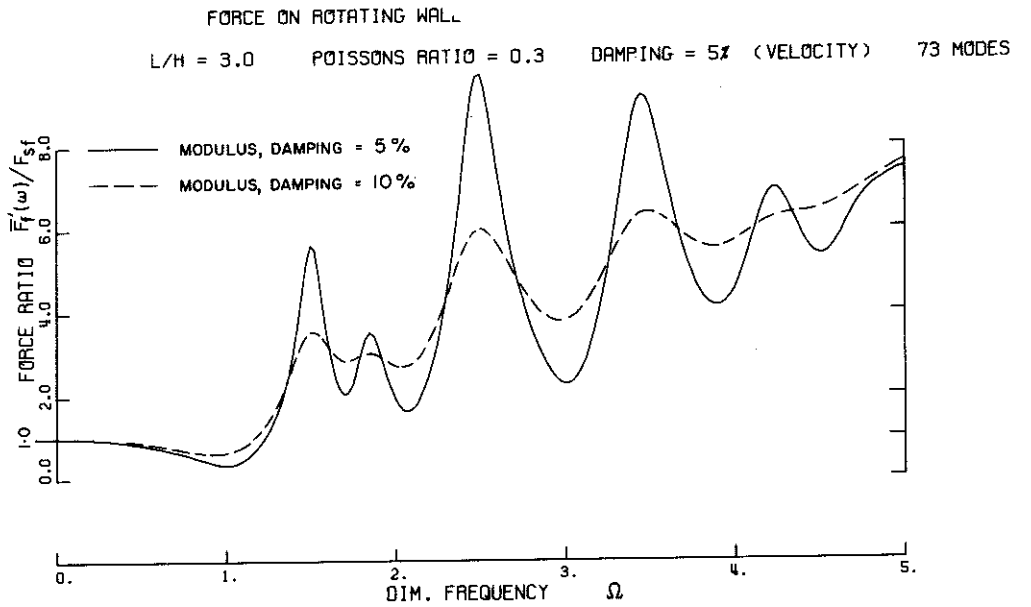

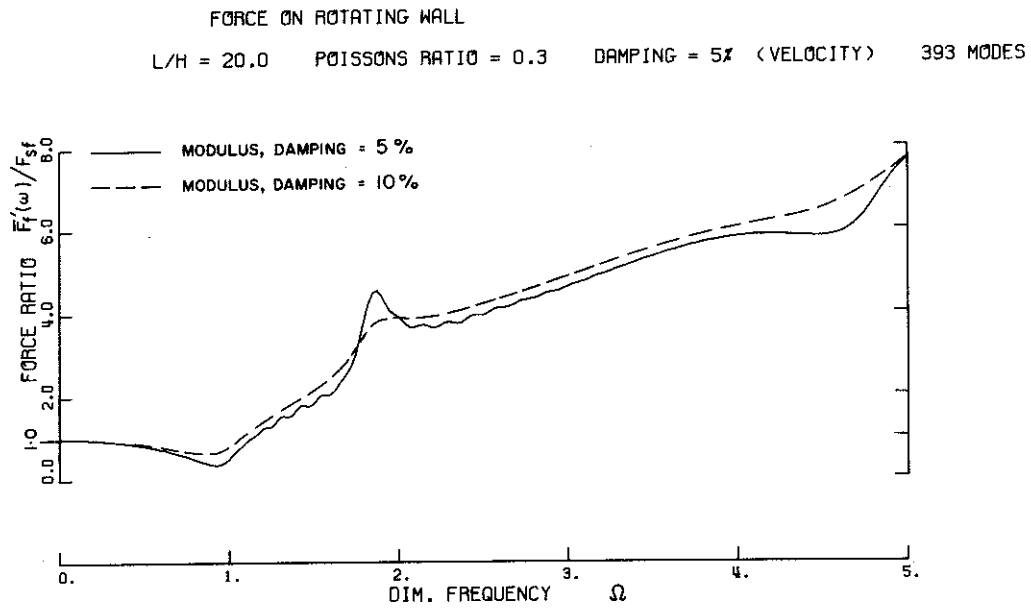

Figure 6.19 Complex-amplitude of force ratio on harmonically forced smooth rotating wall. Comparison between 5% and 10% damping.

quite large fluctuations occur in the moduli corresponding to resonances with the natural frequencies of the soil body. The solutions for $\frac{L}{H} = 10.0$ were found to be good approximations for problems with larger $\frac{L}{H}$ values.

For the $\frac{L}{H} \geq 2.0$ solutions, about 15 modes were found to have significant contributions to the wall force over the frequency range computed. For larger $\frac{L}{H}$ values a greater number of modes contribute. Hence for $\frac{L}{H}$ values greater than two it is not possible to obtain an accurate representation of the dynamic behavior with a relatively small number of modes.

An approximation employing two modified modes of vibration was found to give a moderately good representation of the dynamic wall force and moment for $\frac{L}{H}$ values greater than five. The following parameters for the two-mode model were found to be suitable for a Poisson's ratio of 0.3,

	Mode 1	Mode 2
dimensionless frequency	1.7	3.0
damping ratio	18%	18%
analogous spring constant $k_{n,m}$	1.0 F_{sf}	1.5 F_{sf}
$k_{n,m}h_{n,m}$	0.85 M_{sf}	1.2 M_{sf}

The complex-amplitudes of the two-mode model are compared in Fig. 6.20 with the more exact solution evaluated for $\frac{L}{H} = 20$, $\nu = 0.3$ and a 10% damping ratio.

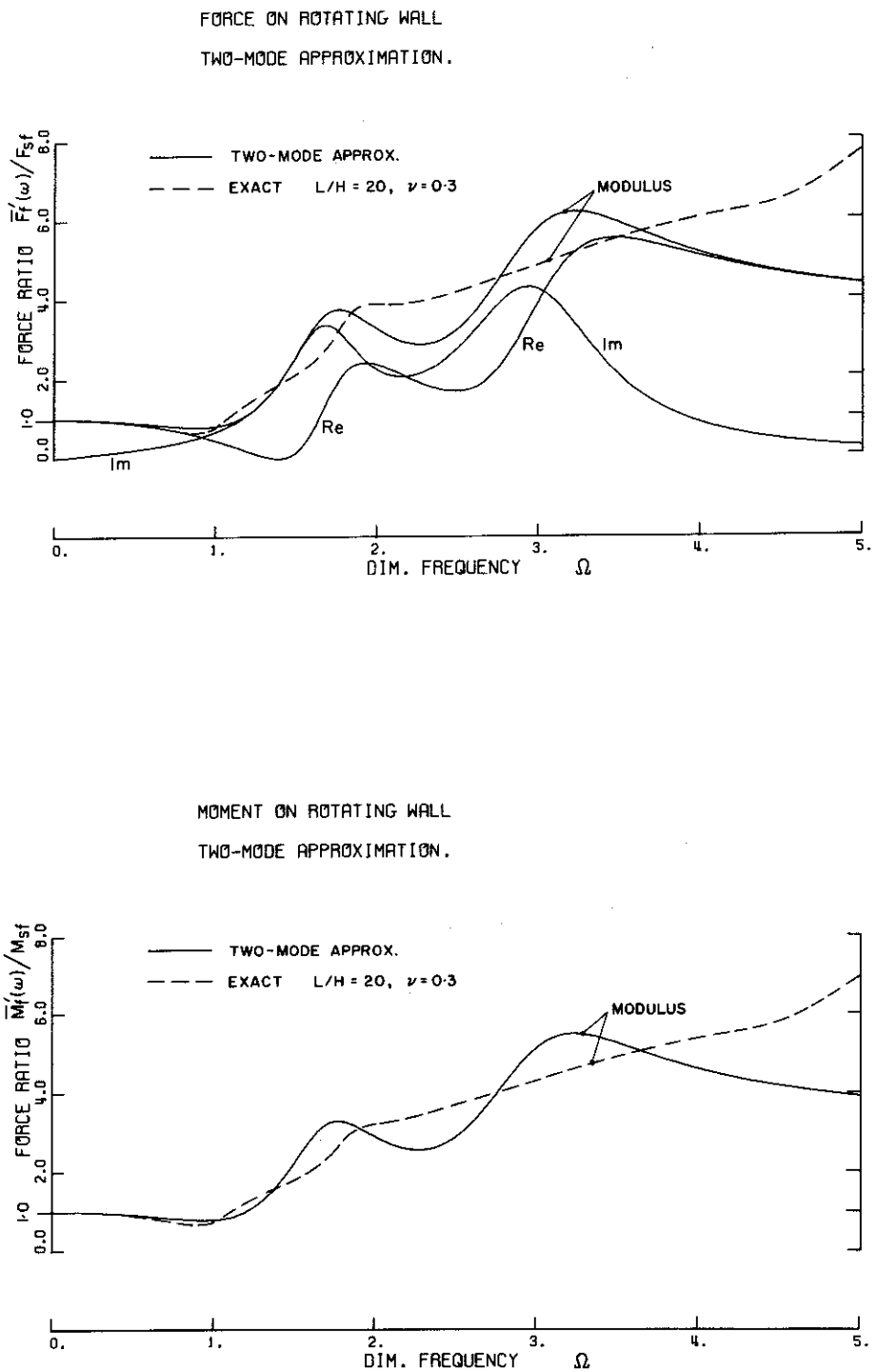

Figure 6.20 Complex-amplitude of force ratio on harmonically forced smooth rotating wall. Comparison between equivalent two-mode system and exact solutions.

6.5. HARMONIC FORCING: FINITE ELEMENT METHOD

The finite element method can be used to compute solutions for harmonically forced problems. Details of the application of the finite element method to problems of this type have been presented by Lysmer and Kuhlemeyer[30]. The general applicability of the method enables problems involving inhomogeneity of material properties and complex boundary configurations to be solved. The finite element equations of motion for forced vibration may be written as

$$M\ddot{\underline{u}}(t) + C\dot{\underline{u}}(t) + K\underline{u}(t) = \underline{f}(t) \tag{6.38}$$

in which

M = assemblage mass matrix

C = assemblage damping matrix

K = assemblage stiffness matrix

$\underline{u}(t)$ = nodal displacement vector

$\underline{f}(t)$ = nodal forcing vector

Let $\underline{f}(t) = \overline{\underline{f}}\, e^{i\omega t}$, then the solution of equation (6.38) is of the form

$$\underline{u}(t) = \overline{\underline{u}}\, e^{i\omega t} \tag{6.39}$$

Hence equations (6.38) can be written as

$$\tilde{K}\overline{\underline{u}} = \overline{\underline{f}} \tag{6.40}$$

in which

$$\tilde{K} = K + i\omega C - \omega^2 M$$

The complex linear algebraic equations (6.40) can be solved by standard methods to give the complex displacements $\underline{\bar{u}}$ and the associated stress field. A complete solution of the equations is required for each value of forcing frequency and the computational effort for each solution is approximately equivalent to that required in a static finite element analysis for a single load system. If this method is used a considerable amount of computation is required to define wall force and moment response curves equivalent to those presented in the previous section. The numerical evaluation of analytical solutions will probably be a computationally more efficient approach but obviously the number of problems solvable by analytical methods is limited.

7. DEFORMABLE WALL

In this chapter the previously presented rigid-wall and forced-wall solutions are superimposed to give total earthquake-induced forces and moments on a wall structure that undergoes rotational deformation. The methods employed can be readily extended to other types of wall deformation.

7.1. STATIC SOLUTION

The problem studied in this section is shown in Fig. 7.1. A deformable wall is loaded by a uniform static horizontal body force in the homogeneous linearly elastic soil. The wall deformation is assumed to be limited to rigid rotation about the base of the wall, and the rotational stiffness of the wall per unit length is represented by a spring of stiffness k_w placed at the top of the wall. The problem boundary conditions are detailed in Fig. 7.1.

In terms of the displacements the equilibrium equations for the elastic soil can be expressed as

$$L\underline{u}(x,y) + \underline{F} = \underline{0} \tag{7.1}$$

in which

$$\underline{F} = \begin{Bmatrix} -\gamma \\ 0 \end{Bmatrix}$$

Let $\underline{u}_{sr}(x,y)$ be the rigid-wall solution of equation (7.1); that is, the solution satisfying $u = 0$, $\tau_{xy} = 0$ on the wall boundary and the other boundary conditions of Fig. 7.1. Let $\underline{u}_{sf}(x,y)$ be the forced-

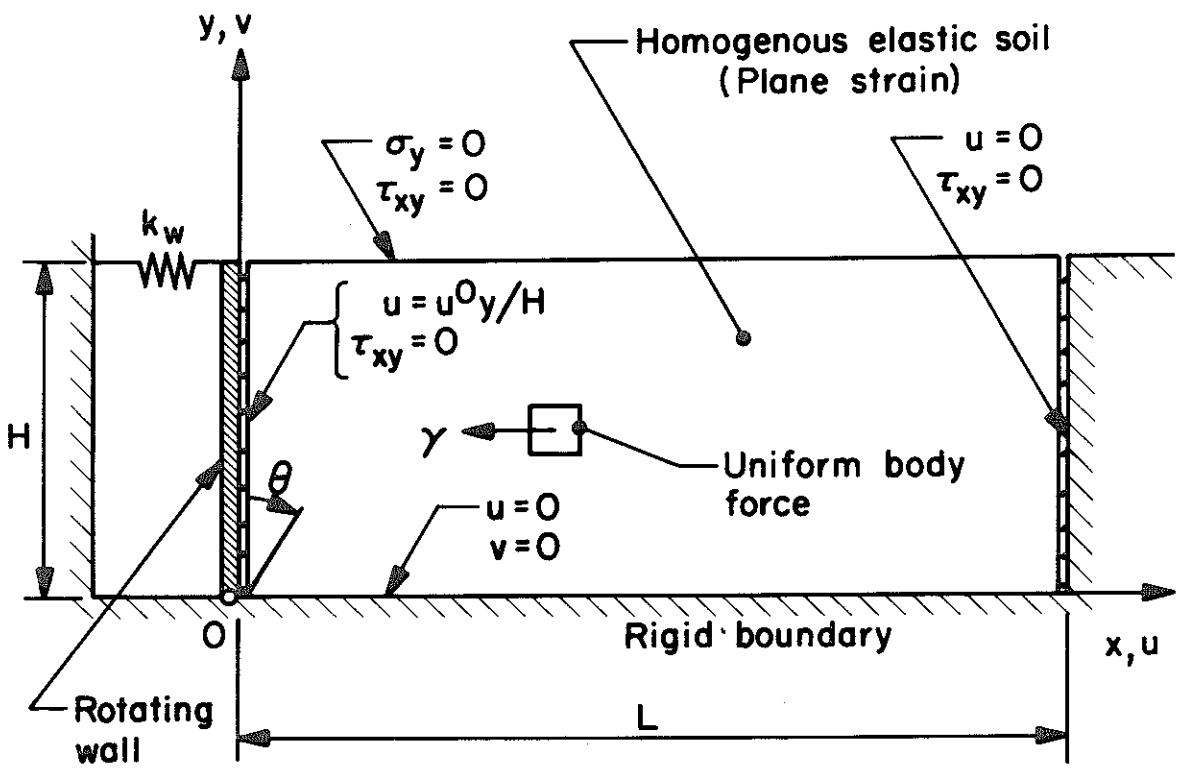

ROTATING WALL PROBLEM

Figure 7.1

wall solution for unit wall rotation; that is, the solution of equation (7.1) for zero body force that satisfies the boundary conditions of Fig. 7.1. By superposition the general solution of equations (7.1) can be expressed as

$$\underline{u}(x,y) = \underline{u}_{sr}(x,y) + \theta \underline{u}_{sf}(x,y) \tag{7.2}$$

in which

θ = angle of rotation of wall

The unknown wall rotation θ can be determined from the moment equilibrium condition for the wall which can be expressed as

$$M_{sr} + \theta M_{sf} - \theta k_w H^2 = 0 \tag{7.3}$$

in which

$$M_{sr} = \int_0^H y L_p \underline{u}_{sr}\, dy, \quad \text{moment on rigid wall from one-g static horizontal body force}$$

$$M_{sf} = \int_0^H y L_p \underline{u}_{sf}\, dy, \quad \text{moment on statically forced wall for unit rotation}$$

(A unit length of structure is implied in these definitions. M_{sr} and M_{sf} are positive in the clockwise direction.) Rearrangement of equation (7.3) gives

$$\theta = \frac{-M_{sr}}{(M_{sf} - k_w H^2)} \tag{7.4}$$

Substitution of expression (7.4) into (7.2) gives the general displacement solution in terms of the partial solutions $\underline{u}_{sr}$ and $\underline{u}_{sf}$. The

pressure distribution on the wall can be derived from the general displacement solution by applying the stress-strain relations in the usual way.

7.2. DYNAMIC SOLUTION

The problem studied in this section is shown in Fig. 7.2. The rigid boundaries are forced by a time-dependent horizontal acceleration. Once again the wall deformation is assumed to be limited to rigid rotation about the base of the wall. The wall rotational stiffness per unit length is represented by a spring of stiffness k_w and the dissipation associated with the rotational deformation of the structure is represented by a dashpot with damping coefficient c_w. By replacing the boundary forcing by d'Alembert body forcing the displacement equations of motion of the elastic soil can be written in vector form as

$$L\underline{u}(x,y,t) = \rho\ddot{\underline{u}}(x,y,t) + c\dot{\underline{u}}(x,y,t) + \rho\ddot{\underline{u}}_b(t) \qquad (7.5)$$

in which

$$\underline{u}_b(t) = \begin{Bmatrix} u_b(t) \\ 0 \end{Bmatrix} \text{ , vector of displacements on rigid boundary}$$

By superposition it is readily shown that the general solution of equation (7.5) can be expressed as

$$\underline{u}(x,y,t) = \underline{u}_r(x,y,t) + \underline{u}_f(x,y,t) \qquad (7.6)$$

in which

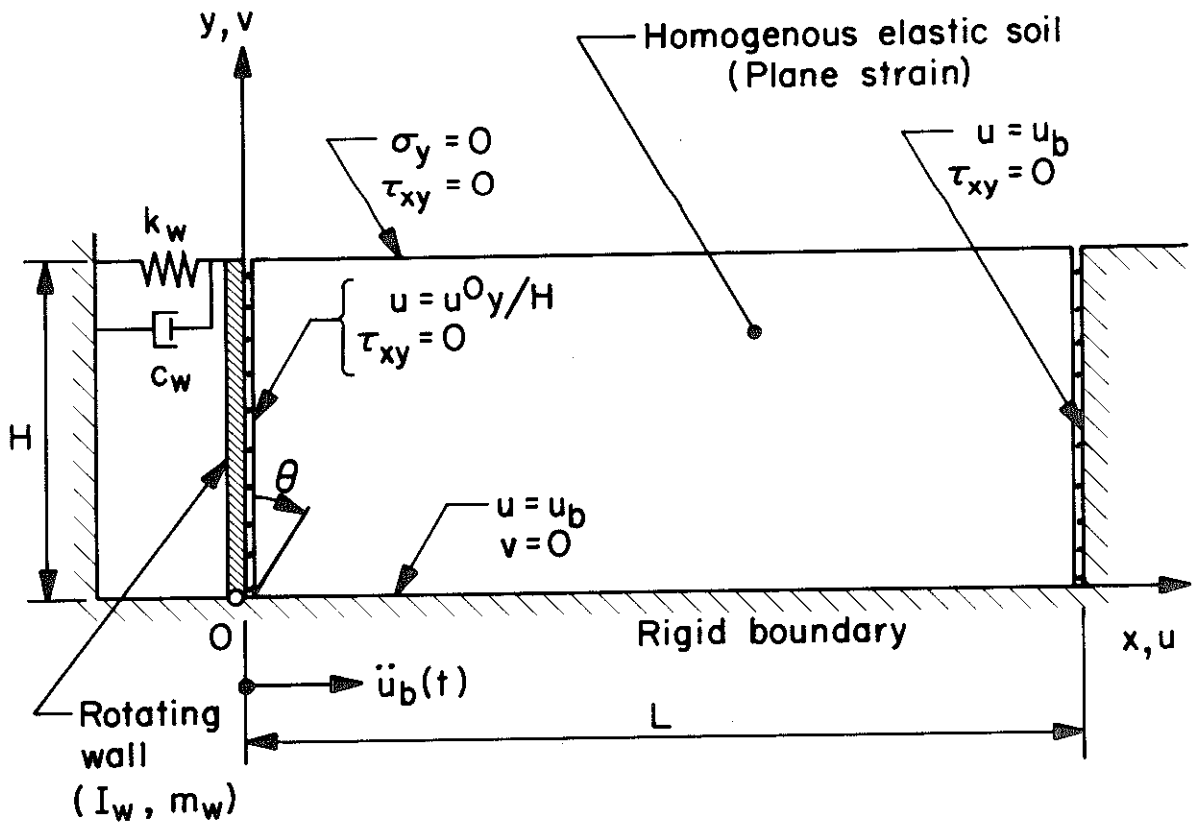

ROTATING WALL PROBLEM

Figure 7.2

$\underline{u}_r(x,y,t)$ = rigid-wall solution; that is, solution for $u(0,y,t) = 0$

$\underline{u}_f(x,y,t)$ = forced-wall solution; that is, solution of equation (7.5) with $\underline{u}_b(t) = \underline{0}$, for forcing of the wall boundary by the horizontal wall displacement $u(0,y,t)$ from the general solution of equation (7.5)

The equation of motion for the wall structure may be written as

$$I_w\ddot{\theta}(t) + c_w H^2\dot{\theta}(t) + k_w H^2\theta(t) + m_w h_c\ddot{u}_b(t) - M_r(t) - M_f(t) = 0 \qquad (7.7)$$

in which

I_w = moment of inertia of wall about the base

m_w = mass of wall structure

k_w = spring constant for wall structure

c_w = damping coefficient for wall structure

h_c = height of center of gravity of wall structure above the base

$M_r(t) = \int_0^H yL_p\underline{u}_r(x,y,t)\,dy$, dynamic moment on rigid wall

$M_f(t) = \int_0^H yL_p\underline{u}_f(x,y,t)\,dy$, moment on dynamically forced wall

A unit length of structure is implied in the definitions of all the above parameters (except h_c). M_f and M_r are taken as positive in the clockwise direction.

Let the Fourier transform of the function $\ddot{u}_b(t)$ be defined as

$$\overline{\ddot{u}}_b(\omega) = \int_{-\infty}^{\infty} \ddot{u}_b(t) e^{-i\omega t}\, dt \tag{7.8}$$

Using this definition the Fourier transformation of equation (7.7) can be written as

$$\left\{-\omega^2 I_w + i\omega c_w H^2 + k_w H^2\right\} \overline{\theta}(\omega) + \overline{\ddot{u}}_b(\omega) m_w h_c - \overline{M}_r(\omega) - \overline{M}_f(\omega) = 0 \tag{7.9}$$

(A bar over the symbol is used to denote a transformed variable.)

The transformed moments can be expressed as

$$\begin{aligned} \overline{M}_r(\omega) &= \overline{M}'_r(\omega)\, \frac{\overline{\ddot{u}}_b(\omega)}{g} \\ \overline{M}_f(\omega) &= \overline{M}'_f(\omega)\, \overline{\theta}(\omega) \end{aligned} \tag{7.10}$$

in which

$\overline{M}'_r(\omega)$ = complex-amplitude of steady-state moment on rigid-wall for one-g amplitude base forcing

$\overline{M}'_f(\omega)$ = complex-amplitude of steady-state moment for harmonic wall-forcing of unit rotational amplitude

Let

$$\begin{aligned} \omega_w &= \sqrt{\frac{k_w H^2}{I_w}} \\ \zeta_w &= \frac{c_w H^2}{2\omega_w I_w} \end{aligned} \tag{7.11}$$

Rearrangement of equation (7.9) and substitution of equations (7.10)

and (7.11) gives

$$\bar{\theta}(\omega) = \frac{-\left\{m_w g h_c - \bar{M}'_r(\omega)\right\} \ddot{\bar{u}}_b(\omega)}{g\omega_w^2 I_w \left\{1 - \frac{\omega^2}{\omega_w^2} + 2i\zeta_w \frac{\omega}{\omega_w} - \frac{\bar{M}'_f(\omega)}{\omega_w^2 I_w}\right\}} \tag{7.12}$$

The transformed total wall moment $\bar{M}_T(\omega)$ can be expressed as

$$\frac{M_T(\omega)}{M_{sr}} = \frac{M_{sf}}{M_{sr}} \frac{\bar{M}'_f(\omega)\bar{\theta}(\omega)}{M_{sf}} + \frac{\bar{M}'_r(\omega)}{M_{sr}} \frac{\ddot{\bar{u}}_g(\omega)}{g} \tag{7.13}$$

in which

M_{sf} = moment on statically forced wall for unit rotation

M_{sr} = moment on rigid wall from one-g static horizontal body force

Let

$$\frac{\bar{M}'_r(\omega)}{M_{sr}} = r_1(\omega) + ir_2(\omega)$$

$$\frac{\bar{M}'_f(\omega)}{M_{sf}} = f_1(\omega) + if_2(\omega) \tag{7.14}$$

The functions $r_1(\omega)$ and $r_2(\omega)$ are the real and imaginary parts of the complex-amplitude of moment ratio for harmonic base forcing of the rigid-wall problem. The functions $f_1(\omega)$ and $f_2(\omega)$ are the real and imaginary parts of the complex-amplitude of moment ratio for the harmonically-forced rotating wall problem. Plots of the

functions r_1, r_2 and f_1, f_2 are given in Sections 3.5 and 6.4 respectively. Substitution of expressions (7.12) and (7.14) into (7.13) gives

$$\frac{M_T(\omega)}{M_{sr}} = -\left[\frac{M_s^r(f_1 + if_2)\left\{1 - M_{sr}^d(r_1 + ir_2)\right\}}{\left\{\left(1 - \frac{\omega^2}{\omega_w^2}\right) + 2i\zeta_w \frac{\omega}{\omega_w} - M_{sf}^d(f_1 + if_2)\right\}} - (r_1 + ir_2)\right] \frac{\ddot{u}_b(\omega)}{g} \tag{7.15}$$

in which

$$M_{sf}^d = \frac{M_{sf}}{\omega_w^2 I_w}$$

$$M_{sr}^d = \frac{M_{sr}}{m_w g h_c}$$

$$M_s^r = \frac{M_{sf}^d}{M_{sr}^d}$$

Separating the numerator and denominator of expression (7.15) into real and imaginary parts gives

$$\frac{M_T(\omega)}{M_{sr}} = -\left[\frac{\left\{f_1 M_s^r - r_1\left(1 - \frac{\omega^2}{\omega_w^2}\right) + 2r_2\zeta_w \frac{\omega}{\omega_w}\right\} + i\left\{f_2 M_s^r - r_2\left(1 - \frac{\omega^2}{\omega_w^2}\right) - 2r_1\zeta_w \frac{\omega}{\omega_w}\right\}}{\left(1 - \frac{\omega^2}{\omega_w^2} - M_{sf}^d f_1\right) + i\left(2\zeta_w \frac{\omega}{\omega_w} - M_{sf}^d f_2\right)} \right]$$

$$\times \frac{\ddot{\bar{u}}_b(\omega)}{g} \tag{7.16}$$

Let

$$\overline{M}_T(\omega) = \overline{M}'_T(\omega) \frac{\ddot{\bar{u}}_b(\omega)}{g} \tag{7.17}$$

Then

$$\frac{|M_T'(\omega)|}{M_{sr}} = \sqrt{\frac{\left\{f_1 M_s^r - r_1\left(1-\frac{\omega^2}{\omega_w^2}\right)+2r_2\zeta_w\frac{\omega}{\omega_w}\right\}^2+\left\{f_2 M_s^r - r_2\left(1-\frac{\omega^2}{\omega_w^2}\right)-2r_1\zeta_w\frac{\omega}{\omega_w}\right\}^2}{\left(1-\frac{\omega^2}{\omega_w^2}-M_{sf}^d f_1\right)^2+\left(2\zeta_w\frac{\omega}{\omega_w}-M_{sf}^d f_2\right)^2}} \tag{7.18}$$

The time-history of the total wall moment can be computed by taking the inverse transform of expression (7.17). That is

$$M_T(t) = \frac{1}{2\pi}\int_{-\infty}^{\infty} \overline{M}_T'(\omega)\,\frac{\ddot{\overline{u}}_b(\omega)}{g}\,e^{i\omega t}\,d\omega \tag{7.19}$$

Thus to evaluate $M_T(t)$ it is necessary to compute the Fourier transform of the base acceleration and to compute the inverse transform of the product specified in expression (7.19). The Fourier transformation and the inverse transformation can be readily evaluated using a Fast Fourier Transform computer program. Applications of the Fast Fourier Transform algorithm to solve structure interaction problems have been previously described by Chopra[6], and Liu and Fagel[29].

Frequently an estimate of the maximum earthquake-induced wall moment or pressure distribution is sufficient information for design purposes. If a suitable earthquake power spectral density function is available, it is significantly more efficient to obtain statistical estimates of the maximum forces and pressures using random vibration theory than to compute the complete time-history of these values using the Fourier transform approach. From

equation (3.49) the variance of the total wall moment can be expressed as

$$s_M^2 = \int_0^\infty |\overline{M}_T'(\omega)|^2 G(\omega)\, d\omega \qquad (7.20)$$

in which

s_M^2 = variance of the total wall moment

$G(\omega)$ = power spectral density of earthquake

$|\overline{M}_T'(\omega)|$ is defined by expression (7.18). A statistical estimate of the maximum value of the wall moment can be found from the value of s_M^2 and the properties of the normal distribution. Details of the application of this method are given in Section 8.3.

7.3. BUILDING-BASEMENT STRUCTURE

The results of the foregoing sections can be applied to the study of dynamic wall pressures on structures that may be considerably more complex in their dynamic behaivor than the simple rotating wall structure. The application of the results to more complex structures is illustrated in this section by developing a solution for the dynamic soil moment on the rigid basement of the building structure shown in Fig. 7.3. The building consists of a flexible superstructure supported on a rigid basement-structure which is founded on a rock layer. An elastic soil layer, that is assumed to be relatively soft in comparison to the rock, overlies the rock layer and is in contact with the basement walls. The rock layer is assumed to permit elastic rotational deformation of

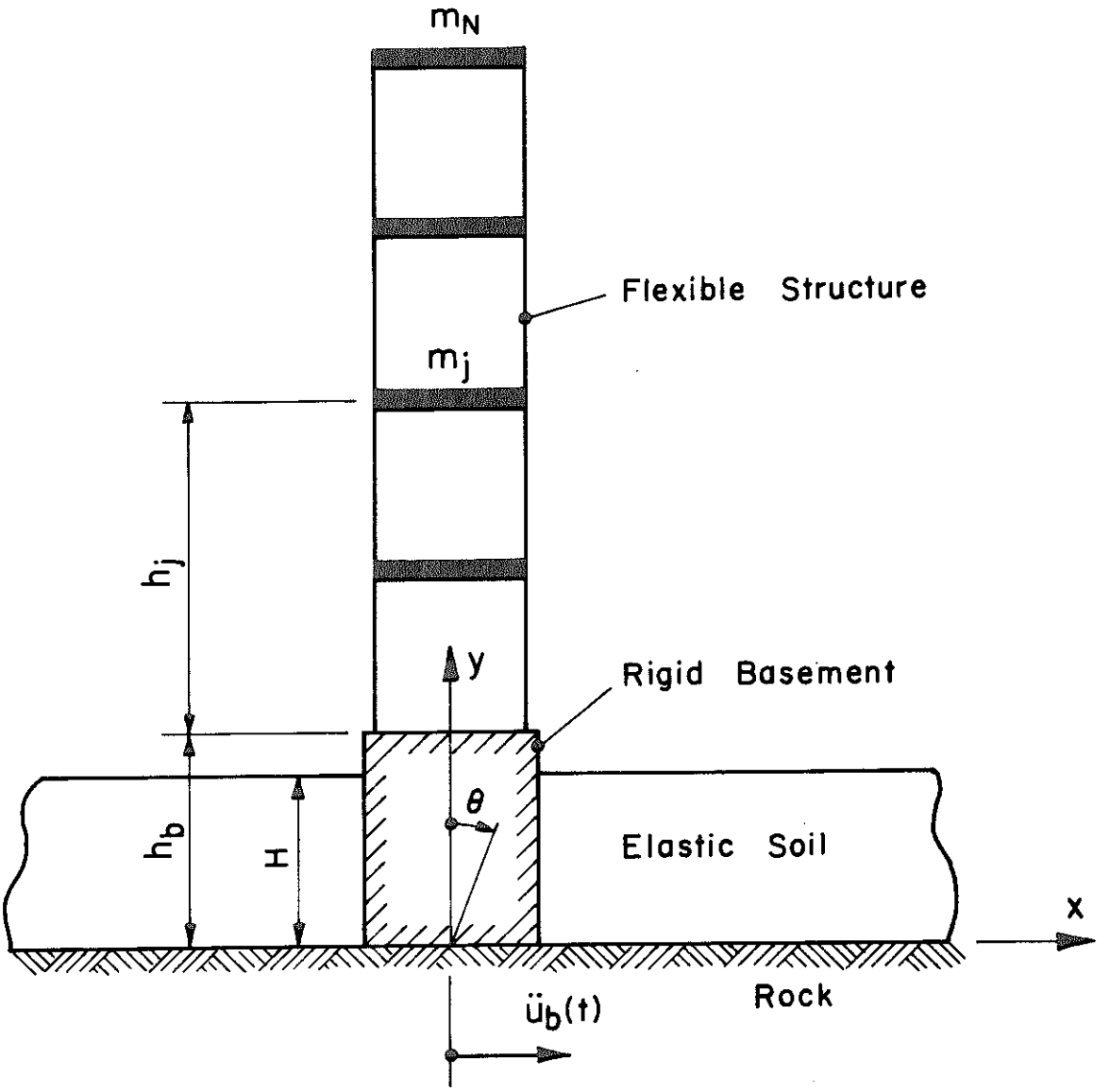

Figure 7.3 Flexible superstructure on rotating basement structure.

the basement but prevent significant translation. It is also assumed that the displacements of the rock surface resulting from the rotation of the basement have no significant influence on the wall pressures. The rock foundation is subjected to a horizontal time-varying acceleration $\ddot{u}_b(t)$.

The equation of motion describing the rotation of the basement can be expressed as

$$I_b\ddot{\theta}(t) + c_b\dot{\theta}(t) + k_b\theta(t) + m_b h_c \ddot{u}_b(t) - M_f(t) - M_r(t) - M_b(t) - S_b(t)h_b = 0 \qquad (7.21)$$

in which

$\theta(t)$ = rotation of the basement structure

I_b = moment of inertia of basement structure about foundation

m_b = mass of basement structure

h_b = height of basement structure

h_c = height of center of gravity of basement above the foundation

k_b = spring constant for rotation of basement on foundation

c_b = damping coefficient for rotation of basement on foundation

$S_b(t), M_b(t)$ = superstructure base shear and moment respectively

$M_f(t)$ and $M_r(t)$ are the soil-basement interaction moments and are

as defined for equation (7.7).* Carrying out the Fourier transformation of equation (7.21) gives

$$\left\{-\omega^2 I_b + i\omega c_b + k_b\right\}\bar{\theta}(\omega) + m_b h_c \bar{\ddot{u}}_b(\omega) - \bar{M}_f(\omega) - \bar{M}_r(\omega) - \bar{M}_b(\omega) - \bar{S}_b(\omega) h_b = 0 \qquad (7.22)$$

The relationship between the transformed superstructure base shear and moment, and the transformed accelerations at the base of the superstructure (top of the basement) can be written as

$$\begin{Bmatrix} \bar{S}_b(\omega) \\ \bar{M}_b(\omega) \end{Bmatrix} = -\begin{bmatrix} H_{11}(\omega) & H_{12}(\omega) \\ H_{21}(\omega) & H_{22}(\omega) \end{bmatrix} \begin{Bmatrix} \bar{\ddot{u}}_b(\omega) + h_b \bar{\ddot{\theta}}(\omega) \\ \bar{\ddot{\theta}}(\omega) \end{Bmatrix} \qquad (7.23)$$

The matrix coefficients $H_{ij}(\omega)$, $i = 1,2$; $j = 1,2$, can be derived from the solution of the equations of motion of the superstructure. On the assumption that the superstructure satisfies the conditions for the existance of classical normal modes the coefficients can be expressed as

---

*The interaction moments are assumed to act on two wall faces of the basement-structure. Tension will in general exist over part of one of the faces at any time during an earthquake. Under tensile conditions most soils will separate from the wall and consequently the total interaction moment will be less than given by elastic theory. For a particular problem an estimate of the extent of the tension region can be used to make an arbitrary reduction in the total interaction moment.

$$H_{11}(\omega) = \sum_{j=1}^{N} m_j + \sum_{n=1}^{N} \frac{(\underline{\phi}_n^T \underline{M})^2 R_n(\omega)}{\underline{\phi}_n^T M \underline{\phi}_n}$$

$$H_{22}(\omega) = \sum_{j=1}^{N} m_j h_j^2 + \sum_{n=1}^{N} \frac{(\underline{\phi}_n^T M \underline{h})^2 R_n(\omega)}{\underline{\phi}_n^T M \underline{\phi}_n} \qquad (7.24)$$

$$H_{12}(\omega) = H_{21}(\omega) = \sum_{j=1}^{N} m_j h_j + \sum_{n=1}^{N} \frac{\underline{\phi}_n^T M \underline{h} \underline{\phi}_n^T \underline{M}}{\underline{\phi}_n^T M \underline{\phi}_n} R_n(\omega)$$

in which

N = number of lumped story masses of superstructure

m_j = story mass at floor j

M = diagonal matrix of story masses

$\underline{M}$ = vector of story masses

h_j = height of story mass j above base of superstructure

$\underline{h}$ = vector of floor heights h_j

$\underline{\phi}_n$ = mode shape for mode n

$$R_n(\omega) = \frac{\omega^2/\omega_n^2}{1 - \frac{\omega^2}{\omega_n^2} + 2i\zeta_n \frac{\omega}{\omega_n}}$$

ω_n = natural angular frequency for mode n

ζ_n = damping ratio for mode n

Rearrangement of equation (7.22) and substitution from expression

(7.23) gives

$$\bar{\theta}(\omega) = \frac{-\left\{m_b g h_c - M_r'(\omega) + g(H_{11}(\omega)h_b + H_{12}(\omega)\right\}\ddot{\bar{u}}_b(\omega)}{g\omega_b^2 I_b\left\{1 - \frac{\omega^2}{\omega_b^2} + 2i\zeta_b\frac{\omega}{\omega_b} - \frac{\bar{M}_f'(\omega)}{\omega_b^2 I_b} - \frac{\omega^2}{\omega_b^2 I_b}(H_{11}(\omega)h_b^2 + 2H_{12}(\omega)h_b + H_{22}(\omega))\right\}} \tag{7.25}$$

in which

$$\omega_b = \sqrt{\frac{k_b}{I_b}}$$

$$\zeta_b = \frac{c_b}{2\omega_b I_b}$$

The transformed total wall moment is found by substituting expression (7.25) into (7.13). The resulting expression can be separated into real and imaginary parts to facilitate the solution obtained by using either the Fast Fourier Transform or the random vibration methods.

In the above derivation it has been assumed that the equivalent spring stiffness k_b and the equivalent damping factor c_b for the rotational motion of the basement structure on the rock foundation are independent of frequency; however, no additional complexity is added by assuming frequency dependence for these parameters. Published solutions for the forced vibration of rigid foundations resting on an elastic half-space can be used to estimate the frequency dependence of the parameters k_b and c_b. Solutions for a rigid strip are given by Karasudhi et al.[23] and Oien[41], and solutions for a rigid rectangle are given by Kobori et al.[25].

8. DEFORMABLE WALL: CASTAIC POWER STATION

In Chapter 5 the earthquake-induced soil pressures on the Castaic power generating station were computed using the assumption of a perfectly rigid wall structure. In this section the effects on the wall pressures of the elastic rotation of the structure on its foundation are investigated and results are presented to illustrate the application of the foregoing theory for deformable-wall solutions.

It can be seen from the typical cross-section of the power station shown in Fig. 5.1 that the contact between the structure and the rock foundation is effectively below the base of the soil-retaining wall. In order to simplify the problem for the purpose of an illustrative example the foundation of the structure was assumed to be at the same level as the base of the wall. The idealization of the soil-structure system used in the following analysis is shown in Fig. 8.1. An effective $\frac{L}{H}$ of about 1.7 is obtained by taking the average length between the wall and sloping far-end boundary. A value of $\frac{L}{H} = 2.0$ was used for the analysis presented here because analytical solutions had been fully evaluated for this case.

Approximate estimates of the soil properties and structural parameters required for the analysis were obtained from Scott[47] and White[58], and the structural drawings. The following values were used:

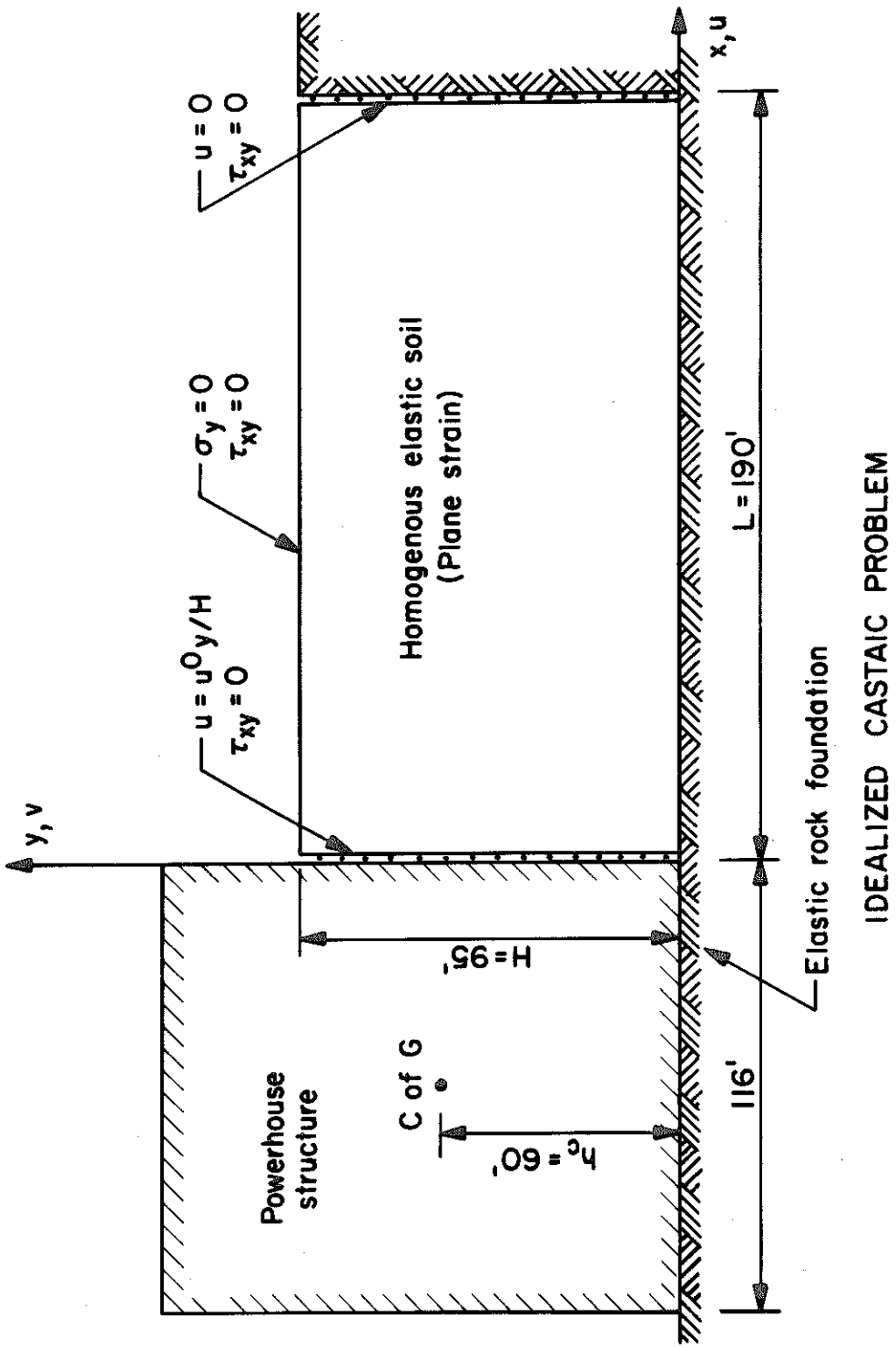

IDEALIZED CASTAIC PROBLEM

Figure 8.1

uniform elastic soil:

$$E = 10^6 \text{ lb/ft}^2$$

$$\nu = 0.4$$

$$\gamma = 120 \text{ lb/ft}^3$$

rigid-body rotation of structure on elastic rock foundation:

period, $T_w = 0.25$ sec

damping, $\zeta_w = 5.0\%$

weight of structure, $m_w g = 1.5 \times 10^6$ lb/ft

height of center of gravity above base, $h_c = 60$ ft

moment of inertia about base, $I_w = m_w \times (7{,}110 \text{ ft}^2)$

length of structure = 420 ft

The above elastic soil properties correspond to a soil shear wave velocity of 310 ft/sec. The period of vibration was computed by the Los Angeles City Department of Power and Water and exact details of the method used are unknown to the writer. The periods of vibration of a rigid rectangular body on an elastic half-space can be readily computed from solutions given by Whitman and Richart[59] and Kobori et al.[25]. From the solution presented by Whitman and Richart the period of 0.25 sec was found to correspond to a rock shear wave velocity of 2,500 ft/sec, and the damping ratio for the rocking mode was found to be approximately 5%.

Deformation of the soil-retaining wall also results from elastic rigid-body translation of the structure on the foundation and from strains within the structural elements. In this analysis the effects of these deformations on the pressure distributions were

considered to be of second order relative to the effects of rotation. Because the Castaic facility is designed to pump storage water, under normal operating conditions a considerable head of water is present on the downstream face of the structure. The influence of the hydrodynamic pressures was not included in the following analyses of the dynamic behavior of the structure. However, it would be of interest to extend the work presented here to include this effect and it appears that appropriate hydrodynamic forces can be obtained from the work on dam-reservoir interaction presented by Chopra[6].

8.1. STATIC ANALYSIS

An estimate of the effects of structure rotation on the dynamic soil pressures was made by a preliminary static analysis. The following static moments were evaluated using the previously presented analytical solutions:

Moment from horizontal one-g soil body force (rigid-wall), $\frac{M_{sr}}{\gamma H^3} = 0.389$

Moment from horizontal one-g force on structure, $\frac{m_w g h_c}{\gamma H^3} = 0.875$

Moment produced by soil pressure due to structure rotation, $\frac{M_{sf}}{E\theta H^2} = 0.308$

(These moments are for a unit length of structure.) From the structure period and moment of inertia the rotational spring-stiffness of the rock foundation was computed to be 2.1×10^{11} lb.ft/rad./ft of structure. The one-g rotation of the structure

was computed from the above moments and the rotational stiffness using expression (7.4). A rotation of 0.61×10^{-3} rad. was obtained, which corresponds to a horizontal displacement of 0.70 in. at the top level of the soil. This rotation reduces the soil body force moment computed for the rigid-wall assumption (M_{sr}) by 4.2%.

Inspection of the plots of the complex-amplitudes of force and moment for harmonic rotational forcing given in Section 6.4 shows that if the structure has a fundamental frequency significantly higher than the lowest natural frequencies of the soil body, considerable amplification of the deformation component in the total static moment may occur. It is of interest to consider the possibility of this amplification effect occurring for the example under discussion. The natural angular frequency ω_w of the structure rotating as a rigid-body on the rock foundation (without the presence of the soil) can be expressed in dimensionless form as

$$\frac{\omega_w}{\omega_s} = \frac{4H}{T_w V_s} \tag{8.1}$$

(in which $\omega_s = \pi V_s/2H$; V_s = shear wave speed of soil.) Evaluating expression (8.1) gives $\omega_w/\omega_s = 4.91$. From Fig. 6.11 it can be seen that at this value of dimensionless frequency the dynamic amplification of the rotational moment component is about 5.3. Consequently it can be expected that for this example the wall pressures will be modified to a significant extent by the dynamic displacements of the structure.

8.2. APPROXIMATE DYNAMIC ANALYSIS

Approximate dynamic soil pressures on certain relatively rigid wall structures may be estimated by decomposing the problem into two idealized uncoupled dynamic problems and superimposing the maximum pressures computed for each case by taking an rms sum. The decomposition into the two separate problems is shown diagramatically in Fig. 8.2. In applying this approximation it is assumed that only weak dynamic coupling exists between the wall structure and the soil body. This will be the case when the lowest natural frequencies of the soil body differ significantly from the lowest natural frequencies of the structure.

Problem I. Only the d'Alembert body forcing of the soil layer is considered in this part of the solution. If the structure is relatively rigid an acceptable Problem I solution can be derived from rigid-wall dynamic solutions. An improvement to the rigid-wall solution can be made by computing the deflection of the structure under the maximum rigid-wall dynamic pressure and adjusting the solution in accordance with this deflection.

Problem II. Only the d'Alembert forcing on the structure is considered in this part of the solution. A good approximation for the wall pressures can be obtained in many cases by considering the participation of the first mode of vibration of the structure. If the first mode shape is approximately linear the solutions given in this study for the harmonically forced rotating wall may be

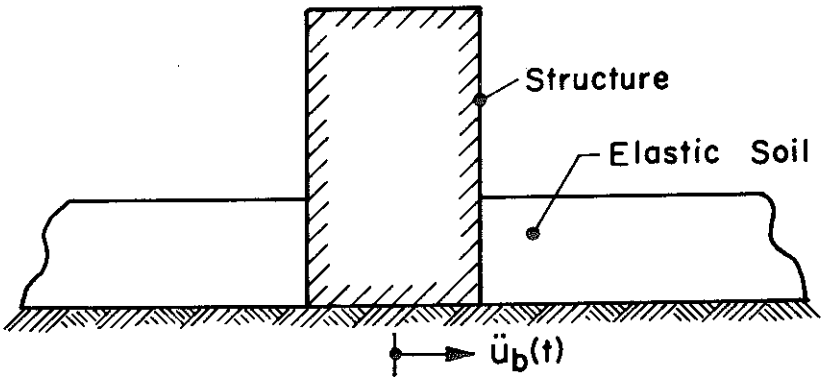

BASIC PROBLEM : FORCING ON RIGID BOUNDARY

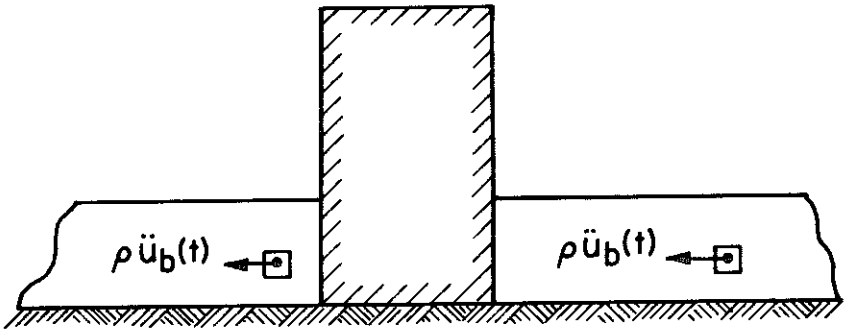

PROBLEM I

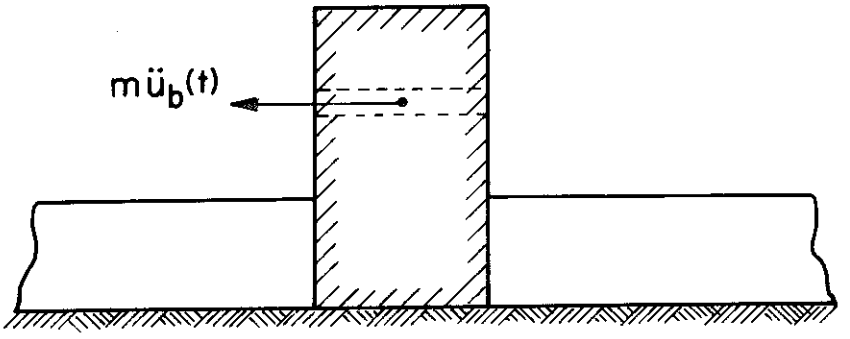

PROBLEM II

Figure 8.2

applied to give a direct solution. In most cases the fundamental frequency of the structure will not be significantly modified by the restraint imposed by the soil in contact with the walls.

From Appendix VI the three lowest dimensionless natural frequencies of the soil body in the example under discussion ($\frac{L}{H} = 2.0$, $\nu = 0.4$) are 1.85, 2.41 and 3.94. Thus, since significant coupling between the structure and the soil body is unlikely the approximate method is suitable for this example.

The static rotational stiffness of the rock foundation was computed to be about 75 times greater than the static rotational restraint provided by the soil layer. From the real part of the complex-amplitude of moment plotted in Fig. 6.11 it can be seen that at the fundamental frequency of the structure the effective soil stiffness increases by about 2.3 times the static value. From the results of Kobori et al.[25] it is found that the rotational stiffness of the rock foundation (for the geometry of this problem) does not change significantly from the static value over the frequency range of interest. Thus, the lowest structure mode has a natural frequency effectively governed by the stiffness of the rock foundation and to a good degree of approximation this frequency can be computed from the foundation static stiffness. (It is assumed in the foregoing discussion that structural deformations are negligible.)

A satisfactory Problem I moment M_I for the present example can be evaluated using the rigid-wall assumption. The rigid-wall moment computed in Chapter 5 using the Response Spectrum method and the rms sum of the modal contributions can

be expressed in dimensionless form as $M_I/\gamma H^3 = 0.071$. The maximum rotational response of the structure was computed using the 5% damped relative-velocity spectrum given in Appendix VIII. From this rotation and the complex-amplitude of moment plotted in Fig. 6.11 the Problem II dimensionless moment was evaluated to be $M_{II}/\gamma H^3 = 0.031$. Using the rms sum of M_I and M_{II} a total maximum wall moment of $M_T/\gamma H^3 = 0.078$ was obtained; that is, a 10% increase in the rigid-wall moment.

8.3. EXACT DYNAMIC ANALYSIS

A more exact dynamic analysis may be undertaken by evaluating the steady-state complex-amplitude response function for total moment given by expression (7.16). This expression was evaluated using the soil and structural parameters given above and the complex-amplitude moment functions plotted in Fig. 3.19 and Fig. 6.11 for $\frac{L}{H} = 2.0$ and $\nu = 0.4$. The solution obtained for the modulus of the complex-amplitude of total moment is compared in Fig. 8.3 with the modulus of the complex-amplitude of the rigid-wall moment. Rotation of the structure reduces the rigid-wall moment in the dimensionless frequency range between 0 and 1.25. At dimensionless frequencies between 1.25 and 5.5 the total moment is greater than the rigid-wall moment and the maximum difference between the moments occurs close to the natural frequency of the structure ($\Omega = 4.9$).

Random vibration theory was used to compute the $P = 0.988$ total wall moment in the same manner as described in Chapter 5 for the rigid-wall assumption. A value of $M_T/\gamma H^2 = 0.083$ was

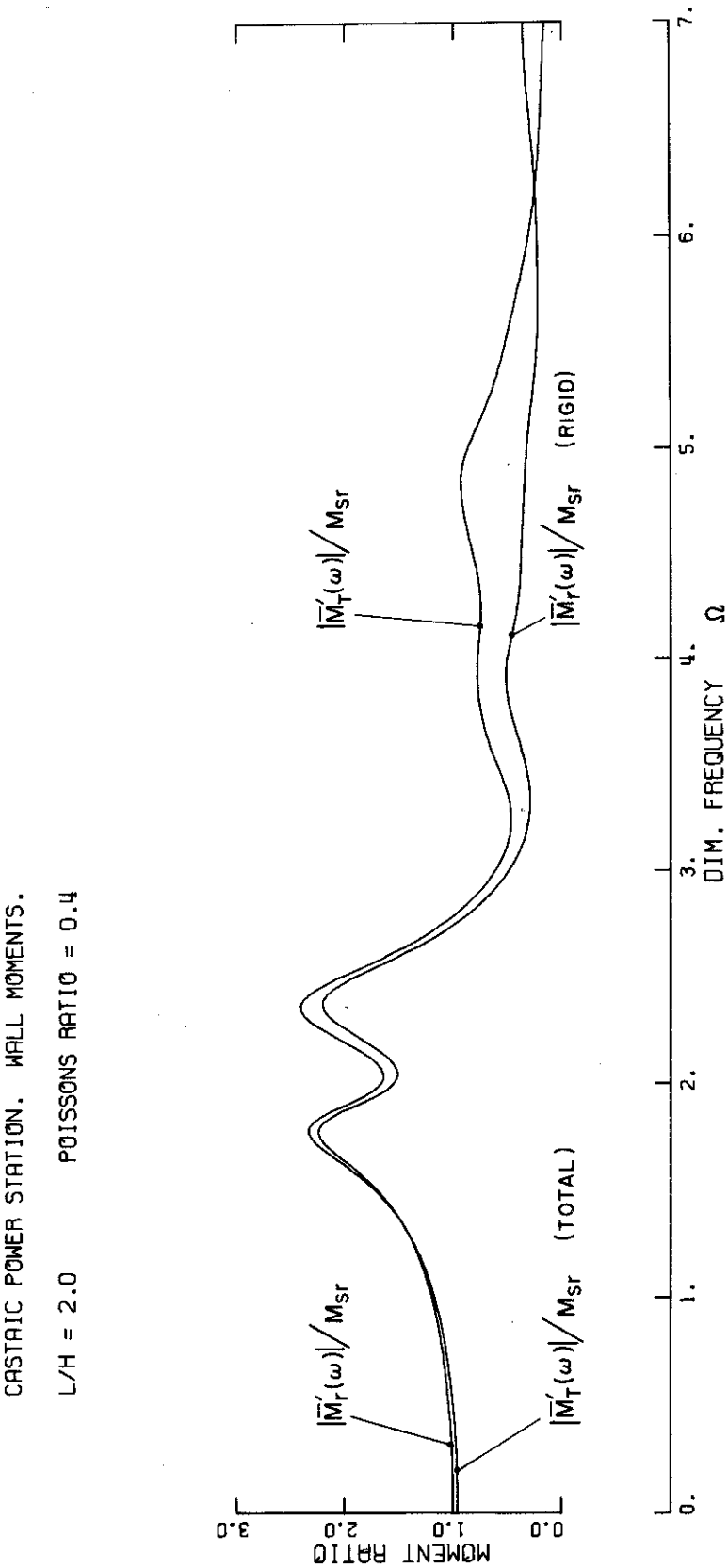

Figure 8.3 Castaic example. Complex-amplitudes of moment ratios. Total moment and rigid wall component.

obtained which is 9% higher than the rigid-wall moment previously evaluated by random vibration theory.

The earthquake-induced pressure distribution was not evaluated for the example under discussion. Complete details of the pressure distributions can be included without difficulty in the frequency domain superposition approach used for the wall moments; however, this requires quite a considerable increase in computational effort. In most cases an approximate pressure distribution suitable for design purposes can be evaluated by applying the rms superposition principle in the same manner as used above to evaluate approximate dynamic wall moments. The previously presented plots of the rigid-wall modal pressures and the forced-wall dynamic pressures enable this approach to be readily applied. The area of the approximate pressure distribution should be adjusted to agree with the force or moment if these are computed by the more exact method.

9. OTHER WALL SYSTEMS

9.1. THREE-DIMENSIONAL EFFECTS

Although quite a large number of wall structures approximately satisfy the plane strain assumption, the degree of error involved in applying the plane strain results to some building basement wall problems may be significant. Three-dimensional effects can be studied using the finite element method; however, in comparison with the two-dimensional case this requires considerably more time for both preparation of input data and computation. It is possible to reduce the computing time by performing only static analyses. The static three-dimensional results can then be used to improve dynamic plane strain solutions.

The following points are relevant in estimating some of the influences of three-dimensional effects.

(1) If the wall length is greater than about four times the wall height the plane strain solutions for wall pressures are expected to be satisfactory.

(2) If the wall structure is embedded in a soil layer of lateral extent large in comparison to the plan dimensions of the wall, then the maximum three-dimensional static pressures are probably greater than in the idealized plane strain representation. The largest pressure increases are probably near either end of the wall.

(3) The presence of a structure embedded in a soil layer of lateral extent large in comparison to the plan dimension of the

structure is unlikely to produce significant modification of the natural frequencies of the soil layer acting alone.

9.2. EMBEDDED PROBLEM

Satisfactory analytical solutions giving the dynamic pressures on the embedded building problem shown as Type VII in Fig. 1.1 are at the present time unavailable. The results of this study may be used as an informative guide when the soil foundation is relatively firm. Probably the most satisfactory approach for the case of a soft foundation soil is to perform a two-dimensional dynamic finite element analysis. A rigid boundary can be imposed some distance below the structure and the normal modes of the system computed.

The results from Tajimi's solution for the harmonic displacement forcing of the wall of the idealized problem shown in Fig. 1.7 are informative in the study of the embedded building problem. However, because of the geometric simplifications necessary in the derivation of this analytical solution the results do not have direct application. One comparatively simple method of making use of these results is to perform a static finite element analysis of a reasonably exact model of the embedded structure. An approximate dynamic solution can then be obtained by using the frequency dependence of Tajimi's results to modify the static finite element solution. This approach gives an approximate solution for dynamic forcing of the structure but does not give the complete solution for the earthquake-induced pressures since the effective

body forcing of the soil by the earthquake motions is not included.

9.3. CANTILEVER WALLS

A fully plastic stress condition develops in the soil retained by most relatively high cantilever walls. For low cantilever walls and in cases where the rotation and translation of the cantilever foundation is restrained, pressure distributions computed using elastic theory may often be satisfactory approximations. Dynamic amplification effects are seldom pronounced in earthquake excitation of low wall-soil systems. Thus, a pseudo-static elastic analysis may be satisfactory for most relatively low cantilever wall structures. Pressure distributions for a number of rigidly-founded cantilever walls loaded by vertical gravity and horizontal body forces in the soil were computed using the finite element method and are presented in Appendix VII.

10. SUMMARY AND CONCLUSIONS

10.1. SUMMARY

A study has been made of the earthquake-induced pressures on soil-retaining structures using linear elastic theory and idealized representations of the wall-soil system.

Static and dynamic analytical solutions were given for the case of a perfectly rigid smooth wall supporting a homogeneous elastic soil layer of finite length bonded to a rigid foundation. The static solution was presented for the case of a uniform horizontal body force, and the wall pressure distributions, forces and moments were plotted for a range of the parameters, ν and $\frac{L}{H}$. The wall forces and moments increased with both increasing ν and $\frac{L}{H}$ values. For $\frac{L}{H} = 6.0$ the force and moment were within about 5% of the asymptotic value for $\frac{L}{H} \to \infty$. The natural frequencies and normal modes were computed for the dynamic problem and expressions in terms of the modal properties were given for the wall pressure and force response to an arbitrarily time-varying forcing of the rigid boundaries. Plots of the natural frequencies, modal pressure distributions and modal wall forces were given to show the influence of the parameters ν and $\frac{L}{H}$ on the solutions. The frequency equation solutions showed that for $\frac{L}{nH} = 10$ the natural frequencies were within 10% of the values for $\frac{L}{nH} \to \infty$. Steady-state wall force and moment responses were computed for harmonic forcing of the rigid boundaries. These solutions showed that for a

10% modal damping ratio the responses for $\frac{L}{H} = 20$ were a reasonably good approximation for greater $\frac{L}{H}$ values. The steady-state solutions were used to determine an equivalent two-mode system for representing problems with an $\frac{L}{H}$ ratio greater than 10.

The Response Spectrum method of computing maximum earthquake responses from the modal properties was found to be satisfactory for the rigid-wall problem and results were given in a convenient form for its application. For $\frac{L}{H}$ values greater than 10 a relatively large number of modes were found to contribute to the pressure and force responses; however, for this case the equivalent two-mode approximation is satisfactory. It was also found that for $\frac{L}{H} < 2.0$ and $\nu > 0.45$ the wall force contributions from the lower modes were small. In these cases a satisfactory dynamic solution can be evaluated from the static solution.

The finite element method was used to investigate static and normal mode solutions of the rigid-wall problem for the case of a bonded contact on the wall-soil interface. Good agreement was found between the smooth and bonded pressure distributions except over the top 20% of the wall height which is the region of the stress singularity for the bonded case. The finite element method was also used to investigate the effect of a linear increase in E and G with increasing depth from the surface of the soil layer (ν assumed constant). Over the top half of the wall, the static pressure distributions had lower values than the distributions for the uniform layer counterparts resulting in lower wall forces and moments for the nonuniform soil. This was also generally the case for the modal

forces and pressure distributions. The natural frequencies of the significant lower modes, computed for $\frac{L}{H} = 3.0$, $\nu = 0.3$ and E (and G) varied from 0.1 at the top of the soil to 1.0 at the base, were within 30% of the equivalent frequencies for a uniform soil with elastic properties equal to the average of the nonuniform soil properties. From the analytical solutions for a nonuniform infinite stratum it was concluded that for large $\frac{L}{nH}$ values (greater than 10) the natural frequencies would be expected to be within about 25% of the frequencies of the uniform problem with average properties. The first mode natural frequency of a nonuniform problem with a large $\frac{L}{nH}$ ratio would be expected to be within 10% of the frequency of the average uniform problem.

An analytical solution was derived for static rotational forcing of the wall boundary of the idealized smooth deformable wall problem. Numerical results were evaluated using the finite element method, and the wall pressure distributions, forces and moments were plotted for a range of the parameters ν and $\frac{L}{H}$. The force and moment were found to decrease with increasing $\frac{L}{H}$ values and at $\frac{L}{H} = 3.0$ were within about 5% of the asymptotic value for $\frac{L}{H} \rightarrow \infty$. The pressure distributions, forces and moments showed relatively small changes for variations of ν from 0.3 to 0.45. Solutions were also computed for the bonded contact assumption. Differences between the smooth and bonded pressure distributions were greater than observed for the rigid-wall problems; however, the differences were not sufficiently large to have practical

significance. Solutions computed for linear increases of E and G with increasing depth showed that the pressures on the top half of the wall were lower than for the uniform soil case.

Two analytical approaches for evaluating the steady-state solution of the idealized smooth deformable wall problem, subjected to harmonic displacement forcing on the wall boundary, were investigated. Numerical results were evaluated for harmonic rotational forcing of the wall over a range of dimensionless forcing frequency from 0 to 5.0. A 10% modal damping ratio was used for most of the solutions. Wall pressures, forces and moments were computed for a range of $\frac{L}{H}$ values from 1.0 to 20.0 with $\nu = 0.3$ and 0.4. The solutions for $\frac{L}{H} = 10.0$ were found to be reasonably good approximations for problems with greater values of the $\frac{L}{H}$ ratio. The moduli of the wall forces and moments were found to decrease from the static values (at zero frequency) to about 60% of the static values at a dimensionless forcing frequency of 1.0. As the forcing frequency was increased beyond the fundamental frequency of the soil body, the moduli were found to increase significantly with the force modulus reaching about eight times the static value at a dimensionless forcing frequency of 5.0. For $\frac{L}{H}$ values less than 5.0 and between dimensionless frequencies 1.0 and 5.0, quite large fluctuations occurred in the moduli corresponding to resonances with the natural frequencies of the soil body.

The solution of the idealized deformable-wall problem subjected to an arbitrarily time-varying horizontal acceleration of the rigid base was obtained by superimposing in the frequency

domain the steady-state solutions for the rigid wall and forced wall problems. It was found convenient to idealize the earthquake forcing as a stationary, Gaussian random process and to evaluate statistical estimates of the maximum wall force and moment during the earthquake from the steady-state frequency domain solution using random vibration theory.

The application of the results and methods presented was demonstrated by computing the earthquake-induced pressures on a soil-retaining wall in a large power-generating plant. The structure was founded on rock and the soil body in contact with the wall was confined by rock boundaries. The structure was assumed to deform by rigid-body rotation on its rock foundation.

A number of topics related to this study that require further research are outlined in the following discussion.

The influence of nonlinear soil properties on the wall pressure distribution is an aspect of the problem that needs further study, especially for the case of large deformations. One approach would be to use a nonlinear finite element method to compute solutions to simplified problems using idealized stress-strain relations for the soil. The normal mode approach is unsuitable if nonlinear behavior is significant and dynamic solutions for this case would need to be evaluated using a direct numerical integration of the finite element equations of motion.

Further research of a number of possible refinements to the Mononobe-Okabe method is desirable. It appears that the Mononobe-Okabe method can be applied in a more rational manner by computing

the permanent wall displacement resulting from a prescribed ground acceleration rather than basing the analysis on an arbitrary selection of a static earthquake coefficient. An analysis to determine the wall pressure distribution for static horizontal body force with the soil in a fully plastic stress state would be informative. Analyses for these conditions can be undertaken by numerical solution of the plastic equilibrium equations.

Investigation is required to determine more exactly the physical nature of the dissipation in wall-soil systems subjected to strong earthquake ground motions. The testing of large-scale wall-soil models on large shaking tables may provide further insight to this aspect of the problem.

The dynamic behavior of embedded wall structures on soft deformable foundations (Fig. 1.1, Type VII) needs further investigation. A finite element study of a number of idealized embedded problems would be informative. The influence of three-dimensional effects in this and other types of wall problems also needs to be investigated. To study these effects it is probably necessary to resort to a finite element approach.

10.2 CONCLUSIONS

(1) It is important to establish the most appropriate method of analysis for each particular wall problem. For relatively rigid structures on firm foundations the behavior during earthquakes may be essentially elastic and the analysis should be based on an elastic theory. If large relative displacements of the wall structure are induced by the earthquake loads a fully plastic state may develop in the soil and maximum pressures should be computed by plastic

theory. For cases intermediate between these two limiting conditions significant nonlinear behavior of the soil will probably occur. In such cases it is often satisfactory to determine pressure bounds by using both the elastic and plastic theories. It is commonly assumed that if the relative displacement of the top of the wall is greater than 0.5% of the wall height a fully plastic stress condition develops. If the soil properties have been established by suitable testing it is desirable to make a more precise estimate of the soil behavior. (In many cases the results given in this study can be used to check whether an analysis based on elastic theory is valid).

For a perfectly rigid wall (that is a rigid structure on a rigid foundation) supporting a relatively long layer of soil it was found that the earthquake force component computed by elastic theory was likely to be greater than twice the force computed by the Mononobe-Okabe method. This result is based on the static solution for the elastic case and the assumption of identical horizontal earthquake coefficients for each case.

(2) Throughout this study solutions have been normalized with respect to a one-g acceleration. This was for convenience and is not intended to imply that an acceleration of this level would be suitable for design of wall structures. In general, the earthquake coefficient, response spectrum or design accelerograms used for wall design should be selected by consideration of a number of factors and in view of the large number of circumstances that can arise in practice it is not possible to make specific recommendations. The factors that need to be considered include the seismicity of the locality, the consequences of damage or failure, the economies of seismic resistance versus the cost of damage repair, and the magnitude of the resistance provided for other infrequent

loads such as water pressures. For walls of minor importance, the factors of safety commonly used in gravity load design may provide satisfactory resistance against small or moderate earthquakes and the possibility of damage or failure in strong earthquakes might well be an acceptable risk.

In most cases the arbitrary reductions to the elastic design coefficients, the elastic response spectra or the design accelerograms that are normally made because of ductility considerations should not be made for wall structures. Wherever possible it is desirable to estimate the maximum wall displacements and pressures occurring in the unfactored design earthquake and base the design on tolerance levels for structural damage and permanent wall displacements. That is, an approach analogous to the ultimate-load design method should be used. Frequently only approximate estimates can be made of the inelastic behavior during an earthquake. However, even very approximate solutions give insight into the actual behavior that might be overlooked if arbitrary reductions are used as a general design procedure.

(3) The Mononobe-Okabe method can be applied in a more rational manner by computing the magnitude of the outward sliding displacement of the soil wedge. The method proposed by Newmark[39] for the study of earthquake-induced sliding in dams and embankments is applicable to most wall structures that satisfy the Mononobe-Okabe assumptions. If this approach is used it is unnecessary to make an arbitrary reduction to the earthquake coefficient and the acceptable limit of outward displacement of the wall becomes the basic design criterion. It may often be desirable to insure that outward movement

occurs as a result of sliding of the structure on soil failure surfaces rather than as a result of a structural yielding in the wall. If this is the case, then it is important to design the structural elements of the wall for at least the force required to produce outward sliding of the wall as a result of soil failure.

(4) Dynamic tests performed on models have assisted the understanding of wall behavior during earthquakes. However, it is very difficult to adequately satisfy all the similarity conditions involved and care is required in applying model results to prototype walls. Experimental errors from the influence of the soil-supporting side and far-end walls of the test equipment can result in an underestimation of the wall force.

(5) In the analysis of earthquake behavior of wall structures imprecision is introduced by the uncertainties in the dynamic soil properties and the nature of the earthquake motions. Consequently the simplification of complex wall problems to readily solvable idealized systems may often be an acceptable approach. In this study idealized problems have been solved using the theory of elasticity. The solutions given are suitable for application in the design of wall structures that approximately satisfy the assumptions made. The solutions may also be informative for other cases that satisfy the basic assumption of linear elastic behavior.

(6) Results evaluated from the analytical normal mode solution of the idealized rigid-wall problem showed that satisfactory dynamic solutions for this type of problem can be computed by the conventional modal superposition methods. It was found that a good

dynamic representation of the rigid-wall problem can be achieved with five or less modes. By deriving the appropriate static solution it is possible to approximately include the influence of the higher modes by using an equivalent "rigid" mode. The Response Spectrum method employing an rms summation of the modal responses appears suitable for most rigid-wall problems.

The normal modes of deformable wall structures were not computed in this study; however, normal mode solutions can be computed for particular problems of this type by the finite element method. Although further study is required it appears reasonable to expect that modal superposition methods would also be satisfactory for computing earthquake pressures on elastic deformable wall problems.

(7) The natural frequencies of the idealized rigid-wall problem for wall heights less than about 15 ft and for moderately firm soils tend to be higher than the predominant frequencies in typical strong-motion accelerograms. Thus, for many relatively rigid low walls a static solution may be a satisfactory approximation. If a damping ratio of 10% can be justified for the wall-soil system the dynamic amplification resulting from earthquake loading is not very pronounced over the entire frequency range of interest and static solutions employing the peak acceleration tend to give conservative approximations for rigid-walls of any height.

(8) Good agreement was found between the analytical and finite element solutions for the smooth rigid-wall problem. This agreement justifies confidence in using the finite element method

for more complex wall problems. Since at present there is no method of determining bounds for the accuracy of finite element solutions, the analytical results obtained in this investigation give useful information regarding the most economical mesh sizes for the study of related problems. It was concluded that the finite element method gives reasonable accuracy for the modal properties of modes that have at least four elements within the modal wave lengths (in both the vertical and horizontal direction).

(9) Good agreement was found between the solutions of the idealized rigid-wall problem using the exact equations of elasticity and solutions based on the assumption of no vertical displacement in the elastic soil ($v = 0$ assumption). However, this agreement was only investigated for a Poisson's ratio of 0.3 and because the $v = 0$ solutions are singular for Poisson's ratio equal to 0.5 the agreement is expected to deteriorate as the ratio is increased above 0.3. The $v = 0$ approximation may be useful for the analytical investigation of more complex problems.

(10) Analytical solutions for wall problems can only be readily derived for the case of a smooth contact on the wall-soil interface (that is a mixed boundary condition). For the horizontally loaded problems considered in this study relatively good agreement was found between the pressure distributions computed for both smooth and bonded contact assumptions. In theory a stress singularity develops near the top of the wall for the bonded case, but in practice because of the variation in soil properties with depth and

the nonlinear behavior of soils at moderate stress levels the stress singularity is unlikely to develop to a significant degree. It is concluded that the analytical smooth wall results presented in this study are satisfactory for practical applications in which a more complex interface condition exists.

(11) It is concluded that even for the case where the relative displacements of the wall structure are sufficiently small to ensure essentially elastic response of the soil it is important to check the influence of the wall deformation on the pressure distribution. If the wall structure has significant mass it is important to include the dynamic properties of the structure in the analysis. In cases where the wall structure has a fundamental frequency higher than the lowest natural frequencies of the retained soil body, significant dynamic amplification of the pressure component due to the structural deformation may occur.

(12) A satisfactory estimate of the maximum earthquake-induced pressures and forces on relatively rigid structures with significant mass can often be made by taking an rms sum of the values computed for the rigid-wall solution and the values from the forced-wall solution evaluated for the response of the first mode of vibration of the structure. This approach is probably unsuitable for the case where the fundamental frequency of the wall structure is close to the lowest natural frequencies of the soil layer.

REFERENCES

1. Archer, J. S., "Consistent Mass Matrix for Distributed Systems," Journal of the Structural Division, ASCE, Vol. 89, No. ST4, August, 1963.

2. Askilsrud, Odd G., Los Angeles County Flood Control District, Personal Communication, 1971.

3. Baligh, Moshen M., "Applications of Plasticity Theory to Selected Problems in Soil Mechanics," Soil Mechanics Laboratory, California Institute of Technology, Pasadena, California, 1972.

4. Bielak, J., "Base Moment for a Class of Linear Systems," Journal of the Engineering Mechanics Division, ASCE, Vol. 95, No. EM5, Oct. 1969.

5. Bycroft, G. N., "Forced Vibrations of a Rigid Circular Plate on a Semi-Infinite Elastic Space and on an Elastic Stratum," Phil. Trans. Roy. Soc. London, Series A, Vol. 248, 1956.

6. Chopra, Anil K., "Earthquake Response of Concrete Gravity Dams," Journal of the Engineering Mechanics Division, ASCE, Vol. 96, No. EM4, August, 1970.

7. Clough, G. Wayne, and Duncan, James M., "Finite Element Analyses of Retaining Wall Behavior," Journal of the Soil Mechanics and Foundations Division, ASCE, Vol. 97, No. SM12, December, 1971.

8. Doherty, W. P., Wilson, E. L. and Taylor, R. L., "Stress Analysis of Axisymmetric Solids Utilizing Higher-Order Quadrilateral Finite Elements," Report No. SESM 69-3 Structural Engineering Laboratory, University of California, Berkeley, California, January 1969.

9. Duncan, James M. and Clough, G. Wayne, "Finite Element Analyses of Port Allen Lock," Journal of the Soil Mechanics and Foundations Division, ASCE, Vol. 97, No. SM8, August, 1971.

10. Frazier, G. A. and Roberts, J. E., "A Mathematical Approach to the Influence of Geological Formations on Seismic Motions," Lawrence Radiation Laboratory, University of California, Livermore, California, June 1970.

11. Hardin, Bobby O. and Drnevich, Vincent P., "Shear Modulus and Damping in Soils: Measurement and Parameter Effects," Journal of the Soil Mechanics and Foundations Division, ASCE, Vol. 98, No. SM6, June 1972.

12. Hardin, Bobby O. and Drnevich, Vincent P., "Shear Modulus and Damping in Soils: Design Equations and Curves," Journal of the Soil Mechanics and Foundations Division, ASCE, Vol. 98, No. SM7, July 1972.

13. Hayashi, Satoshi and Katayama, Takeo, "Damage to Harbor Structures by the Tokachioki Earthquake," Soils and Foundations, Vol. X, No. 2, June 1970.

14. Housner, G. W., "Behavior of Structures During Earthquakes," Journal of the Engineering Mechanics Division, ASCE, Vol. 85, No. EM4, October, 1957.

15. Housner, G. W., Response spectra prepared for, "Nuclear Reactors and Earthquakes," Report No. TID 7024, U.S. Atomic Energy Commission, August, 1963.

16. Housner, G. W., "Dynamic Pressures on Accelerated Fluid Containers," Bulletin Seismological Society of America, Vol. 47, No. 1, January, 1967.

17. Housner, G. W. and Jennings, P. C., "Generation of Artificial Earthquakes," Journal of the Engineering Mechanics Division, ASCE, Vol. 90, No. EM1, January, 1964.

18. Hradilek, P. J., "Behavior of Underground Box Conduits in the San Fernando Earthquake," U.S. Army Engineer District, Los Angeles Corps of Engineers, January, 1972.

19. Ishii, Y., Arai, M. and Tsuchida, H., "Lateral Earth Pressure in an Earthquake," Proceedings, Second World Conference on Earthquake Engineering, Tokyo, 1960.

20. International Association for Earthquake Engineering, "Earthquake Resistant Regulations: A World List," November 1970.

21. Jennings, Paul C., Editor, "Engineering Features of the San Fernando Earthquake," Report No. EERL 71-02, Earthquake Engineering Research Laboratory, California Institute of Technology, Pasadena, California, June 1971.

22. Jennings, P. C., Housner, G. W. and Tsai, N. C., "Simulated Earthquake Motions," Earthquake Engineering Research Laboratory, California Institute of Technology, Pasadena, California, April, 1968.

23. Karasudhi, P., Keer, L. M. and Lee, S. L., "Vibratory Motion of a Body on an Elastic Half Plane," Journal of Applied Mechanics, Vol. 35, Transactions of the ASME, Series E, December 1968.

24. Ko, Hon-Yim and Scott, Ronald F., "Bearing Capacities by Plasticity Theory," Journal of the Soil Mechanics and Foundations Division, ASCE, Vol. 99, No. SM1, January, 1973.

25. Kobori, T., Minai, R., Suzuki, T. and Kusakabe, K., "Dynamical Ground Compliance of Rectangular Foundation," Proceedings of the Sixteenth Japan National Congress for Applied Mechanics, 1966.

26. Kovacs, William D., Seed, H. Bolton and Chan, Clarence K., "Dynamic Moduli and Damping Ratios for a Soft Clay," Journal of the Soil Mechanics and Foundations Division, ASCE, Vol. 97, No. SM1, January 1971.

27. Lemcoe, M. M., "Stresses in Layered Elastic Solids," Transactions, ASCE, Vol. 126, Pt. 1, 1961.

28. Lew, H. S., Leyendecker, E. V. and Dikkers, R. D., "Engineering Aspects of the 1971 San Fernando Earthquake," Building Research Division, Institute for Applied Technology, National Bureau of Standards, Washington D.C., Building Science Series 40, December, 1971.

29. Liu, Shih-Chi and Fagel, Lawrence, "Earthquake Interaction by Fast Fourier Transform," Journal of the Engineering Mechanics Division, ASCE, Vol. 97, No. EM4, August, 1972.

30. Lysmer, John and Kuhlemeyer, Rober L., "Finite Dynamic Model for Infinite Media," Journal of the Engineering Mechanics Division, ASCE, Vol. 95, No. EM4, August, 1969.

31. Marguerre, K., "Druckverteilung durch eine elastische Schict auf starrer rauher Unterlage," Ingenieur-Archiv, 1931.

32. Matuo, M. and Ohara, S., "Lateral Earth Pressures and Stability of Quay Walls During Earthquakes," Proceedings, Second World Conference on Earthquake Engineering, Tokyo, 1960.

33. Matuo, H. and Ohara, S., "Dynamic Pore Water Pressure Acting on Quay Walls During Earthquakes," Proceedings, Third World Conference on Earthquake Engineering, New Zealand, 1965.

34. McCormick, C. W., "Plane Stress Analysis," Journal of the Structural Division, ASCE, Vol. 89, No. ST4, August, 1963.

35. Merchant, H. C. and Hudson, D. E., "Mode Superposition in Multi-Degree of Freedom Systems Using Earthquake Response Spectrum Data," Bulletin of the Seismological Society of America, Vol. 52, No. 2, April 1962.

36. Miklowitz, Julius, "Analysis of Elastic Waveguides Involving an Edge," in "Wave Propagation in Solids," ASME Publications, New York, 1969.

37. Mononobe, N. and Matsuo, M., "On the Determination of Earth Pressures During Earthquakes," Proceedings, World Engineering Congress, Vol. 9, 1929.

38. Murphy, V. A., "The Effect of Ground Characteristics on the Aseismic Design of Structures," Proceedings, Second World Conference on Earthquake Engineering, Tokyo, 1960.

39. Newmark, N. M., "Effects of Earthquakes on Dams and Embankments," Geotechnique, Vol. XV, No. 2, June, 1965.

40. Ohara, S., "Experimental Studies of Seismic Active and Seismic Passive Earth Pressure," Proceedings of the Third Japan Earthquake Engineering Symposium, Tokyo, November, 1960.

41. Oien, M. A., "Steady Motion of a Rigid Strip Bonded to an Elastic Half-Space," Journal of Applied Mechanics, Vol. 38, Trans. ASME, Vol. 93, Series E, June, 1971.

42. Okabe, S., "General Theory of Earth Pressure," Journal, Japan Society of Civil Engineers, Vol. 12, No. 1, 1926.

43. Pickett, Gerald, "Stress Distribution in a Loaded Soil with Some Rigid Boundaries," Proceedings, 18th Annual Meeting Highway Research Board, Vol. 18, Part II, November, 1938.

44. Prakash, Shamsher and Basavanna, B. M., "Earth Pressure Distribution Behind Retaining Wall During Earthquake," Proceedings, Fourth World Conference on Earthquake Engineering, Santiago, Chile, 1969.

45. Przemieniecki, J. S. Theory of Matrix Structural Analysis, McGraw-Hill, 1968.

46. Scott, Ronald F., Principles of Soil Mechanics, Addison-Wesley Publishing Co., 1963.

47. Scott, Ronald F., California Institute of Technology, Personal Communication, 1972.

48. Scott, R. F., "Earthquake-Induced Pressures on Retaining Walls," to be presented at the Fifth World Conference on Earthquake Engineering, Rome, 1973.

49. Seed, H. Bolton and Idriss, I. M., "Soil Moduli and Damping Factors for Dynamic Response Analyses," Report No. EERC, 70-10, Earthquake Engineering Center, University of California, Berkeley, California, December 1970.

50. Seed, H. B. and Whitman, R. V., "Design of Earth Retaining Structures for Dynamic Loads," ASCE, Specialty Conference, Lateral Stresses in the Ground and the Design of Earth-Retaining Structures, Cornell University, 1970.

51. Skinner, R. I., "Earthquake-generated Forces and Movements in Tall Buildings," Bulletin 166, New Zealand Department of Scientific and Industrial Research, 1964.

52. Sokolovski, V. V., Statics of Soil Media, Butterworths, London, 1960.

53. Tajimi, H., "Dynamic Earth Pressure on Basement Walls in the Elastic Ground," Proceedings of the Third Japan Earthquake Engineering Symposium, Tokyo, November, 1970.

54. Tajimi, Hiroshi, "A Statistical Method of Determining the Maximum Response of a Building Structure During an Earthquake," Proceedings, Second World Conference on Earthquake Engineering, Tokyo, 1960.

55. Tajimi, H., "Dynamic Analysis of a Structure Embedded in an Elastic Stratum," Proceedings, Fourth World Conference on Earthquake Engineering, Chile, 1969.

56. Tajimi, Hiroshi, "Dynamic Earth Pressures on Basement Wall," to be presented at the Fifth World Conference on Earthquake Engineering, Rome, 1973.

57. Tennessee Valley Authority, U.S.A., "The Kentucky Project," Technical Report No. 13, 1951. Experimental work by L. S. Jacobsen (1939) reported in Appendix D of this reference.

58. White, R. L., Los Angeles City, Department of Water and Power, Personal Communication, 1972.

59. Whitman, R. V. and Richart, F. E. Jr., "Design Procedures for Dynamically Loaded Foundations," Journal of the Soil Mechanics and Foundations Division, ASCE, Vol. 93, No. SM6, November, 1967.

60. Zienkiewicz, O. C.. The Finite Element Method in Engineering Science, (2nd Edition), McGraw-Hill, 1971.

61. Zienkiewicz, O. C. and Holister, G. S. (Editors), Stress Analysis, John Wiley and Sons, 1965. Chapter 7. Ray W. Clough, "The Finite Element Method in Structural Mechanics."

APPENDIX I

NOTATION

Symbols are defined where they first appear in the text. A summary of the symbols employed is given in this appendix.

Dots above a symbol denote differentiation with respect to time. A bar beneath a symbol denotes a vector quantity. In general a bar above a symbol denotes a transformed parameter. A unit length of structure is implied in the force and moment definitions.

Lower Case Symbols

a_n	Fourier series coefficient for nth term
$a_{0,1,2,...}$	Element displacement function coefficient
b_n	Fourier series coefficient for nth term
$b_{0,1,2,...}$	Element displacement function coefficient
c	Damping coefficient
c_b	Rotational damping coefficient for basement structure
$c_{n,m}$	Analogous damping coefficient for mode n,m
c_w	Damping coefficient for wall structure
d_n	$\frac{p^2}{r^2}\left[(k^2-2) - \frac{np}{r}(k^2-1)\right] + 1$
e	Exponential constant
f'_c	Compressive strength of concrete
f_m, f_p	Frequency of vibration in model and prototype respectively

f_n	$\frac{p^2}{r^2}(k^2-2)(1-\frac{np}{r})$
f_y	Yield strength of reinforcement
$f^o(y)$	Displacement function for forced wall
f_1, f_2	Real and Imaginary parts of $\frac{\overline{M}_f'(\omega)}{M_{sf}}$ respectively
$\underline{f}$	Nodal load vector
$\underline{f}(t)$	Nodal forcing vector
g	Acceleration due to gravity
$g^o(t)$	Time function for forced wall
h	One-half of plate thickness
h_b	Height of basement structure
h_c	Height of center of gravity of wall or basement structure
h_j	Height of story mass j above base of superstructure
$h_{n,m}$	Height of center of pressure for mode n,m
h_r	Height of center of pressure for "rigid" mode
h_s	Height of center of pressure on statically-forced wall
$\underline{h}$	Vector of floor heights h_j
i	Angle of soil slope
i	$\sqrt{-1}$
k	$\frac{V_d}{V_s}$, wave speed ratio
k'	$3 - 4\nu$
k_b	Rotational spring constant for basement structure
k_h	Horizontal earthquake coefficient
$k_{n,m}$	Analogous spring constant for mode n,m

k_s	Analogous spring constant for statically forced wall
k_v	Vertical earthquake coefficient
k_w	Spring constant for wall structure
m	Integer
m	Mode order
m	Mass per unit length
m_b	Mass of basement structure
m_j	Story mass at floor j
$m_{n,m}$	Analogous mass for node n,m
m_r	Analogous mass for rigid mode
m_w	Mass of wall structure
n	Integer
n	mode type
p	$\frac{\pi}{2L}$
$p_{n,m}$	Static-one-g modal wall pressure distribution for mode n,m
q	Nonuniform soil parameter
r	$\frac{n\pi}{L}$
r_1, r_2	Real and imaginary parts of $\frac{\overline{M}'_r(\omega)}{M_{sr}}$ respectively
s_F^2	Variance of wall force
s_M^2	Variance of wall moment
t	Time
u	Displacement in coordinate x-direction
u_b	Displacement in x-direction of rigid boundary
$\overline{u}_n(y)$	Displacement function in x-direction for nth term

u_w	Wall displacement in x-direction
$u_{n,m}$	Displacement in x-direction of mode n,m
u^o	Displacement in x-direction at top of wall
$\underline{u}$	Displacement vector
$\underline{u}_b$	Vector of displacements on rigid boundary
$\underline{u}^e$	Vector of element nodal displacements
$\underline{u}_f$	Vector displacement solution for dynamic wall-forcing
$\underline{u}^i$	Vector of displacements within element
$\underline{u}_r$	Vector displacement solution for dynamic horizontal acceleration of rigid-wall problem
$\underline{u}_{sf}$	Vector displacement solution for static wall-forcing of unit rotational amplitude or unit displacement at wall top
$\underline{u}_{sr}$	Vector displacement solution for one-g static horizontal load on rigid-wall problem
$\underline{u}_1$	Partial vector-displacement solution
v	Displacement in coordinate y-direction
$\overline{v}_n(y)$	Displacement function in y-direction for nth term
$v_{n,m}$	Displacement in y-direction of mode n,m
x	Coordinate direction
y	Coordinate direction
$\overline{y}$	$(1 - \frac{qy}{H})$

Upper Case Symbols

A	Constant
A_n	Displacement function constant for nth term

$A_{n,m}$	Constant for mode n,m
B	Constant
B	Matrix relating strains within element to nodal displacements
B_n	Displacement function constant for nth term
$B_{n,m}$	Constant for mode n,m
C	Assemblage damping matrix
C_n	Displacement function constant for nth term
$C_{n,m}$	Constant for mode n,m
D_n	Displacement function constant for nth term
$D_{n,m}$	Constant for mode n,m
$D_{n,m}(t)$	Relative displacement response of single-degree-of-freedom oscillator with parameters $\omega_{n,m}$ and $\zeta_{n,m}$
E	Young's modulus
$E[y^2]$	Mean-square-response
E_s	Young's modulus for soil
E_w	Young's modulus for wall
F_h	Horizontal force
$\overline{F}'_f(\omega)$	Complex-amplitude of steady-state force for harmonic wall-forcing of unit amplitude
$F_{n,m}$	Static-one-g modal force on rigid wall from mode n,m
$\overline{F}'_r(\omega)$	Complex-amplitude of steady-state force on rigid wall for one-g amplitude harmonic base forcing
F_{sf}	Force on statically forced wall for unit rotation or unit displacement at wall top

F_{sr}	Force on rigid wall from one-g static horizontal loading
F_x, F_y	Body force per unit volume in x- and y-direction respectively
$\underline{F}$	Vector of body forces
G	Shear modulus
$G(\omega)$	Power spectral density of earthquake
G_a	Average shear modulus of soil
G_b	Shear modulus of soil at bottom of stratum
G_m, G_p	Shear moduli of soil in model and prototype respectively
$G_x(\omega)$	Power spectral density of input
H	Height of wall
H	Height of soil stratum
$H(\omega)$	System transfer function
H_{ij}	Building transfer matrix
H_m, H_p	Height of model and prototype walls respectively
I	Unity matrix
I_b	Moment of inertia of basement structure
I_D	$\int_v \underline{\phi}_{n,m} \cdot \underline{\phi}_{n,m} \, dV$
Im	Imaginary part
I_N	$\int_v u_{n,m} \, dV$
I_w	Moment of inertia of wall structure
J_0	Zero-order Bessel function of the first kind
J_1	First-order Bessel function of the first kind

K	Assemblage stiffness matrix
$\overline{K}$	$L^{-1}K(L^T)^{-1}$
$\tilde{K}$	$K + i\omega C - \omega^2 M$
K_{AE}	Active earth-pressure coefficient for combined gravity and earthquake loads
K_e	Element stiffness matrix
K_p	Passive earth-pressure coefficient
K_2	Soil modulus parameter
L	Length of soil layer
L	lower triangular matrix
L	Linear operator
L_p	Linear operator
M	Assemblage mass matrix
M	Diagonal matrix of story masses
$M_b(t)$	Superstructure base moment
M^e	Element mass matrix
M_E	Earthquake moment on wall
$M_f(t)$	Moment on dynamically forced wall
$\overline{M}_f(\omega)$	Complex-amplitude of steady-state moment for harmonic wall forcing
$\overline{M}'_f(\omega)$	Complex-amplitude of steady-state moment for harmonic wall forcing of unit amplitude
M_g	Gravity moment on wall
$M_{n,m}$	Static one-g modal moment on rigid-wall from mode n,m
$M_r(t)$	Dynamic moment on rigid wall

$\overline{M}_r(\omega)$	Complex-amplitude of steady-state moment on rigid wall for harmonic base forcing
$\overline{M}'_r(\omega)$	Complex-amplitude of steady-state moment on rigid wall for one-g amplitude harmonic base forcing
M_{sf}	Moment on statically forced wall for unit rotation or unit displacement at top of wall
M^d_{sf}	$\frac{M_{sf}}{\omega_w^2 I_w}$, dimensionless moment
M_{sr}	Moment on rigid wall from one-g static horizontal loading
M^d_{sr}	$\frac{M_{sr}}{m_w g h_c}$, dimensionless moment
M_T	Total wall moment
$\overline{M}_T(\omega)$	Complex-amplitude of total steady-state wall moment for harmonic base forcing
$\overline{M}'_T(\omega)$	Complex-amplitude of total steady-state wall moment for one-g amplitude harmonic base forcing
M_u	Ultimate resisting moment of wall
M_I	Maximum wall moment for problem I
M_{II}	Maximum wall moment for problem II
$\underline{M}$	Vector of story masses
N	Number of significant modes
N	Number of lumped story masses
N	Matrix relating displacements within element to nodal displacements
P_{AE}	Active wall force for combined gravity and earthquake loads
$P_{n,m}$	Static-one-g modal participation factor for mode n,m

$P^s_{n,m}$ $\quad -\dfrac{\int_V \underline{u}_{sf} \cdot \underline{\phi}_{n,m}\, dV}{\int_V \underline{\phi}_{n,m} \cdot \underline{\phi}_{n,m}\, dV}$

$PA_{n,m}$ Pseudo-acceleration response for single-degree-of-freedom oscillator with parameters $\omega_{n,m}$ and $\zeta_{n,m}$

$Q_{n,m}(t)$ Participation coefficient for mode n,m

$Q'_{n,m}$ Static participation coefficient for mode n,m

R rH

Re Real part

$R_n(\omega)$ $\quad \dfrac{\omega^2/\omega_n^2}{1 - \dfrac{\omega^2}{\omega_n^2} + 2i\zeta_n \dfrac{\omega}{\omega_n}}$

S $\quad \dfrac{E_s H^3}{E_w I_w}$, soil-wall stiffness ratio

$S_b(t)$ Superstructure base shear

S_v Relative velocity spectrum

T Accelerogram duration

T_w Period of vibration of wall structure

V Volume

V_d Dilitational wave speed

V_s Shear wave speed

W Weight of soil wedge

Y_0 Zero-order Bessel function of the second kind

Y_1 First order Bessel function of the second kind

Greek Symbols

α $\sqrt{r^2 - \frac{\omega_{n,m}^2}{V_d^2}}$ or $\sqrt{r^2 - \frac{\omega^2}{V_d^2}}$

α' $\pi\sqrt{\left(\frac{nH}{L}\right)^2 - \frac{\Omega_{n,m}^2}{4K^2}}$

β Angle of wall slope

β $\sqrt{r^2 - \frac{\omega_{n,m}^2}{V_s^2}}$ or $\sqrt{r^2 - \frac{\omega^2}{V_s^2}}$

β' $\pi\sqrt{\left(\frac{nH}{L}\right)^2 - \frac{\Omega_{n,m}^2}{4}}$

$\tilde{\beta}$ $\frac{2H\omega_m}{q}\sqrt{\frac{\rho}{G_b}}$

γ Unit weight of soil

γ_m, γ_p Unit weight of soil in model and prototype respectively

γ_s Unit weight of soil

$\gamma_{x,y}$ Shear strain for the x- and y-direction

δ Angle of wall friction

$\underline{\epsilon}$ Vector of strains within element

ϵ_x, ϵ_y Normal strains in x- and y-direction respectively

ζ Damping ratio, fraction of critical

ζ_b Equivalent damping ratio for rotation of basement structure

ζ_n Damping ratio for mode n

$\zeta_{n,m}$ Damping ratio for mode n,m

ζ_w	Equivalent damping ratio for rotation of wall structure
η	Coordinate direction for element
θ	Angle of rotation
θ	$\tan^{-1}\left(\frac{k_h}{1-k_v}\right)$, direction of total earthquake force
ν	Poisson's ratio
ξ	Coordinate direction for element
π	Numerical constant
ρ	Mass density
ρ_m, ρ_p	Mass density in model and prototype respectively
σ_m, σ_p	Stresses in model and prototype respectively
σ'_m	Mean principal effective-stress
σ_x, σ_y	Normal stresses in x- and y-directions respectively
σ^o_x	Normal stress on wall
σ_1, σ_2	Principal stresses in x-y plane
$\underline{\sigma}$	Vector of stresses within element
τ	Time parameter in integration
τ_d	Deviatoric stress
τ_{xy}	Shear stress in x- and y-directions
τ^o_{xy}	Shear stress on wall
ϕ	Angle of internal friction of soil
$\underline{\phi}$	Mode shape
$\underline{\phi}_n$	Mode shape for mode n
$\underline{\phi}_{n,m}$	Mode shape for mode n,m
$\underline{\psi}$	$L^T\underline{\phi}$, transformed mode shape

ω	Angular frequency
ω_b	Natural angular frequency for rotation of basement structure
ω_n	Natural angular frequency of mode n
ω_m	Natural angular frequency of mode m
$\omega_{n,m}$	Natural angular frequency of mode n,m
ω_s	$\pi V_s/2H$, natural angular frequency of lowest pure shear mode of an infinite elastic stratum
$\omega_{s,m}$	$\frac{(2m-1)\pi}{2H}\sqrt{\frac{G_a}{\rho}}$, natural angular frequency of mode m of a uniform infinite elastic stratum with shear modulus equal to the average of the nonuniform stratum
ω_w	Natural angular frequency for rotation of wall structure
Ω	ω/ω_s, dimensionless frequency
Ω_m	$\omega_m/\omega_{s,m}$, dimensionless natural frequency for mode m
$\Omega_{n,m}$	$\omega_{n,m}/\omega_s$, dimensionless natural frequency for mode n,m
Δ	Value of determinant
ΔP_{AE}	Active wall force increment due to earthquake load

APPENDIX II

FINITE ELEMENT METHOD

(1) STATIC SOLUTIONS

The static finite element solutions were computed using a conventional direct stiffness method. In this approach an assumed element displacement field is chosen and the principle of virtual displacements and internal virtual work is used to derive the element stiffness matrix. It can be readily shown that the element stiffness matrix K^e is given by

$$K^e = \int_V B^T D B \, dV \tag{A.1}$$

where the matrix B is defined by

$$\underline{\epsilon} = B\underline{u}^e \tag{A.2}$$

in which

$$\underline{\epsilon} = \begin{Bmatrix} \epsilon_x \\ \epsilon_y \\ \gamma_{xy} \end{Bmatrix}$$, a vector of the strains within the element

$\underline{u}^e$ = a vector of the element nodal displacements

and matrix D is defined by

$$\underline{\sigma} = D\underline{\epsilon} \tag{A.3}$$

in which

$$\underline{\sigma} = \begin{Bmatrix} \sigma_x \\ \sigma_y \\ \tau_{xy} \end{Bmatrix}$$, a vector of the stresses within the element

The forces and displacements at the nodes of the total assemblage of elements are related by a set of linear algebraic equations that can be expressed as

$$\underline{f} = K\underline{u} \tag{A.4}$$

in which

$\underline{f}$ = a vector of nodal forces

$\underline{u}$ = a vector of nodal displacements

K = the assemblage stiffness matrix

The assemblage stiffness matrix K is derived from the element stiffness matrices by satisfying the equilibrium equations at each of the nodal points.

In this study equations (A.4) were solved for the unknown displacement field $\underline{u}$ by employing a computational method developed by McCormick[34]. This method is efficient for large banded-matrices and utilizes an iterative improvement scheme which allows any desired degree of accuracy to be obtained in the solution. In most finite element programs the stresses at the centroid of each element are computed from the nodal displacements using expressions (A.2) and (A.3). In this study, because the evaluation of the boundary stress distributions was the primary objective, stresses were computed at the nodal points instead of the element centroids.

Two types of elements were used; a first-order rectangular element and a second-order quadrilateral element. These elements

are shown in Fig. A.1.

The rectangular element has an assumed displacement field defined by

$$u(\xi,\eta) = a_0 + a_1\xi + a_2\eta + a_3\xi\eta$$
$$v(\xi,\eta) = b_0 + b_1\xi + b_2\eta + b_3\xi\eta \qquad (A.5)$$

The element stiffness matrix is derived from these displacement functions by determining the constant coefficients a_i and b_i in terms of the nodal displacements and the nodal coordinates and then evaluating expression (A.1). The simple shape of this element allows the required integration to be readily undertaken to give a closed form expression for the element stiffness matrix. Details of this matrix are given by Przemieniecki[45].

The quadrilateral element used was developed by Doherty et al.[8] and was called by these investigators the QM5 element. It is a refined five-point element having a constant shear strain taken as the value of the shear strain at the central point. The assumed displacement field for this element is given by

$$u(\xi,\eta) = a_0+a_1\xi+a_2\eta+a_3\xi\eta+a_4(1-\xi^2)(1-\eta^2)$$
$$v(\xi,\eta) = b_0+b_1\xi+b_2\eta+b_3\xi\eta+b_4(1-\xi^2)(1-\eta^2) \qquad (A.6)$$

The integration required to evaluate the stiffness matrix was carried out numerically by employing a four-point Gaussian quadrature formula.

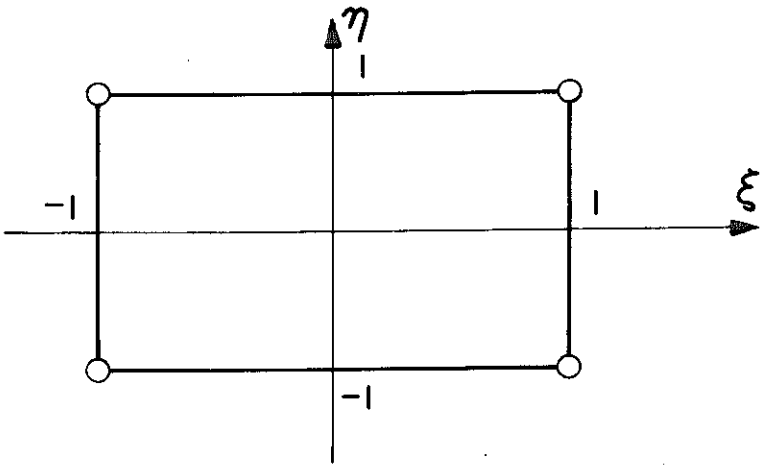

RECTANGULAR ELEMENT

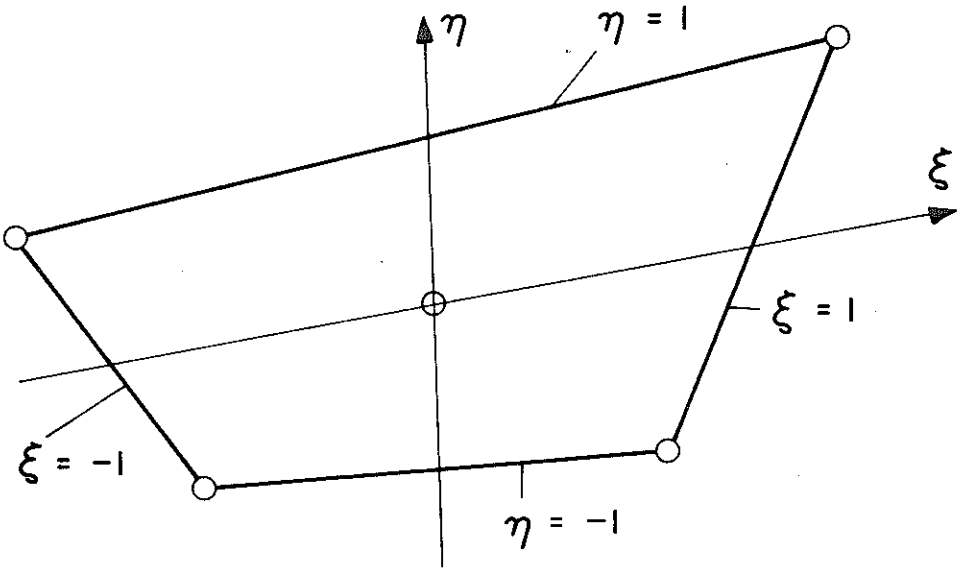

QUADRILATERAL ELEMENT

Figure A. 1

Both the elements used have displacement fields that vary in a linear manner along their sides, thus ensuring continuity of the displacement field between elements.

(2) NORMAL MODE SOLUTIONS

The equations of motion for free undamped vibration of the finite element system can be written as

$$M\ddot{\underline{u}} + K\underline{u} = 0 \qquad (A.7)$$

in which

M = the assemblage mass matrix

The assemblage mass matrix M is derived from the element mass matrices by a method analogous to that used to derive the assemblage stiffness matrix. The analogy between the mass and stiffness matrix derivation is easily demonstrated by using d'Alembert's principle to reduce the dynamic problem to an equivalent static problem.

The solutions of equations (A.7) can be written as

$$\underline{u} = \underline{\phi} e^{i\omega t} \qquad (A.8)$$

in which

$\underline{\phi}$ = mode shape associated with the natural frequency ω

Substitution of (A.8) into (A.7) gives

$$(K - \omega^2 M)\underline{\phi} = 0 \qquad (A.9)$$

In this study the standard eigenvalue problem represented by expression (A.9) was transformed to a more convenient form by using Cholesky's method to perform a triangular decomposition of the mass matrix. Defining the lower triangular matrix L such that $M = LL^T$, and letting

$$\underline{\psi} = L^T \underline{\phi}$$

enables equations (A.9) to be expressed as

$$(\overline{K} - \omega^2 I)\underline{\psi} = 0 \qquad (A.10)$$

in which

$\overline{K} = L^{-1}K(L^T)^{-1}$, a symmetric matrix

I = the unity matrix

Equations (A.10) can be solved by standard computational methods to give the mode shapes and natural frequencies. In this study a library program was used that employed Jacobi's method.

The normal mode solutions were evaluated using the two elements previously described for the static analyses. Element mass matrices were derived using the consistent mass approach of Archer[1]. The consistent element-mass matrix is defined by

$$M^e = \int_V N^T \rho N \, dV \qquad (A.11)$$

in which

M^e = element mass matrix

ρ = material mass density

The interpolation matrix N is defined by

$$\underline{u}^i = N\underline{u}^e \qquad (A.12)$$

in which

$\underline{u}^i$ = a vector of displacements within the element

APPENDIX III

RIGID WALL: DYNAMIC SOLUTION: TYPICAL MODE SHAPES AND FREQUENCIES

The analytical solution presented in Section 3.1 for the natural frequencies and mode shapes of the smooth rigid-wall problem was numerically evaluated for various values of the parameters $\frac{L}{H}$ and ν. The ratio $D_{n,m}/C_{n,m}$ and the dimensionless frequencies $\Omega_{n,m}$ of a number of the antisymmetric modes for $\nu = 0.3$ and $\frac{L}{H} = 2.0$, 5.0 and 10.0 are listed in Table A.1 below. The mode shapes can be readily computed by substituting the values of $D_{n,m}/C_{n,m}$ and $\Omega_{n,m}$ into expressions (3.11), (3.13) and (3.15) Typical mode shapes are plotted for $\frac{L}{H} = 5.0$ and $\nu = 0.3$ in Figs. A.2, A.3 and A.4.

TABLE A.1

Mode Shape Ratio and Natural Frequencies

L/H = 2.0, 5.0 and 10.0; $\nu = 0.3$

Mode Type, Order	L/H = 2.0		L/H = 5.0		L/H = 10.0	
	$\Omega_{n,m}$	$\frac{D_{n,m}}{C_{n,m}}$	$\Omega_{n,m}$	$\frac{D_{n,m}}{C_{n,m}}$	$\Omega_{n,m}$	$\frac{D_{n,m}}{C_{n,m}}$
1,1	1.805	1.574	1.211	-0.337	1.057	-0.179
1,2	2.01	-9.268	1.849	5.721	1.864	10.770
1,3	3.57	-1.176	3.11	-0.494	3.03	-0.252
1,4	4.87	0.853	4.96	0.517	4.99	0.284
1,5	6.05	-5.382	5.70	-8.145	5.64	-14.618
3,1	2.90	1.299	1.849	1.770	1.429	-0.393
3,2	4.49	1.724	2.29	-5.786	1.837	4.310
3,3	5.71	2.382	3.77	-1.422	3.23	-0.724
3,4	5.98	-2.285	4.86	0.885	4.93	0.681
3,5	7.69	-0.0144	6.20	-5.435	5.80	-6.302
5,1	4.65	1.181	2.18	1.492	1.805	1.574
5,2	5.93	1.288	3.44	5.624	2.01	-9.268
5,3	7.34	1.609	4.67	-3.579	3.57	-1.176
5,4	8.61	2.812	5.01	0.733	4.87	0.853
7,1	6.49	1.158	2.74	1.325	1.905	1.713
7,2	7.58	1.226	4.33	1.910	2.58	-9.002
7,3	8.76	1.346	5.52	2.566	3.98	-1.707
7,4	10.16	1.586	5.72	-1.590	4.87	0.892
9,1	8.35	1.153	3.40	1.242	2.07	1.556
9,2	9.40	1.205	4.92	1.460	3.16	12.896
9,3	10.35	1.268	6.27	2.202	4.43	-2.597
9,4	11.59	1.379	6.83	-7.154	4.94	0.829

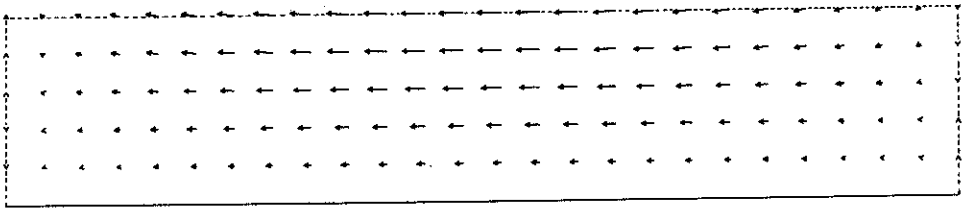

MODE 1,1

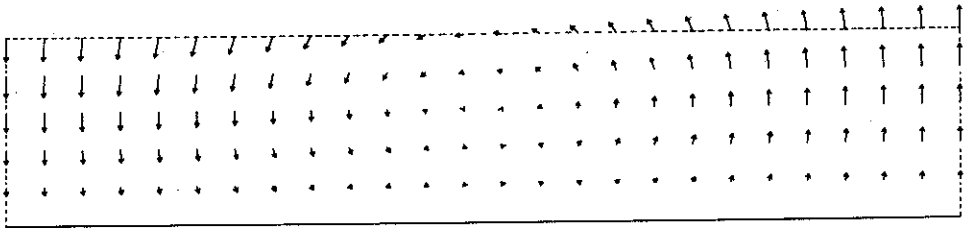

MODE 1,2

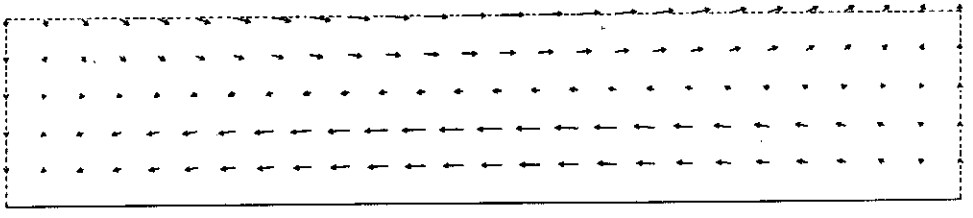

MODE 1,3

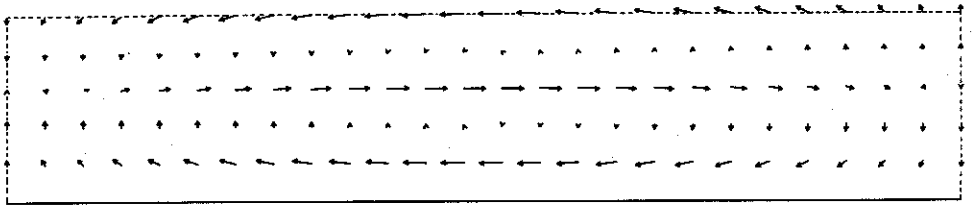

MODE 1,4

Figure A.2 Typical mode shapes. L/H = 5.0. Poisson's ratio = 0.3.

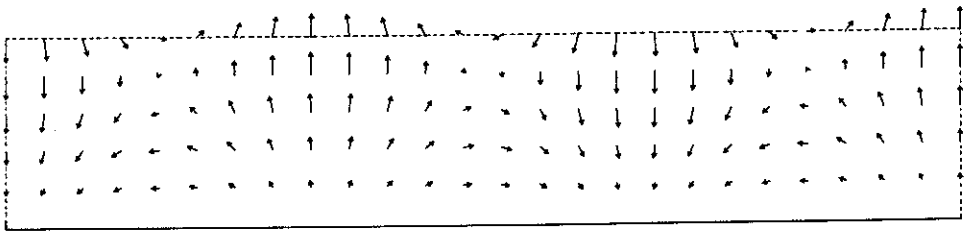

MODE 3,1

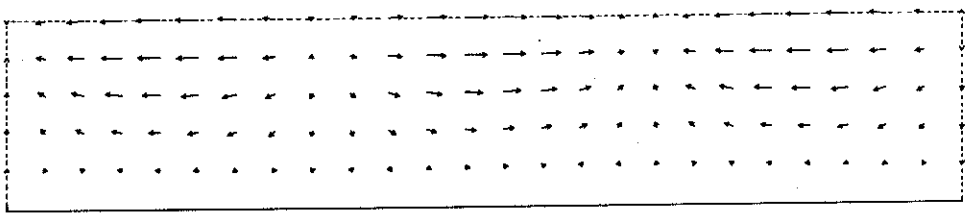

MODE 3,2

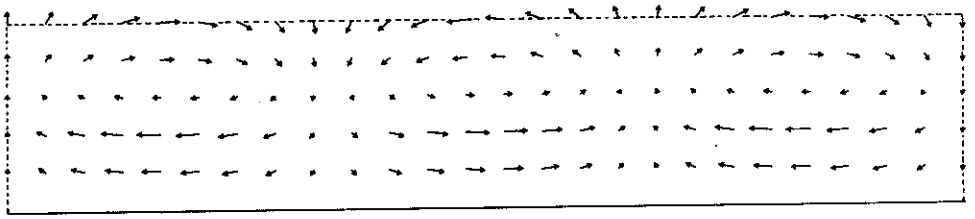

MODE 3,3

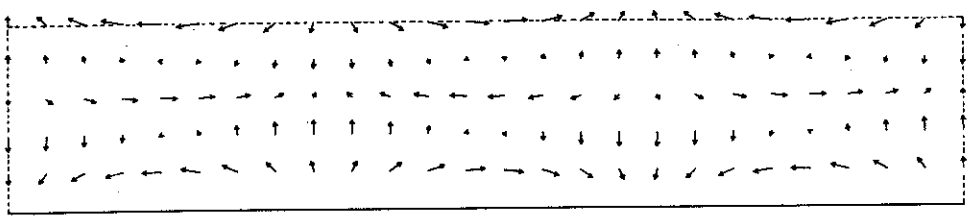

MODE 3,4

Figure A.3 Typical mode shapes. L/H = 5.0. Poisson's ratio = 0.3.

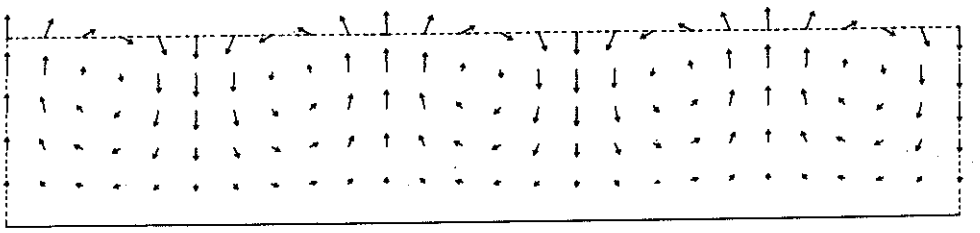

MODE 5,1

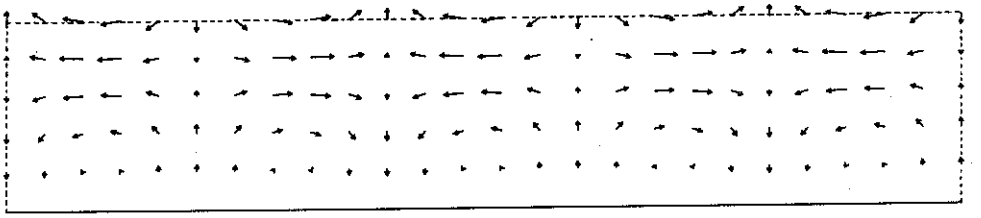

MODE 5,2

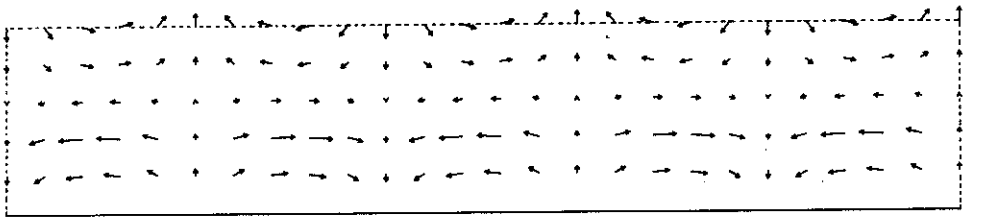

MODE 5,3

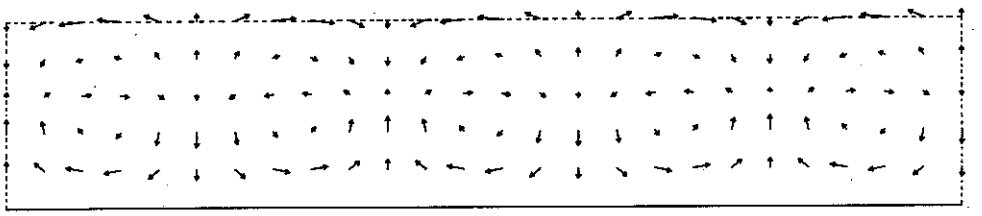

MODE 5,4

Figure A.4 Typical mode shapes. L/H = 5.0. Poisson's ratio = 0.3.

APPENDIX IV

RIGID WALL: DYNAMIC SOLUTION: PARTICIPATION FACTOR INTEGRALS

The static-one-g modal participation factor for mode n,m is defined in Section 3.2 by the relationship

$$P_{n,m} = \frac{-g}{\omega_{n,m}^2} \frac{\int_V u_{n,m}\, dV}{\int_V \underline{\phi}_{n,m} \cdot \underline{\phi}_{n,m}\, dV} \tag{A.13}$$

Let

$$I_N = \int_V u_{n,m}\, dV$$

$$I_D = \int_V \underline{\phi}_{n,m} \cdot \underline{\phi}_{n,m}\, dV \tag{A.14}$$

Closed-form expressions for I_N and I_D were derived for the smooth rigid-wall problem using expressions (A.14) and the modal displacement functions given in Section 3.1.1. The following expressions were obtained.

$\underline{\left(\frac{nH}{L}\right)^2 > \frac{\Omega_{n,m}^2}{4}}$

$$I_N = \frac{2C_{n,m}H^2}{R} \left\{ -\frac{R}{\alpha'^2}(1 - \cosh\alpha') + \frac{1}{R}(1 - \cosh\beta') + \frac{D_{n,m}}{C_{n,m}} \left(\frac{\sinh\alpha'}{\alpha'} - \frac{\sinh\beta'}{\beta'} \right) \right\} \tag{A.15}$$

$$I_D = \frac{C_{n,m}^2 HL}{4}\left[A_1\left(\frac{\sinh 2\alpha'}{2\alpha'} - 1\right) + A_2\left(\frac{\sinh 2\beta'}{2\beta'} - 1\right)\right.$$

$$+ A_3\left(\frac{\sinh 2\alpha'}{2\alpha'} + \frac{\sinh 2\beta'}{2\beta'} + 2\right) - \frac{4}{\beta'}\left(\frac{D_{n,m}}{C_{n,m}}\right)^2 \cosh\alpha' \sinh\beta'$$

$$- \frac{4}{\alpha'}\sinh\alpha'\cosh\beta' - \frac{D_{n,m}}{C_{n,m}}\left\{\frac{4R}{\alpha'\beta'}\sinh\alpha'\sinh\beta'\right.$$

$$+ \frac{4}{R}\cosh\alpha'\mathrm{Cosh}\,\beta' - \left(\frac{1}{R} + \frac{R}{\alpha'^2}\right)\cosh 2\alpha'$$

$$\left.\left. -\left(\frac{1}{R} + \frac{R}{\beta'^2}\right)\cosh 2\beta' + R\left(\frac{1}{\alpha'^2} + \frac{1}{\beta'^2}\right) + \frac{2}{R} - 4\right\}\right] \qquad (A.16)$$

in which

$$A_1 = \left(\frac{R}{\alpha'}\right)^2 + \left(\frac{D_{n,m}}{C_{n,m}}\frac{\alpha'}{R}\right)^2$$

$$A_2 = \left(\frac{\beta'}{R}\right)^2 + \left(\frac{D_{n,m}}{C_{n,m}}\frac{R}{\beta'}\right)^2$$

$$A_3 = 1 + \left(\frac{D_{n,m}}{C_{n,m}}\right)^2$$

$$\frac{\Omega_{n,m}^2}{4} > \left(\frac{nH}{L}\right)^2 > \frac{\Omega_{n,m}^2}{4K^2}$$

$$I_N = \frac{2C_{n,m}H^2}{R}\left\{ - \frac{R}{\alpha'^2}(1 - \cosh\alpha') + \frac{1}{R}(1 - \cos\beta')\right.$$

$$\left. + \frac{D_{n,m}}{C_{n,m}}\left(\frac{\sinh\alpha'}{\alpha'} - \frac{\sin\beta'}{\beta'}\right)\right\} \qquad (A.17)$$

$$I_D = \frac{C_{n,m}^2 HL}{4}\left[A_1\left(\frac{\sinh 2\alpha'}{2\alpha'} - 1\right) - A_2\left(\frac{\sin 2\beta'}{2\beta'} - 1\right)\right.$$

$$+ A_3\left(\frac{\sinh 2\alpha'}{2\alpha'} + \frac{\sin 2\beta'}{2\beta'} + 2\right) - \frac{4}{\beta'}\left(\frac{D_{n,m}}{C_{n,m}}\right)^2 \cosh\alpha' \sin\beta'$$

$$- \frac{4}{\alpha'}\sinh\alpha' \cos\beta' - \frac{D_{n,m}}{C_{n,m}}\left\{\frac{4R}{\alpha'\beta'}\sinh\alpha'\sin\beta'\right.$$

$$+ \frac{4}{R}\cosh\alpha'\cos\beta' - \left(\frac{1}{R} + \frac{R}{\alpha'^2}\right)\cosh 2\alpha'$$

$$\left.\left. - \left(\frac{1}{R} - \frac{R}{\beta'^2}\right)\cos 2\beta' + R\left(\frac{1}{\alpha'^2} - \frac{1}{\beta'^2}\right) + \frac{2}{R} - 4\right\}\right] \qquad \text{(A.18)}$$

$$\frac{\Omega_{n,m}^2}{4K^2} > \left(\frac{nH}{L}\right)^2$$

$$I_N = \frac{2C_{n,m}H^2}{R}\left\{\frac{R}{\alpha'^2}(1 - \cos\alpha') + \frac{1}{R}(1 - \cos\beta')\right.$$

$$\left. + \frac{D_{n,m}}{C_{n,m}}\left(\frac{\sin\alpha'}{\alpha'} - \frac{\sin\beta'}{\beta'}\right)\right\} \qquad \text{(A.19)}$$

$$I_D = \frac{C_{n,m}^2 HL}{4}\left[-A_1\left(\frac{\sin 2\alpha'}{2\alpha'} - 1\right) - A_2\left(\frac{\sin 2\beta'}{2\beta'} - 1\right)\right.$$

$$+ A_3\left(\frac{\sin 2\alpha'}{2\alpha'} + \frac{\sin 2\beta'}{2\beta'} + 2\right) - \frac{4}{\beta'}\left(\frac{D_{n,m}}{C_{n,m}}\right)^2 \cos\alpha' \sin\beta'$$

$$- \frac{4}{\alpha'} \sin\alpha' \cos\beta' - \frac{D_{n,m}}{C_{n,m}}\left\{\frac{4R}{\alpha'\beta'} \sin\alpha' \sin\beta'\right.$$

$$+ \frac{4}{R} \cos\alpha' \cos\beta' - \left(\frac{1}{R} - \frac{R}{\alpha'^2}\right)\cos 2\alpha'$$

$$\left.\left. - \left(\frac{1}{R} - \frac{R}{\beta'^2}\right)\cos 2\beta' - R\left(\frac{1}{\alpha'^2} + \frac{1}{\beta'^2}\right) + \frac{2}{R} - 4\right\}\right] \qquad (A.20)$$

Note: $I_N = 0$ for even values of n.

APPENDIX V

RIGID WALL: DYNAMIC SOLUTION: MODAL PRESSURES

The static-one-g modal wall pressure distribution for mode n,m is given by

$$p_{n,m}(y) = P_{n,m} L_p \underline{\phi}_{n,m}(x,y) \qquad (A.21)$$

The linear operator L_p is determined by the stress-strain relation

$$\frac{\sigma_x}{G} = k^2 \frac{\partial u}{\partial x} + (k^2-2) \frac{\partial v}{\partial y} \qquad (A.22)$$

Expressions for the static-one-g modal pressure distributions of the smooth rigid-wall problem were evaluated using relations (A.21), (A.22) and the modal displacement functions given in Section 3.1.1. The following expressions were obtained.

$\underline{\left(\frac{nH}{L}\right)^2 > \frac{\Omega^2_{n,m}}{4}}$

$$\frac{p_{n,m}}{\gamma H} = \frac{P_{n,m}\omega^2_{n,m}C_{n,m}}{g\Omega^2_{n,m}} \frac{4nH}{\pi L} \left\{ \frac{R\tilde{R}}{\alpha'} \sinh \frac{\alpha' y}{H} - \frac{2\beta'}{R} \sinh \frac{\beta' y}{H} + \frac{D_{n,m}}{C_{n,m}} \left(\tilde{R} \cosh \frac{\alpha' y}{H} - 2 \cosh \frac{\beta' y}{H} \right) \right\} \qquad (A.19)$$

in which

$$\tilde{R} = \left(\frac{\Omega_{n,m} L}{2nH}\right)^2 + 2\left(\frac{\alpha'}{R}\right)^2$$

$$\frac{\Omega_{n,m}^2}{4} > \left(\frac{nH}{L}\right)^2 > \frac{\Omega_{n,m}^2}{4k^2}$$

$$\frac{P_{n,m}}{\gamma H} = \frac{P_{n,m}\omega_{n,m}^2 C_{n,m}}{g\Omega_{n,m}^2} \frac{4nH}{\pi L} \left\{ \frac{R\tilde{R}}{\alpha'} \sinh \frac{\alpha' y}{H} + \frac{2\beta'}{R} \sin \frac{\beta' y}{H} + \frac{D_{n,m}}{C_{n,m}} \left(\tilde{R} \cosh \frac{\alpha' y}{H} - 2 \cos \frac{\beta' y}{H} \right) \right\} \qquad (A.20)$$

$$\frac{\Omega_{n,m}^2}{4k^2} > \left(\frac{nH}{L}\right)^2$$

$$\frac{P_{n,m}}{\gamma H} = \frac{P_{n,m}\omega_{n,m}^2 C_{n,m}}{g\Omega_{n,m}^2} \frac{4nH}{\pi L} \left\{ \frac{R\tilde{S}}{\alpha'} \sin \frac{\alpha' y}{H} + \frac{2\beta'}{R} \sin \frac{\beta' y}{H} + \frac{D_{n,m}}{C_{n,m}} \left(\tilde{S} \cos \frac{\alpha' y}{H} - 2 \cos \frac{\beta' y}{H} \right) \right\} \qquad (A.21)$$

in which

$$\tilde{S} = \left(\frac{\Omega_{n,m} L}{2nH}\right)^2 - 2\left(\frac{\alpha'}{R}\right)^2$$

APPENDIX VI

RIGID WALL: DYNAMIC SOLUTION: STATIC-ONE-g MODAL FORCES

Expressions for the static-one-g modal wall forces and moments can be derived by simple integration of the modal pressure distributions given in Appendix V. Static-one-g modal forces and moments about the wall base were evaluated for a number of values of the parameters $\frac{L}{H}$ and ν, and are listed in Table A.2 below. All the modes that had force contributions greater than 7% of the one-g static force solutions are listed and values for some of the less significant modes are also tabulated. For each case the sum of the listed modal forces exceeds 65% of the static force solution.

TABLE A.2

Static-one-g Modal Forces and Moments

Sign Convention: + = Net Compression
- = Net Tension
Signs of moments are consistent with forces

$\frac{L}{H} = 0.5$

Poisson's Ratio	Mode Type, Order	Dim. Freq. $\Omega_{n,m}$	Dim. Force $F_{n,m}/\gamma H^2$	Dim. Mom. $M_{n,m}/\gamma H^3$
0.2	1,2	5.17	0.016	0.012
	1,4	6.69	0.157	0.088
	1,6	8.17	0.008	0.003
	Static	-	0.226	0.120
0.3	1,2	5.20	0.014	0.011
	1,4	7.40	0.127	0.069
	1,5	8.58	0.030	0.006
	1,6	8.74	0.013	0.012
	Static	-	0.230	0.120
0.4	1,2	5.24	0.012	0.009
	1,4	8.02	0.038	0.022
	1,6	10.24	0.113	0.051
	1,7	11.72	0.018	0.008
	Static	-	0.235	0.119
0.45	1,2	5.26	0.010	0.009
	1,4	8.19	0.018	0.011
	1,6	11.39	0.020	0.009
	1,7	13.11	0.017	0.003
	1,8	13.97	0.096	0.041
	Static	-	0.239	0.118

$\frac{L}{H} = 1.0$

Poisson's Ratio	Mode Type, Order	Dim. Freq. $\Omega_{n,m}$	Dim. Force $F_{n,m}/\gamma H^2$	Dim. Mom. $M_{n,m}/\gamma H^3$
0.2	1,2	3.24	0.281	0.175
	1,3	4.42	0.025	0.000
	1,4	4.72	0.025	0.016
	3,5	10.07	0.022	0.015
	Static	-	0.414	0.229
0.3	1,2	3.43	0.242	0.154
	1,3	4.67	0.048	0.008
	1,4	5.01	0.049	0.030
	3,6	11.36	0.032	0.033
	Static	-	0.423	0.227
0.4	1,2	3.68	0.156	0.103
	1,4	5.62	0.167	0.072
	1,5	7.41	0.014	0.003
	1,6	8.41	0.010	0.011
	3,8	14.95	0.027	0.012
	Static	-	0.436	0.224
0.45	1,2	3.79	0.107	0.074
	1,4	6.63	0.113	0.047
	1,5	7.97	0.094	0.031
	1,6	9.12	0.023	0.014
	Static	-	0.446	0.221

$\frac{L}{H} = 2.0$

Poisson's Ratio	Mode Type, Order	Dim. Freq. $\Omega_{n,m}$	Dim. Force $F_{n,m}/\gamma H^2$	Dim. Mom. $M_{n,m}/\gamma H^3$
0.2	1,1	1.671	0.048	0.031
	1,2	1.874	0.432	0.267
	1,3	3.46	0.019	-0.001
	3,2	4.41	0.031	0.021
	3,3	5.37	0.042	0.025
	5,4	8.14	0.023	0.013
	Static	-	0.664	0.384
0.3	1,1	1.805	0.018	0.016
	1,2	2.01	0.462	0.277
	1,3	3.57	0.035	0.004
	3,2	4.49	0.021	0.014
	3,4	5.98	0.053	0.025
	Static	-	0.687	0.387
0.4	1,1	1.852	0.151	0.107
	1,2	2.41	0.276	0.155
	1,3	3.94	0.097	0.028
	1,4	5.02	0.019	0.011
	3,4	7.01	0.035	0.017
	Static	-	0.714	0.389
0.45	1,1	1.867	0.183	0.131
	1,2	2.71	0.158	0.089
	1,3	4.67	0.111	0.036
	1,4	5.16	0.092	0.039
	3,4	7.43	0.011	0.006
	Static	-	0.734	0.391

$\frac{L}{H} = 3.0$

Poisson's Ratio	Mode Type, Order	Dim. Freq. $\Omega_{n,m}$	Dim. Force $F_{n,m}/\gamma H^2$	Dim. Mom. $M_{n,m}/\gamma H^3$
0.2	1,1	1.438	0.548	0.337
	1,3	3.22	0.015	-0.001
	3,2	3.24	0.094	0.059
	5,3	5.76	0.027	0.017
	7,4	7.66	0.019	0.011
	Static	-	0.788	0.460
0.3	1,1	1.510	0.534	0.330
	1,2	1.836	0.027	0.013
	1,3	3.28	0.028	0.003
	3,2	3.44	0.081	0.051
	5,4	6.44	0.032	0.016
	Static	-	0.829	0.474
0.4	1,1	1.548	0.460	0.295
	1,2	2.28	0.082	0.039
	1,3	3.51	0.081	0.023
	3,2	3.67	0.052	0.034
	3,4	5.62	0.056	0.024
	5,4	7.36	0.015	0.008
	Static	-	0.996	0.560
0.45	1,1	1.562	0.437	0.286
	1,2	2.64	0.029	0.014
	1,3	4.15	0.160	0.055
	3,2	3.79	0.036	0.025
	3,4	6.63	0.038	0.016
	3,5	7.97	0.031	0.010
	Static	-	0.910	0.497

$\frac{L}{H} = 5.0$

Poisson's Ratio	Mode Type, Order	Dim. Freq. $\Omega_{n,m}$	Dim. Force $F_{n,m}/\gamma H^2$	Dim. Mom. $M_{n,m}/\gamma H^3$
0.2	1,1	1.179	0.504	0.309
	3,2	2.13	0.142	0.088
	5,2	3.24	0.056	0.036
	7,2	4.22	0.018	0.012
	Static	-	0.854	0.502
0.3	1,1	1.211	0.535	0.328
	1,3	3.11	0.019	0.002
	3,2	2.28	0.147	0.089
	5,2	3.44	0.049	0.031
	7,4	5.72	0.022	0.010
	Static	-	0.918	0.529
0.4	1,1	1.241	0.543	0.337
	1,3	3.22	0.061	0.018
	3,2	2.63	0.105	0.062
	3,3	4.21	0.033	0.010
	5,4	5.62	0.033	0.014
	Static	-	0.996	0.560
0.45	1,1	1.255	0.541	0.341
	1,2	2.75	-0.041	-0.018
	1,3	3.73	0.146	0.051
	3,2	2.88	0.065	0.039
	3,4	5.38	0.057	0.023
	Static	-	1.048	0.581

$\frac{L}{H} = 10.0$

Poisson's Ratio	Mode Type, Order	Dim. Freq. $\Omega_{n,m}$	Dim. Force $F_{n,m}/\gamma H^2$	Dim. Mom. $M_{n,m}/\gamma H^3$
0.2	1,1	1.048	0.320	0.196
	3,1	1.368	0.185	0.113
	5,2	1.874	0.087	0.054
	7,2	2.41	0.056	0.035
	Static	-	0.867	0.509
0.3	1,1	1.057	0.357	0.218
	3,1	1.429	0.184	0.114
	5,2	2.01	0.092	0.055
	7,2	2.58	0.055	0.034
	9,2	3.16	0.032	0.020
	Static	-	0.939	0.541
0.4	1,1	1.067	0.391	0.241
	1,3	3.07	0.038	0.011
	3,1	1.469	0.167	0.011
	5,1	1.852	0.030	0.021
	5,2	2.41	0.055	0.031
	7,2	2.90	0.041	0.025
	Static	-	1.029	0.580
0.45	1,1	1.072	0.408	0.253
	1,2	2.90	-0.063	-0.026
	1,3	3.46	0.115	0.041
	3,1	1.485	0.159	0.103
	3,3	4.04	0.053	0.018
	5,1	1.867	0.037	0.026
	5,2	2.71	0.032	0.018
	Static	-	1.085	0.603

$\frac{L}{H} = 20.0$

Poisson's Ratio	Mode Type, Order	Dim. Freq. $\Omega_{n,m}$	Dim. Force $F_{n,m}/\gamma H^2$	Dim. Mom. $M_{n,m}/\gamma H^3$
0.3	1,1	1.014	0.194	0.119
	3,1	1.124	0.157	0.096
	5,1	1.314	0.112	0.069
	7,1	1.551	0.074	0.046
	9,2	1.896	0.037	0.022
	11,2	2.141	0.042	0.025
0.4	1,1	1.017	0.218	0.134
	1,3	3.02	0.021	0.006
	3,1	1.144	0.166	0.103
	5,1	1.352	0.108	0.068
	7,1	1.243	0.062	0.040
	9,1	1.784	0.027	0.019
	9,2	2.34	0.024	0.013
	11,2	2.51	0.028	0.016
	13,2	2.76	0.023	0.014
0.45	1,1	1.018	0.231	0.143
	1,2	2.97	-0.053	-0.021
	1,3	3.36	0.078	0.028
	3,1	1.153	0.170	0.106
	3,3	3.59	0.045	0.016
	5,1	1.368	0.105	0.067
	5,3	3.88	0.031	0.011
	7,1	1.60	0.059	0.039
	7,3	4.20	0.023	0.008
	9,1	1.794	0.029	0.020
	11,2	2.79	0.017	0.015

APPENDIX VII

CANTILEVER WALLS: STATIC PRESSURE DISTRIBUTIONS

The finite element method was used to compute the pressure distributions on a slender rigidly-founded vertical cantilever wall for static body force loading and elastic behavior. Details of the problem investigated are shown in Fig. A.5. Because of the relatively slender dimensions of the wall its flexural deformational behavior predominates. The QM5 quadrilateral element described in Appendix II was adopted for this investigation. A mesh similar in detail to that shown in Fig. 2.7 was used to model the soil and the wall was modelled with the mesh shown in Fig. A.5. Pressure distributions were computed for a one-g vertical body force using a smooth wall contact and for a one-g horizontal body force using both smooth and bonded wall contacts. Solutions were obtained for a range of relative wall to soil stiffnesses. Poisson's ratio was taken as 0.3 for both the wall and the soil in all solutions. Plots of the dimensionless wall pressures and displacements are shown in Figs. A.6, A.7 and A.8. The symbols used in these figures are defined as follows:

$$S = \frac{E_s H^3}{E_w I_w} = \text{soil-wall stiffness ratio}$$

E_s = Young's modulus for soil

E_w = Young's modulus for wall

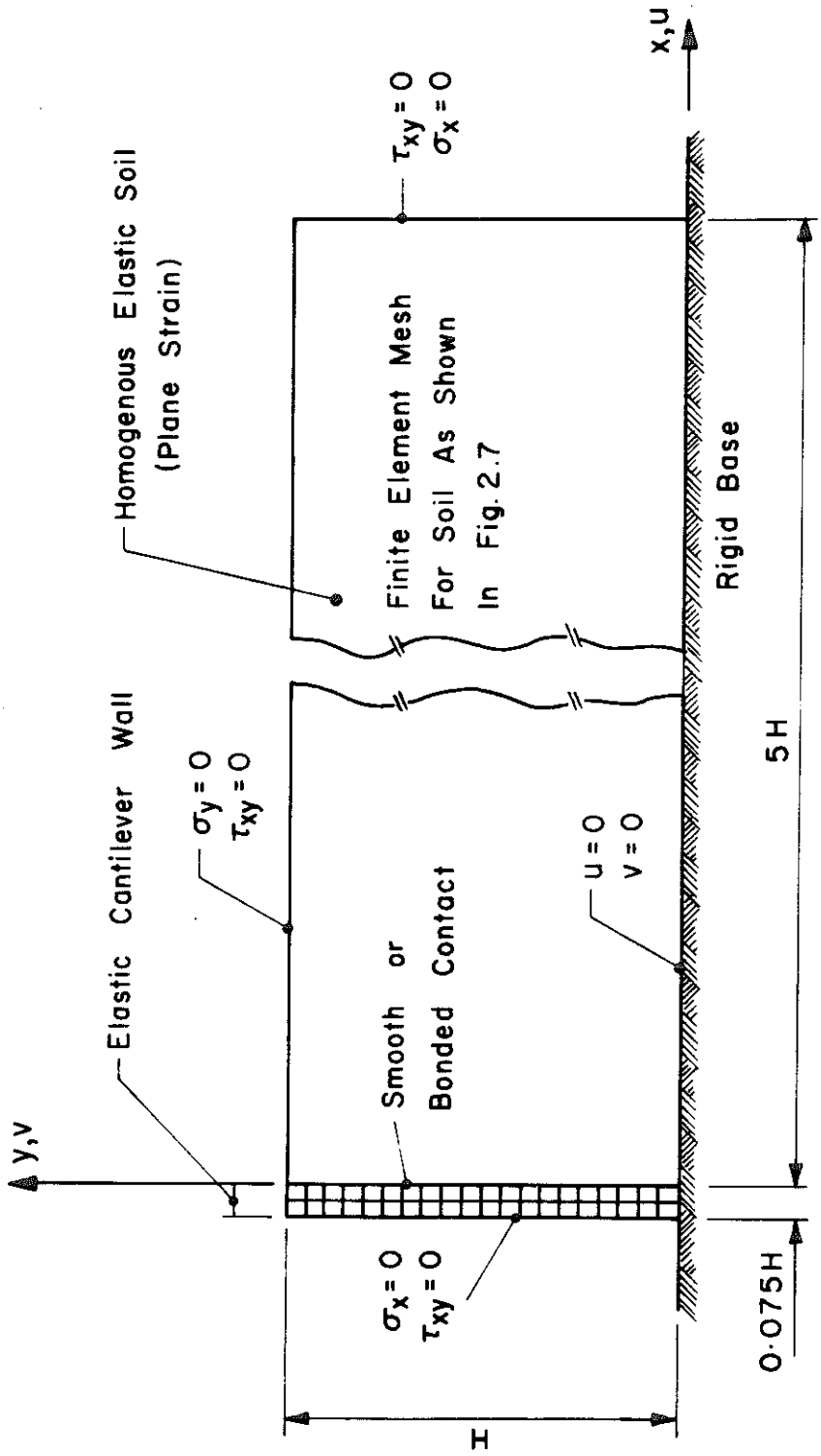

CANTILEVER WALL PROBLEM

Figure A. 5

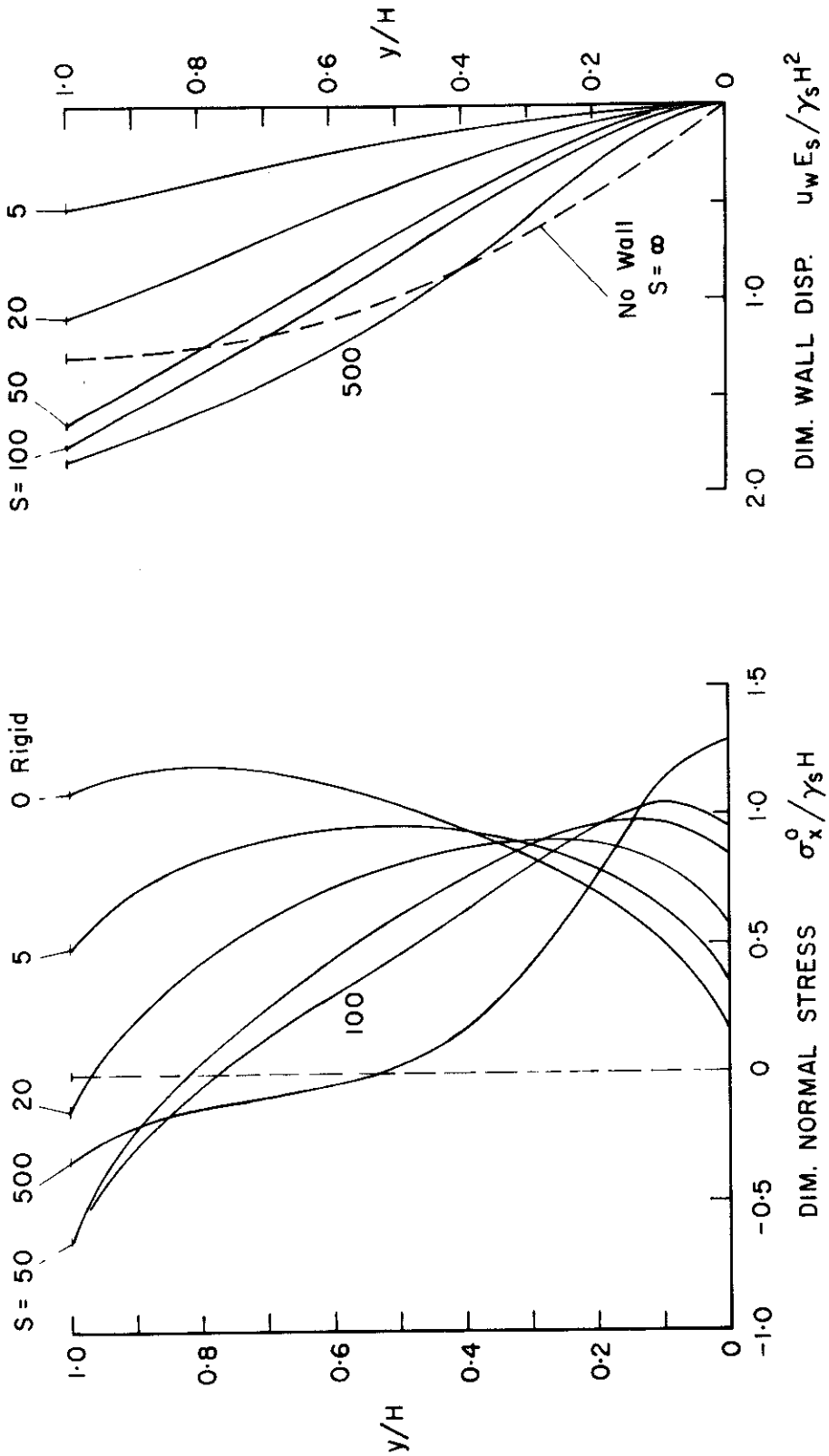

Figure A.6 Pressure distributions and displacements for cantilever wall. One-g static horizontal body force. Smooth contact.

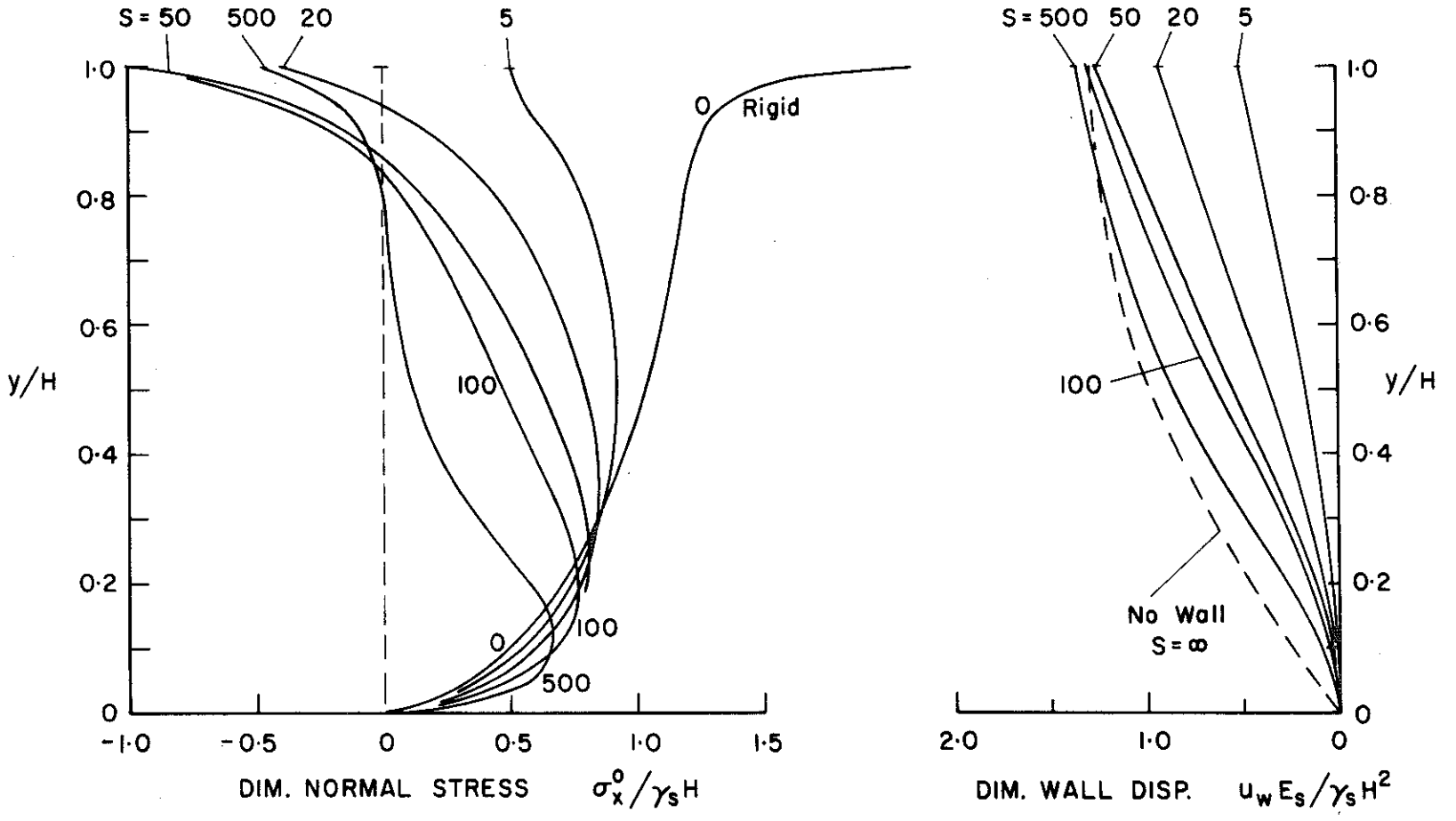

Figure A. 7 Pressure distributions and displacements for cantilever wall. One-g static horizontal body force. Bonded contact.

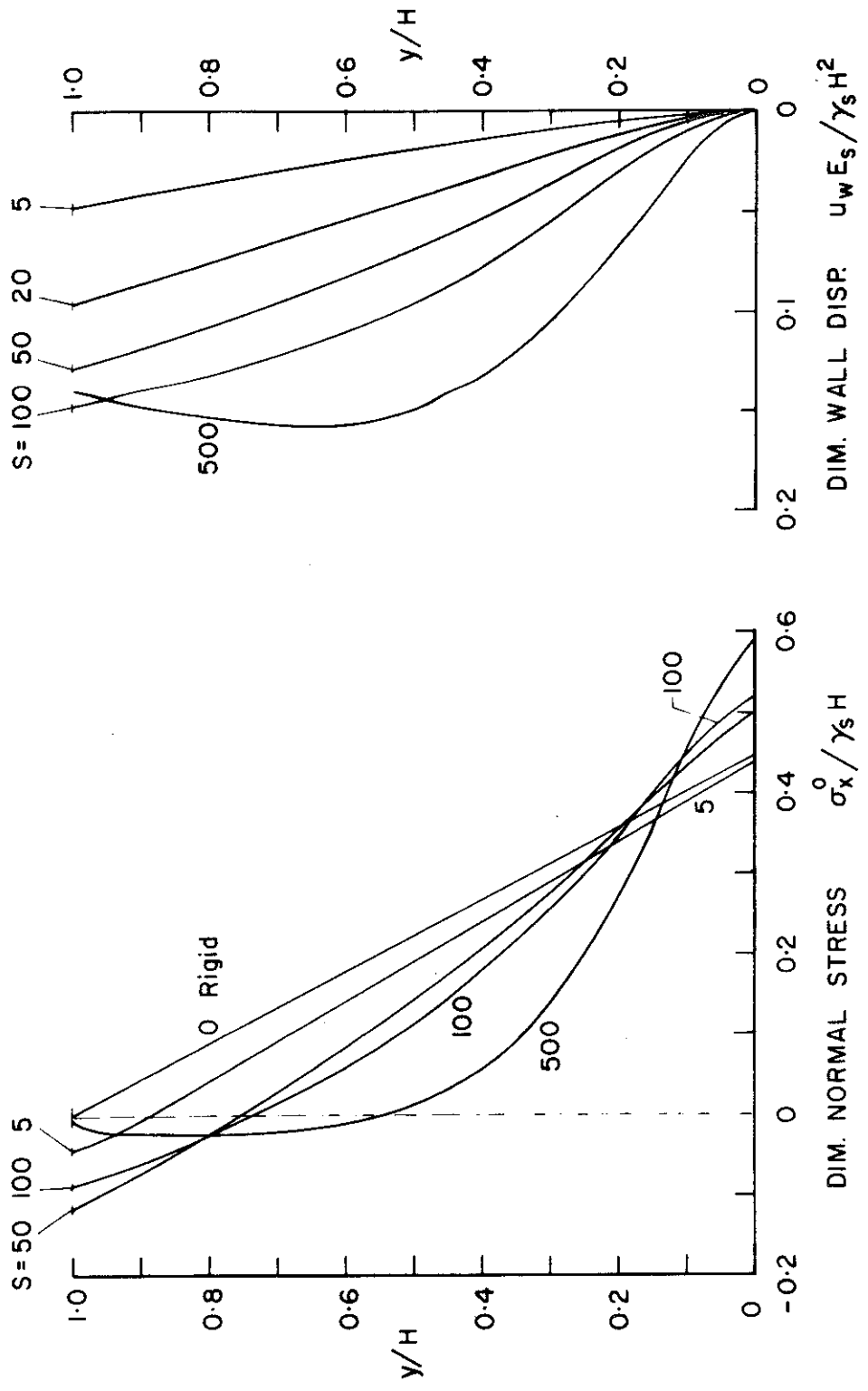

Figure A.8 Pressure distributions and displacements for cantilever wall. One-g static vertical body force. Smooth contact.

I_w = second moment of area of the wall section for unit length of wall

γ_s = unit weight of soil

u_w = wall displacement in x-direction

As the wall stiffness is decreased tension develops at the top of the wall and progresses downwards. In most practical cases no appreciable tensile stress will develop between the wall and soil and so in the region of the tensile pressures the wall will separate from the soil. The solutions given are not exact for cases when wall separation occurs. These cases can be analyzed by using an iterative or nonlinear finite element approach. The possibility that appreciable yielding will develop in the soil as the wall stiffness is decreased imposes a further restriction on the applicability of the elastic solutions. The solutions shown can be used directly for relatively stiff walls and also provide useful information concerning the applicability of linear elastic solutions for more flexible walls.

The solutions for the smooth horizontally loaded walls were checked using a finite element technique in which the wall was modelled with a single flexural beam element. The contact between the soil and wall for this case was approximated by assuming smooth "point" contacts at each of the nodes on the interface. The stiffness of the wall element was computed using the conventional Euler beam equations (Shearing deformation was not considered.) Good agreement was found between the solutions obtained by both methods.

APPENDIX VIII

RESPONSE SPECTRA

Reproductions from Reference (15) of Housner's smoothed average velocity and acceleration spectra are shown in Fig. A.9 and A.10. These spectra were computed by taking the average of the values obtained from both components of the four strong-motion accelerograms: El Centro, Calif., Dec. 30, 1934; El Centro, Calif., May 18, 1940; Olympia, Wash., Apr. 13, 1949; and Taft, Calif., July 21, 1952. The average values were smoothed and scaled so that the velocity spectrum was equivalent to the average spectrum obtained from the two components of the El Centro 1940 record. The zero period acceleration spectrum value was taken as the maximum value of the ground acceleration in the El Centro, 1940 records and not the average of the maximum values. The smoothed average spectra are suitable for design applications within moderate distances of the epicenters of large earthquakes.

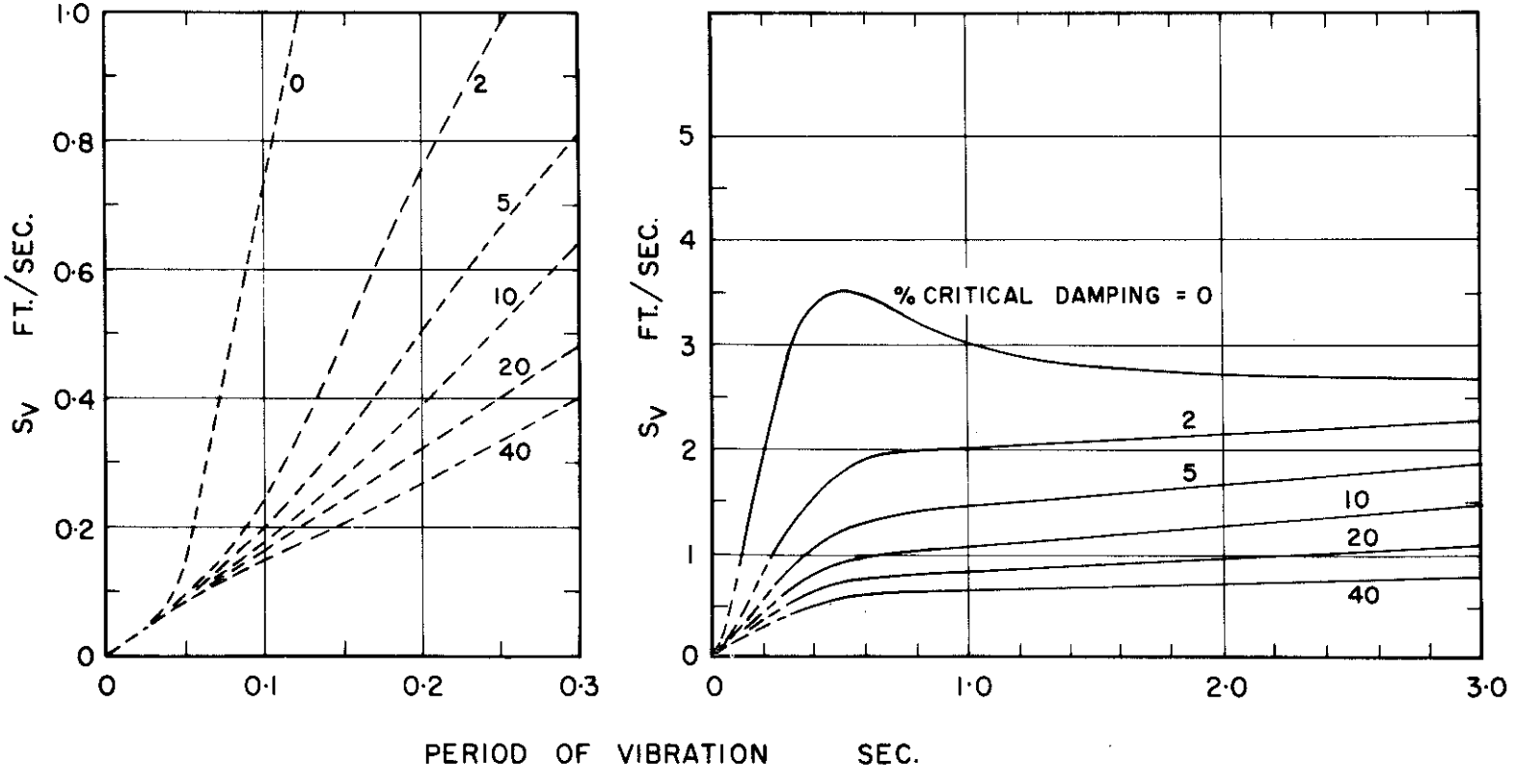

Figure A. 9 Smoothed relative-velocity response spectra for strong-motion earthquakes.

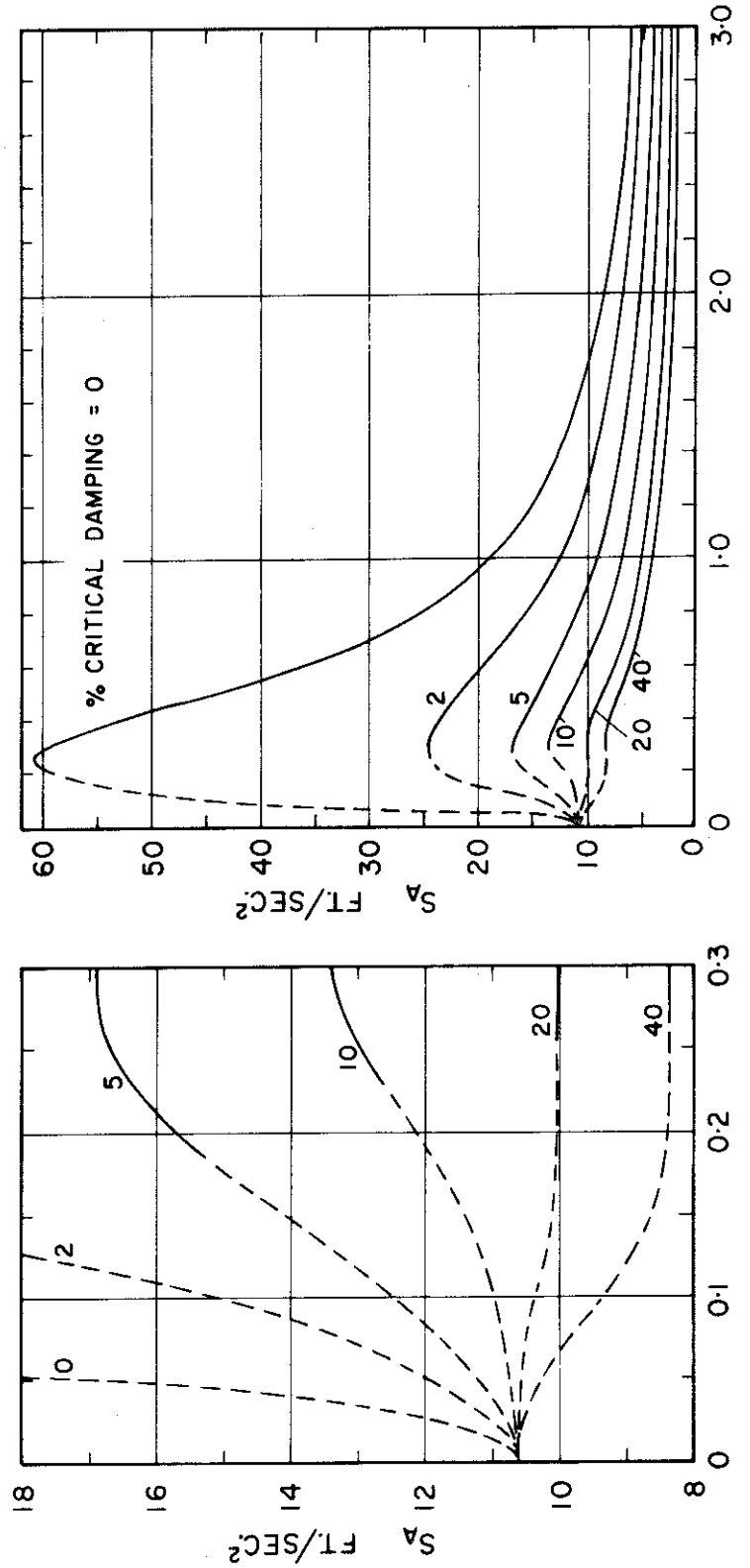

Figure A.10 Smoothed acceleration response spectra for strong-motion earthquakes.